Do changes in the expression of Gαi2 affect cardiac electrophysiology?

Jem Daniel Hardee Lane

Submitted in partial fulfilment of the requirements of the Degree of Doctor of Philosophy

Statement of originality

I, Jem Daniel Hardee Lane, confirm that the research included within this thesis is my own work or that where it has been carried out in collaboration with, or supported by others, that this is duly acknowledged below and my contribution indicated. Previously published material is also acknowledged below.

I attest that I have exercised reasonable care to ensure that the work is original, and does not to the best of my knowledge break any UK law, infringe any third party's copyright or other Intellectual Property Right, or contain any confidential material.

I accept that the College has the right to use plagiarism detection software to check the electronic version of the thesis.

I confirm that this thesis has not been previously submitted for the award of a degree by this or any other university.

Signature:

Date: 23rd October, 2015

Details of collaboration and publications:

Collaboration with Dr David Montaigne. Paper in preparation combining my work on microelectrode array with ventricular slices, and his work utilising murine atria.

Statement regarding experimental work

The experiments contained in this thesis were almost entirely performed by myself alone. These include: all ear-notching of mice for DNA samples used to genotype, digestions of tissue, polymerase chain reactions (PCRs) and electrophoretic gels; all procedures related to the isoprenaline model (insertion of pellets, administration of injections, echocardiography); all procedures related to the coronary ligation MI model (ECGenie recording and analysis, echocardiography, coronary ligation, electrophysiological studies); all procedures related to the MEA system (organ harvest and Langendorff perfusion, tissue slicing, stimulation of tissue and recording, interpretation of signals). All data and statistical analyses were performed by myself. Sanger sequencing and the first mRNA RT-qPCR was performed by the Genome Centre, William Harvey Research Institute. The second mRNA RT-qPCR was performed by myself. I wish to acknowledge the assistance of Dr David Montaigne who wrote the stimulation scripts for use with the MEA system.

Abstract

The heterotrimeric G protein subunit, $G\alpha_{i2}$, is involved in signal transduction from muscarinic acetylcholine and other receptor systems in cardiomyocytes. $G\alpha_{i2}$ expression is elevated in human heart failure, though whether this is beneficial or maladaptive remains unknown. Better understanding could guide therapeutics development. Previous work with $G\alpha_{i2}$ knockout mice suggested a pro-arrhythmic phenotype. We hypothesised that increased $G\alpha_{i2}$ expression is anti-arrhythmic in the ventricles. To investigate this, an *in vivo* murine model of myocardial infarction was used to approximate the human pathophysiology, with wild-type (WT) mice compared to those with cardiospecific $G\alpha_{i2}$ knockout. Subsequently, an *ex vivo* model of cardiac tissue slices was used to evaluate normal electrophysiological properties of murine ventricular tissue, alterations with β-adrenoceptor and muscarinic agonists and temperature, and comparison of these properties in WT mice and those with $G\alpha_{i2}$ globally deleted.

With the myocardial infarction model, there were no significant cardiac phenotypic differences between cardiospecific knockouts and WTs. The cardiac slice model, which utilised a micro-electrode array, showed stable activation and repolarisation properties in WT slices. Comparison of WTs to $G\alpha_{i2}$ global knockouts in the presence of carbachol found no significant differences between groups in terms of repolarisation or conduction properties. In WT slices, isoprenaline was associated with a small increase in effective refractory period, but did not alter conduction properties. There was a highly significant negative linear relationship between temperature and both activation, and repolarisation.

Murine models were used to investigate the electrophysiological effects of autonomic signalling pathways, and in particular, the protein $G\alpha_{i2.}$ No observable electrophysiological differences between WT and $G\alpha_{i2}$ knockout mice were demonstrated. β-adrenergic agonism produced small changes in repolarisation only. Effects of temperature on activation and refractoriness suggest modulation of sodium and potassium currents, in keeping with published work. These findings contribute to our understanding of autonomic modulation of murine cardiac electrophysiology.

Acknowledgements

It seems strange now to think I was apprehensive about undertaking a PhD. Over four years ago, I went to talk to Pier Lambiase in his office at The Heart about research, and he suggested I have a chat with Andy Tinker. Having worked in hospital for ten years, the decision to work in a lab again for three years was not one I took lightly. However, I remember Andy saying to me before I started, "most clinicians enjoy their time in research". Despite the challenges, there is no doubt I enjoyed my time studying for a PhD.

For the opportunity of spending three years in which I was free to take a late-morning coffee every day, many on the grass of Charterhouse Square, I must thank my supervisor Andy. Not only for coming up with a research project, but for granting me the flexibility to work in the way that suited me, and for his trust that I would do the work. For his encouragement, and his fostering of my attempts to achieve an understanding of 'basic science'. Thanks Pier for pointing me in Andy's direction.

My gratitude also to members of his group without whose help I could not have completed this work. Steve Harmer, Qadeer Aziz, Sonia Sebastian, Muriel Nobles, Keat-Eng Ng and Alison Thomas. Thanks also to Amie Moyes, Kristen Bubb and Conchi Villar. As I was starting, four of my contemporaries were in the midst of their PhDs - Aaisha Opel, Richard Ang, Malcolm Finlay and Justine Bha-Amato. Not only were they welcoming, but they helped both teach, and inspire me, and I would like to think the fact we have all been through a similar experience means we have something more in common than just a career path. At the beginning of 2014, an emissary arrived from Lille, France. David Montaigne's experience and intellectual endeavour, coupled with his abilities as a French tutor, made him a great research companion.

One of the nicest things about my three years in research was the freely-given help I received from many people. Thank you to Rachel Dongworth, without whose assistance I may never have got started. And to Yasunori Shintani. Thank you to Alan Hackshaw, who supported me in my early (re-)encounters with statistics, and to Amy Kirkwood who generously assisted with my queries about Stata. My secondary supervisor Patsy Munroe has been most generous with her time and provided much valued critique and commentary on my work.

My gratitude also to the British Heart Foundation for their funding, and to Mark Caulfield, Denise Elliot and the William Harvey Research Institute for their support.

When I began my research, I was quite happy to embrace my time away from hospital, though I soon found I missed it. My thanks to Mark Earley, Richard Schilling, Simon Sporton, and Ross Hunter, for welcoming me to Bart's, and being so supportive in my ambitions. I feel fortunate both to have had the opportunity to work there, and with such inspirational people.
Finally, thanks to my family for their unwavering support, inspiration, and encouragement. For their patience and generosity, for giving me the opportunities to experience and appreciate life outside science and medicine, and for keeping me grounded. No team is better.

The three years spent at the WHRI were rejuvenating. One of the best things about this time was the opportunity to read and explore new concepts, and the enjoyment that comes with understanding. I hope that this has been a foundation.

This work was supported by the British Heart Foundation, grant number FS/12/11/29289.

Table of contents

List of figures

List of tables

Note on thesis presentation

As will be evident from the table of contents, each results chapter is followed a discussion chapter. The thesis is presented in this way rather than using the more traditional approach of combining results and discussion in a single chapter, so as to facilitate readability, ease of locating and cross-referencing.

Abbreviations

AC	Adenylyl cyclase
ACh	Acetylcholine
AF	Atrial fibrillation
ANOVA	Analysis of variance
ANS	Autonomic nervous system
APD	Action potential duration
ARI	Activation-recovery interval
ARP	Absolute refractory period
ATP	Adenosine triphosphate
AV	Atrioventricular
βAR	Beta-adrenoceptor
BDM	2,3-butanedione monoxime
BEG	Bipolar electrogram
bp	Base pairs
BP	Blood pressure
bpm	Beats per minute
BRS	Baroreflex sensitivity
CamKII	Ca2+/calmodulin-dependent protein kinase II
cAMP	Cyclic adenosine monophosphate
cKO	Cardiospecific knockout (gene only deleted in cardiomyocytes)
CL	Cycle length
Cre	Cre recombinase
Ct	Threshold cycle
DAD	Delayed afterdepolarisation
DNA	Deoxyribonucleic acid
EAD	Early afterdepolarisation
ECG	Electrocardiogram
EF	Ejection fraction
EGM	Electrogram
EPS	Electrophysiological study
ERP	Effective refractory period
ESC	Embryonic stem cell
FAC	Fractional area change
Flx	Flanked by loxP
FP	Field potential
FPD	Field potential duration
FS	Fractional shortening
GAPDH	Glyceraldehyde 3-phosphate dehydrogenase
GDP	Guanosine diphosphate
GEF	Guanine exchange factor
GIRK	G protein regulated inwardly-rectifying potassium channel
gKO	Global knockout (gene deleted in all cells of the body)
GNAI2	The gene producing the Galpha-i2 protein

GP	Ganglionated plexi
GPCR	G protein coupled receptor
GRK	GPCR kinase
GTP	Guanosine triphosphate
HCN	Hyperpolarisation-activated cyclic nucleotide-gated [channel]
HF	High frequency band of heart rate variability power spectrum
HFnu	High frequency value of HRV in normalised units
HRV	Heart rate variability
ICD	Implantable cardioverter defibrillator
KO	Knockout
LF	Low frequency band of heart rate variability power spectrum
LFnu	Low frequency value of HRV in normalised units
LFP	Local field potential
LQTS	Long QT syndrome
LTCC	L-type calcium channel
LV	Left ventricle/left ventricular
LVIDd	Left ventricular internal dimension in diastole
mAChR	Muscarinic acetylcholine receptor
MAP	Monophasic action potential
MEA	Microelectrode array
MHC	Myosin heavy chain
MI	Myocardial infarction
mRNA	Messenger ribonucleic acid
NO	Nitric oxide
NSVT	Non-sustained VT
PCR	Polymerase chain reaction
PI3K	Phosphoinositide 3-kinase
PKA	Protein kinase A
PKC	Protein kinase C
PLC	Phospholipase C
PNS	Parasympathetic nervous system
PTX	Pertussis toxin
PVC	Premature ventricular complex
QTc	QT interval corrected for heart rate
RGS	Regulator of G protein signalling
RMP	Resting membrane potential
RMSSD	Root mean square of successive differences
RT-qPCR	Real-time quantitative polymerase chain reaction
RWMA	Regional wall motion abnormality
RyR	Ryanodine receptor
S.D.	Standard deviation
SADS	Sudden arrhythmic death syndrome
SCD	Sudden cardiac death
SDNN	Standard deviation of N-N interval
SERCA2	Sarco/endoplasmic reticulum Ca2+ ATPase 2
SNS	Sympathetic nervous system

TAP	Transmembrane action potential
UEG	Unipolar electrogram
VA	Ventricular arrhythmia
VERP	Ventricular effective refractory period
VF	Ventricular fibrillation
VLF	Very low frequency band of heart rate variability power spectrum
VT	Ventricular tachycardia
WT	Wild-type

1. INTRODUCTION

1.1 Background – the clinical problems

1.1.1 Ventricular arrhythmias

Ventricular arrhythmias (VAs) are often life-threatening abnormalities in cardiac rhythm, occurring when the rate and rhythm of the heart are driven by tissue in one of the heart's two larger chambers, the ventricles. This contrasts with normal 'sinus' rhythm, where the heart's natural pacemaker in the right atrium produces electrical impulses which are conducted through the heart's specialized conducting system, leading to coordinated contraction of the atria, followed by the ventricles.

The causes of ventricular arrhythmias are many and varied, and include 'structural' heart disease, related to the heart muscle or valves; 'ion channel disorders', related to the cardiac action potential and its propagation; and other less common causes such as drugs, and idiopathic disorders[1,2]. Sudden cardiac death (SCD), of which ventricular arrhythmias are a leading cause, is estimated to account for between 180,000 to 450,000 deaths per year in the United States and in Europe, equivalent to an annual population incidence of 1-2 per 1000[1,3,4]. In the UK, there are an estimated 50-70,000 SCDs annually[5]. However, this incidence varies depending on a number of factors such as definition, geographic area, age and sex. For example, SCD is most commonly defined as death within an hour of symptom onset, although 24 hours has also been used, resulting in an increased incidence[3].

More specifically, sudden arrhythmic death syndrome (SADS), is defined as sudden death in a person with no known cardiac disease, where they were seen alive within 12 hours of death, with negative toxicological screen and no cause found by a cardiac pathologist[6]. In England and Wales, the incidence is estimated at 0.24 per 100,000 population in the 1-34 age group[7], and 0.16 per 100,000 in those aged 4-64, equivalent to over 500 cases per year[6]. It is important to appreciate however, some of the inherent difficulties in making these estimates, particularly for SCD: although accurate death certification and inclusion/exclusion of cardiac causes is taken for granted, the reality is that diagnostic errors, coding inaccuracies, and unreliable post mortem examinations make accurate analyses difficult[8].

1.1.2 Heart failure

Heart failure is a well-recognised and common substrate for VAs. This umbrella term encompasses many disease processes and has been defined as "an abnormality of cardiac structure or function leading to failure of the heart to deliver oxygen at a rate commensurate with the requirements of the metabolising tissues, despite normal filling pressures (or only at the expense of increased filling pressures)[9]. Changes subsequently develop at systemic, organ, and cellular levels, some of which are initially adaptive, but many of which become maladaptive as the disease progresses.
Ischaemic heart disease is the commonest cause of heart failure in the UK and other developed countries, accounting for approximately 70% of cases[9]. In this setting, left ventricular (LV) impairment develops largely due to myocyte necrosis, following interruption of the heart's blood supply during myocardial infarction. An arrhythmic substrate may then develop, in large part due to areas of viable myocardium interspersed with fibrotic scar tissue; this provides the basis necessary to support re-entrant tachycardias within the ventricles (see *Section 1.5*). However, other processes, including changes in gene expression, ion channel function, signalling cascades, neurohormonal adaptation, and drugs, all contribute to the milieu favourable to arrhythmogenesis.

With the recognition that heart failure greatly increases the risk of life-threatening VAs, a number of treatments have been developed for both treatment and prevention. Implantable cardioverter-defibrillators (ICDs) have been shown to reduce mortality in patients with LV impairment at risk of VAs[10,11], and superiority over amiodarone therapy has been established[10,12,13]. Catheter-delivered radiofrequency ablation has been assessed in two randomised trials in patients receiving ICDs following myocardial infarction[14,15]; both showed lower rates of appropriate defibrillator therapy in the ablation group. A meta-analysis reported lower rates of VT recurrence with adjunctive catheter ablation, but no effect on mortality[16]. A further randomised trial is underway to assess this treatment strategy[17].
With the exception of beta-blockers and possibly amiodarone[18,19], most anti-arrhythmic drugs have been associated with a lack of efficacy, and in some cases, increased mortality, due to either pro-arrhythmogenicity or heart failure[20–23].
Therefore there exists a need to develop new options for pharmacotherapy in this common condition.

1.2 Cardiac Electrophysiology

1.2.1 Normal cardiac structure

Macroscopically, the normal heart comprises right and left atria, and corresponding right and left ventricles. The right atrium connects to the right ventricle via the tricuspid valve, and the right ventricle ejects blood through the pulmonic valve into the pulmonary artery which delivers blood to the lungs for oxygenation. This blood then returns to the left atrium via the pulmonary veins, whereupon it passes through the mitral valve into the left ventricle. It is ejected through the aortic valve into the aorta, the main conduit of the systemic circulation before finally returning via the systemic veins to the right atrium, as established by Harvey in 1628 [24].

This sequential return of blood, filling of chambers, followed by ejection, is governed by the heart's cyclical electrical activity in coordination with cellular contractile processes, a phenomenon known as excitation-contraction coupling. This in turn is ultimately driven by a pacemaker, which in normal hearts is the sinus node. Located principally at the junction of the superior caval vein and right atrium, it extends inferiorly to varying degrees[25] (see Figure 1). As the group of cells with the highest frequency of spontaneous discharge, this pacemaker determines the frequency of atrial and ventricular contraction. However, for physiological functioning, the impulses of the sinus node must spread through the working myocardium of the atria, and then into the ventricles. In order for contraction of the chambers to occur in a synchronised way, sufficient to both generate high pressures and overcome those of the arterial systems, the time from original impulse generation to activation of the whole of the large muscle mass of the ventricles is necessarily brief. This requires an impulse conduction system, analogous to wiring, to facilitate the rapid dispersion of the electrical impulse to all regions of the heart (Figure 1). The key components of this are the atrioventricular (AV) node, penetrating bundle of His, common AV bundle, branching bundle, right and left bundle branches, and Purkinje fibres[26]. Impulses arriving at the AV node in the atria proceed sequentially through these, exiting through the Purkinje fibre network which provides multiple points of ventricular cardiomyocyte activation. Although other muscular tissue connections exist within the heart such as Bachmann's bundle, the conduction system is differentiated by its fibrous sheath insulation, ion channel expression, and action potential morphologies. Despite the functional resemblance to neurones in the ability of the His-Purkinje system to rapidly transmit impulses, the

cells comprising the system are derived principally from cardiomyocytes rather than neural crest tissue, although are innervated by ganglia originating from the latter[27].

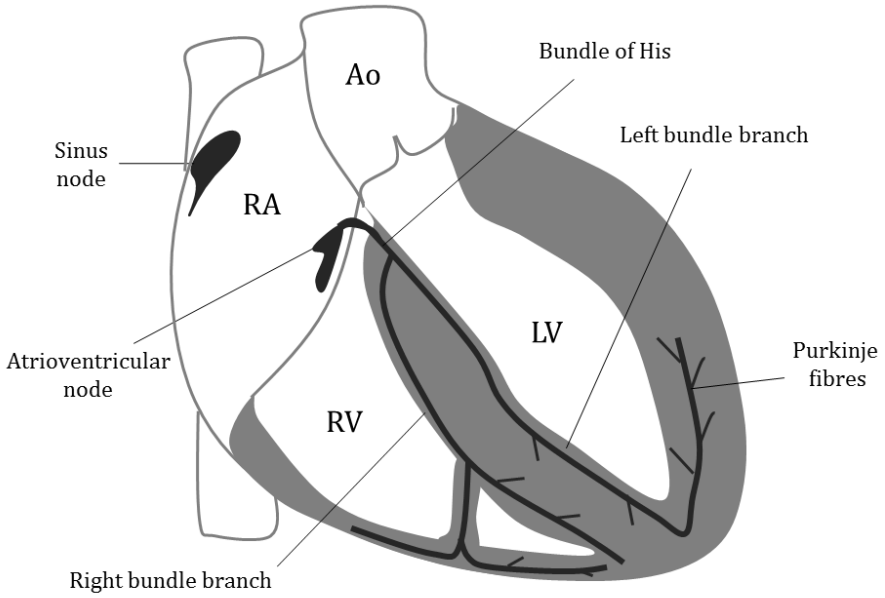

Figure 1 Cardiac conduction system. RA: right atrium, Ao: aorta, RV: right ventricle, LV: left ventricle.

Microscopically, the heart is comprised of a variety of cell types. A classification based on cell differentiation and functional properties could divide the cell types into atrial and ventricular working myocardium (cardiomyocytes), sinus and atrioventricular nodal tissue, His-Purkinje tissue, fibroblasts and myofibroblasts, smooth muscle, endothelial, and epicardial cells[28].

Of these, fibroblasts are most numerous, accounting for over 50% of the total number of cells. These spindle-like cells are components of the supportive extracellular matrix, and produce different types of collagen to cardiomyocytes, as well as fibronectin and matrix metalloproteinases[29]. Interestingly, this collagen undergoes continual turnover. Expression of ion channels, and fibroblast-cardiomyocyte interactions through current-conducting 'gap junction' protein complexes for example, suggest that fibroblasts are not simply inert, supportive cells, and there is interest in their potential roles in arrhythmogenesis[30,31].

Cardiomyocytes account for only around a third of the total number of cells within the heart, yet constitute approximately 75% of its volume. Human atrial and ventricular myocytes are long, narrow and cylindrical in shape, with approximate dimensions of

10-20 μM diameter, and 60-140 μM length[32,33]. Cardiomyocytes are composed largely of contractile proteins bundled together as myofibrils, and mitochondria, required due to the cells' high energy demands. This composition gives cardiomyocytes their contractile function, a feature not seen in other cardiac cells. Cardiomyocytes are connected to each other via intercalated discs. These provide both a structural continuum between cells via desmosomal proteins and adherens junctions, and an electrical continuum through protein channels known as gap junctions, as well as ion channels (Figure 2). Desmosomes and adherens junctions are classically regarded as proteins involved in mechanical cellular continuity, providing structural linkage and integrity. Gap junctions – low resistance intercellular channels – are formed by proteins known as connexins, and are understood to facilitate the rapid passage of currents between neighbouring cells. The voltage-gated sodium channel complex, comprising α and β subunits, is also found at the intercalated disc, where it plays an important role in impulse conductance[34]. However, there may be species differences in the extent to which the main α subunit, Nav1.5 localises here[35].

Whilst these functional categorisations largely hold true, there is some overlap, and co-regulation, as might be expected given the proteins' physical proximity. Desmosomal proteins modulate the voltage-gated sodium channel complex, and therefore its current I_{Na} for example, as well as the function of connexin43 (Cx43)[34].

The cardiac conduction system may be thought to comprise the sinus and AV nodes, and the His-Purkinje system. These cell groups share some properties such as poorly-developed sarcomeres and sarcoplasmic reticulum, with a relative paucity of mitochondria[27]. However, there are distinctions too: the nodal areas both exhibit spontaneous depolarisation immediately after attaining their hyperpolarised membrane voltage, a property governed by expression of certain ion channels as discussed later. This gives rise to their natural pacemaker activity. The upstroke of their action potentials is largely dependent on L-type calcium channel opening and the resultant inward current I_{CaL}, which has a lower gradient than cardiomyocytes; hence nodal cells are considered to be 'slowly conducting'. In contrast, cells of the His-Purkinje system show a different pattern of intercellular gap junction protein expression, and are depolarised by the fast inward sodium current I_{Na}. These properties result in their ability to conduct impulses much more quickly, and they are therefore referred to as 'rapidly conducting' tissues[36].

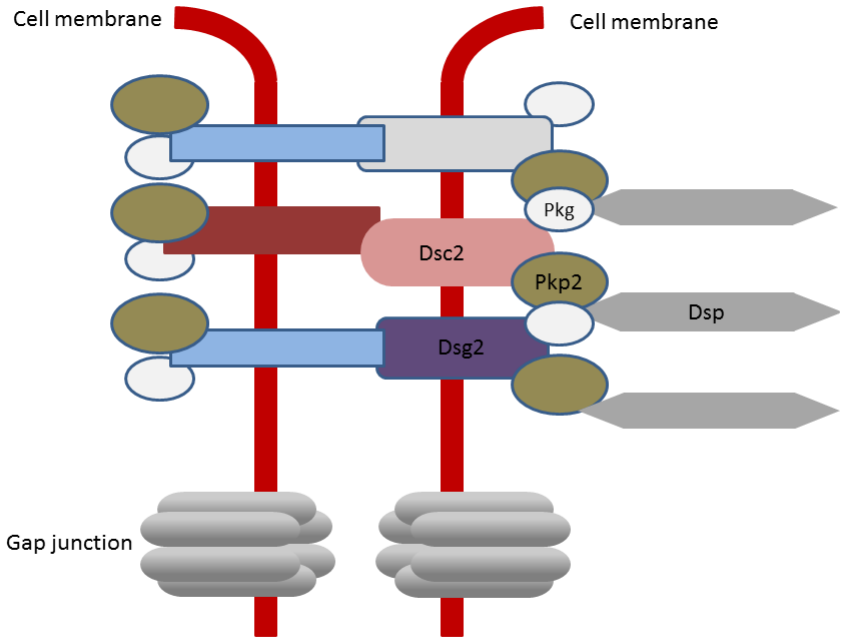

Figure 2 The intercalated disc. Dsc2: desmocollin-2, Dsg2: desmoglein-2, Pkg: plakoglobin, Pkp2: plakophilin-2, Dsp: desmoplakin. Modified from Awad et al[37].

1.2.2 An overview of ion channels, currents and action potentials

Cardiac physiology relies on an elaborate, cyclical system of cellular ionic fluxes generating impulses, which are conducted through the myocardium, resulting in cardiomyocyte contraction and relaxation. The interplay between these electrical and mechanical processes is termed 'excitation-contraction coupling'. Fluxes of three ions – Na^+, K^+, and Ca^{2+} - and to a lesser extent Cl^-, across the specialized cardiomyocyte membrane known as the sarcolemma, regulate both the concentration and compartmentalization of intracellular Ca^{2+}, the key link in the processes. Movements of ions into and out of the cell are governed by flow down concentration gradients through channels, and active movement by pumps and exchangers. The latter ensure that in the resting (diastolic) state, intracellular Na^+ concentration ($[Na^+]_i$) is low, intracellular K^+ ($[K^+]_i$) is high, and that intracellular Ca^{2+} ($[Ca^{2+}]_i$) is sequestered in the sarcoplasmic reticulum.

Ion channels

Ion channels have two main properties: selective permeability and gating[38]. The former refers to the ionic selectivity of most channels, determined by amino acid residues. The HCN (hyperpolarisation-activated cyclic nucleotide-gated) channel is an exception, allowing passage of both Na^+ and K^+ ions. Structurally, two of the channels generating the largest currents, Nav1.5 and the L-type Ca^{2+} channel (LTCC), Cav1.2, are similar, despite allowing passage of different ions. There are several K^+ channels, and a main structural difference between them and Na^+/ Ca^{2+} channels relates to the accessory β-subunits which modify some K^+ channel activity and have been implicated in some forms of Long QT Syndrome (LQTS).

Channel gating refers the regulated opening and closure of a channel, and its consequent ability to pass ions. This property is most commonly dependent on membrane voltage, but ligands or mechanical stimuli are alternative mechanisms. The work of Hodgkin and Huxley in the early 1950s modelled the conductance of the Na^+ and K^+ channels of the giant squid axon[39], and provided a framework with which to understand this property. Gating is believed to result from reversible conformational changes of the channel apparatus that regulate passage of ions[40]. In the simplest model, channels may be described as being in one of three 'states': open, closed, or inactivated. Inactivation underlies the property of refractoriness in cardiomyocytes (see below). Recovery from this state and re-acquisition of the ability to open is dependent on both time and hyperpolarisation[38]. Gating is incompletely understood; many of the models have been derived from single ion channel analysis, and more recently, work on crystal structures and molecular interactions. Mathematical approaches such as Markov models have also been used to estimate the number of states and their transitions. The three state model above is probably too simplistic, and an alternative is shown in Figure 3, illustrating the possibility of more than one 'closed' state.

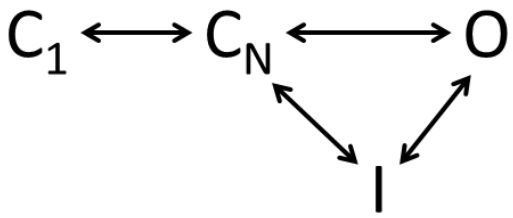

Figure 3 Ion channel states implicated in gating. C_1: initial closed state, C_N: closed state before the O state, O: open state, I: inactivated state. From Grant[38].

Action potentials in different regions of the heart

Figure 4 illustrates the action potentials of atrial, ventricular and sinus nodal tissues, with their most important currents. Cardiac action potentials are divided into phases according to the ionic shifts into and out of the cell. These correspond to the following events:

- Phase 0: rapid depolarisation
- Phase 1: transient repolarisation
- Phase 2: Ca2+ inflow and K+ outflow
- Phase 3: terminal, rapid repolarisation
- Phase 4: resting potential, during which there may be gradual depolarisation.

As can be seen, although there are some differences in the dominant ionic currents, atrial and ventricular myocytes essentially follow the pattern of Na^+ influx-mediated depolarisation, following by plateau phase maintained by the balance of inward Ca^{2+} flow and outward K^+ flow. Finally, outward K^+ flow leads to repolarisation of the cell. In sinus nodal cells, the action potential frequency is determined by a combination of the 'pacemaker current', I_f, and the 'intracellular Ca^{2+} clock'[36]. The HCN channel produces the slowly-depolarising I_f current during diastole. This net inward current leads to activation of T-type Ca^{2+} channels which produce Ca^{2+} sparks – brief releases from the sarcoplasmic reticulum. Elevated intracellular Ca^{2+} concentrations activate the Na^+/ Ca^{2+} exchanger, leading to a net influx of Na^+ which depolarizes the cell sufficiently to activate LTCCs (Cav1.2). Rapid Ca^{2+} influx ensues leading to

depolarisation of the cell and initiation of the action potential. Depolarisation activates the K^+ channels which repolarise the cell, and the process begins again[41].

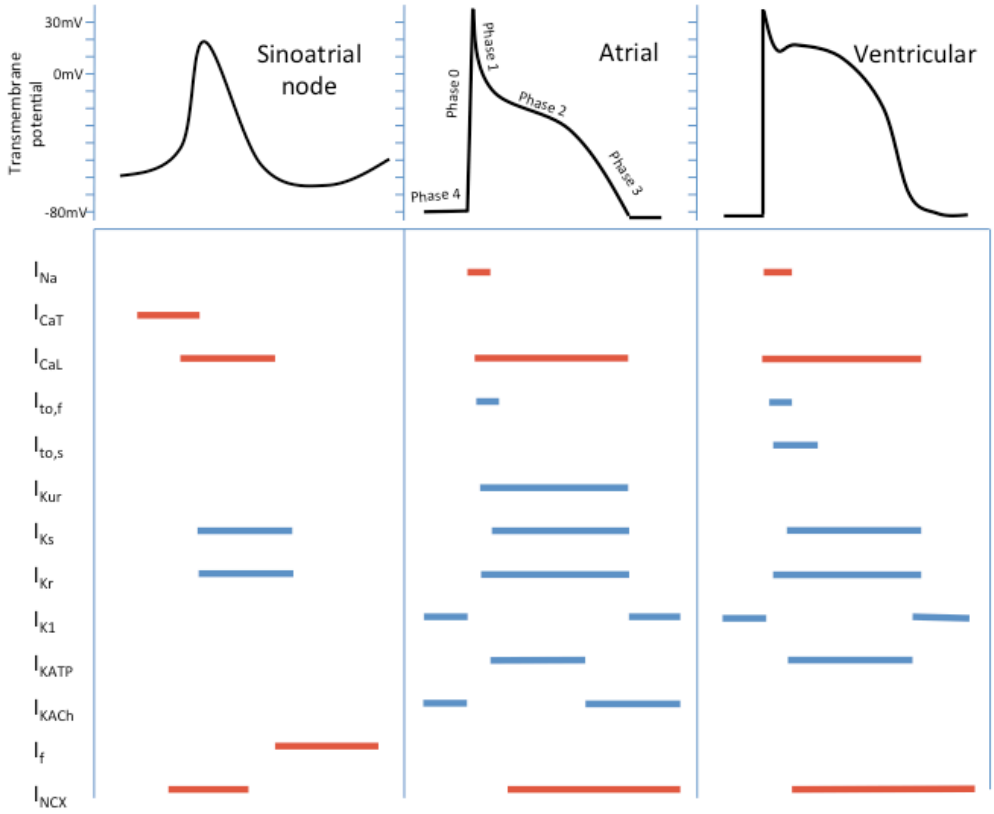

Figure 4 Cardiac action potentials from different regions of the heart, with the currents that generate them. Coloured lines indicate the phase of the action potential that the current participates in. Inward currents are in red, outward currents in blue. Currents - I_{Na}: inward Na^+, I_{CaT}: T-type Ca^{2+}, I_{CaL}: L-type Ca^{2+}, $I_{to,f}$: fast transient outward, $I_{to,s}$: slow transient outward, I_{Kur}: ultra-rapid K^+ delayed rectifier, I_{Ks}: slow K^+ delayed rectifier, I_{Kr}: rapid K^+ delayed rectifier, I_{K1}: inward rectifier, I_{KATP}: ADP-activated K^+ channel, I_{KACh}: muscarinic-gated K^+ channel, I_f: 'funny' current, I_{NCX}: Na^+/Ca^{2+} exchange current.

There are differences in cardiac action potentials between species, including between mammals, which are important to bear in mind when using animal models of arrhythmias. This is illustrated in Figure 5, which contrasts human and murine electrocardiograms (ECGs) and ventricular action potentials. A noticeable difference exists between the two in the repolarisation phase: the major outward currents in humans are I_{Kr} and I_{Ks}, whereas in the mouse are I_{to}, $I_{K,slow1}$, $I_{K,slow2}$ and I_{SS}[42,43]. The majority of repolarisation takes place within a proportionately much shorter timeframe in the mouse, although full repolarisation continues for longer as a slower decline in transmembrane potential. These differences are necessary given the nine- to ten-fold higher heart rate in the mouse, with consequent shorter coupling interval. As

can be seen from the representative ECG complexes at the top of Figure 5, the initial T wave peak in the mouse occurs soon after the QRS complex, but this is followed by a prolonged dip below the isoelectric line. The origin of the T wave in both species is incompletely understood, and the subject of much debate[44,45].

Although depolarisation appears similar for humans and mice, and is indeed mediated by a fast inward sodium current, there may in fact be differences here too. Several Nav protein isoforms have been shown to be expressed in murine hearts, whereas Nav1.5 is by far the most abundantly expressed in humans (see below). β1-4 subunits co-localise with these other α-subunits in the mouse, suggesting some redundancy. Together with possible differential localisation of these protein subunits in the cell, these findings raise the potential for differences in activation and conduction[35,46].

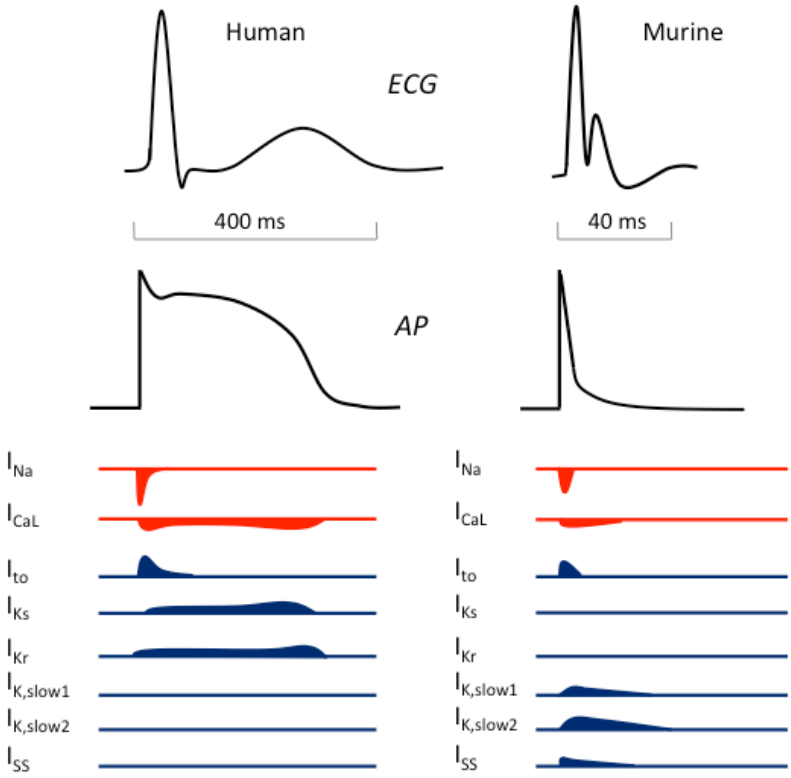

Figure 5 Comparison of human and murine ECGs and ventricular action potentials (APs), with the key currents that generate these. Currents - I_{Na}: inward Na^+, I_{CaL}: L-type Ca^{2+}, I_{to}: transient outward, I_{Ks}: slow K^+ delayed rectifier, I_{Kr}: rapid K^+ delayed rectifier, $I_{K,slow1}$ and $I_{K,slow2}$: K^+ delayed rectifier, I_{SS}: steady state. Modified from Davis et al[47].

Thus, despite similar overall sequences of depolarisation and repolarisation in humans and mice, and some overlap in transmembrane currents, particularly I_{Na} and I_{CaL}, repolarisation differs substantially between the two species. We must therefore be

cautious in interpreting alterations in repolarisation in humans and extrapolating them to the mouse, and vice versa.

1.2.3 Excitability of cardiomyocytes

As described above, cardiomyocytes relay from cell to cell the stimulatory action potentials necessary to initiate contraction. This relay of activation between millions of cells occurs rapidly, as it must if the contractile forces of each cell are to be synchronised, so as to work collectively in ejecting blood forcefully from the cardiac chambers. The corollary of this is that a period of inexcitability or refractoriness of cardiomyocytes is required, both to prevent uncoordinated contractions and ensure propagation in one direction, and to prevent contractions occurring too frequently. This period also serves as a time for the redistribution of ions necessary prior to the next cycle, and in mechanical terms, permits relaxation. As such, cardiomyocyte excitability may be considered to comprise two parts: activation, and refractoriness. Whilst these fundamental properties are largely governed by different proteins, there is also some overlap. These will now be considered in turn in relation to ventricular myocytes.

Activation

Cardiomyocytes are considered to be 'at rest' during phase 4 of the action potential. Their resting membrane potential (RMP) remains steady at around -80 mV. This value, known as the equilibrium potential (E_m), is determined by the balance of chemical and electrical gradients generated by different concentrations of ions intra- and extracellularly. Its magnitude is similar to the equilibrium potential of K^+, due to this being the ion with the highest intracellular concentration, and reflects the fact that the I_{K1} current is its major determinant. E_m can be calculated for single ions with the Nernst equation, or for multiple ions with the Goldman-Hodgkin-Katz equation[48]. Maintaining E_m at such a low value on the one hand is believed to be one of the inherent protective measures against spontaneous depolarisation of cardiomyocytes outside the sinus node, whilst on the other, it ensures sodium channel availability in a non-inactivated state.

When an action potential (or more generally, a stimulatory impulse) is relayed from one cardiomyocyte to another, provided the cell receiving the impulse is not refractory, it will depolarise from its RMP. In order for a large amplitude rapid inward current to result, the excitatory stimulus must be of sufficient magnitude to depolarise the membrane beyond a threshold level of -55 to -65 mV [36,42]. As shown in Figures 4 and 5, the main current responsible for this rapid depolarisation in cardiomyocytes is the inward sodium current, I_{Na}. This sets off the sequence of opening and closure of different ion channels that together produce the action potential.

The voltage-gated sodium channel, through which passes I_{Na}, is in fact a multi-protein complex with two core components, the α- and β-subunits[49]. There are 10 α-subunit genes in humans, and these are expressed in different tissues. A key characteristic of sodium channels is their sensitivity to tetrodotoxin (TTX). Nav1.5 is the principal, though not exclusive cardiac isoform. Indeed, 12-27% of sodium current is due to other isoforms such as Nav1.2 and Nav1.1[35]. There are some differences in localisation of the different isoforms, e.g. intercalated disc vs. cardiomyocyte cell membrane, and these appear to differ between species. The β-subunits that are expressed in the heart (SCN1B-4B) have all been reported to associate with Nav1.5. Although experimental data are somewhat conflicting, the importance of these subunits in modulation of the α-subunit is borne out by the fact that mutations in these genes lead to serious arrhythmic phenotypes, such as Brugada syndrome, atrial fibrillation (AF) and cardiac conduction disease[46]. β-subunits are believed to modulate both channel function, and expression.

The α-subunit has the ability to conduct Na^+ independently, and incorporates voltage-sensing and pore-forming modules. The three-dimensional (3D) shape of the channel is dependent somewhat on electrostatic forces related to the membrane potential. At a RMP of -80 mV, this results in a conformation with a closed pore. Upon depolarisation, changes in electrostatic forces permit channel segment movement and pore opening. These geometric fluxes permit Na^+ ion flows that depolarise the membrane from -80 mV to +30 mV within around 1 ms. An important feature differentiating sodium channels from potassium or calcium channels is that inactivation commences almost immediately after opening, and the majority of the channels are wholly inactivated within a few milliseconds. However, a 'late' inward current may result from persistence of an open state or re-opening of some channels during phase 2 of the action potential[42,49].

Various putative modulators of sodium channel function have been investigated. Those for which there is most evidence of modulation include protein kinase A (PKA) phosphorylation, $G\alpha_S$ (PKA-independent), and temperature. However, other factors possible factors include protein kinase C (PKC), glycosylation, calcium/ calmodulin, Ca^{2+}/calmodulin-dependent protein kinase II (CamKII), tyrosine phosphorylation, and pH[46,48].

Refractoriness

Activation, or phase 0, is followed by a brief slight repolarisation (phase 1), and then by a plateau (phase 2) during which an inward predominantly calcium current, I_{CaL}, is balanced by potassium efflux. This outflow occurs almost wholly through the voltage-gated delayed rectifier potassium channels I_{Kr} (rapid-activating) and I_{Ks} (slowly-activing), and during phase 3 these currents outweigh I_{CaL} and repolarise the cell completely to its resting membrane potential. Another class of potassium channel, the inward rectifiers (Kir) are also involved in repolarisation. One of these, the G-protein regulated inwardly-rectifying potassium channel (GIRK), through which passes the I_{KACh} current, is thought to contribute little if anything to repolarisation in the ventricle. Kir2.1 which produces the I_{K1} current however, is important, and as already mentioned, largely determines the phase 4 RMP[42,50].
However, Kir2.1/I_{K1} is not limited to these roles; various lines of evidence support the idea that it also has a reciprocating regulatory relationship with Nav1.5/I_{Na}[50]. For example, Nav1.5 expression and density appear to be dependent in part on Kir2.1. As components of a common macromolecular complex, this dependency could be expected. In addition, by setting the RMP sodium channel availability and therefore cell excitability are influenced.

Repolarisation can be quantified in several ways: perhaps the most logical and easily understood is to measure the action potential duration (APD) from its onset to when repolarisation has brought E_m to where it has returned 90% from its peak value[51] (see Figure 6), an interval known as APD_{90}. The related but distinct property of refractoriness, can be described in terms of refractory periods. These time intervals are measured from the onset of the action potential to a predefined level of refractoriness, which is determined by the ability of a stimulus to elicit a response from the cell or tissue. The absolute refractory period (ARP) is the period when no stimulus,

no matter how strong, can elicit another depolarisation. This extends from phase 0 to the beginning of phase 3[36]. After this, in the mid and terminal portions of phase 3 typically, is the relative refractory period (RRP). This describes the time during which a cell or tissue is able to generate a complete action potential, but only with a stimulus larger than is required during phase 4 (i.e. diastolic threshold). In addition, the action potential elicited has a slower upstroke, lower amplitude, and is propagated more slowly than normal (see Figure 6).

In clinical electrophysiology, or with *in vivo* experiments, a further measure is used: the effective refractory period (ERP). This is defined as the longest stimulus coupling interval that fails to capture the tissue or to be conducted through it[52]. This therefore potentially encompasses both repolarisation and conduction, at the tissue rather than cellular level. It exists somewhere near the boundary of the ARP and RRP.

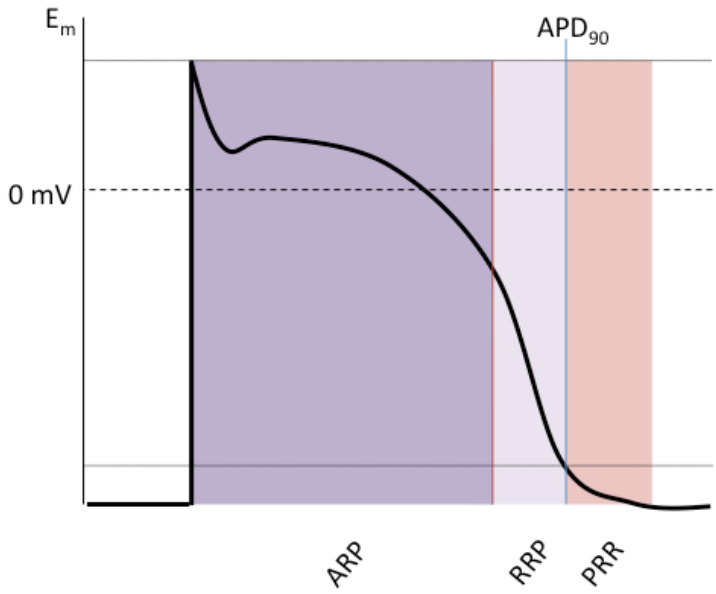

Figure 6 Relation of refractory periods to the action potential. Note: APD_{90} and RRP do not necessarily coincide. Absolute: absolute refractory period, ERP: effective refractory period, RRP: relative refractory period, PRR: post-repolarisation refractoriness, APD90: action potential duration at 90% repolarisation.

Two human studies have found ventricular ERP (VERP) to be consistently shorter than APD_{90} in the drug-free state, though their results differ slightly in the VERP/APD_{90} ratio in relation to cycle length. It is also worth noting that both studies involved patients with heart disease undergoing investigation for ventricular tachycardia (VT)[53,54]. Nevertheless, the demonstration of a positive correlation between both parameters

and steady state paced cycle length is in keeping with the relationship noted in atria and the His-Purkinje system in a heterogeneous cohort, including those without heart disease[55]. This physiological adaptation of APD to heart rate is the means by which the heart ensures cardiomyocyte refractoriness can vary; this ensures the cells are no longer refractory as the coupling interval between successive beats shortens, as occurs with exercise for example. This adaptive response is mediated by several processes, though the I_{Ks} current is thought to be a major determinant[56].

An allied theme is that of restitution, which describes the alteration of APD that occurs following an abrupt change in the preceding diastolic interval[57]. The slope of this relationship may be important in arrhythmogenesis[58].

Finally, the above discussion pertains to physiological repolarisation and refractoriness. The efficacy, and harmful effects, of antiarrhythmic drugs often depend upon alteration of these properties. When refractoriness of a cell or tissue is extended beyond full repolarisation, it is termed 'post-repolarisation refractoriness', a situation that may be induced with drugs[59].

To summarise what has been described above: upon receiving a propagated impulse, opening of sodium channels occurs very rapidly, initiating the action potential. The majority of these channels are then inactivated quickly, i.e. within a matter of milliseconds, preventing physiological re-activation of the cardiomyocyte which becomes refractory. In order to relieve this inactivated state, the membrane potential must be repolarised, and this is dependent on termination of calcium inflow, and potassium channels' outward currents. As such, although contributing to different parts of the action potential, sodium and potassium fluxes are inextricably linked.

1.2.4 Impulse propagation in the ventricles

The preceding discussion has focused on the action potential – the summative change in transmembrane voltage of a cardiomyocyte over time. Action potentials in the sinus nodal cells are initiative, whereas in health, those in ventricular cardiomyocytes are regenerative and involved in relay of the impulse rather than its initiation. As described previously, this change in membrane potential of a cell is passed on through low resistance channels at the intercalated disc known as gap junctions. This section will focus on the intercellular transmission that occurs within the ventricles.

Voltage decays with increasing distance from a current source when conduction is passive, as predicted by cable theory[48]. In physiology, this passive spread is known as electrotonus. Thus, if a depolarising impulse occurs (e.g. the impulse leaving a Purkinje fibre, or an external stimulus), and is of sufficient magnitude to raise E_m above threshold, sodium channel activation will occur leading to a fast inward current, and an action potential. Some of this current will pass into an adjoining cell via gap junctions, where again, provided it is of sufficient magnitude, the same will occur. However, due to the decay of voltage over distance, the impulse will not be sufficient to depolarise cells further away. In order for relay to occur therefore, when the impulse passes from one cell to its immediate neighbours through gap junctions, those neighbouring cells must initiate action potentials of their own so as to regenerate the voltage required to depolarise their neighbours without attenuation (see Figure 7).

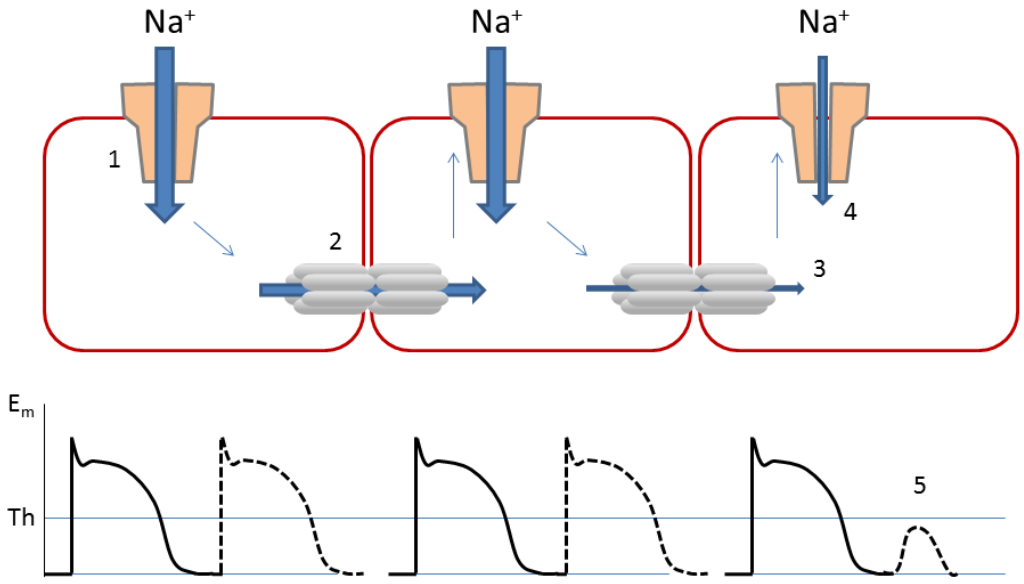

Figure 7 Activation of cardiomyocytes and impulse propagation. Cardiomyocytes (red outline) have sodium channels in the sarcolemma and gap junctions at the intercalated disc. An action potential is initiated by rapid Na^+ influx (1) which depolarises the cell membrane. Some of this charge passes through gap junctions to a neighbouring cell (2), and if this charge is of sufficient magnitude, it will regenerate an action potential through the same process of sodium influx. Only a tiny portion of the charge from the original cell on the left would pass through to the cell on the right (3) without the regenerative action potential in the middle cell. This would induce only a small Na^+ influx (4), insufficient to elevate the cell membrane potential (Em) above threshold (Th), so that a full action potential would not regenerate (5). In the lower panel, solid lines represent action potentials that have just occurred. Dashed lines show the action potentials that would be elicited following Na^+ influx in the left hand cell only. Arrows indicate the normal pattern of Na^+ influx, transfer of charge, and induction of Na^+ influx in the neighbouring cell.

At a molecular level, it can be seen from the description above that there are two key determinants of propagation, i.e. whether the impulse conducts at all, and its speed. These are sodium channel conductance, and gap junction conductance[35,36,48,60]. Both of

these in turn depend on the number of channels at the sarcolemma or intercalated disc respectively, their unitary conductance, and their state, or availability to open[61]. The importance of sodium channels in propagation is reflected in the fact that conduction velocity is directly related to the rate of rise (i.e. dV/dt of phase 0) and the amplitude of the action potential (i.e. difference in voltage between RMP and full depolarisation). Gap junctions are discussed further below.

At a multi-cellular or tissue level, it is useful to scale up the way in which propagation is considered, although the underlying determinants remain the same. Thus, the concepts of source and sink, and safety factor are useful at this level, and tissue geometry or architecture become more important. Early modelling considered impulse propagation to occur along a one-dimensional (1D) array of cardiomyocytes. This was a physiological extrapolation of the principles of cable theory, which had been developed to understand electrical transmission along telegraph cables. Using this approach, the concept of liminal length was developed, which describes the minimal length of a cellular array that must be activated if propagation is to occur[48,60]. The idea of a critical mass of cells required to excite cells downstream remains useful, but the inadequacies of a 1D model of cardiac tissue are immediately apparent. A generalisation applicable to 3D tissue structures utilises the concept of 'source' and 'sink'. The former describes the cell or cells which have been depolarised, and are able to transfer current to neighbouring cells so that they can be depolarised. The latter describes the neighbouring, hyperpolarised cells, which 'accept' current from the source[62]. Taking this further, 'safety factor' is defined as the ratio of the current generated by the source to that consumed during excitation of the sink. A safety factor of more than one ensures impulse propagation, whereas conduction failure will occur if less than one. In addition to sodium channel and gap junction conductance, tissue architecture is relevant here. If cardiomyocyte density is reduced, by fibroblasts in scarred tissue for example, the source:sink ratio will fall, resulting in reduced conduction velocity or failure of propagation.

Gap junctions

These intercellular connection channels have already been mentioned. Their existence was predicted *a priori* based on theoretical assumptions regarding current transmission and voltage decay[63]. Structurally they can be broken down as follows: six connexin proteins oligomerise to form a hemichannel known as a connexon, which

resides in the cell membrane. When two connexons in adjoining cells appose each other, they form a gap junction[64]. There are 21 human connexin genes, and they are expressed in most tissues, albeit with tissue specificity of proteins. When connexons are composed of different connexins they are known as heteromeric, and heterotypic gap junctions are those where the connexons are different[61]. Connexins 43, 40 and 45 are expressed in the heart, although connexin43 (Cx43) is predominant, and in the ventricles is essentially the only isoform expressed[65]. In the atria, Cx40 and Cx43 are expressed, while Cx40 is the major isoform in the ventricular conduction system. Cx45 is primarily expressed in the sinus and AV nodes[66]. They are permeable not only to ions (particularly K^+), but also to second messengers such as cyclic adenosine monophosphate (cAMP), and possibly small interfering RNAs (siRNAs). Expression, trafficking and turnover affect the number of connexins and hence gap junctions present at the intercalated disc. But in a similar way to membrane-bound ion channels, gap junctions exhibit several conductance states. This property of gating appears to be more dependent on transjunctional than transmembrane voltage, though both may have a role. The other two key regulators are pH and intracellular calcium concentration ($[Ca^{2+}]_i$)[61,67].

There is some debate as to the relationship between gap junction conductance and conduction velocity through the myocardium. Modelling has suggested that cell-to-cell electrical uncoupling, i.e. via reduction in gap junction conductance, will lead to reductions in conduction velocity, but that propagation will persist at very low velocities until near complete uncoupling has occurred[68]. Based on theoretical and experimental data, others have suggested a positive, non-linear relationship between the number of gap junctions at the intercalated disc and conduction velocity[67]. A view that has gained widespread acceptance is that near complete loss of Cx43 expression must occur before conduction velocity declines. This came from studies in Cx43 knockout mice, which found that conduction velocity was unaltered in heterozygotes with Cx43 expression at 50% of normal levels, whereas it diminished when reduced by more than 95% [69,70]. However, this notion has been challenged recently by Dhillon et al, who suggest there is in fact a continuous, linear relationship between conduction velocity and gap junction conductance[71].

Estimates of conduction velocity

Measurement of conduction velocity through the myocardium is more difficult than might at first be assumed. It is complicated by a number of factors: first and foremost, these include the need to define the activation of small, localised clusters of cardiomyocytes throughout the tissue. It must be possible to spatially locate these clusters with accuracy, as well as to temporally define their activation precisely. Finally, an estimate of the path of impulse propagation is required. With regard to defining activation, the intracellular techniques that offer precision with *in vitro* work are not feasible *in vivo*, and extracellular analogues utilising surrogate markers must be used. For the latter, it is possible to conceptualise a path of propagation in a two-dimensional (2D) piece of tissue, although even here the word path is probably inappropriate. In the intact heart, which is not only a 3D structure at the chamber level, but also within the myocardial walls, impulses neither emanate from a single point source, nor do they proceed linearly. The spread of excitation is akin to a wavefront, which must adjust to the contours and limits of the myocardium and to other interacting wavefronts.

Coupled with these factors are the intrinsic differences in speed of conduction between subpopulations of cells within the heart, e.g. atrial versus ventricular myocytes, or Purkinje fibres versus AV nodal cells. Also, the inherent property whereby conduction is faster along the longitudinal axis of cardiomyocytes rather than their transverse axis. This directional dependence is known as anisotropy, and is related to cellular structure, connectivity and gap junction localisation[60,72]. Cardiomyocytes are cylindrical rods and have a length:width ratio of over five. It is generally assumed that most propagation delay occurs at gap junctions rather than within the cardiomyocyte. Ventricular myocytes are typically connected to around 10 other myocytes, whereas this number is smaller in the atria. Finally, there is some evidence that gap junctions are clustered more at the cell ends than along their length[60,61]. Together these factors indicate a preference for passage of current in the longitudinal as opposed to the transverse direction throughout the tissue. They also explain differences in the anisotropy ratio of the atria compared to the ventricles for example (i.e. longitudinal to transverse conduction velocity ratio).

A couple of other factors deserving mention are the health of the tissue, and the stimulation parameters, where an external stimulus is used. Scarred or damaged tissue, either *in vivo* following myocardial infarction for example, or *ex vivo* following traumatic tissue harvest, will display abnormal conduction properties. And tissue can

be stimulated in various ways and to various levels, but briefly, the size of the electrode, whether a point source or linear electrode is used, and the amplitude of the stimulus, are all relevant to subsequent measurements on impulse propagation. Experimental estimates vary, but in ventricular tissue have been found to be in the region of 50 cm s^{-1}, whilst in the His-Purkinje system approximately 2 m/s[60,73] (see also *Chapter 8*).

Murine cardiac conduction

Anatomically, the main components of the conduction system are similar in mice to humans[27,74,75]. Mice also show a similar expression pattern of connexins, but in addition express murine connexin30.2 (mCx30.2) primarily in the sinus and AV nodes. The human orthologue, Cx31.9, does not appear to be so important[73]. That these connexins are important in the mouse heart is illustrated by the phenotypes of knockouts. $Cx43^{-/-}$ mice for example, survive to term, but die shortly after from right ventricular outflow obstruction, suggesting this protein also has a developmental role[76]. Conduction velocities obtained with murine hearts or tissue are similar to those reported in humans[69,74].

1.3 Cell signalling

The study of intracellular signalling relates to the cascades linking a stimulus or initiator, to a relay or effector, and the subsequent cellular response. A large number of these pathways exist, serving diverse physiological processes. Broadly they can be divided into those pathways responding to stimuli arriving at the cell membrane, and those arising within the cell[77]. Neurotransmitters, hormones and growth factors interact with cell membrane receptors, resulting in activation of the latter, and initiation of signalling pathways. In this way, the behaviour of cells or tissues of one organ can be modified by other organs.

Some of the features that make this branch of physiology particularly complex are: cross-talk between pathways, multiple isoforms of receptors or enzymes due to slight differences in sequence homology, and redundancy, in part resulting from this, but also from pathway interactions. Indeed, the fact that separate pathways can converge on an

effector, or that a receptor or downstream signalling molecule can exert disparate (even paradoxical) effects (e.g. β2-adrenoceptor (β2AR), M2-Acetylcholine (M2-mACh) receptor[78]), as well as the presence of autoregulatory feedback, makes attempts to understand these systems especially challenging. To add to this, the structural similarities of receptors/enzymes of the same class often make quantification and functional assays difficult. Despite these difficulties however, huge amounts of progress have been made in this field over the last few decades, and development of novel therapeutics is reliant on the insights gleaned.

Although many messenger molecules exist, one of particular importance, both generally, and in relation to subsequent discussion here, is cyclic adenosine monophosphate (cAMP). This prototypical 'second messenger' was identified by Earl Sutherland and colleagues in the late 1950s[79]. It serves to regulate cellular responses in tissues as varied as brain, the adrenal glands, skeletal and cardiac muscle, lung, kidney and liver[77]. It is generated by the enzyme adenylyl cylase (AC) through a sequence of interactions that begin with a hormone or neurotransmitter typically.

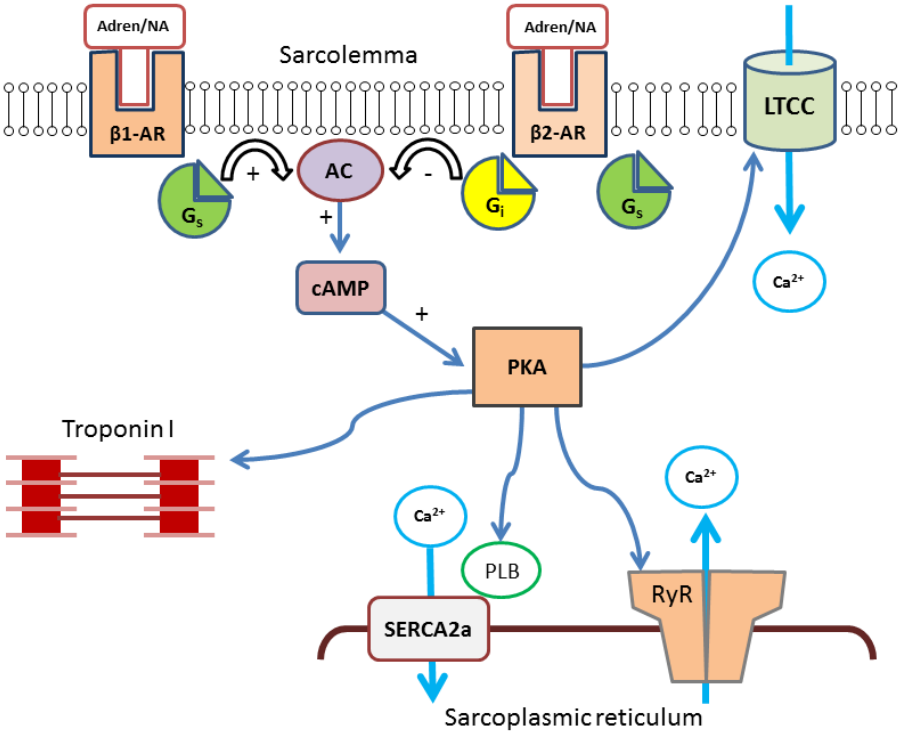

Figure 8 G protein and cAMP signalling in the heart. Modified from Lee et al[80]. Adren/NA: (nor)adrenaline, Gs: stimulatory G protein, Gi: inhibitory G protein, AC: adenylyl cyclase, LTCC: L-type Ca^{2+} channel, cAMP: cyclic adenosine monophosphate, PKA: protein kinase A, PLB: phospholamban, SERCA2a: sarco/endoplasmic reticulum calcium ATPase, RyR: ryanodine receptor.

Upon binding to a special class of cell membrane-bound receptor known as G-protein coupled receptors (GPCRs, see below), heterotrimeric G-proteins are activated which in turn regulate AC (see Figure 8). It is worth noting that AC is not in fact one molecule, but a family of isoforms, the majority of which are membrane-bound.
As can be seen in Figure 8, cAMP exerts most of its effects through protein kinase A (PKA), though other targets include the exchange proteins activated by cAMP (EPACs). Its action is terminated through either hydrolysis by phosphodiesterases, or efflux from the cell[80].

1.3.1 G-protein coupled receptors (GPCRs)

GPCRs constitute the largest superfamily of cell membrane receptors, numbering approximately 800[78,81], the other two types being ion channel-linked, and enzyme-linked receptors. Within this superfamily, there are five subfamilies: glutamate, rhodopsin, adhesion, frizzled/taste2, and secretin[82]. They respond to stimuli as diverse as hormones, neurotransmitters, light, tastes and amino acids, and collectively represent major targets for drug action.
Structurally GPCRs are all similar, sharing a seven transmembrane domain structure. More precisely, there are seven alpha-helical domains, three interhelical loops either side of the membrane, an extracellular N-terminus and an intracellular C-terminus[81]. The second and third intracellular loops and the C-terminal tail are important for interaction with their intracellular messengers, the heterotrimeric G proteins (termed 'G proteins' from hereon in).
In terms of activation, agonist binding induces a conformational change in cytoplasmic domains allowing interaction with G-proteins. However, these receptors do not necessarily require an agonist; some show constitutive activity. Once activated, the receptor functions as a guanine exchange factor (GEF), exchanging guanosine diphosphate (GDP) for triphosphate (GTP) on the G protein α subunit, thereby activating the G protein. It is noteworthy that different agonists bound to the same receptor can stimulate distinct signalling pathways, a phenomenon termed 'ligand-directed signalling'.
With regard to how GPCRs and G proteins come to be in the proximity required for interaction, there are two models: 'collision-coupling' holds that G proteins can only interact with activated receptors, whereas 'pre-coupling' describes a model where the G protein is able to interact with a receptor prior to agonist binding[81]. Receptors show

preference for specific G protein isoforms; however, this does not preclude interaction with more than one G protein (see *Section 1.8*).
Deactivation is brought about by receptor phosphorylation by protein kinase A (PKA) or C (PKC), or by GPCR kinases (GRKs), which results in uncoupling from G proteins[83]. GRK phosphorylation leads to binding of arrestins, resulting in internalisation[77,78]. The GPCR may then either be dephosphorylated and returned to the membrane, or trafficked to lysosomes for degradation.
Within the cardiovascular system, important examples of GPCRs include the α1- and β-adrenoceptors, the A_{2A}-adenosine, M2-muscarinic (mACh), angiotensin II AT1, and endothelin-1 ET_A receptors.

1.3.2 Heterotrimeric G proteins

These extrinsic membrane proteins are molecular mediators in the pathway from stimulus to cellular response. They comprise alpha, beta and gamma subunits, which in the inactive state combine to form a trimer. In the active state, the beta and gamma subunits separate as a dimer from the alpha subunit, and both these components have roles in signalling. There are 21 known alpha, 6 beta, and 12 gamma subunits[81], and these exist in various combinations, both in terms of the beta-gamma dimer, and its association with an alpha subunit. Not all possible combinations have been shown to occur however.

Heterotrimers are divided into four classes based on the alpha subunit sequence: Gs, Gi, Gq and G12. Those in the Gi class (sometimes written Gi/o) are known as 'inhibitory' G proteins, due to their effect on adenylyl cyclase, and include Gi_1, Gi_2, Gi_3, Go_1 and Go_2. Activity of all these isoforms is inhibited by pertussis toxin, and they are sometimes referred to as 'pertussis toxin sensitive' G proteins.
Sites of contact with GPCRs are unsurprisingly important in determining coupling specificity to the receptors. Important sites on the G protein are thought to be the C terminal helix and certain adjacent loops of the Gα subunit, as well as the C-terminal of the Gγ subunit[83]. In the inactive trimeric state, the α subunit is bound to GDP. As already described, GPCRs facilitate exchange of this for GTP, thereby activating the G protein, inducing a conformational change and leading to separation of the α subunit from the βγ dimer[77].

Both the α and βγ components can function as signal transducers, acting on a variety of downstream targets (see also below). Interestingly, despite separation on activation, it has been shown that with neuronal GIRK channels the α subunit is required to act as a kind of chaperone or co-factor in determining receptor specificity for the channel[84].
G protein signalling may continue until GTP is hydrolysed to GDP, allowing the heterotrimer to reform, thus completing the G protein cycle (see Figure 9).

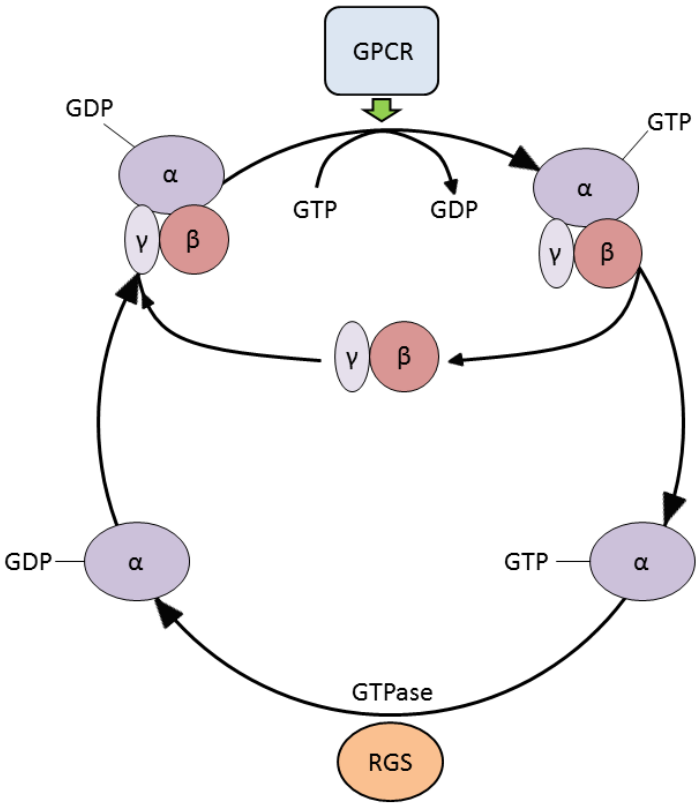

Figure 9 The G protein cycle, modified from Milligan et al[85]. GPCR: G protein coupled receptor, GTP: guanosine triphosphate, GDP: guanosine diphosphate, GTPase: GTP hydrolase, RGS: regulator of G protein signalling.

This hydrolysis may result from intrinsic hydrolase activity of the α subunit, or be catalysed by regulators of G protein signalling (RGS).
In the cardiovascular system, Gi proteins have been shown to transduce signals from the M2 mACh receptor to G protein-regulated inwardly rectifying K^+ (GIRK) channels, and it has been shown that the βγ dimer is key here[86,87], although the α subunit has a co-factor role similar to that described above. α subunits from each of the four classes are expressed within the cardiovascular system as a whole, i.e. heart and vasculature, but in the human heart it is members of the Gi and Gs classes which are most important (see below and *Section 1.8*).

1.3.3 Regulators of G protein signalling

The rate of GTP hydrolysis by the G protein α subunit can be accelerated by a group of proteins known as regulators of G protein signalling (RGS), of which there are about 20 members[88]. Within the heart and vascular system, a number of these have been shown to be expressed: RGS2, 3, 4, 5, 6, 9 11, 19 and p115RhoGEF. Of these, RGS2 seems to be important in regulating vascular tone. Levels of RGS2, 3 and 4 have been shown to be altered in cardiac hypertrophy and heart failure, possibly implicating them in the pathophysiology, although results have not all been consistent[78].

1.3.4 G alpha i2

This is the predominant cardiac Gi isoform, at least in the mouse[89], and is of particular interest in cardiac physiology, due to its participation in the signalling pathways linking M2-mACh receptors to GIRK channels, and possibly β-adrenoceptors (βARs) to the L-type calcium channel (LTCC), Cav1.2[90–96] (see Figure 10). Cardiac GIRK channels, heterotetramers of Kir3.1 and 3.4 proteins, are expressed in the atria and conduction system tissue, whereas LTCCs are expressed throughout the heart, and of importance in arrhythmias originating in both atria and ventricles[97].

By the late 1980s, it was known that G proteins mediated the link between βARs and cAMP production by adenylyl cyclase. It had also been shown that β1ARs are downregulated in heart failure (see *Section 1.8.2*), yet this did not appear to account for all the observed reduction in cAMP seen. As such, it was hypothesised that alterations in G protein expression may explain some of the differences in cAMP levels, and therefore contractile function in failing hearts[98].

In 1988, two groups reported increased expression of Gi proteins in myocardial tissue from patients with heart failure[98,99]. In 1990, Böhm et al noted increased expression of Gi α subunits in dilated, but not ischaemic cardiomyopathy[100], and in 1992, Eschenhagen et al showed increased messenger RNA (mRNA) expression of $G\alpha_{i2}$ in patients with both dilated and ischaemic cardiomyopathy, whereas $G\alpha_s$ and $G\alpha_{i3}$ levels were unaltered compared to controls[101]; findings that were recapitulated in rats[102].

The reasons for altered expression of $G\alpha_{i2}$ were unclear: was it related to compensatory hypercontractility in viable segments of the heart, or was it somehow related to the neurohumoural response to LV impairment and its consequent elevation

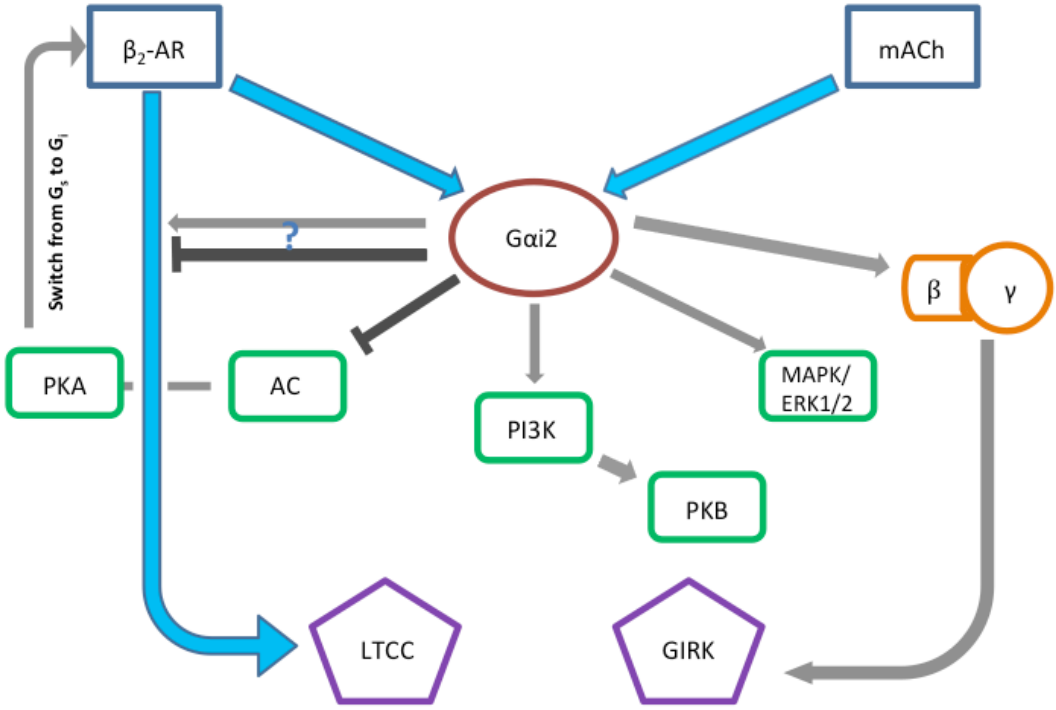

Figure 10 The signalling pathways in the heart for which there is most evidence of $G\alpha_{i2}$'s involvement. The diagram is structured hierarchically, such that receptors are in rectangles at the top, signalling enzymes downstream of $G\alpha_{i2}$ are in rounded rectangles/diamonds below it, and ion channels are in pentagons at the bottom. AR: adrenoceptor, mACh: muscarinic acetylcholine receptor, PKA: protein kinase A, AC: adenylyl cyclase, PI3K: phosphoinositide 3-kinase, MAPK: mitogen-activated protein kinase, ERK: extracellular signal-related kinase, Akt/PKB: protein kinase B, LTCC: L-type calcium channel, GIRK: G protein regulated inwardly-rectifying potassium channel.

of LV diastolic and pulmonary venous pressures? If the latter, was it through a direct hormonal effect on the myocardium, or a signalling cascade initiated by elevated pressures, and resulting in upregulation of $G\alpha_{i2}$ production? The possible effects were equally unclear: was this change a beneficial, adaptive response of the heart, or was it maladaptive?

Various lines of evidence support the possibility of an antiarrhythmic role for $G\alpha_{i2}$. Lerman et al found a somatic mutation in the *GNAI2* gene (which encodes the $G\alpha_{i2}$ protein) in a patient with ventricular tachycardia originating in the right ventricular outflow tract. The mutation was localised to the arrhythmogenic focus, led to increases in cellular cAMP, and rendered the arrhythmia resistant to adenosine-mediated suppression[103]. Na^+/Ca^{2+} exchange currents, believed to be a contributor to early and delayed afterdepolarisations (EADs and DADs, as described in *Section 1.5*), may be stimulated by βAR activation. Zhang et al showed that adenosine can antagonise this

effect via inhibitory G proteins[104]. In a similar vein, Grimm et al used pertussis toxin to inactivate $G\alpha_i$ subunits and observed the effects on right atrial and papillary muscle tissue from rats, stimulated with the non-selective βAR agonist isoprenaline. This resulted in increased arrhythmogenic effects of βAR stimulation[105]. Utilising a cross of two transgenic mouse lines, Foerster et al investigated the effects of human β2AR overexpression in mice deficient in $G\alpha_{i2}$[96]. Their results suggested that $G\alpha_{i2}$ exerts a protective role in this setting in terms of wall hypertrophy and cardiac failure. Interestingly, analysis of Ca^{2+} currents from the LTCC following pertussis toxin administration raised the possibility that $G\alpha_{i3}$ rather than $G\alpha_{i2}$ is one of the key regulators of this channel in contrast to the findings of Zuberi et al[94]. However, the situation is complicated further by the fact that although both $G\alpha_{i2}$ and $G\alpha_{i3}$ may couple to the β2AR, $G\alpha_{i2}$ coupled to the mACh receptor is able to negatively regulate the LTCC[106,107].

Previous work using mice with globally-deleted $G\alpha_{i2}$ showed that compared to controls, they exhibited a faster resting heart rate, and autonomic tone assessment using heart rate variability (HRV) suggested parasympathetic withdrawal[108]. Subsequently, they were shown to experience more spontaneous ventricular ectopy (premature beats originating in the ventricles), manifest action potential prolongation, were more prone to inducible ventricular arrhythmias, and had increased expression of LTCCs, with increased Ca^{2+} currents using patch-clamp[94]. Taken together with previous studies[92,96,106], these results therefore indicate there is some divergence of opinion as to whether $G\alpha_{i2}$ signalling enhances, restricts or has no effect on βAR-induced LTCC activity.

1.4 The autonomic nervous system control of ventricular function

The autonomic nervous system (ANS) comprises the sympathetic nervous system (SNS) and parasympathetic nervous system (PNS). Traditionally, these two limbs have been considered both anatomically and physiologically distinct, exerting opposing effects on the heart and other organs. Whereas the SNS is associated with excitability and a heightened sense of arousal, the PNS is associated with relaxation and calmness. Both branches convey afferent and efferent fibres, and it is likely that both are implicated in propensity to, and triggering of arrhythmias in different disease states of

the heart. There is increasing recognition however of a degree of anatomical co-localisation even in the vagus nerve, and of functional integration[109,110].

The ANS supply of the heart can be divided anatomically into extrinsic and intrinsic components. The former refers to neurons connecting the brain or spinal cord to the heart, located outside the pericardial sac. For the SNS this consists of the neurons connecting the cervical and thoracic spinal cord to their localised autonomic ganglia – the superior cervical, cervicothoracic (stellate), and thoracic ganglia – and the postganglionic fibres whose cell bodies originate in these. Of these, the stellate ganglia are most important for the heart[111]. In addition, the SNS is usually considered to include circulating catecholamines released from the adrenal medulla. The PNS on the other hand, has origins in the nucleus ambiguus of the medulla oblongata. Its preganglionic fibres travel predominantly in the right and left branches of the vagus nerve, which subdivide near the heart[112,113].

The intrinsic cardiac nervous system is comprised of autonomic nerve fibres within the pericardial sac and sympathetic and parasympathetic divisions are anatomically and physiologically less distinct. Fibres from the extrinsic SNS and PNS converge at numerous ganglia on the epicardial surface of the heart, most of which are organised into ganglionated plexi (GPs). These GPs appear to be situated in defined regions of the

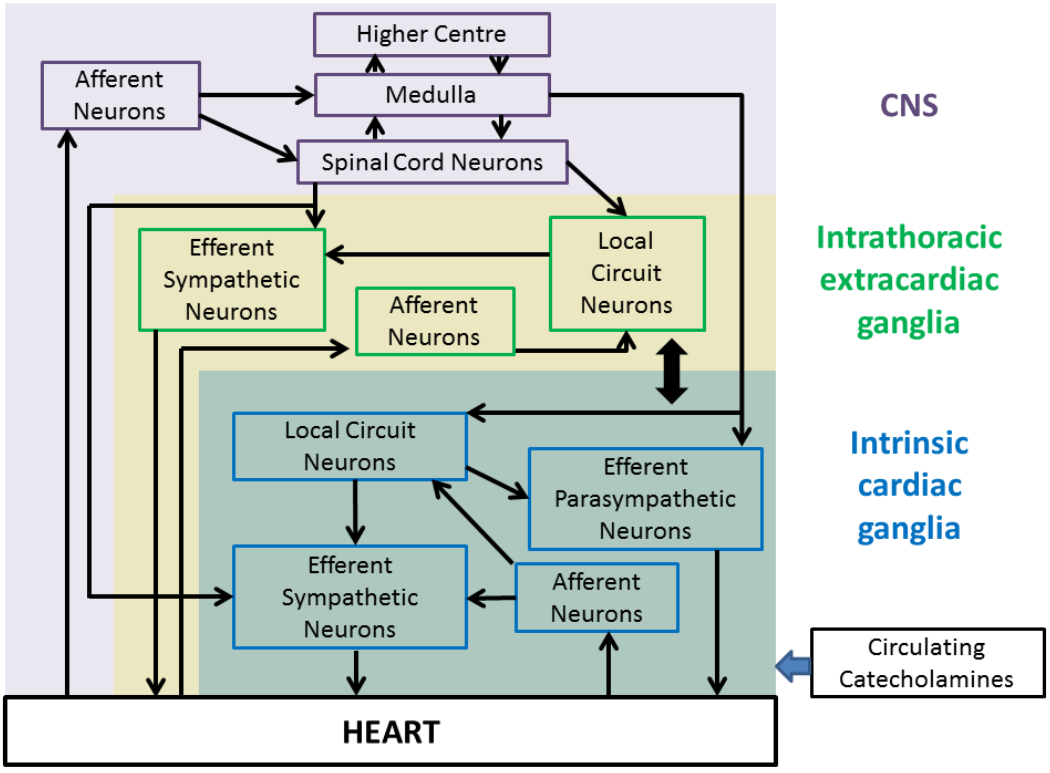

Figure 11 Anatomical and functional relationships of the autonomic nervous system. CNS: central nervous system. After Armour[119].

atria and ventricles, and are concentrated in fat pads on the epicardium[114]. They are interconnected, and their function appears to be to integrate the signals from each limb of the ANS and other GPs, before communicating the output to different regions of the heart such as the sinus and AV nodes[115] (see Figure 11).

The orthodoxy that there is little or no parasympathetic innervation in the ventricles is increasingly challenged[116,117]. In fact, it is surprising that this view has held sway for so long given results from over 150 years ago indicating the ability of vagal input to modify arrhythmogenicity[118] (see below).

The discussion above has focused on subcortical neurons; there is however interest in the modulation exerted by higher centres within the brain on these pathways, and the role of such modulation in arrhythmogenesis[120,121]. That these are important is exemplified most convincingly by ECG changes that occur following intracranial events such as subarachnoid haemorrhage, and the reported association of sudden death with mental stress[121].

1.4.1 Receptors and signal transduction

At a molecular level, the SNS communicates with cardiomyocytes via adrenergic receptors/adrenoceptors (ARs), whilst the PNS communicates primarily via muscarinic acetylcholine (ACh) receptors (mAChRs). α-adrenoceptors can be subdivided into α1 and α2, of which the latter is barely expressed, if at all, in the human heart. α1-ARs comprise three subtypes: α_1A, α_1B, and α_1D, all of which are expressed in the heart, though it is α_1A and α_1B which predominate in the working myocardium[122,123]. Most species show fairly similar levels of expression of α1-ARs, except for rats which show markedly higher levels, and a relative abundance of the α_1B subtype - an important consideration in dose-response experiments and heart failure models[122]. Cell membrane-bound α1-ARs signal through the pertussis toxin (PTX) insensitive Gq class of G proteins, which in turn activate the phospholipase C (PLC) β1 – inositol trisphosphate (IP3) – PKC pathway, amongst others. There is also some evidence for nuclear localisation of these receptors[123]. α1-AR stimulation exerts inotropic effects, though these appear to be less marked than with βAR stimulation. Perhaps neglected somewhat due to their relative lack of expression, there is nevertheless interest in the role of α1-ARs in myocardial adaptation, for example in heart failure, and in cardioprotection[123].

Beta-adrenoceptors (βARs) are situated in the sarcolemma and constitute approximately 90% of the total ARs in the heart. There are three subtypes - β1-3 - although in mammalian hearts, β1 and β2 are by far the most abundant, and of greatest importance[124].

In normal human hearts, the ratio of β1: β2 ARs is approximately 75:25 in the ventricle, with a slightly lower proportion of β1ARs in the atria[122]. With regard to signal transduction, β1ARs signal exclusively through the stimulatory G-protein, Gs, whereas β2ARs are able to signal through both Gs and Gi, the inhibitory counterpart[125,126] (see Figure 8 in *Section 1.3*). Of the Gi isoforms, there is evidence to support $G\alpha_{i2}$'s coupling to the β2AR, though $G\alpha_{i3}$ may also be an important mediator, particularly with regard to regulation of the LTCC[94,96].

Murine knockout models suggest that of β1 and β2, the former is the predominant driver of heart rate and contractility, although human studies suggest that β2 does have modest inotropic effects[127]. Differences are somewhat difficult to tease out due to the shared Gs signalling pathway. At a molecular level, the βAR/Gs – AC - cAMP – PKA signalling cascade increases phosphorylation of LTCCs, phospholamban, troponins and the ryanodine receptor (RyR), actions which enhance inotropy and lusitropy[77,124,127]. In humans, the two main repolarising potassium currents, I_{Kr} and I_{Ks}, are also regulated through this cascade, as is the pacemaker current, I_f, which is in fact directly sensitive to cAMP[38]. As noted earlier, I_{Kr} and I_{Ks} are not present in the mouse, and the main repolarising currents in this species, and their modulation by βAR agonism, are less well-studied.

Efferent parasympathetic neural activity from the vagus nerves releases ACh. Of the five mAChR subtypes, the predominant one in mammalian hearts is the M_2 receptor. Unlike the M_1, M_3 and M_5 receptors, which typically couple to Gq/PLC, the M_2 receptor preferentially interacts with Gi[122]. The main effects of ACh signalling differ slightly between atria and ventricles. In both sets of chambers, Gi activation leads to AC inhibition, reducing cAMP and downstream PKA signalling effects. Consequent reduction of LTCC currents, amongst other things, results in reduced inotropy. In the atria, additional electrophysiological effects occur as a result of lower levels of cAMP and GIRK channel activation (see also *Section 1.3*). The former through direct effects on I_f in the sinus node, reduces heart rate, whereas the latter induces K^+ outflow, with resultant hyperpolarisation and APD abbreviation[38,128] (see Figure 12). In contrast with the atria where the PNS can directly lead to reduced chronotropy and inotropy,

the ventricles appear to require pre-existing sympathetic activity in order for the PNS to elicit the same effects[122,129].

These differences between chambers including the restriction of GIRK expression largely to the atria, coupled with the evidence supporting the anti-arrhythmic effects of PNS signalling in the ventricles[118,130,131], suggest the possibility of other intrinsic ANS neurotransmitters and anti-arrhythmic mediators[111]. Experiments suggest that nitric oxide (NO) may be one such mediator, effecting changes in the ventricular fibrillation (VF) threshold and APD restitution slope. Additionally, it appears that this may operate independently of vagal nerve ACh signalling[117].

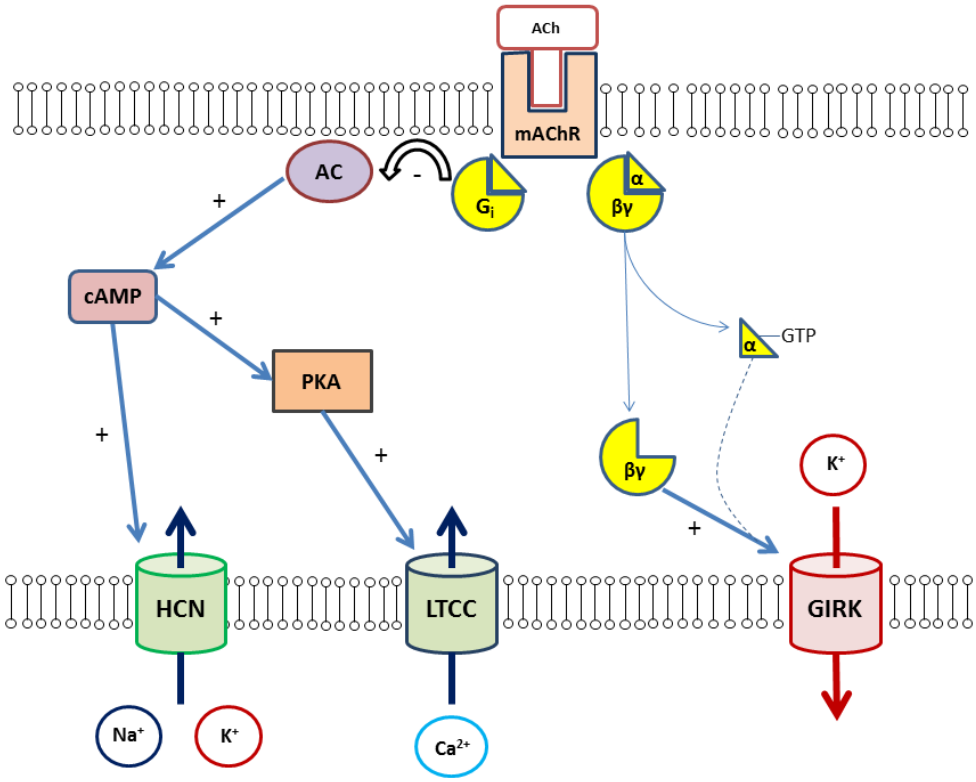

Figure 12 Key signalling pathways and ion channels modulated by mACh receptor agonism. ACh – acetylcholine; mAChR – mACh receptor; AC: adenylyl cyclase; cAMP – cyclic adenosine monophosphate; PKA – protein kinase A; HCN – hyperpolarisation-activated cyclic nucleotide gated channel; LTCC – L-type calcium channel; GIRK – G protein regulated inwardly rectifying potassium channel.

1.4.2 Assessment of the ANS: methods of measurement

In humans, cardiac sympathetic and parasympathetic activity can only be studied indirectly at present. Several measurement techniques and indices have been developed to this end[132]. They are all based on analysis of variations in the beat to beat

interval of the heart. Of these, probably the two best-studied are heart rate variability (HRV) and baroreflex sensitivity (BRS).

HRV is the term used to describe the quantification of the normal oscillation in the beat to beat interval of the heart (the R-R interval from the ECG). During normal sinus rhythm, heart rate is governed by the spontaneous discharge of the sinus node. The sinus node however, is under the influence of the SNS and PNS, and these opposing influences lead to fluctuations in its rate of discharge. HRV analysis utilises the ECG to quantify this variability and is a non-invasive means of making inferences about the relative contributions of the sympathetic and parasympathetic arms of the autonomic nervous inputs to the heart. The technique developed from research into foetal distress in the 1960s [133]. Its applicability to cardiac disease was obvious, and in the 1980s and '90s, much work was performed utilising the technique. Time domain measures are the simplest, and in general are indices reflecting variation in R-R interval, such as standard deviation. Frequency domain measures can be performed using shorter recordings, but are more complex: they require conversion of the R-R interval data into a power spectral density via a transform. This power spectrum is then divided into three frequency bands: very low frequency (VLF), low frequency (LF), and high frequency (HF). It has been determined that the HF component is governed to a large extent by the heart's parasympathetic input, whereas the LF component reflects both sympathetic and parasympathetic inputs. The origin of the VLF component is uncertain[134].

BRS refers to the adjustment of heart rate that occurs in response to changes in blood pressure (BP), and is a reflection of the feedback and co-regulation of both limbs of the ANS, though is predominantly regarded as an index of vagal efferent activity[135,136]. Measurement commonly involves administration of a bolus of an α-AR agonist to increase BP. Aortic and carotid baroreceptors convey afferent information via cranial nerves nine and ten to the medulla, resulting in the arterial baroreflex, whereby increased parasympathetic output results in a reduction in heart rate[137]. BP and heart rate are measured simultaneously, and the change in each parameter is plotted. The slope of the line is determined, i.e. change in R-R interval (ms) per change in unit blood pressure (mmHg). This technique was shown to have prognostic value in the ATRAMI trial[138].

1.4.3 The ANS in the pathophysiology of arrhythmias

There is abundant, albeit largely circumstantial evidence that the ANS is implicated in the pathophysiology of a range of arrhythmias and inherited arrhythmia syndromes. From experiments performed over 100 years ago demonstrating the protection afforded by vagal stimulation against VF, to studies showing the prognostic value of HRV and BRS, and the efficacy of reduction in SNS activity, either through pharmacological blockade or neural ablation.

Reduced HRV has been shown to be a poor prognostic marker in heart failure. In the UK-Heart study, reduced SDNN (standard deviation of N-N intervals) was found to be a significant predictor of all-cause mortality in patients with chronic heart failure, and the strongest predictor of death due to progressive heart failure[139]. However, not all studies have shown utility in risk stratification[132,140]. And it is interesting to note that HRV has not been shown to be directly linked to arrhythmic death (though see below). Eckberg et al showed reduced parasympathetic activity in patients with heart failure compared to normal subjects. Elevation of heart rate following PNS blockade with atropine was less marked in patients, and BRS was reduced[135]. In the ATRAMI trial involving 1284 post-MI patients BRS was shown to have prognostic value independent of HRV and left ventricular (LV) ejection fraction (EF)[138]. Though these do not provide direct evidence of a role in arrhythmogenesis, arrhythmias are the commonest cause of death in patients with heart failure, and account for much of the morbidity associated with this condition.

More direct evidence comes from both animal and human studies. In a canine study involving simultaneous recordings of left stellate ganglion activity and ambulatory ECGs in dogs surviving myocardial infarction (MI), Zhou et al showed that increased stellate activity tended to precede onset of ventricular arrhythmias[141]. Consistent with these findings, Schwartz et al found that left cardiac sympathetic denervation was effective in reducing sudden death amongst survivors of myocardial infarction complicated by ventricular arrhythmias[142]. A randomised trial of bilateral cardiac sympathetic denervation in patients with ICDs who experience VAs is planned[143].

In Brugada Syndrome, it is possibly the PNS that appears to have more of a role in arrhythmia induction, or perhaps a relative lack of sympathetic activity. An analysis of the temporal distributions of VF in patients with this syndrome found a higher incidence between midnight and 06:00[144]. And Miyazaki et al were able to exacerbate the ST elevation seen on the ECG with muscarinic agonists, whereas isoprenaline reduced this[145]; the latter is suggested as a possible therapy in such patients who

experience recurrent VAs in rapid succession ('electrical storm')[146]. In the LQTS, there is a correlation between genotype and triggers for cardiac events, with LQT1 genotype associated with exercise in particular, and LQT3 with sleep or rest[147]. Beta-blockers form the mainstay of management in this condition.

Finally, although designed with heart failure rather than arrhythmias in mind, vagal nerve stimulation is currently under investigation. Results of the NECTAR-HF trial failed to show any benefit in the primary or secondary endpoint measures[148]; a further trial, INOVATE-HF is underway[149].

1.5 Arrhythmia mechanisms

Understanding of the mechanisms underlying arrhythmias continues to evolve. Traditionally, at a cellular and tissue level these have been divided into disorders of impulse formation, disorders of conduction/propagation, or a combination of both[32]. With regards to tachyarrhythmias, the three most common mechanisms are triggered activity, abnormal automaticity, and re-entry. The first two can be considered disorders of impulse formation, whereas re-entry is a disorder of conduction/propagation. Without further explanation, it could be understood that each of these three mechanisms is equally capable of both initiating and sustaining an arrhythmia. However, this is unlikely: triggered activity is, as the name suggests, more often an arrhythmic trigger than a sustaining mechanism. Re-entry in its various forms, is the most common sustaining mechanism, but requires a trigger or at least a change in the myocardial substrate to allow its initiation.

1.5.1 Triggered activity

Triggered activity may take the form of either EADs or DADs (Figure 13). EADs usually occur with delayed repolarisation, which can cause 'repolarisation instability', rendering cells more susceptible to premature depolarisation[150]. The postulated mechanisms relate either to arrest of repolarisation due to diminished outward K^+ currents, or abnormal Ca^{2+} influx, either through L-type calcium channels or the Na^+/Ca^{2+} exchange pump[150,151]. They are most well-described as triggers for torsade de pointes, in the setting of LQTS.

DADs occur during phase 4, following completion of repolarisation. They result from release of Ca^{2+} from the sarcoplasmic reticulum, which raises intracellular Ca^{2+} concentration ($[Ca^{2+}]_i$). The Na^+/Ca^{2+} exchanger extrudes this, with resultant import of Na^+ which causes premature depolarisation[150,152]. They may occur with digitalis, in the context of arrhythmias associated with myocardial infarction, or some right ventricular outflow tract tachycardias.

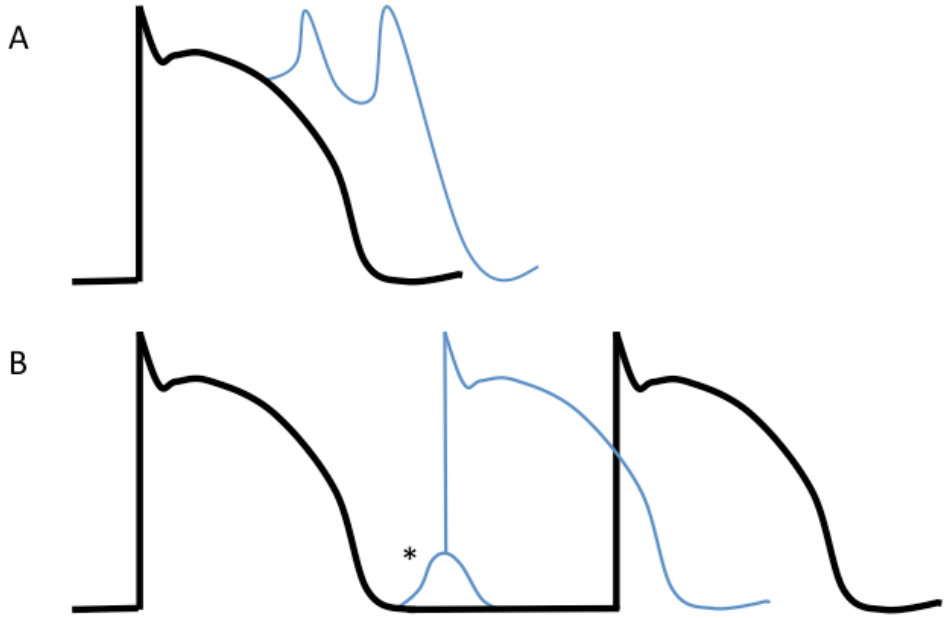

Figure 13 Afterdepolarisations. A: Early afterdepolarisations (EADs) occur during phase 2 or 3 of the action potential (shown in blue). B: Delayed afterdepolarisations (DADs) occur following completion of repolarisation, in phase 4. If of sufficient magnitude to depolarise the cell to the activation threshold (*), a premature action potential is initiated (shown in blue).

1.5.2 Disorders of automaticity

Disorders of automaticity are divided into those of enhanced normal, and abnormal automaticity. The former occurs in cells with intrinsic pacemaker function, such as the sinus node or subsidiary regions in the atria or AV node. Alterations in the maximum diastolic potential, threshold potential, or phase 4 depolarisation slope underlie changes in the frequency of action potential generation, and the resultant arrhythmia. Inappropriate sinus tachycardia is an example of enhanced normal automaticity.

In tissue without intrinsic pacemaker capacity, abnormal automaticity may result if cells become partially depolarised from their normal phase 4 transmembrane voltage. In such pathological states, this can enable these cells to spontaneously depolarise repetitively[36]. This may occur in atrial tachycardia or accelerated idioventricular rhythm for example.

1.5.3 Re-entry

Re-entry refers to a circus movement of wavefront propagation. First demonstrated in jellyfish by Mayer in 1908, it was subsequently shown to be possible in cardiac tissue by Mines in 1913[60,153]. In the classical model of a wavefront progressing around an anatomical barrier in a fixed ring-like path, there are several prerequisites for re-entry to occur:

- areas of block or altered refractoriness defining the re-entry path
- unidirectional conduction block (set up by source-sink mismatch, for example – see *Section 1.2.4*)
- wave travel in a single direction
- termination if the pathway is cut or blocked
- region(s) of slow conduction.

An important concept in this setting is that of wavelength. This is defined as the product of conduction velocity and ERP, and as such, it represents the length (in reality, volume) of tissue that is refractory to new impulses. For re-entry to occur, wavelength must be shorter than the length of the re-entrant circuit (path length). The difference between these is known as the 'excitable gap' – the zone of non-refractory tissue between the wavefront and wavetail (Figure 14). In theory therefore, prolonging wavelength should be antiarrhythmic, if it can be made to exceed path length; however, this implies either increasing conduction velocity or ERP, both of which in the right circumstances may also be pro-arrhythmic.

Anatomical re-entry operates in a range of arrhythmias, although the scale of the re-entrant circuit varies. Typical cavo-tricuspid isthmus-dependent flutter and scar-related monomorphic VT are good examples. The former is probably the closest to a classical re-entrant circuit, though even this is thought to require functional block along the crista terminalis. In contrast to anatomical block at sites of unexcitable non-cardiomyocyte tissue such as a valve annulus, this functional block occurs in regions of

cardiomyoctyes where altered refractoriness, induced by tachycardia for example, leads to temporary unexcitability.

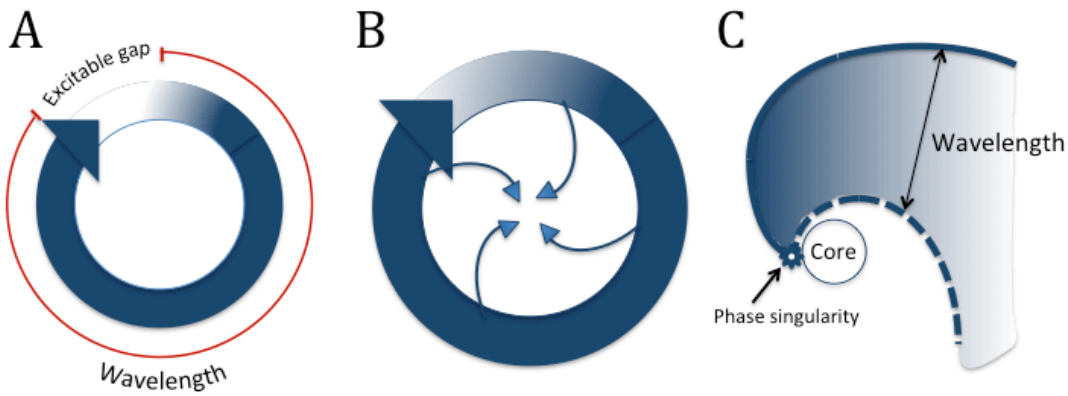

Figure 14 Types of re-entry. A: Classical anatomical re-entry. The wavelength is the product of conduction velocity and refractory period (shown in red). The excitable gap is the section of the circuit which is unexcited, ahead of the wavefront. B: Leading circle re-entry. The wavefront impinges on the wavetail such that there is no excitable gap. In addition, centripetal invasion creates a central region of functional refractoriness. C: Rotor re-entry. The wavefront and wavetail meet at a phase singularity, which rotates around an unexcited core. The wavelength (distance between the wavefront and tail) varies according to distance from the phase singularity. Modified from Pandit and Jalife[154].

Functional re-entry: the Leading Circle model and rotors

In 1977, Allessie et al proposed a new model of re-entry in which a typical circular activation wavefront would occur, without the requirement for the central anatomical obstacle (e.g. blood pool). In this model, which they termed the 'leading circle' concept, the circuit is formed by the smallest possible circle permitted by the electrophysiological properties of the tissue[155]. A central area of functional block is produced by centripetal invasion from the leading circle. The length of the circuit can vary, dependent on the electrophysiological properties of the tissue, and in contrast to the classical anatomical re-entry model, there is no excitable gap: the wavefront is constantly impinging on the wavetail (Figure 14).

Developments in understanding of fibrillation came from work on multiple wavelets and rotors[154,156,157]. These alternatives to the uniform, cyclical nature of anatomical re-entry offered a means of accounting for the absolute irregularity observed with fibrillation.

A rotor is a form of functional re-entrant activity in which a curved wavefront and wavetail meet at a point known as the phase singularity. When stationary, this point rotates around a small circle or core (Figure 14). The curvature properties of the wavefront at the singularity prevent invasion of the core, such that it remains unexcited, in contrast to what occurs in leading circle re-entry. One consequence of this is that the rotor can meander, in which case more complex core geometries will result. The rotor is therefore the 'driver', while spiral waves are the 2-dimensional propagating wavefronts, emanating from the phase singularity. In 3-dimensions, the term 'scroll wave' is used, and the core is considered a filament.

A further important characteristic of rotors and spiral waves is that the wavelength varies with distance from the core (see Figure 14). And spin frequency rather than wavelength may be a more appropriate index of arrhythmogenicity and measure of the effect of therapies. Phase mapping and dominant frequency mapping are two techniques that have been employed to analyse such properties of rotors.

Rotors and spiral waves are initiated by events that lead to wavebreak. This may occur with collision of impulses, encounter with an obstacle with sharp edges, or result from heterogeneity in tissue characteristics. The curvature of the wavefront is one of the key properties in determining rotor initiation. Termination typically occurs upon collision of a phase singularity with a boundary[154].

1.5.4 Mechanisms of ventricular fibrillation

While scar-related monomorphic VT is usually due to anatomical re-entry, maintenance of polymorphic VT and VF necessitate alternate mechanistic explanations due to their irregularity. Three main mechanisms have been put forward[158]:

- mother rotor re-entry
- wandering wavelet re-entry
- Purkinje fibre activity

With the first, a stable, high frequency re-entrant circuit drives the arrhythmia. The edges of the generated spiral waves fractionate, producing short-lived daughter wavefronts. Wandering wavelet re-entry consists of multiple short-lived wavefronts which meander, collide, fractionate, and annihilate. Following a triggering event, this behaviour facilitates maintenance of the fibrillation, supported by the presence of abnormal myocardial substrates, e.g. regional tissue heterogeneities. Finally, based on

differences in endocardial-epicardial activation rates during VF, and Purkinje fibre anatomy in different species, studies have investigated the role of the Purkinje system in maintaining VF, particularly once the arrhythmia has been present for two to three minutes. The cellular events underlying this are believed to include elevation of calcium levels with triggered activity in Purkinje fibres[158].

1.6 Measurement of cardiac electrical activity

At a single cellular and tissue level there are three key measurable electrophysiological parameters: activation, repolarisation, and refractoriness. A fourth parameter, impulse propagation, is important at a multicellular or tissue level. As the foregoing discussion has illustrated, each of these properties is determined by the interplay of a multitude of ionic fluxes. However, these four properties are the common denominators, and disturbances in them underpin arrhythmogenesis. Repolarisation and refractoriness are considered two entities, as although closely linked, their relationship is not fixed. Given that research is performed on substrates ranging from single cardiomyocytes to the whole heart, these terms form a core vocabulary applicable to all.
Ideally, the spatial location as well as the transmembrane voltage over time (i.e. action potential) for every cardiomyocyte in the heart would be known. If this were possible, each cell's activation and repolarisation could be measured, and the wavefronts of depolarisation and repolarisation could be calculated. For many reasons, this ideal is not possible. Nevertheless, the study of electrophysiology and pathophysiology requires measurement of the four fundamental parameters. At a tissue level, this necessitates use of extracellular proxies which reflect the key changes occurring intracellularly.

Measurement of these surrogates requires recording and analysis of signals. Although analogue components form part of the signal recording equipment, these are almost always converted to digital signals which offer advantages in terms of filtering, storage and reproducibility. In terms of the fidelity of the digital signal to its original counterpart, there are two parameters: sampling frequency and quantisation. The former refers to the number of times per second a signal is recorded, and the latter to the number of gradations of the output scale[159]. Filters are also important here as a means of reducing signal noise and enabling the key components to clearly seen.

A variety of techniques are available to measure at least one of the four parameters, and there are pros and cons associated with each. Intracellular voltage measurements using the patch-clamp technique record transmembrane action potentials (TAPs). Recordings made using electrodes which make extracellular contact with cardiomyocytes include unipolar (UEGs) and bipolar electrograms (BEGs) and monophasic action potentials (MAPs). The activation-recovery interval (ARI) is a parameter derived from UEG signals. Refractory periods such as the effective refractory period (ERP) may be determined either intra- or extracellularly with any of these techniques. Finally, the ECG measures global cardiac electrical activity at the body surface (see Figure 15).

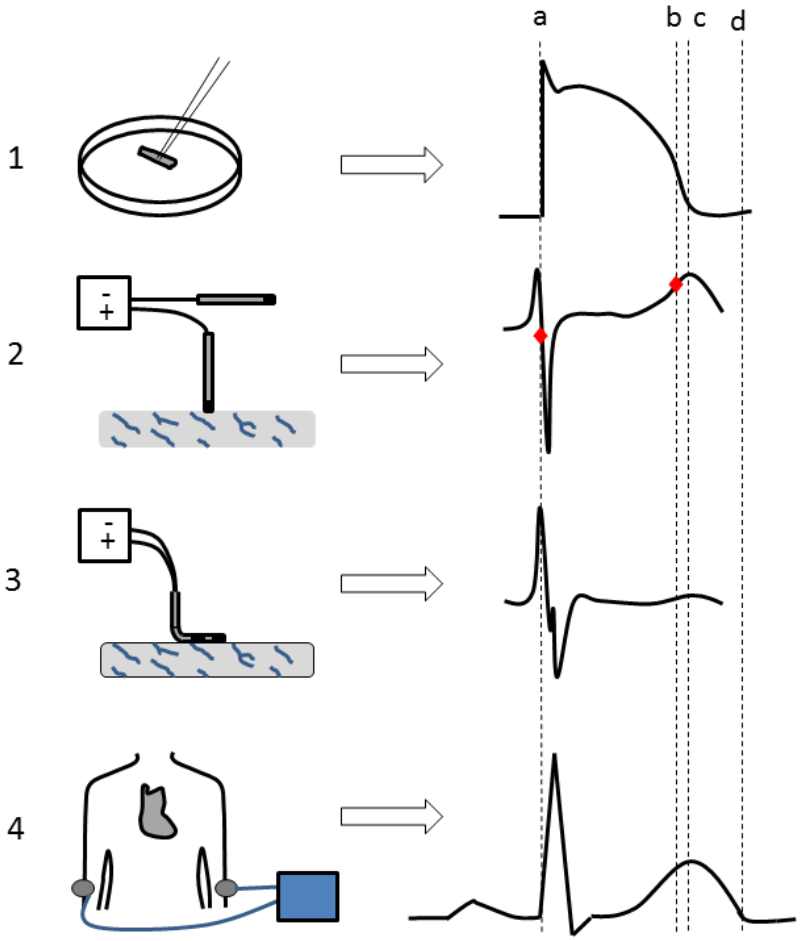

Figure 15 Cardiac bioelectric signals. 1: Patch-clamp of a cardiomyocyte with resulting TAP. 2: Unipolar extracellular tissue recording with UEG. 3: Bipolar tissue recording with BEG. 4: Lead I electrocardiography with ECG. Dashed vertical line (a): phase 0 of TAP. This coincides with dV/dt_{min} in the UEG, shown by the first red dot, and the peak value in the BEG. (b) indicates dV/dt_{min} of the TAP during phase 3, which coincides with dV/dt_{max} of the upstroke of the T wave in the UEG, illustrated by the red dot. The time between red dots is equal to ARI. By coincidence in this figure, (b) occurs at similar points on the T wave of the UEG and ECG. (c) full repolarisation of the TAP. (d) end of the T wave on the body surface ECG.

1.6.1 Unipolar and bipolar signals

The recording of bioelectric signals requires two electrodes – one connected to the anode, and another to the cathode terminal of the recording device. When only one of these electrodes is in contact with the tissue of interest, the signal generated will be 'unipolar'. In such instances, this 'exploring' or 'different' electrode is usually connected to the anode, with the cathodal electrode either situated in a remote, electrically inactive part of the body, or to the Wilson's central terminal, a 'reference' or 'indifferent' electrode derived from the average potential of the right arm, left arm and left leg ECG electrodes[160].

An alternative arrangement occurs when both electrodes (anodal and cathodal, equivalent to exploring and reference) are situated in close proximity (usually a few millimetres) and are both in contact with the tissue of interest. This is known as a bipolar configuration, and the signal from one electrode is subtracted from that of the other to produce the BEG. Unipolar signals offer advantages in that they give an indication of the direction of wavefront propagation, and repolarisation is registered. Their main disadvantage is susceptibility to noise and far-field signals. Bipolar signals on the other hand are unable to reliably indicate direction of propagation, but have negligible far-field effect or noise.

1.6.2 Monophasic action potentials (MAPs)

MAPs are a special type of signal that may be recorded in either unipolar or bipolar configuration. Their name derives from the fact that the electrogram (EGM) recorded shows a deflection in one direction only, coupled with the similarity of this signal to an action potential morphology, which is believed to have an electrophysiological basis rather than being coincidental. MAPs were among the first bioelectric signals to be recorded. As far back as 1882, Burdon-Sanderson and Page used this technique to record the cardiac electrical activity in the frog[161], though it was not used in humans until the 1960s[162,163]. For a number of years, it was believed that in order to record a MAP, an area of tissue injury was required, though the demonstration that MAPs could be recorded using the 'contact' electrode method suggested local cellular depolarisation induced by catheter pressure, rather than injury was necessary[164]. Over the years several techniques have been used, including suction electrodes, the contact electrode method (Franz catheter), and KCl electrodes, and the technique

enjoyed a resurgence of interest in the 1980s and 1990s after the development of the Franz catheter, which permitted safer recordings in humans. Interestingly, the issue of which electrode records the MAP signal has never quite reached consensus[165,166]; the predominant view however is that it is the depolarising electrode[164,167]. The main strength of MAPs is their ability to approximate local APDs, and in particular, repolarisation time.

1.6.3 Transmembrane action potentials (TAPs) and their relation to extracellular measurements

The currents underlying and generation of action potentials have already been discussed (see *Section 1.2.2*). These changes in potential across the cellular membrane are measured by piercing the cell membrane with an extremely fine-tipped glass pipette, in a technique known as sharp microelectrode recording, to yield TAPs. The first descriptions of such recordings are from 1949, by Ling and Gerard using frog sartorius muscle fibres, and Coraboeuf and Weidmann with cardiac tissue[168–170]. Measurement of TAPs was a prerequisite for ascertaining what different components of MAP EGMs, UEGs and BEGs represented. Correlational studies with MAPs showed that the rapid upstroke of the signal corresponded to phase 0 of the action potential[171]. And with UEGs, cellular activation was shown to most closely correlate with the fastest portion of the initial downstroke, dV/dt_{min}[172,173]. The theoretical basis of this is that this short period of time is when rapid sodium influx into the cells occurs, suddenly leaving the extracellular space around them relatively negatively charged. As phase 0 occurs within 1 ms, for the cluster of cells underlying an extracellular electrode, their collective depolarisation will occur within a few milliseconds. Despite the general acceptance, there are only a few direct comparisons between activation time measured by transmembrane action potentials and extracellular EGMs.

There has been less agreement concerning the timing of repolarisation for several reasons. Firstly, phase 3 of the action potential occurs less rapidly than phase 0, and consequently it is common to refer to the time at which a certain level of repolarisaton has occurred, e.g. APD_{90}, for 90% repolarisation, as this may differ from APD_{50} by several milliseconds. Secondly, due to the non-synonymity of the terms repolarisation and refractoriness, an index of repolarisation must be chosen which is both reproducible, and which has a physiological basis. Thirdly, the polarity of the repolarisation (T) wave in a UEG may be positive or negative; it must be decided if one

rule can be applied to both, or if there are separate ways to define the repolarisation time for each. Finally, although it is acknowledged that the T wave in both UEGs and ECGs is related to repolarisation, exactly how it is generated remains unanswered. One of the first and best known indices of repolarisation derived from UEGs is that described by Wyatt et al in 1980[174,175]. These investigators compared TAP duration with the time interval from the initial dV/dt_{min} to dV/dt_{max} of the UEG T wave, and found it to be highly correlated. Defining repolarisation in this way has become known as the 'Wyatt' method with dV/dt_{max} referred to as T_{up}; an alternative utilising dV/dt_{min} of the downslope of positive T waves (T_{down}) has been termed the 'alternative' method[176–178]. Although not named as such until Millar et al's publication in 1985[179], Wyatt et al's work in fact provided the first description of an activation-recovery interval (ARI) measurement. Further evidence of correlation was found by Haws and Lux[180], and Coronel et al provided support for the use of T_{up} regardless of whether the T wave is positive or negative[167]. The physiological significance of T_{up} is supported by *in vivo* work showing a high correlation between ARI measured with this method, and ERP[179].

1.6.4 Electrocardiography

The electrocardiograph, which records ECGs was invented by Einthoven in the early 1900s. Despite its relative simplicity compared to many modern diagnostic technologies used in medicine, it remains the most important non-invasive test in cardiology. The principles underlying electrocardiography are:

- that the whole heart's electrical activity can be measured and recorded graphically, with a degree of spatial specificity
- that because of the 3D structure of the heart, it is useful to 'look' at the heart (i.e. measure its activity) from different spatial locations
- that the depolarisation and repolarisation of cardiomyocytes from each chamber of the heart create specific deflections on the ECG
- that these deflections are commonly altered in disease states of the heart.

In humans, it is usual to record a 12-lead ECG; that is, to record the heart's electrical signals in orthogonal planes from 12 positions on the body. The key deflections and intervals are as follows: the P wave represents combined left and right atrial

depolarisation. The PR interval is the time taken from the start of atrial depolarisation to initial depolarisation within the ventricle, and therefore reflects conduction through the atria, the atrioventricular (AV) node, and down the His-Purkinje system. The QRS complex arises due to depolarisation of the right and left ventricles; this is followed by the T wave, representing ventricular repolarisation. Finally, the QT interval is the time from the onset of the QRS complex to the end of the T wave, reflecting depolarisation and repolarisation of the ventricles (see Figure 21). This interval varies with heart rate, so that a correction must be made to reflect this. Various formulae are available, but Bazett's correction is most commonly used ($QTc = QT/\sqrt{(R - R)}$).
In relation to the preceding discussion on extracellular signals, two points are worth bearing in mind: firstly, the standard ECG records cardiac activity at the body surface, and although individual ECG leads may reflect changes in their vicinity to a degree, ECG signals largely represent summated global activity, and do not offer anywhere near the spatial resolution of EGMs or MAPs. In the same vein, this combined output of all the cellular processes will therefore mask heterogeneities discernible at the cellular or tissue level with TAPs or EGMs. Secondly, although the QRS complex and T wave will have physiological correlates on a global scale, the fact they represent summated activity means there will be no precise relation to local ventricular action potentials within a section of myocardium[181].

1.7 Gene knockout technology

Gene manipulation technology has come a long way over the last three to four decades. In the early 1980s, microinjection of exogenous DNA allowed alteration of gene expression to produce 'transgenic' animals. One limitation of this approach was the often random incorporation of the DNA construct into the genome, with unregulated expression. With the development of embryonic stem cell (ESC) technology, it became possible to 'knock out' specific genes using homologous recombination. Introduction of ESCs carrying the mutant gene into animal embryos permitted generation of lines of 'knockout' mice with specific, known gene mutations[182,183]. Although this latter approach is still in use, two main drawbacks exist: the embryonic lethality conferred by certain gene deletions, and effects outside the organ or interest.

The introduction of the cre-loxP system of gene recombination in the 1980s has enabled a more sophisticated approach, permitting both spatial (i.e. tissue) and temporal specific knockout of genes of interest[184–187].

The elegant technology of the cre-loxP system (Figure 16) has several prerequisites in order to function properly:

- Insertion of 34 base pair 'loxP' sequences within/around the gene of interest to target this section of DNA for deletion
- Confirmation that excision of the sequence between the loxP sites will render any transcribed/translated product (from the remaining exons) non-functional
- Identification of a tissue-specific gene/protein, the promoter of which can be used to drive expression of the cre recombinase enzyme ('Cre')

The principles of how this system can be utilised to produce cardiac-specific knockouts are discussed below. Although only one gene's transcription apparatus (i.e. promoter) is employed, some knowledge of how the relevant protein relates to others at a cellular level is beneficial, and are therefore briefly discussed.

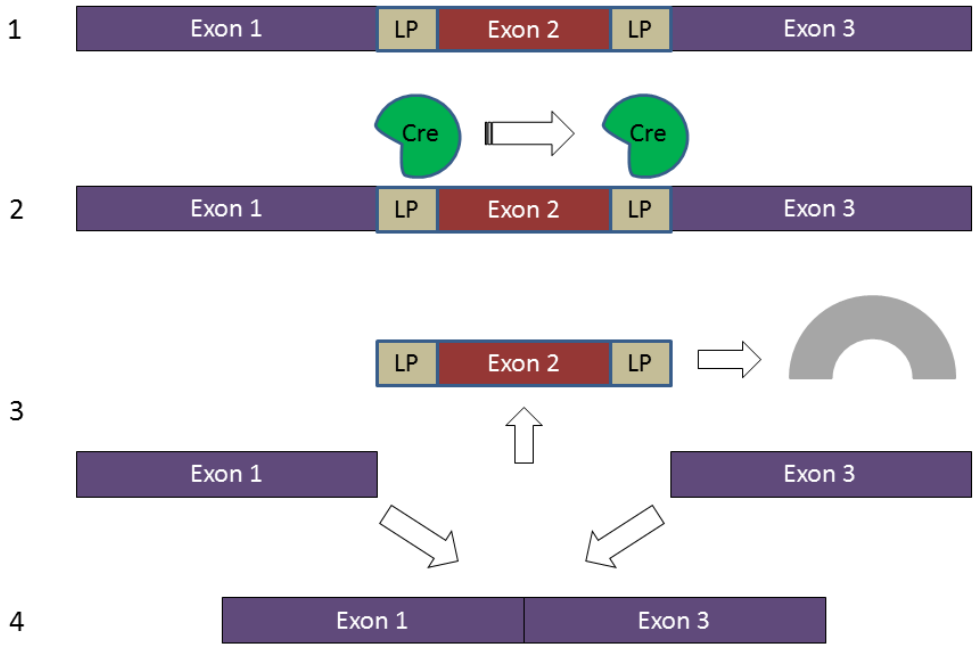

Figure 16 Cre-mediated excision of loxP-flanked DNA. 1: The allele within the genome. 2: Cre recombinase locates loxP sites flanking functionally-important exon. 3: This section of DNA is excised by Cre, leaving remaining exons to rejoin (4). The transcribed DNA will therefore only include exons 1 and 3.

1.7.1 Cardiomyocyte structure-function relationships

A cluster of myocytes together form a myofibre, held together by surrounding connective tissue which comprises the extracellular matrix. At a subcellular level, each myocyte contains bundles of contractile proteins known as myofibrils. These are divided along their length into sarcomeres, the most basic contractile unit. A number of proteins make up these myofibrils; together they interact in a coordinated fashion to produce contraction-relaxation cycles whereby filaments form cross-bridges and slide over one another. Subsequently, the cross-bridges are broken and they return to their resting state. This process is governed by availability of Ca^{2+} ions, the presence of which is closely regulated by ion channels and pumps, and storage and release from the sarcoplasmic reticulum[32].

1.7.2 Myosin heavy chain (MHC) expression

Myosin is an ATP-binding protein that forms the thick filaments of sarcomeres. It is composed of two heavy chains and four light chains. The genes encoding cardiac MHCs are located in on chromosome 14 in humans and chromosome 11 in mice. These chromosomal loci are distinct from their skeletal muscle counterparts. MHCs exist in two isoforms, α and β, which combine to form αα, αβ, or ββ dimers. In the human ventricle, these are referred to as V_1, V_2 or V_3 respectively, and they differ in their ATPase activity, the reaction which induces myofilament sliding[188–190].

Under physiological conditions in human ventricles, it is predominantly the β isoform that is expressed during both foetal life and postnatally, whereas in the atria it is the α isoform.

In murine atria, α-MHC is expressed during foetal life and after birth, and of note, it is also expressed in the pulmonary vasculature. In the ventricles however, β-MHC is the predominant isoform during foetal development, but a switch occurs in the first few days following birth, leading to a rapid rise in α-MHC expression matched by a similarly abrupt decline in β-MHC, such that the former accounts for nearly all ventricular MHC expression by 7 days after birth[188,190,191].

1.7.3 Regulation of expression of α-MHC in the mouse

Expression of α-MHC occurs transiently in the mouse ventricle between days 7.5 and 10 following fertilisation. From day 10 until birth, transcription is reduced after which it increases rapidly, essentially replacing β-MHC[189]. This expression profile is driven by myogenic programmes which differ for cardiac and skeletal muscle.
With regard to the DNA, the region upstream of the transcription start site shows conservation between species suggesting likely similarities in the factors governing transcriptional control. It also differs sufficiently from that of β-MHC to allow temporal and spatial specificity of expression of the isoforms. Two DNA sequences of particular importance have been identified: the thyroid hormone response element (TRE) and an A/T-rich region known as A/T2. These serve as contact points with thyroid hormone receptors (TRs) and myocyte enhancer factor-2 (MEF-2) proteins respectively, which act as transcription factors[190]. Prenatally, MEF-2 binding may be involved in regulation during late foetal life, but postnatally, the transcriptional switch in expression from β- to α- isoforms in the ventricle is largely mediated by thyroid hormones, reinforcing the importance of the TRE. Finally, the GATA family of DNA binding proteins may also have a role as transcription factors, and changes in chromatin structure could be implicated.

1.7.4 Cardiomyocyte-specific knockout using the α-MHC gene promoter

A number of extra-cardiac effects of global $G\alpha_{i2}$ knockout have been described, which have the potential to reduce survival and influence results[192–196]. These reflect the fact that $G\alpha_{i2}$ also participates in signalling pathways outside the heart, and indeed, this fact has been utilised both to understand physiology, and to create models of disease. These issues can be circumvented through use of a cardio-specific knockout model which makes use of the Cre-loxP system of DNA recombination[184,197]. As described above, this requires appropriately sited loxP sites to be inserted within the *GNAI2* gene. These serve as recognition sequences for Cre, expression of which is under the control of the α-MHC gene promoter, which is cardio-specific. Cre recombinase is therefore only produced in cardiomyocytes where it excises sections of the *GNAI2* gene, rendering the protein product, $G\alpha_{i2}$, non-functional. Evidence for the cardiac tissue-specificity of Cre-mediated recombination when under control of the α-MHC promoter is well-established[187,198]. Furthermore, it has been shown that this construct does not

lead to recombination in the sinoatrial node[199], and by inference, possibly not the conducting system tissue either, due to similarities in these cell types. Expression of Cre within the heart is therefore likely limited to cardiomyocytes.

The degree of knockout achieved with this system has been studied by several groups. Using a tamoxifen-inducible α-MHC promoter-driven Cre, levels of cardiac myosin binding protein C were reduced to 50% after two weeks of tamoxifen, and to <10% after eight weeks' treatment[200]. Interestingly, with DNA polymerase chain reaction (PCR) analysis, a faint 'flox' (flanked by loxP) allele band (i.e. amplicon incorporating loxP sites) was still seen after Cre-mediated excision. This likely resulted from non-myocyte cells. Andersson et al showed that with a tamoxifen-inducible Cre under control of the α-MHC promoter, mRNA levels of a cardiac protein (SERCA2) rapidly fell with tamoxifen treatment to <4% of that seen in controls after four days. SERCA2 protein levels were reduced to 20% by one week, and were undetectable after four weeks' treatment[201]. Of note, expression of this protein in non-cardiac tissues (lung and kidney) was negligible in controls as well as knockouts. Cardiac fibroblasts would therefore not be expected to have 'contaminated' the sample, and mRNA/protein knockdown would be expected to be almost complete. Sohal et al demonstrated >80% recombination following treatment with tamoxifen[186], and Kedzierski et al demonstrated 78% knockdown of ET_A mRNA in $ET_A^{flox/flox}$ mice (both alleles incorporating loxP sites), in which Cre was driven by the α-MHC promoter[202].

1.8 Animal models of heart failure

A number of small animal models of heart failure have been developed[203], the aim being to simulate those changes that occur in humans at systemic, organ and cellular level, so that these processes can be elucidated further, and the effects of other changes such as genetic manipulation or drugs, can be studied in a controlled manner. Each model has its merits, and at the outset of the project, it was considered useful to establish two models – one surgical and one pharmacological. In addition to their different complexities, this would also offer the opportunity to look at the effects of different challenges on the cardiovascular system. Most importantly, setting up two models simultaneously would act as an insurance policy, should it prove difficult to establish one of them.

It is worth making a distinction between LV systolic dysfunction and 'heart failure'. Although in terms of pathophysiology there is overlap, there are also some differences, as LV impairment, particularly when mild, is unlikely to induce the neurohumoural response that characterises heart failure. A recent scientific statement on animal models of heart failure recommends the following should be assessed to ensure the model is representative of the syndrome: measures of LV chamber size and wall thickness, functional reserve, echocardiographic indices (LVEF or fractional area change (FAC)), and gravimetric data demonstrating chamber hypertrophy and/or elevation of filling pressures[203].

The uncertainty regarding the driver(s) behind $G\alpha_{i2}$ elevation, and the overlap between LV systolic dysfunction and heart failure, have meant that while I have generally used the term LV impairment in this thesis, 'heart failure' has also been used at times, acknowledging the assumptions and possible inaccuracies inherent in this wording.

1.8.1 Myocardial infarction

The model of MI-induced heart failure has been performed extensively in both small and large animals. The main advantage of this model is that it offers clear parallels with both the pathophysiological process involved in the most common form of heart failure in humans, and the cardiac structural changes observed. Thus, in contrast to other heart failure models, where the 'insult' is more evenly distributed throughout the ventricle, the myocardial infarction model leads to regional necrosis, scar, and contractile dysfunction. The main disadvantages of this model are the technical expertise required, and the fact that the most common process of inducing MI, even in larger animals, namely coronary ligation, is clearly different to the endoluminal rupturing of an atherosclerotic plaque with subsequent thrombosis that occurs in humans.

With regards to the suitability of mice for this model, again there are pros and cons. Mice are cheap, breed easily, are the mammal with the most easily-manipulated genome, and the model is well-established in this animal. However, their cardiorespiratory anatomy and physiology differ from that of humans in several important ways:

- heart rate is 8-9 times faster than that of humans

- oxygen consumption is markedly lower – minute volume (inspired tidal volume x respiratory rate) is 30-40 mL/min in the mouse, compared to 15-30 L/min in humans
- coronary anatomy (see below)

Perhaps more importantly, mice also show a propensity to cardiac rupture following MI, which may reflect differences in wound healing and scar tissue formation[204].
In view of their size, large animals offer some advantages in this regard[203,205]. The coronary circulation of pigs is similar to that of humans, and whilst the occurrence of ventricular arrhythmias in porcine models is problematic in terms of survival[206], it resembles that which can occur in humans without urgent revascularisation and beta blocker therapy. One important disadvantage of the use of dogs is the presence of a collateral coronary circulation. This can limit infarct size and make reproducibility difficult[203].

Differences in the coronary circulation between mice and humans essentially relate to the fact that in mice, the course of the main branch of the left coronary artery is more oblique than in humans, and that there are differences in blood supply to the septum. In humans the right coronary artery supplies the basal-mid inferior septum in about two thirds[207], with the left coronary artery supplying the anterior septum. In mice, the whole septum is more commonly supplied by a branch of the right coronary artery, or a separate septal artery originating from the right sinus of Valsalva[208–210]. The relevance of these findings is that ligation of the left coronary artery is likely to spare the interventricular septum from infarction.

Two surgical techniques used to induce myocardial infarction have been described[211–214]. The classical technique using coronary ligation, involves passing a suture through the ventricular myocardium to encircle the main branch of the left coronary artery, just distal to the left atrium. Recently, Gao et al have described a novel method of coronary ligation involving exteriorisation of the heart, without the requirement for intubation[213]. Cryoinjury-induced infarction is an alternative method that has been shown to produce comparable left ventricular (LV) impairment to that achieved with ligation; infarct size was also shown to be reproducible[214].
Mortality rates vary by research group, and depend amongst other things, on factors such as time post-surgery, technique, strain, and gender of mice[204,211–218]. Peri-procedural mortality rates are reported to be in the range 3.5-15.9%, and up to 52% by

28 days[211–214]. Commonly reported causes of death include myocardial rupture, acute heart failure, arrhythmia, and pneumothorax. Myocardial rupture appears to be particularly common, and there are data to suggest mouse strain and sex may be important in the risk of developing this[204,217–219]. Mechanistically, these differences have been associated with for example, a higher blood pressure and stronger inflammatory response in 129Sv mice[219].

1.8.2 Supraphysiological beta-adrenoceptor agonism (isoprenaline)

As already described, in the normal heart the ratio of β1: β2 ARs is approximately 75:25 in the ventricle[122]. In heart failure however, chronically elevated levels of catecholamines result in a fall in β1ARs, while β2AR density remains largely unaltered[124]. Despite this, Gs activity is paradoxically unaltered, whereas that of its inhibitory counterpart Gi, is increased[124]. This upregulation of Gi signalling is possibly brought about by a switch in β2AR signalling from Gs to Gi, driven by PKA phosphorylation of the receptor[220].

In ischaemic heart disease, heart failure consequent on left ventricular impairment results largely from ischaemia-induced necrosis, although apoptosis and autophagy are also contributory in this and other forms of the syndrome[221]. In untreated LV failure, catecholamine excess develops regardless of underlying aetiology. However, it is uncommon for catecholamines alone to induce LV impairment and/or heart failure in humans: the cardiomyopathy related to phaeochromocytoma, and probably Takotsubo cardiomyopathy are examples infrequently encountered. Therefore, whilst it is accepted they contribute to the syndrome at systemic and organ level, the degree to which these hormones participate in the pathophysiology of cardiomyocyte death is debatable. As such, whilst animal models utilizing βAR agonists (usually the non-selective agonist isoprenaline/isoproterenol) as the sole mechanism of inducing LV impairment/heart failure may shed light on certain disease pathways, the relevance to human pathophysiology must be questioned, particularly given that the drug levels used are chosen to induce hypertrophy/heart failure, rather than to reflect levels of agonism seen in the syndrome. Having said that, the importance of βAR signalling in heart failure is undisputed, and βAR-blocking drugs are a mainstay of therapy.

Accepting that excessive βAR stimulation can lead to cardiomyocyte death, the mechanisms are still being elucidated. Nakayama et al showed in a murine model of LTCC overexpression, that βAR stimulation can augment cellular Ca^{2+} overload and myocyte necrosis, rather than apoptosis[222]. Zhang et al found that βAR signalling can lead to cytosolic and sarcoplasmic reticulum (SR) Ca^{2+} overload, which in turn may result in cell death; this process was blocked by PKA inhibition[223]. It remains unclear whether apoptotic signals originate solely through the β1 signalling pathway; studies investigating β2 signalling through PI3K have shown conflicting results with regard to cell survival/apoptosis[224,225] (see Figure 17).

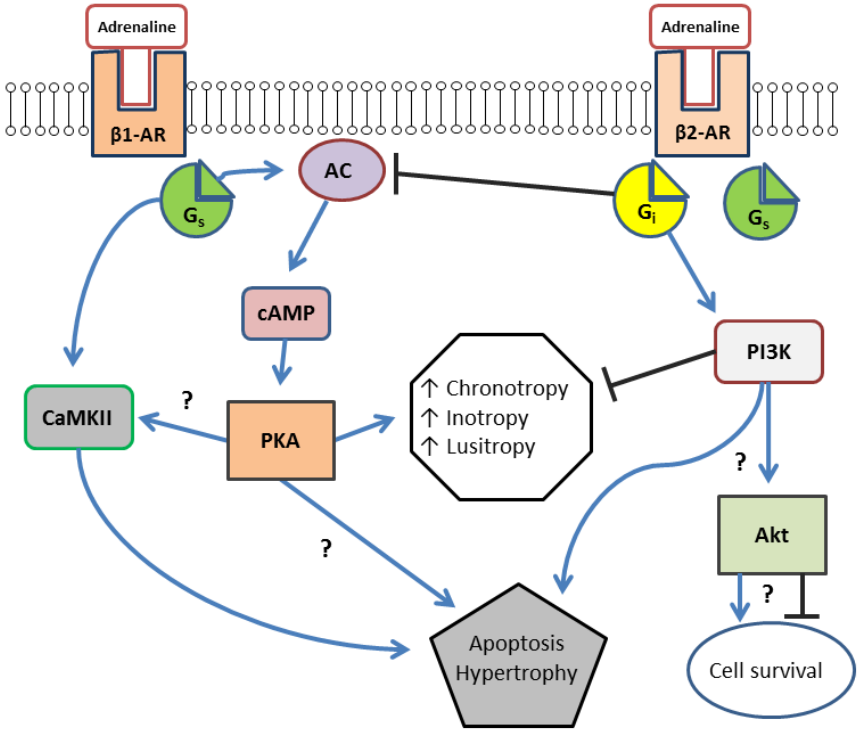

Figure 17 Important β1- and β2-adrenoceptor signalling pathways. AR: adrenoceptor, AC: adenylyl cyclase, Gs: stimulatory G protein, Gi: inhibitory G protein, cAMP: cyclic adenosine monophosphate, PKA: protein kinase A, CaMKII: Ca2+/calmodulin-dependent protein kinase, PI3K: phosphoinositide 3-kinase, Akt: protein kinase B. Modified from Zheng et al[127].

1.9 Microelectrode array studies

1.9.1 Background

There are many similarities between neurological and cardiac electrophysiology, both in terms of underlying mechanisms and measurement techniques. To measure brain activity at the body surface, neuroscientists record electroencephalograms (EEGs), whilst the cardiac equivalent is the ECG. To measure local extracellular electrical activity of tissue, neuroscientists record local field potentials (LFPs) with microelectrode arrays (MEAs), whereas cardiac electrophysiologists record EGMs or MAPs. Despite the differing terminology, the hardware setup and in particular the electrode localisation for recording LFPs and EGMs seem remarkably similar, though the signals obtained differ, as discussed below.

MEAs have been used extensively in neuronal experiments since at least the 1990s[226]. Their obvious attraction is the ability to simultaneously monitor multiple tissue bioelectric signals at potentially very high spatial resolution. Having said that, when neuroscientists have used them *in vivo*, two important findings have emerged. Firstly, the 'local' field potentials (FPs) are not necessarily as local as may be expected[227], and secondly, at least *in vivo*, currents from a host of processes combine to produce the FP. The predominant contributor is synaptic activity due to the relatively slow event rate which facilitates overlap. Although fast action potentials mediated by Na^+ flux produce spikes which contribute to FPs, their brevity and lack of synchrony limit the magnitude of this contribution. Others include calcium spikes, I_h and I_T currents, spike afterhyperpolarisations, gap junction and neuro-glia interactions, and ephaptic effects[228].

The MEA suggests itself as suitable for the study of cardiomyocyte clusters and cardiac tissue given their multicellular composition and electrical activity. A couple of the important differences between the heart and brain in relation to such work *in vivo* include the mechanical activity of the heart, and its vascularity. Though not insurmountable, *ex vivo* techniques offer potential advantages. Several models are available, including the isolated perfused heart, perfused ventricular wedge preparation, papillary muscles, Purkinje fibres and single cardiomyocytes. The isolated perfused heart suffers from the same mechanical issues as *in vivo*, and ensuring stable recordings in the commonly used rodent heart is particularly challenging. Ventricular

wedge preparations maintain 3D architecture, complicating measurements of conduction velocity, and maintaining perfusion and oxygenation of small animal heart sections is challenging. Purkinje fibres and papillary muscle techniques are time-consuming and technically difficult, and single cardiomyocytes must be separated enzymatically and lack the intercellular connections that reflect the tissue environment.

1.9.2 Cardiac tissue slices

Cardiac slices offer an alternative means of tissue study. First used in 1991 to study neonatal rat hearts with patch-clamp recordings[229], this technique was subsequently used in 2005 to study murine embryonic hearts[230]. The first study of adult murine heart slices was reported in 2006[231], and adult human slices in 2011[232]. Proposed advantages include the possibility of using several or even numerous tissue sections from the same heart, relative ease of perfusion/oxygenation, and importantly, maintenance of intact tissue structure. The thinness of the slices (200-300 μM) also means that propagation can be studied in a pseudo-2D manner. The main disadvantages are the requirement for dedicated equipment such as a vibratome and MEA recording hardware, and the need to acquire competence in the Langendorff technique of retrograde cardiac perfusion.

Maintenance of tissue viability is paramount if good quality signals are to be recorded with the MEA. The heart undergoes a good deal of physical trauma and is exposed to metabolically stressful environments. The former is only minimally modifiable, so efforts are concentrated on the latter. The heart is first removed *en masse* from the body, and extraneous tissue is removed prior to retrograde perfusion. This is done in ice-cold liquid or on ice. Retrograde perfusion using the 'Langendorff technique' is then initiated. This was first described by Langendorff in 1895 and is a means of perfusing the ventricles when the heart is removed from the body and has lost the pulmonary circuit through which antegrade blood flow normally occurs[233]. The aorta is cannulated and perfusate pushes the aortic valve closed allowing it to flow down the coronary arteries[234].

The perfusate must supply oxygen and a substrate in order to permit continued metabolism. Although whole blood perfusion is possible, more commonly crystalline solutions are used. The ionic constitution should be similar to that of blood, so that it is

isotonic with the interstitial fluid. Also, the pH should be physiological, achieved with carbon dioxide (95% O_2 and 5% CO_2) and buffered by bicarbonate or inorganic phosphate. The two solutions most frequently used are Krebs-Henseleit buffer, and Tyrode's solution. These are broadly similar, and often modified e.g. with regard to K^+, Ca^{2+} or glucose concentration. Glucose is preferred to the heart's normal energy substrate of free fatty acids due to availability and the relative ease of maintaining the former in solution[234].

To minimise metabolic stress and its consequent effects on viability and physiology, cold media are used to reduce metabolic rate, and high potassium, low calcium solutions are used to achieve cardioplegia. A reversible excitation-contraction uncoupling agent is used to aid mechanical arrest and further reduce metabolic demands. 2,3-butanedione monoxime (BDM) and blebbistatin are both suitable for this purpose, though BDM has been used more frequently in published MEA studies[231,232,235,236].

After cardioplegia has been induced, the ventricles are separated from the atria and glued to a platform, after which the vibratome cuts sequential slices. These are transferred to carbogenated (95% O_2, 5% CO_2) solutions prior to study, which allow a graded return to electromechanical association with more physiological ion concentrations and absence of BDM or blebbistatin.

1.9.3 Field potentials vs. electrograms

To return to the discussion concerning the signals recorded from cardiac slices, it can be seen that heart's coordinated electrophysiology, in conjunction with its relative paucity of synaptic activity mean the signals obtained will more closely reflect the action potentials of localised clusters of cardiomyocytes in the vicinity of the exploring electrode than may be the case with neuronal tissue, particularly *in vivo*. With the MEA as used in neurological investigations, the high spatial density of the exploring electrodes, together with the use of a remote reference electrode[227] suggest the signals obtained (LFPs) to be somewhat analogous to the unipolar EGMs used in cardiac electrophysiology. Thus, although the term 'field potential' has been frequently used in relation to cardiac electrophysiology studied with the MEA, it would appear these FPs are not substantially different to UEGs. This is supported by the morphology of reported FPs which bear resemblance to UEGs[231,235–238]. To an extent, this is a semantic issue, though the transference of terms from other disciplines without explanation of

their similarities and differences can lead to confusion. As such, the signals recorded with the MEA in my study will be termed UEGs in this thesis, although when referring to published studies, FPs will be used.

1.10 Summary

Life-threatening ventricular arrhythmias may arise in a large variety of settings, but scar within, and disruption of the normal myocardial architecture of the ventricles, is the most common predisposing condition. Similarly, the replacement fibrosis that constitutes scar can result from a range of insults, but myocardial infarction is the most common in developed countries such as the United Kingdom. The resultant changes in myocardial architecture produce conditions favourable to re-entrant circuits in particular. If sufficient scarring is present, ventricular function becomes impaired, with elevation of diastolic pressure and transmission of this to the pulmonary circulation; if severe, right heart impairment ensues and systemic venous pressures also become elevated. This chain of events often results in the signs and symptoms of 'heart failure'. This is perpetuated further by maladaptive neurohumoural responses in the body, which result in increased sympathetic, and reduced parasympathetic activity. In addition to elevation of heart rate and sodium and water retention in the kidneys, this autonomic imbalance alters cardiac tissue electrophysiology in ways favourable to arrhythmogenesis. Despite great advances in our understanding of the changes that occur in heart failure, cardiac electrophysiology at the cellular and tissue level, the autonomic nervous system, and mechanisms of arrhythmia, the therapies available to prevent the occurrence of ventricular arrhythmias are suboptimal. Better understanding of receptor signalling cascades in the heart, their effects on ion channels, and the changes that occur to these in the setting of cardiac scarring and heart failure, could help guide development of novel anti-arrhythmic agents.
The signalling protein $G\alpha_{i2}$ has been shown to be elevated in patients with heart failure. $G\alpha_{i2}$ is involved in signal transduction from the mAChR and the β2AR, regulating the GIRK channel and the LTCC. Given the increased risk of ventricular arrhythmias in this syndrome, it is possible that this protein modulates arrhythmogenicity. This is supported by experimental evidence, including from mice with global deletion of $G\alpha_{i2}$, who were shown to have a pro-arrhythmic phenotype. However, there has been little

if any other *in vivo* work reporting electrophysiological phenotypic effects of alterations of $G\alpha_{i2}$.

In order to develop the work previously undertaken in the group with $G\alpha_{i2}$ knockout (KO) mice, and more generally to investigate the electrophysiological effects of autonomic modulation in the murine heart, I utilised *in vivo* and *ex vivo* models. The former involved phenotyping mice before and after coronary ligation-induced MI, with its resultant impairment of LV function. By creating a cohort of wild-type (WT) and $G\alpha_{i2}$ KO mice with regions of scar, and sympathovagal imbalance, I was able to model the pathophysiology of human ischaemic heart disease and heart failure, and probe phenotypic differences due to $G\alpha_{i2}$ at an organ and whole body level. The *ex vivo* ventricular tissue model utilised an MEA system to investigate key electrophysiological parameters in WT and $G\alpha_{i2}$ KO mice, as well as their alteration with pharmacological agonists of βARs and mAChRs, and temperature.

Together, these two sets of experiments took advantage of genetically-manipulated mice to probe the possible electrophysiological effects of a signalling protein $G\alpha_{i2}$, and investigate the effects of parasympathetic and sympathetic agonism on electrophysiological parameters. There has been little published previously on the phenotypic effects of alterations of $G\alpha_{i2}$, and the combination of two approaches to investigate this, and the autonomic control of heart function, provides a distinct contribution to the field of study.

HYPOTHESES

1. $G\alpha_{i2}$ is anti-arrhythmic in the ventricles where it mediates parasympathetic signalling effects on the key electrophysiological parameters of activation, repolarisation, and conduction velocity.
2. Beta-adrenoceptor agonism and changes in temperature exert effects on activation, repolarisation and conduction velocity.

AIMS

1. To establish a pharmacological and a surgical murine model of heart failure, with which to probe hypothesis 1.
2. To test hypothesis 1 by assessing the phenotypic effects of cardiac-specific knockout of $G\alpha_{i2}$ in mice at baseline, and following induction of heart failure.
3. To test hypothesis 1 by assessing the electrophysiological effects of $G\alpha_{i2}$ knockout in ventricular tissue from mice with global deletion of the *GNAI2* gene.
4. To test hypothesis 2 by assessing the electrophysiological effects of beta-adrenoceptor agonism and changes in temperature in ventricular tissue from wild-type mice.

2. METHODS

2.1 Statement on use of laboratory animals

Mice were maintained at the Biological Services Units at Charterhouse Square and Whitechapel sites of Queen Mary University of London. Animal maintenance and experiments conformed to UK Home Office guidelines relating to animal welfare (PPL 70/7665; PIL 70/24330 / I8A749EFA). Mice were housed in individually ventilated cages in temperature-controlled rooms (21-23°C) with 12 hour light/dark cycles. They had access to standard rodent chow and water at all times.
Following general anaesthesia, mice were observed until moving before being replaced in their cage. They received opiate analgesia prior to recovery, were reviewed at 4-6 hours post-operatively, and again the following day. If necessary, a further dose of opiate analgesia was administered at this stage. Post-operatively mice were housed alone.

2.2 Cardio-specific $G\alpha_{i2}$ knockout mice

2.2.1 Generation of cardio-specific Gαi2 knockout mice

Mice with cardiomyocyte-specific knockout of the *GNAI2* gene encoding the $G\alpha_{i2}$ protein (used interchangeably hereafter) were generated through use of the Cre-loxP system of DNA recombination[184,197] as described in Section 1.7. Homozygous 'conditional-ready' mice on a 129Sv background, with loxP sites flanking exons 2 and 4 of the *GNAI2* gene, were provided as a gift by Dr Lutz Birnbaumer (Figure 18). Sections of a gene with loxP sites at each end are termed 'flanked by loxP' or 'floxed', and the allele is written as 'Flx'. Mice homozygous for the floxed *GNAI2* gene are designated $G\alpha_{i2}{}^{Flx/Flx}$; those with two wild-type (WT) alleles are designated $G\alpha_{i2}{}^{WT/WT}$; and those with one copy of each allele, $G\alpha_{i2}{}^{Flx/WT}$.
After initial breeding of $G\alpha_{i2}{}^{Flx/Flx}$ mice and confirmation of $G\alpha_{i2}$ gene status (i.e. Flx or WT), homozygous female offspring were crossed with a male mouse on a C57B6/J

background expressing Cre under control of the α-MHC gene promoter (Figure 19). This Cre+ mouse was provided as a gift by Prof Michael Schneider. Further breeding of offspring was carried out until an extra-cardiac tissue genotype of $G\alpha_{i2}^{Flx/Flx}$ Cre+ was obtained from ear DNA (see below). This would produce a cardiac tissue-specific knockout of $G\alpha_{i2}$ due to Cre-mediated DNA excision as was previously demonstrated in the research group.

Figure 18 Mus musculus *GNAI2* gene indicating exons (numbered blue blocks), inserted LoxP sites and PCR primer binding sites. Retrieved through BLAT and modified from Ustyugova et al[239]

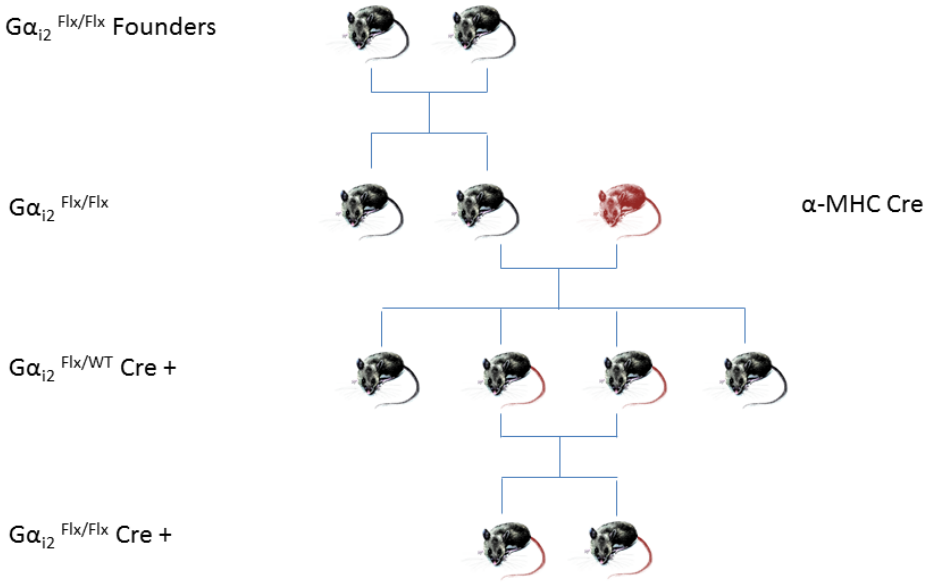

Figure 19 Generation of knockout mice. Black body colour indicates presence of a Flx allele within the *GNAI2* gene, whereas red body colour indicates homozygosity for the WT GNAI2 allele. Red tail indicates presence of Cre recombinase, whereas black tail indicates its absence.

2.2.2 Assessment of genetic status

Tissue was obtained from mice aged 2-4 weeks by 'ear-notching' to enable assessment of *GNAI2* status (Flx/Flx, Flx/WT, or WT/WT), and Cre status (expressed or absent). The tissue was collected in a 1.5ml eppendorf tube, and digested to release DNA suitable for PCR as follows:

i. 150 µl of tail lysis buffer per sample (2 M Tris HCl, 1M $(NH_4)_2SO_4$, 0.5 M $MgCl_2$, Triton X-100, distilled H_20) with 1% β-Mercaptoethanol was added to each sample
ii. The samples were heated at 100 °C for 10 minutes
iii. Samples were cooled for 10 minutes
iv. 5 µl of Proteinase K (20 mg/ml, Sigma-Aldrich, UK**)** was added to each sample for digestion over 12-16 hours, or 7 µl for digestion over 4-5 hours at 55 °C
v. Samples were heated at 100 °C for 10 minutes
vi. Samples were left to cool for 10 minutes, then centrifuged at 14,000 rpm for 3 minutes
vii. The supernatant was collected in new 0.5 ml eppendorf tubes, and stored at -20 °C

For PCR of ear tissue DNA, the following DNA primers (Invitrogen Life Technologies) were used:

$G\alpha_{i2}$ Forward: 5'-GGA GCC TGG ACT TTG CTT CTG ACC-3'
$G\alpha_{i2}$ Reverse: 5'-GGC TAT GAT CCC AAA ACT CCC CG-3'

αMHC Cre Forward: 5'-CCA ATT TAC TGA CCG TAC ACC-3'
αMHC Cre Reverse: 5'-GTT TCA CTA TCC AGG TTA CGG-3'

PCR1

The reaction mix and PCR programme for *GNAI2* genotype of each digested DNA sample was as follows:

- 10 µl HotStarTaq Mastermix (Qiagen) (DNA polymerase, PCR buffer, and deoxynucleotides)
- 9 µl distilled water
- 10 µl primer mixture (5µM forward, 5µM reverse)
- 1 µl DNA

1. Heat lid to 110 °C
2. 94 °C for 15 minutes
3. 35 cycles
    a. 94 °C for 30 seconds
    b. 60 °C for 30 seconds
    c. 72 °C for 1 minute
4. 72 °C for 10 minutes
5. Store at 8 °C

PCR 2

The reaction mix and PCR programme for α-MHC Cre genotype of each digested DNA sample was as follows:

- 12.5 µl HotStarTaq Mastermix (Qiagen)
- 4.5 µl distilled water
- 2.5 µl forward primer (10µM)
- 2.5 µl reverse primer (10µM)
- 310 µl DNA

1. Heat lid to 110 °C
2. 95 °C for 15 minutes
3. 35 cycles
    a. 94 °C for 1 minute
    b. 60 °C for 1 minute
    c. 72 °C for 1 minute
4. 72 °C for 5 minutes
5. Store at 8 °C

TAE buffer (50X) was made up with 242 g Tris Base (MW 121.1), 57.1 ml Glacial Acetic Acid, and 100 ml 0.5 M EDTA, dissolved in distilled deionised water to make 1 litre. From this, 1X TAE buffer was made by adding 20 ml of 50X TAE buffer to 980 ml distilled deionised H_20.
To visualise the amplicons of the PCR, and enable separation of products of different length, a 1% agarose gel was prepared as follows:

1. 1 g of UltraPure™ Agarose (Invitrogen) was dissolved in 100 ml of 1x TAE buffer
2. This was heated for 2 minutes in a microwave to fully dissolve
3. After leaving to cool for a few minutes, 7.5 µl of Midori Green Advanced DNA stain (Nippon Genetics Europe) was added and mixed into the solution
4. The 1% agarose solution was poured into a 15 or 20 lane gel tray and left to set for 45 minutes

Prior to loading the gel with samples, 5 µl of 6X DNA loading dye (New England Biolabs) was added to and mixed with each DNA PCR sample. 20 µl of each PCR/loading dye product was added to each lane. A 100 base pair (bp) DNA ladder (New England Biolabs) was run in the first lane of the gel, which was imaged with ultraviolet light transillumination (Alpha Innotech), exposure time 150 ms. Illustrative examples of PCR products are shown in Figure 42.

2.2.3 Confirmation of knockout status of $G\alpha_{i2}^{Flx/Flx}$ Cre+ mice: analysis of mRNA expression and Sanger sequencing

'Knockout' of a gene can be demonstrated in different ways. At the DNA level, PCR performed with primers either side of the region of interest can be used to produce amplicons of different sizes dependent on the status of the gene, i.e. WT allele, 'floxed' allele, or excised. This can be taken a step further by analysis of the amplicon sequence, using Sanger sequencing, so as to produce a DNA base-by-base readout. The sequence can then be analysed using genome library tools, so as to visualise alignment with the gene of interest and look for unmatched regions suggesting excision.

As DNA is transcribed to mRNA, further confirmatory evidence can be obtained by analysis of the relative amounts of mRNA in tissues from genetic knockouts and

controls, to confirm knockouts have the expected marked reduction. Finally, protein expression can be measured using the technique of western blot. This requires antibodies specific for the protein of interest. In the case of $G\alpha_{i2}$, the specificity of the antibodies available is not sufficient to differentiate from other $G\alpha_i$ isoforms; hence the use of mRNA analysis and Sanger sequencing.

RNA extraction

In order to show tissue-specific knockout of the *GNAI2* gene product, $G\alpha_{i2}$, in mice genotyped as $G\alpha_{i2}^{Flx/Flx}$ Cre+ (termed cKOs hereafter), hearts, livers and tails were harvested from four cKO mice and four mice of wild-type *GNAI2* gene status (three $G\alpha_{i2}^{WT/WT}$ Cre-, and one $G\alpha_{i2}^{WT/WT}$ Cre+). Mice were culled by cervical dislocation, organs excised and stored in RNAlater (Sigma-Aldrich, UK) prior to storage at -80 °C pending RNA extraction.
This was performed using RNEasy Fibrous Tissue mini kit (Qiagen) according to the following product instructions (all reagents supplied within the kit):

1. Buffers and reagents prepared as per protocol
2. Approximately 30 mg of tissue was removed from storage in RNAlater
3. The tissue was frozen with liquid nitrogen, and disruption was performed with a mortar and pestle. Homogenisation was performed with a needle and syringe in 300 µl of Buffer RLT
4. 590 µl of RNAse-free water was added to the lysate. Then 10 µl of proteinase K solution was added and mixed
5. The mixture was incubated at 55 °C for 10 minutes
6. It was then centrifuged for 3 minutes at 12,500 rpm
7. The supernatant was pipetted into a new microcentrifuge tube
8. 450 µl of ethanol (96-100%) was added to the cleared lysate and mixed by pipetting
9. 700 µl of the sample was transferred to an RNeasy Mini spin column placed in a 2 ml collection tube. This was centrifuged for 15 s at 10,000 rpm. The flow-through was discarded
10. Step 9 was repeated with the remainder of the sample
11. 350 µl of Buffer RW1 was added to the RNeasy spin column. This was centrifuged for 15 s at 10,000 rpm. The flow-through was discarded

12. 10 µl of DNase I stock solution was added to 70 µl of Buffer RDD and gently mixed
13. The DNase I incubation mix was added directly to the RNeasy spin column membrane, and placed on the bench top for 15 minutes
14. 350 µl of Buffer RW1 was added to the RNeasy spin column. This was centrifuged for 15 s at 10,000 rpm. The flow-through was discarded
15. 500 µl of Buffer RPE was added to the RNeasy spin column. This was centrifuged for 15 s at 10,000 rpm. The flow through was discarded
16. 500 µl of Buffer RPE was added to the RNeasy spin column. This was centrifuged for 2 minutes at 10,000 rpm. The flow through was discarded
17. The spin column was placed in a new 1.5 ml collection tube. 30-50 µl of RNase-free water was added directly to the spin column membrane. This was centrifuged for 1 minute at 10,000 rpm to elute the RNA
18. Step 17 was repeated with another 30-50 µl of RNase-free water

Extracted RNA was kept on ice and transferred to the Genome Centre, William Harvey Research Institute, QMUL, for analysis with real-time PCR. As extracted total RNA contains several types (mRNA, transfer RNA, and ribosomal RNA), with mRNA being the one of interest, prior to RT-qPCR it was necessary to perform a reverse transcription reaction with High Capacity RNA to cDNA (Applied Biosystems). This uses only the mRNA to produce complementary DNA (cDNA), and is therefore a reflection of the quantity of mRNA for each gene.

Real-time quantitative PCR (RT-qPCR)

mRNA analysis has previously been performed in our group on $G\alpha_{i2}{}^{Flx/Flx}$ Cre+ mice with Cre expression under control of the α-MHC promoter (unpublished results). The primer sequences used (Forward: TGGAGAGTCAGGGAAGAGCA, Reverse: TAGACCACGGCACGGTACT) were provided to Dr Charles Mein at the Genome Centre. The sequences were entered into a BLAT (BLAST-Like Alignment Tool) search which retrieved the murine *GNAI2* gene sequence. The forward primer is located in exon 2, and the reverse primer in exon 3. It was decided to use a TaqMan® Assay (Invitrogen) to assess expression. The previously used primer sequences were not available, so

new primers in near-identical locations were used (Forward: CAGGGAAGAGCACCATCGT, Reverse: GCCGGCACTCCTCTTCTG) (see Figure 20).

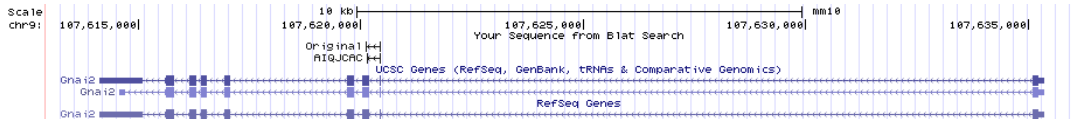

Figure 20 Results from UCSC BLAT search[240] using original and new (labelled 'AIQJCAC') mRNA primer sequences. These are situated over exons 2 and 3 of GNAI2 gene (short purple bars). Diagram illustrates near identical location of original and new primer sequences.

Glyceraldehyde 3-phosphate dehydrogenase (GAPDH) was used as the 'housekeeping' (reference) gene. Threshold cycle (C_t) was determined for each assay as well as for no template controls (NTCs).

Relative expression of the gene of interest can be determined using the 'Comparative Ct Method', described by Livak and Schmittgen[241,242]. Using this method, C_t values were determined for the gene of interest (*GNAI2*) and the housekeeping gene (*GAPDH*) in the tissue of interest (cardiac ventricles), for both knockout and control mice. A delta C_t value (ΔC_t) was obtained by subtracting the C_t for ventricular GAPDH in controls, from the C_t for ventricular $G\alpha_{i2}$ in controls. This 'control' ΔC_t was then subtracted from the corresponding value for knockouts, to obtain $\Delta\Delta C_t$. As each increment of one in C_t represents a halving of mRNA expression (or conversely, each decrement represents a doubling), the relative expression of the gene of interest between controls and knockouts can be calculated using equation 1:

$$\text{Relative expression} = 2^{-\Delta\Delta Ct} \qquad \text{Equation 1}$$

<u>Sanger sequencing</u>

DNA sequences from four mice with the following genotypes were obtained by Sanger sequencing performed by the Genome Centre at the William Harvey Research Institute:

- $G\alpha_{i2}^{Flx/Flx}$ Cre+ (2 mice)
- $G\alpha_{i2}^{WT/WT}$ Cre- (1 mouse)
- $G\alpha_{i2}^{Flx/Flx}$ Cre- (1 mouse)

The two cKO mice used were two of the same ones used in the real-time quantitative PCR (RT-qPCR) experiment described above; the $G\alpha_{i2}^{WT/WT}$ Cre- and $G\alpha_{i2}^{Flx/Flx}$ Cre- mice were not used previously.
DNA extracted from the mice's hearts was provided to the Genome Centre, where it was amplified by PCR using a second forward primer ('F2') designed to produce the following PCR amplicons:

WT allele: 2.1 kb
Flx allele: 2.2 kb
Allele following Cre-mediated excision: 0.4kb

The F2 primer sequence was 5'-GTGGTAAGCCTGTGTTTGTGAGAG-3'. The PCR programme was the same as described above for *GNAI2* genotyping (PCR 1), except for stage 3c which was held at 72 °C for two minutes rather than one.
Sequences were downloaded from a server using the program CoreFtp (Core FTP), and visualised with BioEdit (Ibis Biosciences). Each sequence was then entered into the University of California Santa Cruz (UCSC) BLAST-like alignment tool[240], to confirm alignment within the mouse *GNAI2* gene, and to look for deleted regions.

2.3 Global $G\alpha_{i2}$ knockout mice

2.3.1 Generation of global $G\alpha_{i2}$ knockout mice

Global gene deletion is an alternative means to ensure the relevant protein is not produced anywhere in the body. As described in *Section 1.7*, this is achieved by injecting ESCs with the modified non-functional version of the gene into blastocysts which are implanted into pseudopregnant females. Provided DNA recombination occurs, breeding of the offspring generates mice with the knockout version of the gene at either one or both alleles. Status can be designated in a similar manner to that for cardio-specific knockout: two wild-type alleles - $G\alpha_{i2}^{+/+}$; two knocked out alleles - $G\alpha_{i2}^{-/-}$; heterozygote - $G\alpha i2^{+/-}$.
Heterozygote mice were provided by Dr Lutz Birnbaumer. The KO allele was created by disruption of the *GNAI2* gene within exon 3, a key region involved in binding and hydrolysis of GTP. Insertion of an oligonucleotide 'cassette' induced a frameshift

resulting in a truncated, non-functional protein. This was confirmed structurally[194], and its functional effects have been demonstrated[243].
Mice with global *GNAI2* gene deletion ($G\alpha_{i2}^{-/-}$) were generated by breeding heterozygote males and females. These are termed gKOs hereafter.

2.3.2 Assessment of genetic status

Tissue was obtained from mice aged 2-4 weeks by ear-notching, and digested as for cardio-specific knockout mice.
For PCR of ear tissue DNA, the following DNA primers (Invitrogen Life Technologies) were used:

WT forward: 5'- GAT CAT CCA TGA AGA TGG CTA CTC AGA AG - 3'
WT reverse: 5'- CCC CTC TCA CTC TTG ATT TCC TAC TGA CAC - 3'

KO forward: 5'- CAG GAT CAT CCA TGA AGA TGG CTA C - 3'
KO reverse: 5'- GCA CTC AAA CCG AGG ACT TAC AGA AC - 3'

The reaction mix and PCR programme for *GNAI2* genotype of each sample was as follows:

<u>PCR 3</u>
For WT allele

- 6.1 µl HotStarTaq Mastermix (Qiagen) (DNA polymerase, PCR buffer, and deoxynucleotides)
- 21.8 µl distilled water
- 3.0 µl primer mixture (5 µM forward, 5 µM reverse)
- 1.0 µl $MgCl_2$
- 1.0 µl DNA

For KO allele

- As for WT allele but without $MgCl_2$ and with 22.8 µl water

1. Heat lid to 110 °C
2. 94 °C for 5 minutes

3. 35 cycles
    a. 94 °C for 1 minute
    b. 60 °C for 1 minute
    c. 72 °C for 2 minutes
4. 72 °C for 10 minutes
5. Store at 8 °C

PCR products were run on a 1% agarose gel as for cardio-specific knockout genotyping.

2.4 Phenotypic assessment of cardiovascular function in mice

2.4.1 Assessment of left ventricular contractile function

Various modalities are available for use in assessing murine cardiac contractile function. These include echocardiography (echo), magnetic resonance imaging (MRI), ventricular catheterization with pressure-dimension/volume loops, radiolabelled microspheres, and thermodilution techniques[244,245].

Cardiac catheterisation for example, on the one hand offers the means of directly obtaining indices of left ventricular function, which in themselves are perhaps less operator-dependent than echo. However, the technique is highly invasive, making it a terminal procedure. The values obtained are pre-load dependent, and are pressures, and therefore only surrogates of ventricular function[245]. And the accuracy and relevance of a model in which a catheter of not dissimilar diameter to the aortic valve through which it traverses, and the left ventricular cavity, in which it sits, has to be questioned. In the human these issues are of far less importance given the relative size of the catheter to these structures.

Magnetic resonance imaging assessment of cardiac function in mice is a technology in evolution, and has recently been compared with echocardiographic assessment[246]. This study found better interobserver reproducibility with echo than MRI, and moderate agreement in measurements between the modalities. Radiolabelled microsphere and dilution techniques allow assessment of cardiac output, blood and plasma volume, but not ejection fraction (EF)[247].

Echocardiography

Use of echo was previously restricted by technical limitations such as frame rate relative to heart rate, and appropriate transducer frequency for the small tissue depth of the murine thorax[244]. However, current generations of hardware have overcome these difficulties. Echocardiography offers several advantages over other techniques: first and foremost, it enables real-time, direct visualization of left ventricular contractility; secondly, as it is non-invasive, repeated assessments can be performed at different time points on the same animal; thirdly, although as with any technique there is a learning curve, the fundamentals are easier to grasp than magnetic resonance imaging, for example.
Possible disadvantages of the technique include the use of anaesthesia to immobilise the animal with resultant effects on contractility, and the variability in quality of images obtained, in particular of endocardial definition. This in turn affects reliability of measurements.

With regard to anaesthesia's effects on contractile function, investigators have used various anaesthetic/sedative agents and studied the effects on murine cardiac function, as well as assessing the importance of heart rate under anaesthesia. The increase in contractility seen with faster heart rates is known as the Bowditch effect or 'treppe' phenomenon[248], and was documented as long ago as 1871 in humans. The effect has also been demonstrated *in vivo* in mice undergoing echo[245] and in Langendorff-perfused murine hearts[191], although other investigators have shown a negative force-frequency relationship in rodents, particularly at low stimulation frequencies, suggesting a more complex relationship in these mammals[249,250].
In their study using C57BL/6 mice, Gentry-Smetana et al investigated the effects of different concentrations of isoflurane and sevoflurane on echocardiographic parameters of contractile function[251]. They found that with isoflurane, there was a trend in reduction of fractional shortening (FS) with increasing concentrations, although this did not become significant until an isoflurane concentration of 4%. EF became significantly reduced at 3%, but was still approximately 65% at this concentration. These findings suggest that a reduction in heart rate alone is not the sole cause for the reduction in contractile function observed in other studies, and that anaesthetic agents may exert direct effects in a concentration-dependent manner. Evaluation in conscious, non-anaesthetised mice have been performed but are much more technically challenging. Janssen et al compared cardiovascular parameters

including heart rate and cardiac output in conscious and anaesthetised mice[252]. The anaesthetic agents used were isoflurane at 1% and 2%, ketamine-xylazine alone, and in combination with isoflurane, and pentobarbital sodium. Whilst all anaesthetic regimes induced significant reduction in both heart rate and cardiac index, the differences observed were least for isoflurane 1%. The largest reductions in both cardiac index and heart rate were seen with both ketamine-xylazine regimes.

In summary, it is difficult to tease out whether the reduction in contractile function seen with anaesthetic agents is due to their direct effects, or is a consequence somehow of the concomitant negative chronotropy; possibly both mechanisms operate. Some conclusions can be drawn however: if anaesthesia is to be used for echocardiographic assessment of murine ventricular function, isoflurane appears to be the most suitable agent, as it is easily titratable, and appears to have the least effect on both heart rate and contractile function at low concentrations. In addition, to ensure reproducible measurements, and to obtain good approximations of ventricular function in the conscious mouse, the heart rate during anaesthesia should be at least 400bpm.

Various echo measures of LV contractility are possible. The simplest is FS, which also has the advantage of being a non-derived parameter without assumptions. This involves performing 1D chamber size measurements in systole and diastole. From this, it is possible to calculate an EF, based on assumptions of uniform contractility of all LV walls. Whilst reasonable in baseline studies (prior to intervention), such measurements are clearly likely to be inaccurate in a myocardial infarction model where regional wall motion abnormalities (RWMAs) result from infarction. Fractional area change (FAC) is a means of incorporating these RWMAs into the assessment and is recommended for use in models of myocardial infarction[203,211]. The endocardium is traced at end systole and end diastole (EndoAreaS/D), and used to derive the percentage FAC, according to the formula:

Fractional area change (%) = (EndoAreaD – EndoAreaS) * 100 / (EndoAreaD)

Typically, the endocardium is traced at the mid-ventricular level, although additional measurements at the apical level can be incorporated.

2.4.2 Electrocardiography

As discussed previously, 12-lead ECGs are commonly recorded in humans to enable some assessment of regional myocardial electrophysiology. Nevertheless, a single lead ECG can provide information on heart rate and rhythm, and allow measurement of intervals provided it is of sufficient quality.

Murine heart rates are typically 550-650bpm – approximately eight to ten times faster than that of humans. The shorter intervals on murine ECGs result from smaller cardiac chamber sizes and muscle masses, and hence shorter times required for impulses to propagate throughout the myocardium and for cells to repolarize. For example, a typical corrected QT interval (QTc) in humans is 420ms, whereas in mice it is approximately 45-50 ms, after correction with an alternate formula[253]. From Figure 21 it can also be seen that the morphology of the murine T wave differs substantially from that of the human, as already described.

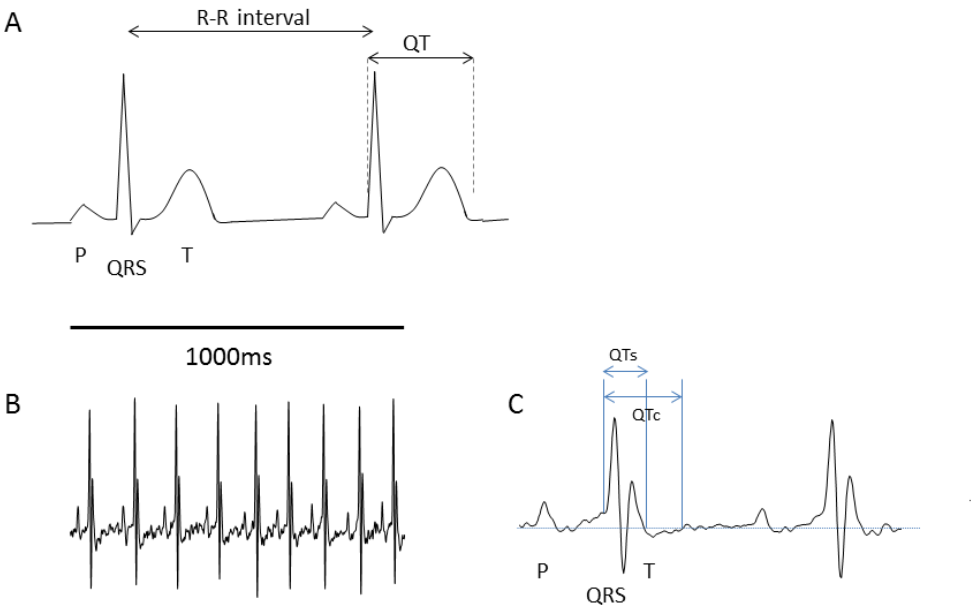

Figure 21 Comparison of human and murine ECGs with intervals. A: human ECG with P and T waves, QRS complex, R-R and QT intervals marked. B: Murine ECG on same time scale as for human. C: Focus on two murine ECG complexes to illustrate difference in T wave morphology compared to that of humans.. QTs: QT interval at intersection of T downstroke with isoelectric line; QTc: QT interval at return of negative limb of T wave to isoelectric line.

There are currently two available systems for recording ECGs in conscious mice: implanted telemetry probes, and recording platforms. The former are small devices that require surgical implantation, either subcutaneously or intra-abdominally. They

record a single lead ECG and transmit to a receiver, typically situated under the cage. Advantages include the ability to record the ECG in the mouse's usual environment, at any time of the day or night, thereby avoiding problems of the stress of an unusual environment, and possibly short, unrepresentative recordings. Disadvantages include surgical implantation, with a recovery period of 1-2 weeks, the unknown effects of a foreign body on heart rate, and expense. These factors also discourage large sample sizes.

The ECGenie is a system designed to allow ECG recording from conscious mice, without the need for surgery[254]. It consists of a recording platform with electrodes on which the mouse is placed (Figure 22). The ECG is recorded through the animal's paws when in contact with the electrodes. Another advantage is the ability to record ECGs from mice in a comparatively short space of time, and to perform repeat recordings.

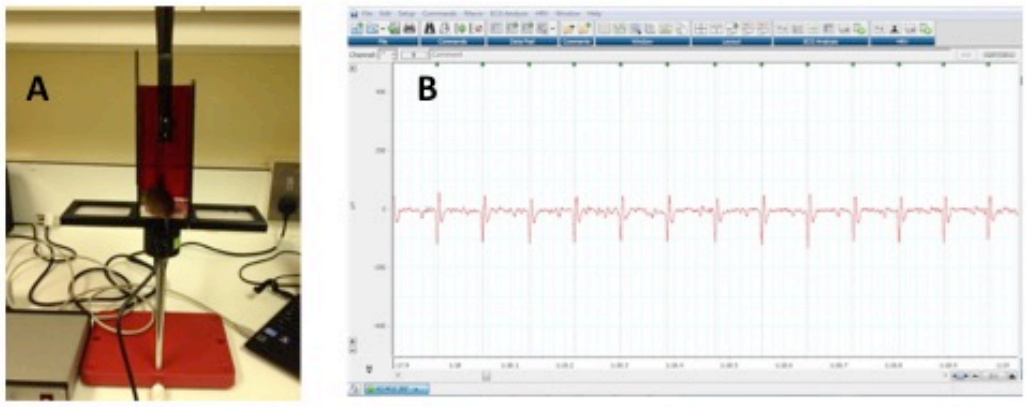

Figure 22 ECGenie. A: platform with mouse on recording pad. B: representative ECG recorded in LabChart with R wave markers.

A number of parameters, measurable from the ECG, have been found to be of prognostic use in humans. These include the durations of the QRS complex and corrected QT intervals, as well as presence of premature ventricular complexes (PVCs) and non-sustained ventricular tachycardia (NSVT)[132,140]. The PR interval is useful in providing a measure of conduction time and AV nodal function.

2.4.3 Heart rate variability (HRV)

The principles underlying this technique, which quantifies the normal oscillation in the beat to beat interval of the heart (the R-R interval from the ECG), were described in

Section 1.4.2. Time and frequency domain measures can be used; with the latter, the HF component of the power spectrum is largely dependent on parasympathetic inputs. Extrapolating these findings, HRV has been used as a means of assessing autonomic balance in mice. As already discussed, murine heart rates are much faster than humans', and adjusted HRV indices are therefore used[255,256].

2.4.4 Electrophysiological study (EPS)

This technique involves transvascular placement of a catheter in the heart, to enable recording of intracardiac EGMs and pacing of either the right atrium or ventricle. Response to pacing enables physiological assessment of the sinoatrial and AV nodes, and propensity to arrhythmia can also be assessed. In the ventricle, this is done with programmed ventricular stimulation, which has been used since the early 1970s [257]. Several indications have been described, including risk stratification following MI to guide decisions on ICD therapy. However, it is has fallen out of favour in recent years due to concerns regarding its specificity and predictive powers. The principle underlying the technique is that in hearts prone to development of ventricular arrhythmias, these can be induced by artificially stimulating the heart, and that this technique can help predict those in whom this is most likely to occur spontaneously.

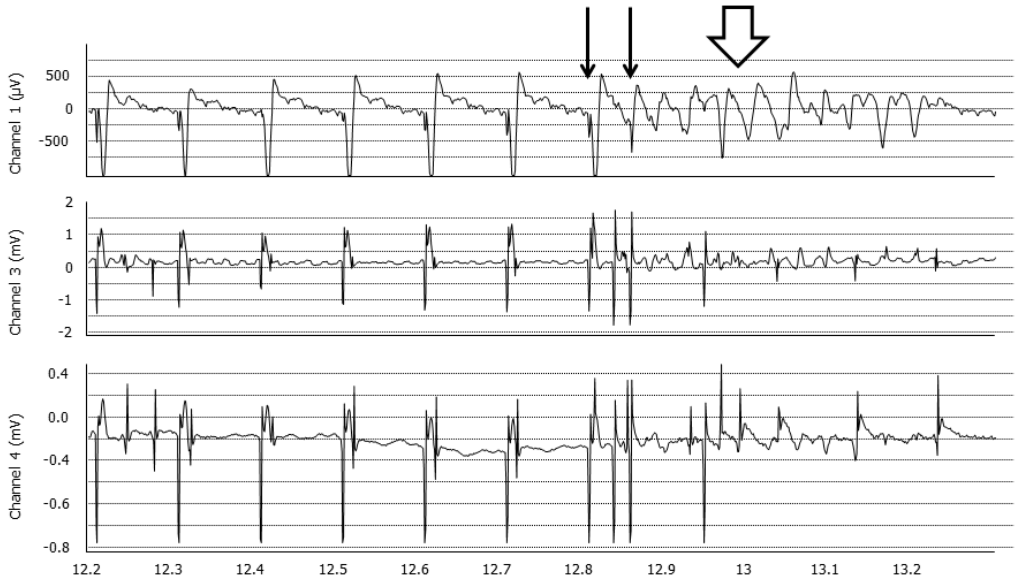

Figure 23 Programmed ventricular stimulation with non-sustained VT (NSVT) in a mouse. Thin arrows indicate last beat of pacing at fixed interval and extrastimulus. Wide arrow indicates NSVT.

Different protocols exist, and pharmacological adjuncts such as isoprenaline may be used, although what the latter mimics is open to debate. The technique can be modified for investigation in mice, with introduction of the catheter through the right internal jugular vein, and hence serves as another tool for assessing arrhythmic potential (see Figure 23).

2.5 Echocardiography

2.5.1 Equipment

All studies were performed using a Visualsonics Vevo 770 Imaging System. A 30 MHz ultrasound probe was used, at a sampling rate of 100 frames per second. Studies were performed in a dedicated room.

2.5.2 Protocol

Mice were anaesthetised initially with a 2% isoflurane/oxygen mixture in an anaesthetic chamber. They were transferred to a heated table incorporating rectal body temperature feedback and heart rate monitoring, which was linked to the echo machine. Anaesthesia was continued at this stage via a nose mask with 1.5% isoflurane in oxygen and a scavenging system.

Chest hair was removed using Veet hair removal cream. The following echocardiographic measurements were obtained from parasternal short axis recordings at the mid-ventricular level: end-diastolic and systolic endocardial areas; anterior and inferior LV wall thickness from 2D images; wall thickness, internal dimensions in diastole and systole from M-mode recordings. Two sets of each measurement were made per mouse (see Figures 24 and 25). All measurements were taken with heart rate over 400 beats per minute (bpm), and body temperature 35-37°C.

In addition, the following calculations/derived measurements were noted: fractional shortening (FS) and EF from M-mode measurements; fractional area change (FAC) for 2D endocardial measurements. The following formulae were used to calculate these:

1. Fractional shortening (%): 100 * ((LVIDd – LVIDs) / LVIDd
2. Ejection fraction (%): 100 * (LVvolD – LVvolS)/LVvolD
3. LVvolD (µL): ((7.0 / (2.4 + LVIDd)) * $LVIDd^3$
4. LVvolS (µL): ((7.0 / (2.4 + LVIDs)) * $LVIDs^3$
5. Fractional area change (%): (EndoAreaD – EndoAreaS) * 100 / (EndoAreaD)

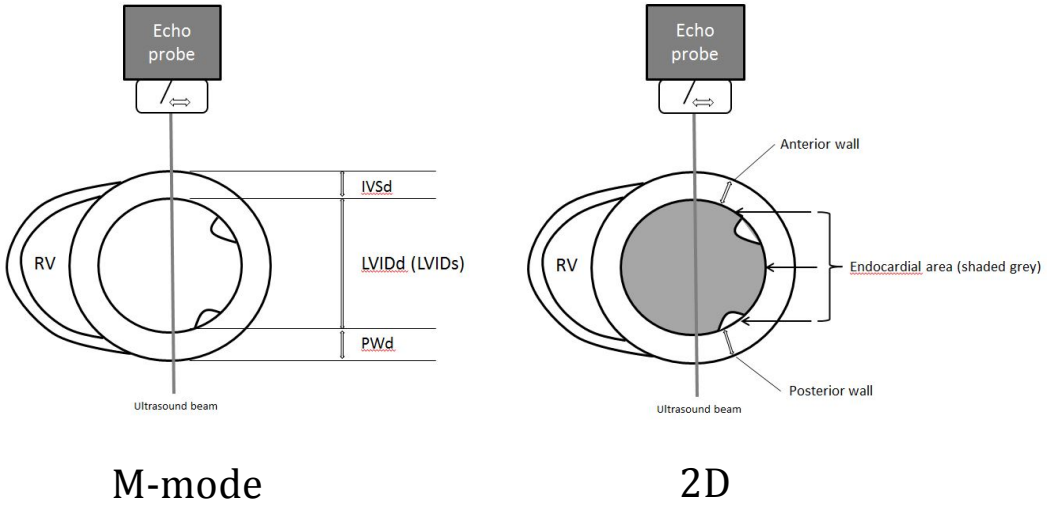

Figure 24 Illustration of echocardiographic measurements made on left ventricle. M-mode (left) and 2D measurements (right). RV: right ventricle, IVSd: interventricular septum in diastole, LVIDd/s: left ventricular internal dimension in diastole/systole, PWd: posterior wall in diastole.

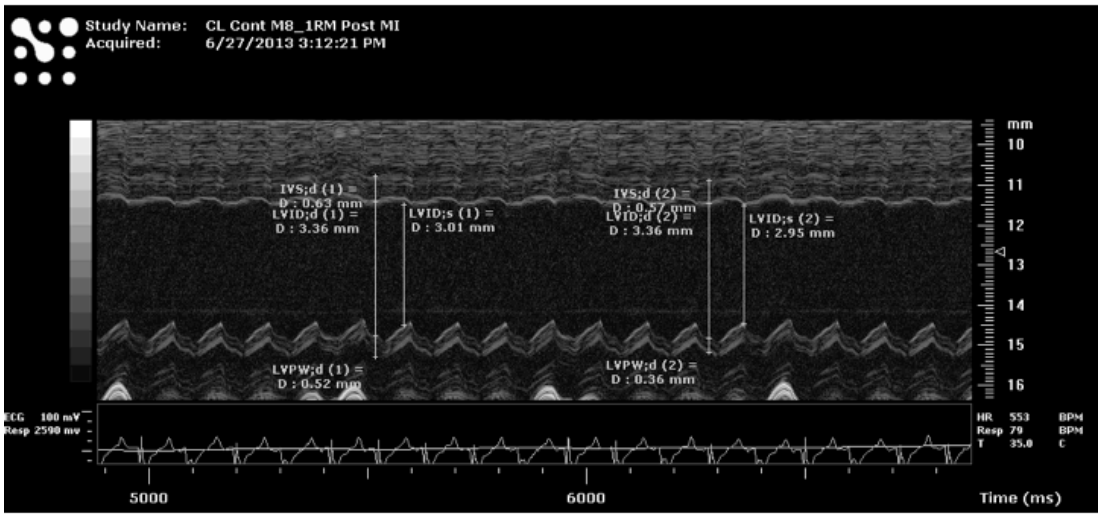

Figure 25 Illustrative example of M-mode echocardiographic recording. Measurements made as illustrated in Figure 24. As can be seen, the anterior wall is barely contracting, although there is impaired but visible contraction of the posterior wall. The FAC post-MI for this mouse was 41%.

2.6 Isoprenaline (isoproterenol) model of heart failure

Two dose-ranging studies were performed, using different methods of administration: subcutaneous pellets designed to release over 21 days, and daily subcutaneous injections. Prior to the first study, the literature was reviewed for previous similar experiments. No studies utilising pellets were found; three studies using mini-osmotic pump delivery or injections were identified and used to guide dosing[225,258,259]. Based on doses of 15, 30, 45 and 60 mg/kg/day for 21 days for mice of 25-30 g, and considering the pellet doses available from the supplier (Innovative Research of America), pellet doses of 7.5 mg, 15 mg, 25 mg and 35 mg were chosen. These were supposed to elute over 21 days, thereby administering the target doses.

In the first part of the dose-ranging study using subcutaneous pellets, 11 WT mice of C57BL/6 strain under 6 months old were weighed, and underwent baseline echocardiogram. Under isoflurane anaesthesia, skin overlying the upper back was cleaned with chlorhexidine gluconate 0.5% (Ecolab Ltd, UK) and a small incision made. The isoprenaline pellet was inserted under the skin, and the wound closed with Mersilk 5.0 (Ethicon LLC, USA). One mouse died two days post-implant; all others underwent repeat echo at day 6-12, day 14-18 and day 22.

Evaluation of the results revealed that none of the mice developed LV impairment (reduced FS or EF) (this fact is mentioned here to explain the rationale for proceeding as described). This second part of the study was initiated using higher doses of 50 mg, 67.5 mg and 75 mg in four mice. These underwent echocardiogram at baseline and 14 days. However, none of these mice developed LV impairment by 14 days and were therefore culled. Some mice from both groups developed sores over the implant site. It was decided to try another route of administration in case the lack of effect was related to delivery from the pellets, and in view of the skin sores and costs of pellets and mini-osmotic pumps.

The protocol was based on a study published by Horiuchi-Hirose et al[260]. (-)-isoproterenol hydrochloride (Sigma-Aldrich) was reconstituted by dissolving 1.8 mg isoproterenol in 3 mL 0.9% saline. Five mice of 129Sv background underwent baseline echocardiogram, and then received daily injections – three at 0.1 mL/10 g, and two at 0.15 mL/10 g bodyweight (equivalent to 6 mg/kg/day or 9 mg/kg/day, respectively). This daily dose was considerably lower than that used with the pellets, but was adopted as the authors of the study had had success in inducing LV impairment with

this approach, and because it was assumed absorption is likely superior with injections compared to pellets.
For the first 15 days, the injections were performed after anaesthetising the mice with isoflurane. However, the mice were bradycardic at the time of echocardiographic studies, and as this was thought possibly related to the repeated exposure to isoflurane, injections for the remaining days were performed without anaesthesia. Echo was performed at 8, 15 and 22 days to measure FS, EF and cavity size (LVIDd).

2.7 Model of myocardial infarction-induced heart failure

All procedures were performed in the Biological Services Unit at the Charterhouse Square campus of Queen Mary University of London by myself.
Coronary ligation is the most common means of inducing myocardial infarction in rodents, and initially this technique was used. Poor survival led to exploration of modifications of the technique, including cauterisation and cryoinjury, as described below. All four mice which underwent cryoinjury died during the procedure, and of the four mice which underwent cauterisation, two died intraoperatively, with the two survivors showing evidence of only small areas of myocardial infarction on echo and histology. Further help with the coronary ligation model was therefore sought, leading to slight modifications of the technique with improved results. These issues are described here for the sake of brevity, so that the Results and Discussion can focus on the main study, performed using coronary ligation.
Two sets of results are reported in *Chapters 3* and *5*: a preliminary histology correlational study (described in *Section 3.5*), and the main study comparing control mice to cKOs (reported in *Section 5.3*). For this, 18 controls (genotype $G\alpha_{i2}^{WT/WT}$ Cre-, $G\alpha_{i2}^{WT/WT}$ Cre+, $G\alpha_{i2}^{Flx/WT}$ Cre-, or $G\alpha_{i2}^{Flx/Flx}$ Cre-) and 16 cKOs (i.e. genotype $G\alpha_{i2}^{Flx/Flx}$ Cre+) were studied. Mice were aged 10-15 weeks old at time of coronary ligation surgery.

2.7.1 Coronary ligation

Operative technique was similar to that described by Tarnavski and Borst[211,212]. The mouse undergoing coronary ligation was anaesthetised in a chamber with 2%

isoflurane, prior to being transferred to the operating field, consisting of a sterile drape placed over a heating mat. Inhalational anaesthesia (2% isoflurane in 1L/min oxygen) was continued here via a nose cone delivery/scavenging system. The mouse's paws were taped to the drape, with the left lower limb pulled across the body to the right side. Hair on the anterior thorax and neck was removed with a clipper, and these areas were cleaned with chlorhexidine gluconate 0.5%. The skin overlying the left lower thorax was cut, and stretched to expose the underlying muscles. The skin overlying the central neck was cut, and the muscles were dissected to expose the trachea. Elastic stay hooks (Harvard Apparatus, UK) were used to retract the paratracheal muscles and maintain visibility of the trachea. At this stage, the isoflurane concentration was increased temporarily to 4% for approximately a minute, to ensure deep anaesthesia during intubation. The nose cone delivery system was removed, and the head retracted using a piece of plastic thread around the upper teeth. A metal cannula attached to the ventilator (Minivent Type 845, Harvard Apparatus UK) was then inserted into the trachea, after which inhalational anaesthesia was resumed (2.5% isoflurane in 1L/min oxygen), with stroke volume of 175 μL and respiratory rate of 180/min.

ECG electrodes (Needle electrodes, ADInstruments) were inserted into the muscles of each limb and connected via a signal amplifier (Bioamp, ADInstruments) and data acquisition device (Powerlab 4/35, ADInstruments) to a computer running LabChart (ADInstruments, UK), so as to record a single lead ECG in real time.

The muscles of the left anterior thorax were dissected to expose the lower ribcage, and an incision was made in either the 3rd or 4th intercostal muscle using a combination of diathermy and blunt dissection. The left lung was deflated partially to allow visualisation of the heart, by temporarily switching off the ventilator and applying pressure to the lung. A retractor was used to open the intercostal incision further. The pericardium was incised, and the heart manipulated into view by pressure on the right thorax. A Prolene 8.0 suture (Ethicon LLC, USA) was passed 1-2 mm distal to the tip of the left atrium to encircle the left main coronary artery, and was tied twice. Coronary ligation was confirmed by noting ensuing pallor of the left ventricle, and by observing ST elevation on the ECG, after which the suture was cut.

The intercostal incision was closed using Mersilk 5.0 (Ethicon LLC, USA) with interrupted sutures. The left lung was re-expanded concomitantly by transient occlusion of the ventilator outflow to increase positive end-expiratory pressure. At this stage, 3 μg buprenorphine (Reckitt Benckiser Healthcare UK) was administered intramuscularly. The skin incisions over the left thorax and neck were subsequently

closed with Mersilk 5.0 using continuous sutures. Inhalational anaesthesia was discontinued, needle electrodes were removed, and tape was removed from the mouse's paws. Once the animal made purposeful movements, the endotracheal tube was removed. The mouse was placed in a cage on a heating mat, with post-operative observation and review as already described.

2.7.2 Cauterisation

The technique used was similar to that of coronary ligation up to the stage of passing the ligature. At this stage, a small-tipped soldering iron was used to cauterise a small area 1-2mm distal to the tip of the left atrium. Several applications of 2-4 seconds were used. The remainder of the procedure was the same as for coronary ligation.

2.7.3 Cryoinjury

The technique used was similar to that of the two techniques above. The small-tipped soldering iron which had been left in dry ice was applied to the anterolateral border of the heart at the stage of passing the ligature. At this stage, all mice studied became bradycardic before asystole ensued.

2.7.4 Post mortems

All mice in the myocardial infarction study that died following coronary ligation underwent post mortem examination within 24 hours of death. This included laparotomy and thoracotomy to examine the liver and chest viscera. The liver's colour was noted, as was the presence of blood in the chest cavity, deemed indicative of myocardial rupture in association with a pale liver. Location of the myocardial ligature was noted, and the left ventricular wall was examined for tears and/or thinning.

2.7.5 Histological assessment of infarct size: preliminary correlational study

As part of a coronary ligation pilot study involving 10 mice, to establish feasibility of the model, and satisfactoriness of echo in assessing extent of left ventricular scar and infarct size, the hearts from the 10 mice underwent histological analysis (for results see *Section 3.5*).

Following echocardiographic assessment one week after coronary ligation, mice were culled by $C0_2$ inhalation and cervical dislocation. Hearts were removed and placed into 10% neutral buffered formaldehyde. They were then prepared in paraffin, and cut into basal, mid-ventricular, and apical segments 3-4 μM wide. Sections of these were stained with Masson's trichome, which stains muscle red/pink, and collagen green/blue.

Photographs of the sections were taken using a digital camera (BZ-8000, Keyence Corp, Japan). For each section, the endocardial and epicardial lengths of the infarcted section of the left ventricle were measured, where collagen was present in ≥ 50% of the wall thickness, using AnalyzingDigitalImages software (Museum of Science, Boston, MA), and the mean calculated; the same calculation was performed for the endo- and epicardial circumferences of the left ventricle. The percentage infarct size was calculated as mean infarct length divided by mean total LV circumference, as has been previously described[261,262]. This was chosen in preference to area measurements which tend to underestimate infarct size once scar tissue has replaced cardiomyocytes, leading to thinning of the ventricular wall.

Other methods of infarct size assessment have been described[211,263], and the method to some extent depends on the timing of organ harvesting in relation to the infarct. Left ventricular wall thinning, and replacement of necrotic tissue with collagen, occurs in the first few days post infarction, and is well-established at one week. Masson's trichome was chosen as it has been used extensively in this setting, and clearly delineates infarcted from healthy tissue[264].

2.8 ECGenie protocol

Recording was carried out in a quiet room in the animal facility. One mouse was placed on the recording pad of the platform, with a second mouse on the side platform. They were left to acclimatise for 15 minutes before recording started. Continuous recording

through LabChart was performed for 5-10 minutes typically, to ensure capture of sufficient length of ECG trace which would allow analysis of PQRST morphology and intervals, and HRV analysis. Sampling and filter settings were as follows: 2 kHz sampling, bandpass 3-100 Hz, with 50 Hz and 'Mains' filters. Due to only intermittent contact of the mouse's paws with the recording electrodes, sections of analysable ECG lasted anywhere from 5 seconds to over 5 minutes. Mice were conscious at all times.

2.8.1 ECG analysis

For analysis of ECG parameters (heart rate, PR and QT intervals, QRS duration), and presence of PVCs or VT, three epochs were recorded to enable averaging and to ensure the impact of transient physiological/environmental fluctuations was minimised. The 'cleanest' sections of ECG (i.e. those with lowest noise and artefact levels) were chosen. Typically, two 10 second epochs and one 20-25 second epoch were used, the latter also serving as the section for HRV analysis.

All recorded sections of 'clean' ECG were reviewed prior to analysis. The LabChart software allows for semi-automated ECG analysis, including R wave marking. Each section was reviewed by myself, with manual adjustments to R wave markers made if necessary. Similarly, the signal averaging tool used to generate an ensemble PQRST complex from which intervals were measured, was also reviewed and manually adjusted to ensure accurate measurements. Two QT interval measurements were made on baseline recordings (see Figure 21): for the first, duration from the onset of the QRS to the intersection of the first slope of the T wave with the isoelectric line was recorded (QTs); for the second, the duration from the QRS onset to the intersection of the more protracted, lower amplitude section of the T wave with the isoelectric line was recorded, and corrected with the formula published by Mitchell et al[253] (QTc).

2.8.2 Heart rate variability analysis

For HRV analysis, the same procedure of review and manual adjustment of R wave markers was performed as described above. All beats were regarded as sinus beats, as observation of numerous recordings revealed that some mice have marked variability in beat to beat interval which is usually sinus rhythm (i.e. sinus arrhythmia), and because the quality of the trace often did not permit P waves to be accurately

identified. Markedly premature beats of ventricular origin were exceptionally rare, and therefore not considered to have any significant impact on results. Analysis settings were as follows: Histogram bin size: 10 ms; FFT (fast Fourier transform) size: the lowest exponent of 2 greater than the recorded number of beats, typically 512; Window: Welch; Overlap: ½; Max frequency 5 Hz, Frequency bands: 0.4 < LF < 1.5 < HF < 4 Hz. There is some debate about the precise limits of frequency bands, as there is in humans. In fact, murine HRV frequency bands are largely derived from extrapolation of those in humans. The values chosen were those from a previous study from our group[108]. The following average indices were recorded:

- mean N-N interval (equivalent to R-R interval)
- median N-N interval

The following time domain indices were recorded:

- N-N range
- standard deviation of N-N (SDNN)
- standard deviation of delta N-N (SD delta NN)
- root mean square of successive differences (RMSSD)

The following frequency domain indices were recorded:

- total power (Tpower)
- very low frequency (VLF, < 0.4Hz)
- low frequency (LF, 0.4-1.5Hz)
- high frequency (HF, 1.5-4Hz)
- low frequency normalised units (LFnu)
- high frequency normalised units (HFnu)
- LF/HF ratio

The low and high frequency normalised units were derived from the formula

(LF or HF) / (TPower – VLF) *100.

2.9 Electrophysiological studies

Mice were anaesthetised with isoflurane: 2% at induction, followed by 1.5-2% maintenance anaesthesia via a face mask. The neck was dissected to expose the right internal jugular vein (RIJ). The cranial end of the vein was tied off with silk suture, and a suture passed around the caudal end (nearest the heart). A small incision was made in the vein, and a 1.1F octapolar miniature electrophysiology catheter (Millar Instruments) was passed through this to the heart. The catheter was connected to a signal amplifier (Bioamp, ADInstruments) and data acquisition device (Powerlab 4/35, ADInstruments),and intracardiac EGMs were recorded using LabChart. The catheter was manipulated until ventricular and atrial EGMs were seen.
Pacing protocols consisted of AV node Wenckebach point, ventricular effective refractory period (VERP), and ventricular tachycardia stimulation ("VT stim"). These protocols are detailed below.

2.9.1 Wenckebach point

In normal hearts, if the sinus nodal/atrial rate is fast enough, impulses fail to continue to conduct in a 1:1 fashion through the AV node to the ventricles. This occurs due to the decremental properties of the AV node. The point at which this begins to occur is known as the Wenckebach cycle length, and describes a situation where there is progressive delay in conduction of impulses, eventually leading to a non-conducted impulse, after which conduction resumes and the cycle repeats. The Wenckebach point/cycle length therefore provides a means of assessing AV nodal function.
Pacing of the right atrium was commenced at 500 bpm (120ms cycle length). If conduction to the ventricle occurred in a 1:1 fashion, the cycle length was reduced by 10ms. This process was repeated until either 1:1 conduction failed, or the AV interval prolonged to greater than the paced cycle length, rendering interpretation of the AV relationship difficult. The cycle length at which this occurred was noted as the Wenckebach point.

2.9.2 Ventricular effective refractory period (VERP)

This provides a measure of excitability of the ventricular tissue. Its relevance to arrhythmogenesis is related to the role of EADs and DADs in triggering tachycardia.

Although not uniformly applicable, a shorter effective refractory period can render tissue more amenable to excitation by EADs/DADs, as wavelength (the product of conduction velocity and refractory period) is reduced, a condition favourable to re-entry.

To ascertain VERP, the ventricle was paced at 600 bpm (100ms cycle length) for 20 beats. A paced beat of shorter cycle length (S2) was introduced at the end of this drive train, starting at a cycle length of 90ms. If the S2 captured the ventricle, the S2 cycle length was reduced by 10 ms. The process was repeated until S2 failed to capture the ventricle. The S2 with the highest cycle length that failed to capture was noted as the VERP.

2.9.3 Ventricular tachycardia stimulation ("VT stim")

This technique is an extension of VERP measurement, and is designed to mimic what may happen in patients when a succession of ventricular premature beats occur. In diseased hearts, this may trigger VT.

The protocol used was a slight modification of that previously described[94]. The ventricle was paced at 600 bpm (100 ms cycle length) for 20 beats. An additional beat (S2) was introduced at the end of this drive train 10 ms above the VERP cycle length. If no VT was induced, a further additional beat was introduced starting at 90 ms (S3), and the S3 cycle length reduced by 10 ms until non-capture. Again, if no VT was induced, S2 was held 10 ms above VERP, S3 was held at the shortest cycle length that achieved capture, and a further beat, S4, was introduced starting at 90 ms and reducing by 10 ms until non-capture. Intrinsic cardiac rhythm immediately following this programmed electrical stimulation was monitored: if at any stage during the process 4 or more intrinsic beats of different morphology to that of sinus rhythm at a rate>600bpm was achieved, this was noted as ventricular tachycardia (VT). Between 4 and 30 beats were classified as NSVT; over 30 beats were classed as sustained VT.

2.10 Microelectrode array (MEA) studies

Mice studied included those of WT *GNAI2* status (Gαi2 $^{+/+}$ littermates of gKOs, and $G\alpha_{i2}$ $^{WT/WT}$ Cre- or Gαi2 $^{Flx/WT}$ Cre- littermates of cKOs). All mice were on a 129Sv background.

Experimentation with various aspects of the technique for analysing tissue with the MEA was performed prior to commencing the studies. This process of optimisation is described below, prior to the methodology used in the MEA studies. Figure 26 illustrates the experimental setup. Detailed description of the steps is provided throughout Section 2.10, but in summary, experiments consisted of retrieval of the heart, perfusion on a Langendorff apparatus, slicing, preservation of slices, stimulation and recording of electrical signals.

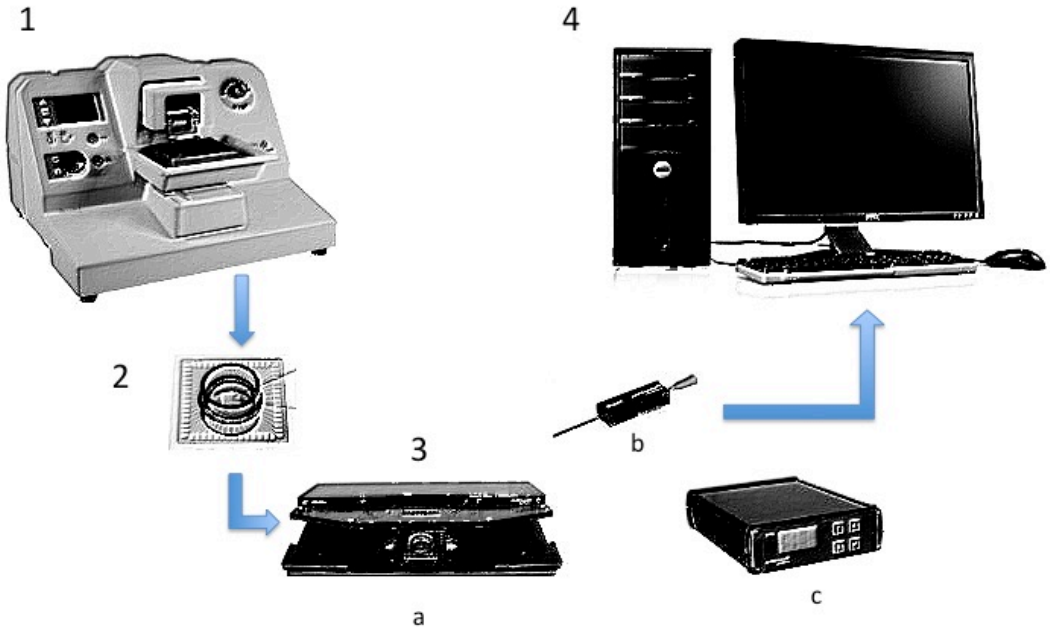

Figure 26 MEA system setup. After retrieval of the heart and retrograde aortic perfusion, the heart is sliced with a vibratome (1). When the slice is ready for use, it is transferred to the MEA (2) which is placed on the recording platform (3a). Modified Krebs is perfused through a cannula (b), the temperature of the perfusate is regulated (c). Signals are recorded and visualised on a computer (4).

2.10.1 Development and optimisation of technique

The technique of murine cardiac slice evaluation with the MEA had been used within our group, so some first hand observation was possible. However, two key aspects of the methodology were not accessible, as they required specialist software and understanding of MATLAB programming. They therefore suggested themselves as amenable to simplification, and possible improvement.

Stimulation: electrode configuration

The first was the means of stimulation of the slice, which had been achieved using a non-commercial external stimulator, with a stimulation program written in MATLAB (MathWorks, USA). This also involved uncertainty as to where exactly on the slice stimulation was occurring. A method of stimulation through the MEA was discovered, with the advantages that the precise location of stimulation would be known, as well as the ability to easily customise stimulation protocols. The 60PedotMEA200/30iR-Au-gr MEA (hereafter termed 'MEA'; Multi Channel Systems MCS GmbH, Germany) was chosen due to its lower electrode impedance, and hence ability to tolerate higher voltages. Its base is made from glass, and there are 60 electrodes made from carbon nanotube – poly 3,4-ethylene-dioxythiophene (PEDOT-CNT), with contact pads made from titanium-gold. Each electrode's diameter is 30 μM, with interelectrode distance of 200 μM.

Due to familiarity with voltage stimulation, this was initially employed in a unipolar manner, i.e. from one electrode. However, it was not possible to achieve capture within the recommended voltage limits, so bipolar current stimulation using adjacent electrodes was attempted. Initially this seemed to be more successful, although after experimentation, it was realised that whilst a bipolar configuration was specified, both electrodes did not always participate. Producing bipolar stimulation protocols was also more complex, and became particularly problematic when needing to restart a protocol after premature discontinuation, e.g. due to non-capture. As a result, unipolar current stimulation was used due to its consistency and relative ease of use. Capture of the whole slice at high currents was the major downside of this, and once appreciated care was taken to ensure this was not occurring, achieved in part by limiting maximum stimulation current to 100 μA.

Signal recording and calculation of conduction velocity

The second aspect was analysis of recorded signals and calculation of conduction velocity. The recording and file conversion were similar to that described below for my experiments. However, analysis and computation was performed using a custom-made MATLAB script. Given the time constraints, as well as the possibility that although mathematically more complex, this did not necessarily offer more accurate

representation of the tissue characteristics, an alternative method was developed using a limited number of signals with the program LabChart.

Heart slicing

An important modification was made to the way the excised heart was prepared for slicing. The dogma had been that it was necessary to structurally support the ventricles on the vibratome stage by embedding them in low melting point agarose. This required immersion of either the whole heart or just the ventricles within warm, liquid agarose, such that it would envelop the heart and fill its cavities. After a number of trials, several problems emerged. Firstly, the additional steps involved in preparing the agarose such that it would be at just the right temperature to remain in liquid form, yet not too hot that it would thermally injure the heart, were difficult to coordinate with the heart retrieval and Langendorff perfusion. Secondly, when agarose encases the epicardial surface and fills the ventricular cavities, there is no means by which the oxygenated buffer can perfuse the tissue. Thirdly, for reasons that were unclear, the block of agarose frequently fell apart when cutting began, or became unstuck from the vibratome stage, necessitating abortion of the experiment.
An alternative means of supporting the heart against cutting was tried and found to be effective. This consisted of gluing the ventricles directly to the removable metal stage, and gluing a small piece of polystyrene directly behind. This provided a buttress to support the heart against the cutting blade, helping to prevent folding or collapse of the ventricles. Despite its efficacy, one problem that emerged was that the glue used to stick the polystyrene occasionally adhered to the epicardial surface causing tissue damage and preventing smooth slicing. Therefore an even simpler method without the polystyrene block was tried; provided the ventricles were stuck to the stage properly, this worked well, and was therefore adopted for the experiments described in the *Chapter 7*.

Stimulation frequency

A resting mouse heart rate is typically 500-600 bpm, equivalent to a cycle length of 100-120 ms. Despite this, most published studies report stimulation at cycle lengths of 500-1000 Hz. Clearly it is desirable to try to test the tissue in a way that resembles *in*

vivo conditions as closely as possible. On the other hand, the tissue undergoes a good deal of physical and metabolic stress as discussed in *Section 1.9*, which reduces its tolerance of 'normal' heart rates. At the outset, stimulation cycle lengths of 150 ms and 250 ms were trialled. Although a number of successful experiments were carried out with the former, capture was less consistent, and the slices were prone to complete loss of capture before completion of the protocol, presumably due to tissue deterioration. Therefore 250 ms was chosen as a compromise.

Signal analysis

A final point in relation to signal appearances and analysis was that signals were rarely ideal, and often varied substantially over the course of an experiment. Familiarisation with signal appearances, what is acceptable, and which part of the signal is likely to represent local activation were learnt through observing and analysing a large number of experiments. Far-field components were recognised through their lower amplitude, lower frequencies, and coincidence with sharper signals elsewhere on the MEA.

2.10.2 Buffer solutions

The following modified Krebs-Henseleit buffer (hereafter termed 'Krebs') master solution was made up prior to slice preparation on the day of procedure (molecular concentration):
NaCl 6.896 g (118 mM), KCl 0.283 g (3.8 mM), $MgSO_4$-$7H_20$ 0.293 g (1.19 mM), $NaHCO_3$ 2.1 g (25 mM), KH_2PO_4 0.162 g (1.19 mM), D-glucose 0.9 g (5 mM), sodium pyruvate 0.220 g (2 mM) were dissolved in 1 L of distilled water.

This 'Calcium-free Krebs' solution was used to produce the following modified Krebs solutions:

1. Normal Krebs (Ca^{2+} 1.4 mM**,** K^+ 5 mM)
2. Perfusion-Slicing Krebs (Ca^{2+} 0.6 mM, K^+ 15 mM, BDM (10 mM, Sigma-Aldrich): 4 °C
3. Resting Krebs (same as Perfusion-Slicing Krebs): 21 °C
4. Preparation Krebs (Ca^{2+} 1.4 mM, K^+ 5 mM, BDM 10 mM): 21 °C
5. Bathing Krebs (Ca^{2+} 1.4 mM, K^+ 5 mM): 37 °C

To produce these from Calcium-free Krebs:

300 mL of Calcium-free Krebs was poured into a bottle and the following added to make Perfusion-Slicing Krebs:

i. 0.18 ml 1 M $CaCl_2$ to get 0.6 mM
ii. 0.224 g KCl to get 15 mM final concentration
iii. 300 mg BDM

50 ml of this was poured into a Falcon tube for use as Resting Krebs, and kept at room temperature. After bubbling with carbogen, some of remainder was used to make ice cubes (Perfusion-Slicing Krebs)

The remaining 700 ml of Calcium-free Krebs was used to make up Normal, Preparation and Bathing Krebs. 0.98 ml of $CaCl_2$ (1 M) was added to this volume. Two volumes of 50 ml were poured into Falcon tubes and chilled after bubbling for 15 mins (Normal Krebs). A further 50 ml was poured into a Falcon tube, to which 50 mg of BDM was added (Preparation Krebs). The remaining 350 ml was left at room temperature (Bathing Krebs).
The pH and oxygen content of Normal Krebs were measured to verify that as expected, they were within the physiological range. The results of three sets of measurements are shown in *Section 7.2*.

2.10.3 Cardiac slice preparation

Mice injected with 200 µl of heparin (5000 IU/ml, Leo Pharma, UK) intra-abdominally. After five minutes, they were culled by cervical dislocation with use of isoflurane anaesthesia only in difficult cases. Hearts were immediately removed after thoracotomy and placed in ice-cold Normal Krebs to remove surface blood and fill cavities with fluid. The heart was placed on ice covered by absorbent paper, and extraneous lung, adipose and thymus tissue was removed. It was then transferred to a petri dish filled with Normal Krebs placed under a microscope, and the aorta was pulled over a metal aortic cannula, secured by tying a thread around the aorta.
The cannula and attached heart were transferred to a perfusion (Langendorff) system with bubble trap primed with ice-cold Normal Krebs. The heart was perfused at a rate

of 2-3 ml/min for 60-90 s, after which the perfusate was changed to Perfusion-Slicing Krebs. This was continued until contractions terminated.

The heart was removed from the Langendorff system and transected at the level of the atrioventricular grooves to separate the atria and ventricles. The ventricular base was glued to a cylindrical metal 'coin', and this was placed in a chamber on the vibratome (Vibrating Microtome 7000-smz2, Campden Instruments Ltd, UK). The chamber was filled with Perfusion-Slicing Krebs at 4 °C, and the previously frozen ice cubes were used to maintain a low temperature. After removal of the apex, three slices of thickness 250 µM were cut with slicing settings – frequency 50 Hz, amplitude 1.00 mm, z-deflection < 2 µM, and advance rate 0.02 mm/s. After each slice was cut, it was transferred to a Falcon tube containing carbogenated Resting Krebs at room temperature. Slices were kept in Resting Krebs for 30 minutes, after which they were transferred to carbogenated Preparation Krebs also at room temperature.

Prior to transferring each slice for recording, the MEA setup was primed by flushing the system with distilled water, followed by Normal Krebs to ensure the inflow tubing and the MEA were both filled with this. Temperature of the perfusate was maintained at 37 °C with a two channel temperature controller and heatable perfusion cannula with temperature sensor (TC02 and PH01, Multi Channel Systems). A slice was subsequently placed in the Krebs-filled MEA, and a small home-made circular mesh 'slice holder' was used to maintain slice contact with the electrodes while allowing simultaneous contact with the perfusate (Figure 27). This was returned to the

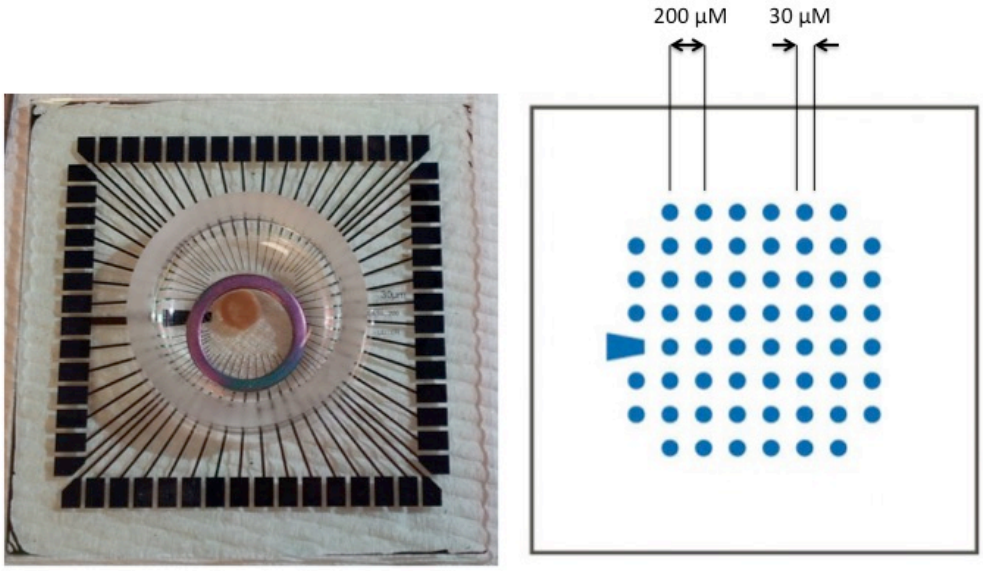

Figure 27 MEA with ventricular tissue slice (left). Illustration of electrode diameter and interelectrode distance (right).

headstage (MEA2100-HS, Multi Channel Systems) and perfusion with Normal Krebs started with a pump (Mini-Peristaltic Pump II, Harvard Apparatus UK). The slice and slice holder were manipulated so that as many of the MEA electrodes as possible were covered by homogeneous, unfolded tissue.

2.10.4 Stimulation

Unipolar stimulation of the slice was commenced straight away using MC_Rack version 4.5.11 (Multi Channel Systems). An electrode at the periphery of the MEA was selected, and the following initial settings were used: a biphasic pulse of -40 μA for 1 ms and 40 μA for 1 ms at a cycle length (CL) of 1000 ms. If no capture was achieved, stimulation via a different peripheral electrode was tried. This was repeated until capture was achieved; if necessary, non-peripheral electrodes were utilised. If no capture was achieved after 15 minutes, the slice was discarded. If stable capture was achieved, the stimulation CL was reduced to 500 ms after 20-25 minutes and threshold was determined. Output current was set at twice diastolic threshold in all experiments. After 30-40 minutes, the CL was reduced to 250 ms; often at this stage, it was necessary to change the stimulating electrode due to either lack of consistent capture, or EGMs of inadequate quality to permit measurement of activation time (a sharp downstroke separate from the pacing stimulus). Care was also taken to avoid stimulating such that wide capture appeared to occur, as indicated by simultaneous activation across the MEA. If the stimulating electrode was changed, the threshold was re-determined and output adjusted accordingly. The electrode was not changed once the experiment proper had begun, i.e. commencement of measurements.
Preconditions for continuing the experiment past this point were:

- Consistent capture
- A discernible downward deflection within 5 ms of the stimulus artefact on an electrode within 400 μM of the stimulating electrode, to allow measurement of local activation time ('reference electrode' signal)
- Increase in activation time with increasing distance from the stimulus
- At least two good quality EGMs ≥ 600 μM from the reference electrode

2.10.5 Stimulation protocols

Once consistent capture at a CL of 250 ms had been achieved, two stimulation protocols were employed in all experiments. The first, to determine ERP, utilised scripts written with MC_Stimulus II version 3.4.4 (Multi Channel Systems) by Dr David Montaigne. Four versions of the same script were written, differing only by the current output specified to allow stimulation at twice diastolic threshold (at 40, 60, 80 and 100 μA). Biphasic current pulses as described above were utilised. S2 decremented by 10 ms between 140 ms and 70 ms, whilst between 62 ms and 20 ms, there were 2 ms decrements after each 10 stimulus drive train of S1. This was to allow precision over the expected range of ERP, whilst not prolonging the experiment unnecessarily. An outline is shown below:

- Initial run-in of 30 stimuli at 250 ms (S1)
- Premature beat (S2) at 140 ms
- 10 x S1 at 250 ms
- 1 x S2 at 130 ms
- 10 x S1 at 250 ms
- 1 x S2 at 120 ms
- …
- 10 x S1 at 250 ms
- 1 x S2 at 70 ms
- 10 x S1 at 250 ms
- 1 x S2 at 62 ms
- 10 x S1 at 250 ms
- 1 x S2 at 60 ms
- …
- 10 x S1 at 250 ms
- 1 x S2 at 20 ms

By setting up a long-term display, and a trigger from the stimulus, two data displays could be set up to allow real-time visualisation of capture adjacent to the stimulating electrode and at a distal electrode. In this way, ERP was ascertained on the fly, and was determined twice for each time point/drug concentration/temperature.

To measure activation times and conduction velocity, stimulation was performed at CL of 250 ms for 8-10 s (32-40 stimuli) to achieve a steady state and ensure consistent capture. On occasion this had to be repeated, for example if there was frequent spontaneous activity which interfered with capture. Sampling frequency was 10 kHz. This whole epoch was recorded using the MC_Rack software as a .mcd format file. This was subsequently converted to an ASCII .txt file using MC_DataTool version 2.6.13 (Multi Channel Systems) for the relevant MEA electrodes/channels, to permit reading and analysis in LabChart.
Each slice was used to obtain one set of ERP and conduction velocity measurements, at each cycle length where appropriate, i.e. one ERP and one conduction velocity protocol was performed per slice, stimulating via the same electrode throughout.

2.10.6 Analysis of activation times and calculation of conduction velocity

The heterogeneity of signals across the MEA meant that the same electrode data had to be used throughout the experiment to avoid erroneous changes being reported. For example, if the activation times at electrodes 12, 31 and 61 (e12, e31, e61) were 2.3, 4.1, and 1.7 ms at baseline, the mean is 2.7 ms. But if the signal in e31 was lost for some reason halfway through the protocol, assuming activation times otherwise remained unchanged, data would only be available for e12 and e61, the mean of which would now be 2.0 ms. Given that typically only a few electrodes distal (> 600 μM) to the reference electrode (the one within 400 μM of the stimulating electrode used to define earliest capture; see Figure 28) would show good quality signals at baseline, and the expectation was that not all of these would persist through the protocol, it was decided to require a minimum of two distal electrodes with good quality signals, in addition to the reference electrode close to the stimulus.
The method of analysis described below assumed linear impulse propagation across the MEA from the reference electrode to distal electrodes at which activation times were measured (see *Chapter 8* for debate regarding the validity of this assumption). This is illustrated in Figure 28.
The ASCII .txt file was opened in LabChart and a new channel created to display the first temporal derivative of the MEA electrode data being analysed. In this way, activation time in milliseconds could be measured from the commencement of the stimulus artefact to the maximum negative value on the derivative channel (Figure 29). By displaying the original channel data concurrently, the value measured could be

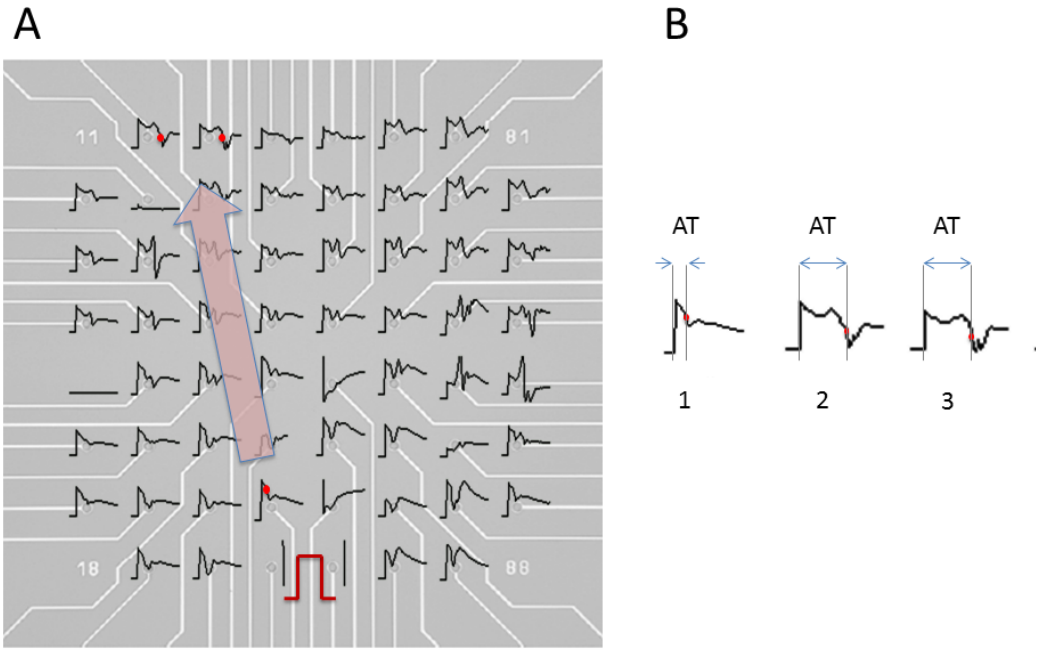

Figure 28 Method of calculation of conduction velocity. A: MEA with EGMs at each electrode. A stimulus is applied at the centre bottom (red open rectangle). The local activation time is marked on an adjacent electrode with a red dot. Propagation is assumed to be linear shown by the arrow, and activation times on two distal electrodes are marked. B: The three EGMs in (A) have been enlarged to show how activation time (AT) is measured. (1: electrode adjacent to stimulus; 2 & 3: distal electrodes).

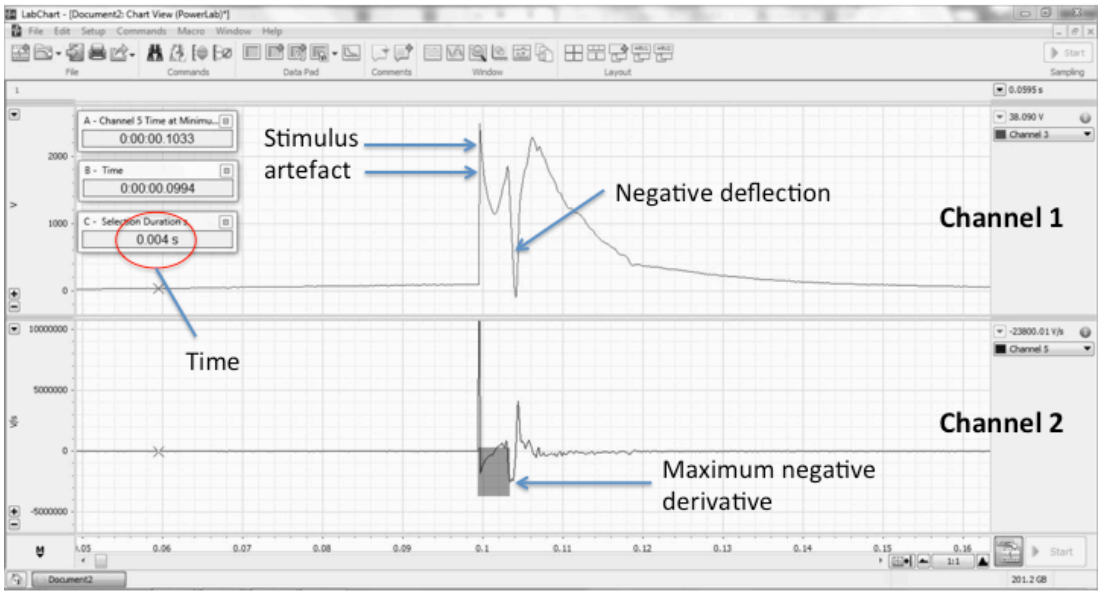

Figure 29 Calculation of activation time (AT). Channel 1 is the unipolar signal from one of the MEA electrodes, indicating stimulus artefact and sharp negative deflection associated with activation of the overlying cardiomyocytes, i.e. phase 0 of action potential. Channel 2 shows the first temporal derivative of Channel 1, indicating the maximum negative derivative. The shaded area represents the time from stimulus artefact to this point (indicated in the red circle - ' Time').

checked to corroborate it occurred at the time of maximum negative downstroke, or in difficult cases, that it was plausible. The process was repeated for the distal electrode channels to determine their activation times. Measurements were entered into a spreadsheet, and the time difference between activation time at the reference electrode and each distal electrode was calculated. The distance between these electrodes was also calculated, and conduction velocity derived from these values. Values < 10 cm/s or > 150 cm/s were excluded from analysis. Mean conduction velocity was determined for each pair of distal electrodes at each time point/drug concentration/temperature.

2.10.7 Control experiments

A series of experiments were performed to assess the stability of ERP and conduction velocity over time, in the absence of any drug or other challenge. These were called 'control experiments'. ERP and conduction velocity were measured at baseline and every 7 minutes for 35 minutes, as described above.

2.10.8 Drug challenge

The effects of several drugs on ERP, local activation time and conduction velocity were determined for WT mice; carbachol experiments involved both WTs and gKO mice. Drugs were reconstituted from powder form to produce stock solutions of 1 mM concentration. During the study, baseline measurements were taken, after which increasing concentrations of the drugs were assessed on the same slice. This was achieved by adding the requisite amount of drug stock solution to the Normal Krebs perfusate according to the formula

$$N_1.V_1 = N_2.V_2 \qquad \text{Equation 2}$$

Where N_1 = concentration of stock solution, V_1 = volume of stock solution, N_2 = desired concentration, and V_2 = desired volume. After measurements were made at this concentration, a further volume of stock solution was added to achieve the new desired concentration. The new concentration of drug in Normal Krebs was perfused for three minutes before commencing measurements, to allow equilibration of the MEA chamber fluid and drug action. This time was a trade-off between the time required to

adequately reflect the drug concentration's effects, and the desire to complete the experimental protocol with a full dataset before tissue deterioration.

For the muscarinic agonist carbachol (Alfa Aesar, UK) and the non-selective βAR agonist isoprenaline, ERP was assessed at the following concentrations: **10^{-9} M**, 10^{-8} M, **3 x 10^{-8} M**, 10^{-7} M, **10^{-6} M** (concentrations written in exponent form to facilitate interpretation of graphs in *Chapter 7*). Conduction velocity was assessed at the three concentrations shown in bold. Following 10^{-6} M carbachol, the muscarinic antagonist 10^{-6} M atropine (Sigma-Aldrich) was perfused from a separate 50 mL volume of Normal Krebs (i.e. drug-naïve), whereas after 10^{-6} M isoprenaline, the non-specific βAR antagonist propranolol hydrochloride (Santa Cruz Biotechnology, Dallas USA) was perfused at a concentration of 10^{-6} M (also from separate 50 mL Normal Krebs). Mexiletine hydrochloride (Sigma-Aldrich) was studied at 10^{-5} M and 10^{-4} M, with ERP and conduction velocity measured at both concentrations.

2.10.9 Thermal challenge

Baseline measurements of ERP and conduction velocity were made at 37 °C in the same way as described above. The temperature of the perfusate in the inflow, and in the MEA chamber was reduced to 34 °C using the TCX-Control version 1.3.4 (Multi Channel Systems). After five minutes of perfusion measurements were made. The temperature was then increased to 40 °C, with measurements made again after 5 minutes. Finally, temperature was reduced to 37 °C before final measurements.

2.11 Statistical Analysis

All statistical analysis was performed with StataIC 12 (StataCorp LP, USA). For comparisons of paired and unpaired observations, assumptions were checked as follows: i. equality of variance in groups was checked with Levene's test; ii. normality of the outcome variable was assessed with a standardised normal probability plot, and if the appearance was equivocal, a skewness and kurtosis test was used to assess more objectively. If the groups had equal variances and were deemed to be normally distributed, a t-test (paired or unpaired) was used. If variances were unequal, but the

outcome variables were considered normal, a t-test with unequal variances was used. If both assumptions were invalid, the appropriate non-parametric test was used, dependent on whether the data were paired (Wilcoxon signed-rank) or unpaired (Wilcoxon Ranksum/Mann-Whitney U).
Correlational analyses report Pearson's product moment coefficient (r) unless otherwise stated. Comparison of number of observations between groups was performed with Fisher's Exact test unless otherwise stated.

MEA studies

Multilevel mixed effects models were employed to analyse repeated measures data after recommendation by a statistician due to their advantages over repeated measures analysis of variance (RM-ANOVA). These include fewer assumptions, or requirement for less strict adherence to them; the ability to build in increasing hierarchical complexity with 'levels' of data corresponding to groupings; and the ability to analyse incomplete datasets. With regard to the assumptions, the lack of comprehensible instructions on how to test data for compound symmetry and sphericity, and more importantly, what to do if your data do not meet these assumptions, made multilevel mixed effects models attractive. Further considerations were that the random effects component provides a means of varying the slope (lines of best fit) for each individual sample's data.
Below is an overview of the steps involved in using multilevel models to analyse ERP, activation time and conduction velocity data, using variable drug concentrations as an exemplar:

i. Input variables and re-shape to long format
ii. Random intercept model with concentration as a continuous variable; store estimates
iii. Random slopes model with concentration as a continuous variable; store estimates
iv. Likelihood ratio test to compare models
v. If $p<0.05$, use random slopes model; if not, restore random intercept estimates
vi. Check assumptions of normality of residuals and homoscedasticity
vii. Plot original data and fitted lines for each sample to visually check model

viii. Generate margins and plot with original data mean values to visually check model
ix. Check for differences between maximum concentration and baseline values
x. If two groups, compare them at each concentration
xi. Re-model with concentration as a discrete variable
xii. Re-check assumptions
xiii. If two groups, compare them at each concentration
xiv. Compare each concentration to baseline

Several of the datasets were also analysed with RM-ANOVA, and the results were similar.

Statistical significance for was assumed if $p<0.05$ in all circumstances.

3. RESULTS - ESTABLISHMENT OF A HEART FAILURE MODEL

3.1 Introduction

Attempts were made to establish two models of heart failure: one pharmacological, and one surgical. The aims were to permit investigation of the pathophysiological changes in cell signalling occurring in the context of different myocardial insults, and to provide some insurance should one of the approaches fail to induce LV impairment/heart failure.

The supraphysiological beta-adrenoceptor agonism model utilised isoprenaline in WT mice. Effects on LV contractility were assessed using echo: LVIDd, FS and EF were measured for all animals. As described in the *Chapter 2*, the initial plan was to use pellets which would elute the drug over three weeks. After preliminary study of ten mice (pellets – standard dose), there was no demonstrable effect, and a further four mice were studied at higher doses (pellets – high dose). After these too did not show an effect, the drug delivery system was changed to subcutaneous injections. The results of the three parts of the isoprenaline dose-ranging studies are reported here (*Sections 3.2* to *3.4*).

These were dose-ranging studies designed to test the efficacy of isoprenaline for inducing LV impairment, and to establish the best dose(s) to use to obtain this effect. As such, and in view of the small numbers of mice receiving similar doses in each part of this study, summary statistics are presented rather than the results of formal statistical tests. Together with the graphs, the former enable more meaningful interpretation than attempting to apply tests to underpowered data.

The coronary ligation model of myocardial infarction-induced heart failure was developed concurrently. Prior to performing the study involving cKOs and controls (*Chapter 5*) which required serial echo measurements, a preliminary correlational study of echocardiographic assessment of LV contractility and histological scar was performed in WT mice to establish echo as a reliable means of assessing MI-induced scar and contractility. The results are reported in *Section 3.5*.

3.2 First isoprenaline dose-ranging study: pellets (standard dose)

The first dose-ranging study involved mice receiving subcutaneous pellets at doses similar to those reported in the literature to induce LV hypertrophy and/or heart failure. Ten mice were studied; those receiving similar doses have been grouped to enable averaging and clearer graphical representation (Figures 30 to 32). The pellets included fixed quantities of isoprenaline (7.5 mg, 15 mg, 25 mg and 35 mg). Although advertised as designed to elute over 21 days, the lack of observable effect calls this rate into question, and the following four dose groups have therefore been chosen based on isoprenaline dose per gram of mouse body weight: 0.25-0.35 mg/g, 0.5-0.6 mg/g, 0.85-1.05 mg/g, and 1.15-1.35 mg/g.

3.2.1 Left ventricular dimensions

As Figure 30 shows, there was a very slight increase in LVIDd over the course of the study.

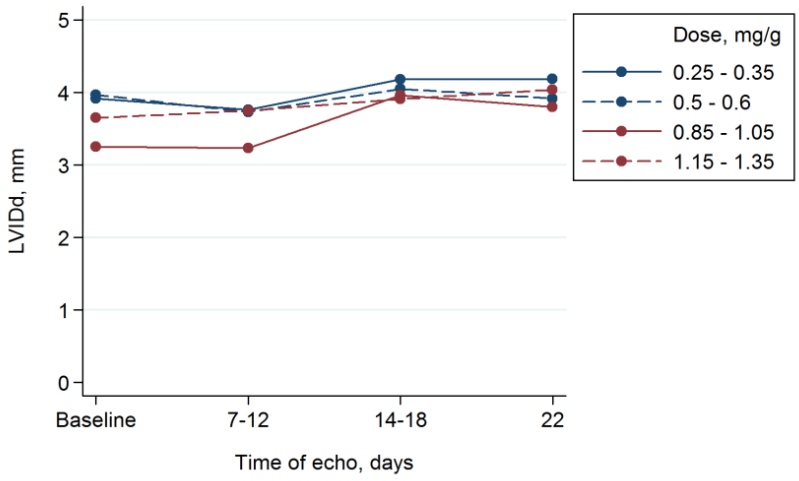

Figure 30 Left ventricular internal dimension in diastole (LVIDd) over time in standard dose part of isoprenaline pellet study for the four dose groups (n=10).

3.2.2 *Fractional shortening*

Figure 31 shows the data for FS. The lowest dose group exhibited an increase between baseline and 7 days, before returning to baseline value. The second highest dose group showed a fall between 7-12 and 14-18 days, after which FS stabilised. Overall, there was no clear trend.

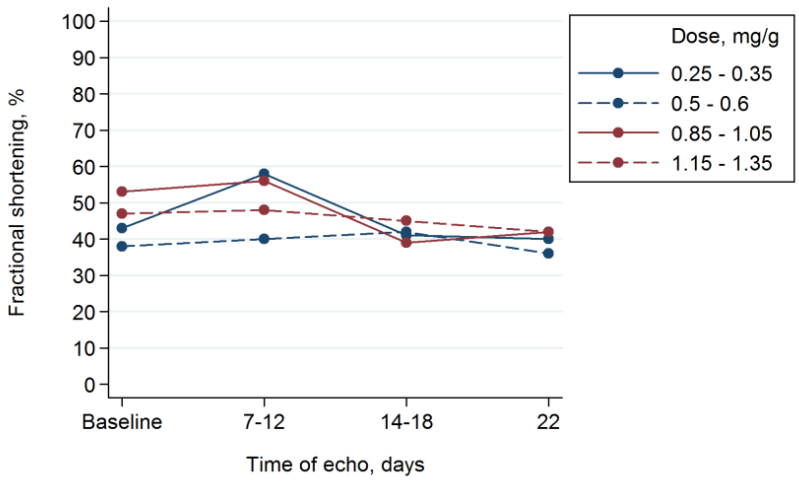

Figure 31 Fractional shortening (FS) over time in standard dose part of isoprenaline pellet study for the four dose groups (n=10).

3.2.3 *Ejection fraction*

EF measurements are derived from those of FS, and as a result, will exhibit the same trends, as shown in Figure 32. They are also presented due to their volumetric rather than linear basis, and because EF is a more intuitive parameter, that is widely understood.

The slight changes noted in FS for two of the groups also occurred in EF, but as before, there was no trend.

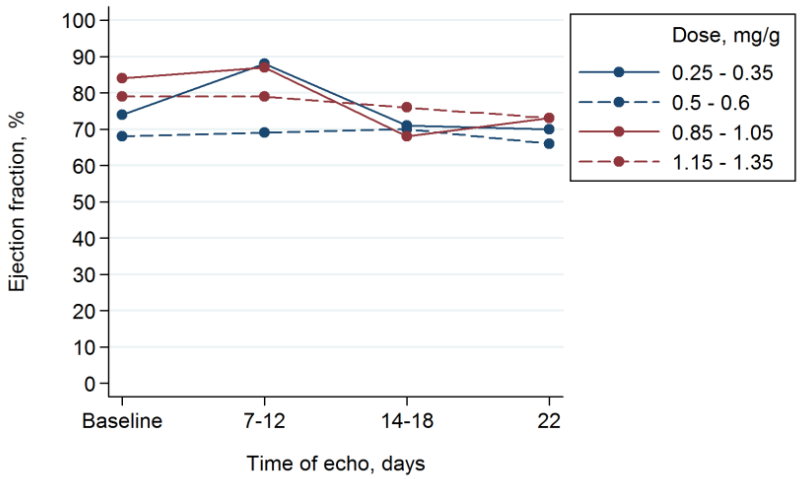

Figure 32 Ejection fraction (EF) over time in standard dose part of isoprenaline pellet study for the four dose groups (n=10).

The data in the graphs above are summarised in Table 1, which presents the percentage change from baseline for each parameter according to dose group. For LVIDd, the percentage change is relative, i.e. the starting value is taken as 100%, whereas for FS and EF which are already measured as percentages, the change from baseline is recorded as absolute: if the baseline value is 55%, and at 7-12 days it is 70%, this is equal to +15%.

		0.25-0.35 mg/g (n=3)	0.5-0.6 mg/g (n=3)	0.85-1.05 mg/g (n=2)	1.15-1.35 mg/g (n=2)
		% change from baseline			
LVIDd	7-12 days	-4	-6	-1	+3
	14-18 days	+7	+2	+22	+7
	22 days	+7	-1	+17	+11
FS	7-12 days	+15	+2	+3	+1
	14-18 days	-2	+4	-14	-2
	22 days	-3	-2	-11	-5
EF	7-12 days	+14	+1	+2	0
	14-18 days	-3	+2	-16	-3
	22 days	-4	-2	-11	-6

Table 1 Change of echocardiographic indices over time in standard dose isoprenaline pellet study. Percentage change for LVIDd is relative, whereas for FS and EF it is absolute.

3.3 First isoprenaline dose-ranging study: pellets (high dose)

Higher doses of the pellets were used in four mice. The corresponding drug doses per gram of bodyweight were 2.4 mg/g, 3.6 mg/g, 4.0 mg/g and 4.1 mg/g. Measurements were made at only two time points for this small study: baseline and 14 days.

3.3.1 Left ventricular dimensions

As shown in Figure 33, there was no change in LVIDd between baseline and 14 days for the cohort.

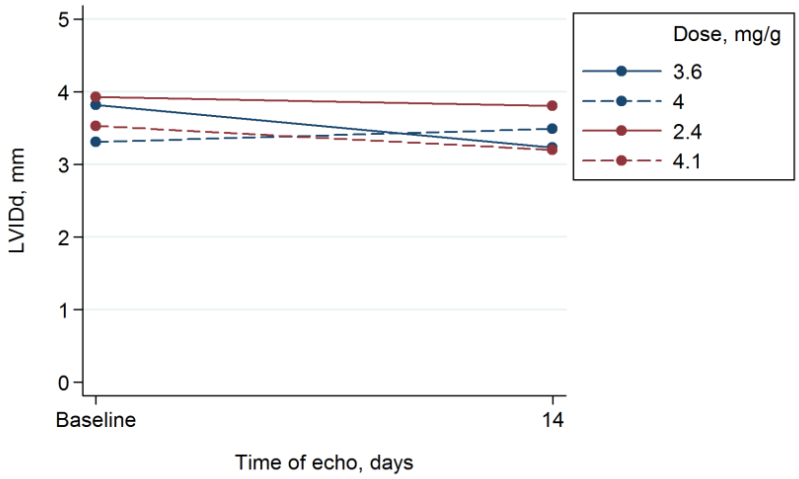

Figure 33 Left ventricular internal dimension in diastole (LVIDd) over time in high dose part of isoprenaline pellet study for the four mice studied (n=4).

3.3.2 Fractional shortening

There was no trend seen here either (Figure 34).

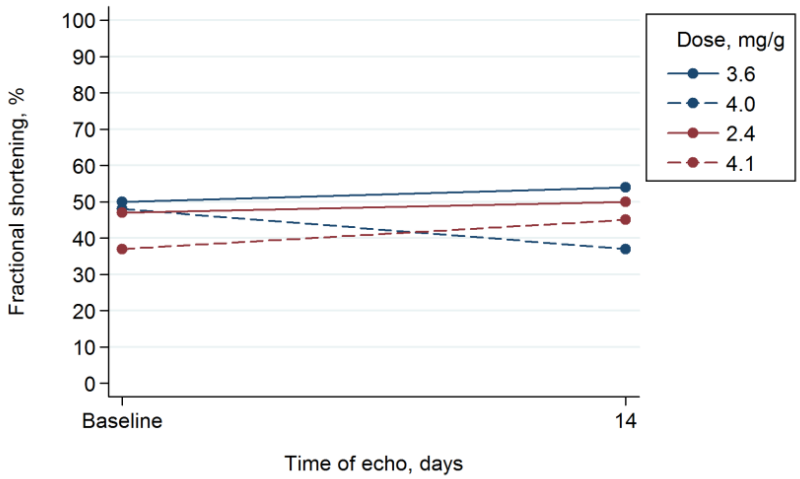

Figure 34 Fractional shortening (FS) over time in high dose part of isoprenaline pellet study for the four mice studied (n=4).

3.3.3 Ejection fraction

As before, EF mirrors FS (Figure 35).

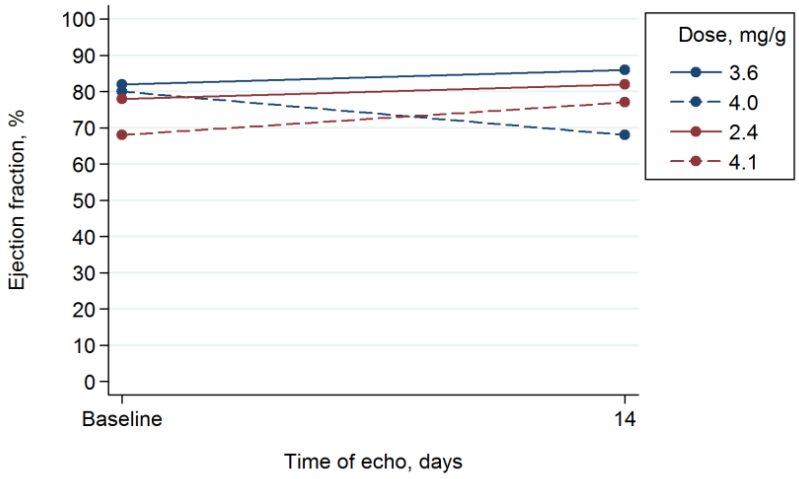

Figure 35 Ejection fraction (EF) over time in high dose part of isoprenaline pellet study for the four mice studied (n=4).

As for the standard dose experiments, the data in the graphs above are summarised in Table 2, which presents the percentage change from baseline for each parameter according to dose group.

		2.4 mg/g (n=1)	3.6 mg/g (n=1)	4.0 mg/g (n=1)	4.1 mg/g (n=1)
		% change from baseline			
LVIDd	14 days	-3	-15	+5	-9
FS	14 days	+6	+8	-23	+22
EF	14 days	+5	+5	-15	+13

Table 2 Change of echocardiographic indices over time in high dose isoprenaline pellet study. Percentage change for LVIDd is relative, whereas for FS and EF it is absolute.

3.4 Second isoprenaline dose-ranging study: injections

For this mini-study, daily injections of isoprenaline were administered to five mice at two doses: three mice received 6 mg/kg/day, and two received 9 mg/kg/day, all for 21 days. In contrast to the pellets where the total dose was known, but not rate of elution, the same isoprenaline dose was administered daily with these injections; hence the dose is stated in mg/kg/day. The results are summarised in Figures 36 to 38.

3.4.1 Left ventricular dimensions

Results for each mouse are plotted in Figure 36 to convey similarities in the responses. Of the five mice, measurements were not possible at 15 days for one receiving the lower dose, and one the higher dose, due to bradycardia and awakening from anaesthesia.

Table 3 summarises the percentage change from baseline of the lower and higher dose groups at each time point for each parameter. As can be seen, there was a small increase in LVIDd at each time point for both dose groups.

		6 mg/kg/day (n=3)	9 mg/kg/day (n=2)
		% change from baseline	
LVIDd	8 days	+12	+9
	15 days	+24	+14
	22 days	+18	+14
FS	8 days	-21	-15
	15 days	-18	-14
	22 days	-11	-8
EF	8 days	-26	-18
	15 days	-22	-15
	22 days	-14	-9

Table 3 Change of echocardiographic indices over time in isoprenaline injection study. Percentage change for LVIDd is relative, whereas for FS and EF it is absolute.

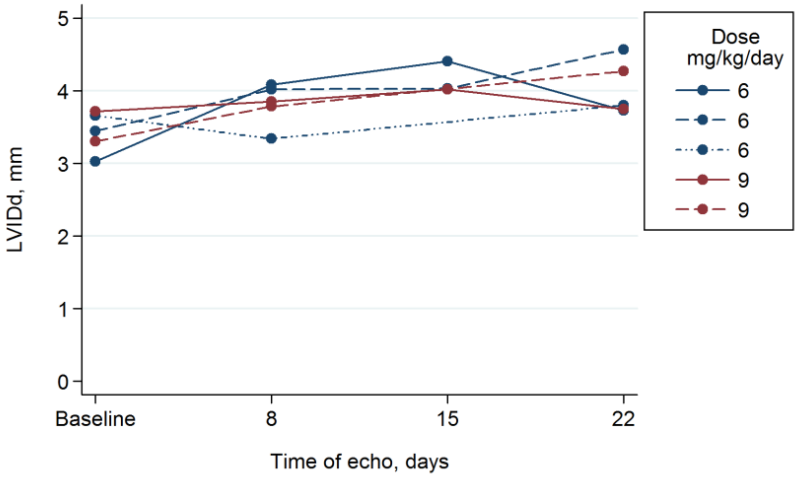

Figure 36 Left ventricular internal dimension in diastole (LVIDd) over time for individual mice in isoprenaline injection study (n=5).

3.4.2 Fractional shortening

This decreased for both dose groups by 8 days, remaining lower than baseline at 15 days before attaining an intermediate level by the end of the study.

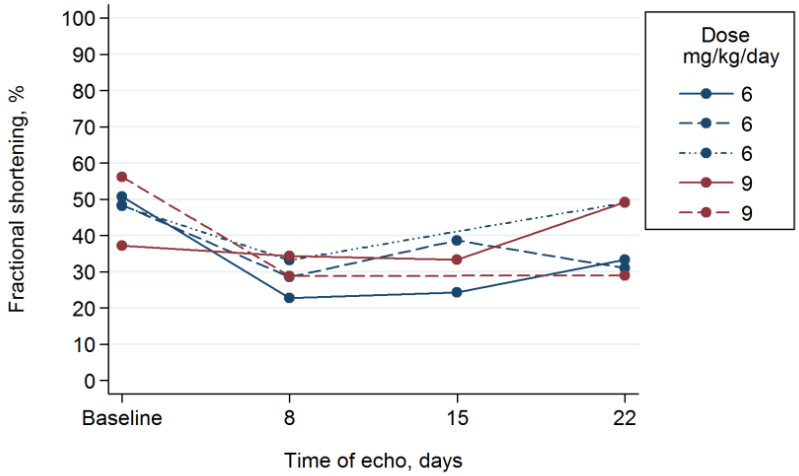

Figure 37 Fractional shortening (FS) over time for individual mice in isoprenaline injection study (n=5).

3.4.3 Ejection fraction

The changes seen in FS were mirrored by EF, i.e. there was a reduction during the middle of the study before a partial recovery.

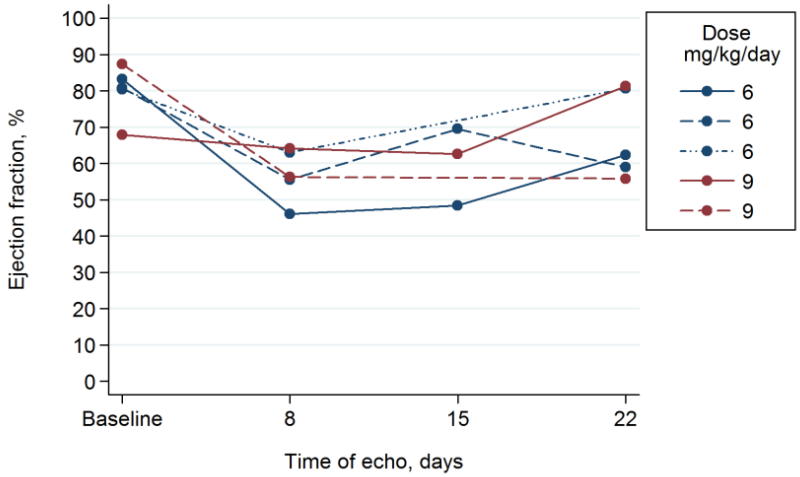

Figure 38 Ejection fraction (EF) over time for individual mice in isoprenaline injection study (n=5).

An illustrative example of echocardiographic measurements is shown in Figure 39.

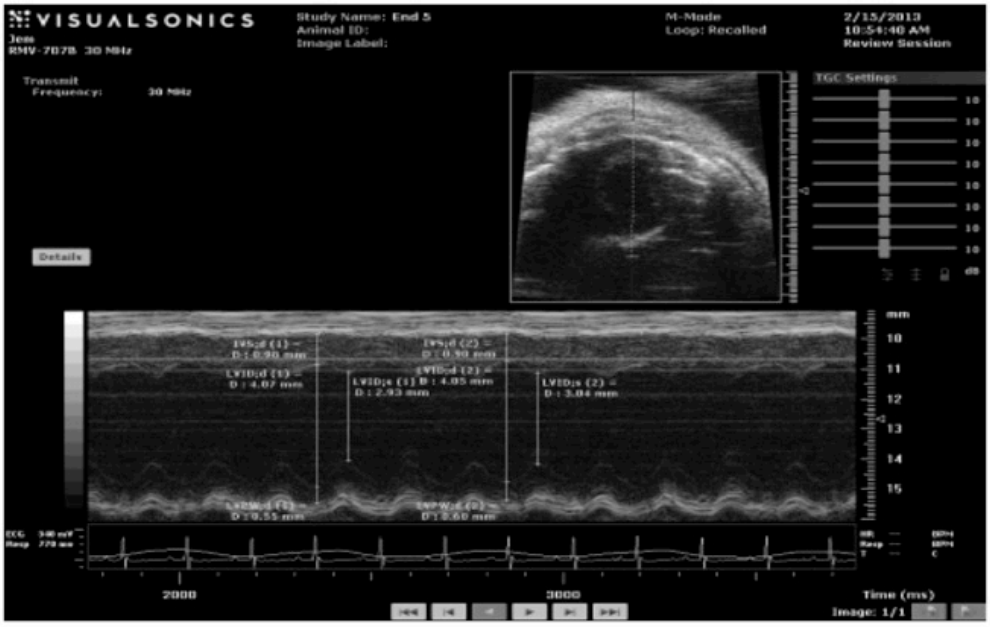

Figure 39 M-mode echocardiography of mouse at day 22 of isoprenaline study. Top right of image shows short axis view; lower part of image shows M-mode with cavity and wall thickness measurements. EF was measured at 56%.

3.5 Preliminary coronary ligation study: correlation of histology with echocardiographic findings

Table 4 shows the percentage scar on histological examination and fractional area change (FAC) on echocardiogram for each of the ten mice studied.

Three examples of heart sections stained with Masson's trichome are shown in Figure 40 to illustrate no scar, moderate, and severe scarring.

The data from Table 4 are displayed graphically in Figure 41 with a linear regression line. As expected, this shows a negative correlation between histological scar and FAC (r= -0.82). Based on these results, FAC was deemed a valid non-invasive method of assessing left ventricular contractility, given that regions with severe scarring do not contract.

Mouse	Histological scar, %	FAC, %
1	3	40
2	11	59
3	38	13
4	17	39
5	5	59
6	6	55
7	50	30
8	3	53
9	32	32
10	36	22

Table 4 Scar measured histologically, and contractility measured by echo with fractional area change (FAC), for the 10 mice in the preliminary coronary ligation study.

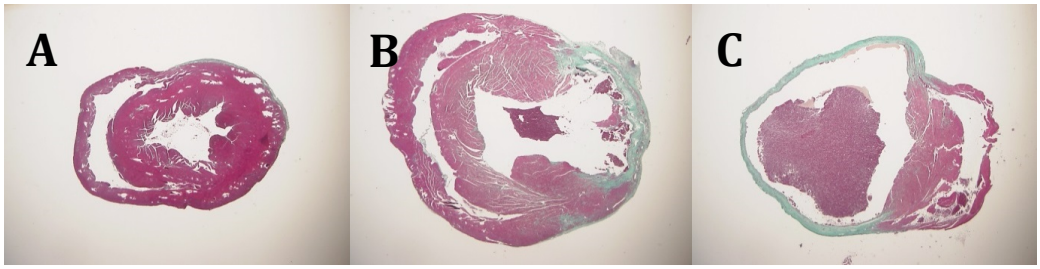

Figure 40 Masson's trichome stain of three short axis sections of heart. Collagen/fibrous tissue stains green. A: no scar, B: moderate scar, C: severe scar.

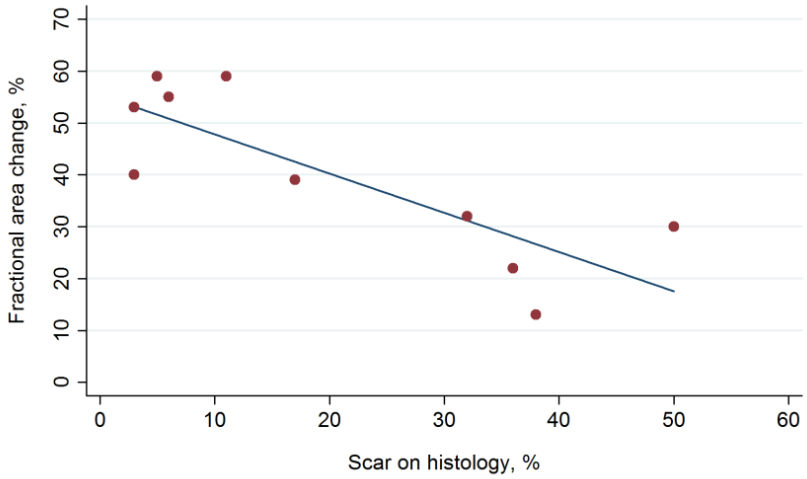

Figure 41 Scar on histological analysis and fractional area change on echo for 10 mice.

4. DISCUSSION – ESTABLISHMENT OF A HEART FAILURE MODEL

4.1 Isoprenaline dose-ranging studies

4.1.1 Isoprenaline model – results

In both the standard and high dose parts of the pellet study, there was no clear change in LVIDd, FS or EF at any of the doses. The suggestion of a small increase in LVIDd with standard doses was not seen with the high doses, making chance or measurement error a more likely explanation. In the standard dose part, the mean FS and EF or the three mice receiving the lowest doses increased at day 7-12 compared to baseline. However, these parameters then fell again by day 14-18. A possible explanation is that the pellets eluted the drug more quickly than expected: in the short term, sympathomimetics usually cause an increase in contractility, at least in low to moderate doses. Tachyphylaxis may then have ensued, with a resultant plateau of effect. Against this possibility is the fact that it only occurred at the lowest doses.
With isoprenaline injections, LVIDd rose progressively for both dose groups from baseline to day 15 at which point it plateaued. Also in both groups, there was a fall in FS and EF between baseline and day 8, maintained at day 15 before rising slightly. Thus it seems, an effect was observed. However, the lowest EFs measured were 55% for the 6 mg/kg/day group, and 60% for the 9 mg/kg/day group, i.e. still within what is probably the normal range. And importantly, these lowest EFs occurred at day 8, with partial recovery over the next two weeks.
So, although a modest effect was seen with isoprenaline injections, isoprenaline did not induce LV impairment in any mice. The reasons for this are not clear. Given the range of doses used with the pellet formulation, it would seem dosage is unlikely to underlie the lack of effect observed. More probable is that the pellet formulation did not dissolve at any appropriate rate, or that the isoprenaline became inactivated or failed to be absorbed. Oxidisation is known to occur with isoprenaline in solution, and for the injection experiments, care was taken to prepare and use the solution within an hour to avoid this.
Despite the isoprenaline model's familiarity to investigators, there is surprisingly little standardisation in the literature with regard to the dose required to induce LV

impairment/heart failure, and how to assess it. The reported means of drug delivery are daily injections, and mini osmotic pumps. While Kaur et al performed intraperitoneal injections of 30 mg/kg/day for seven days[265], Horiuchi-Hirose et al used 6-9 mg/kg/day subcutaneous injections[260], and Faulx et al used 100 mg/kg/day[258]. Neither Kaur et al nor Faulx et al measured contractility with echo; heart:body weight ratio was measured instead as an index of hypertrophy. Oudit et al did not perform baseline echo measurements in drug-naïve animals, and only reported fractional shortening[225], and Matkovich et al reported 'Vcfc' – velocity of circumferential shortening normalised to heart rate – rather than FS, EF or FAC[259]. There was no specific mention of maintaining body temperature 35-37°C, or heart rate over a particular value in the studies that used echo to quantify LV dysfunction.

4.1.2 Isoprenaline model – methodology

With regards to the strengths of the studies, reasonable numbers of mice were used: a total of fourteen received pellets, and five received daily injections. A range of doses were studied based on previously published results, and alternate methods of drug delivery were tried. Repeated measurements were made over two to three weeks to look for chronic effects rather than those of an acute insult, and to ensure stability of measurements. The consistency of the results attests to the studies being conducted properly and in the same manner for each mouse.

There were two possible weaknesses: firstly the use of FS and EF rather than FAC. As discussed in *Section 2.4*, FS is measured along a 1D line through the heart, whereas FAC uses the circumference of the endocardium and may therefore be less prone to error. Having said this, isoprenaline would be expected to induce a global insult rather than the regional scarring seen following myocardial infarction, and contraction along one dimension may in fact be representative of the whole LV's contractility. Secondly, it is possible that trends seen in the injection group may have become clearer with a larger number of animals.

4.1.3 Suitability of supraphysiological βAR agonism as a model of heart failure

Heart failure as a syndrome is characterised at a system level by excessive neurohumoural sympathetic activity – increased circulating catecholamines, and

increased activity from sympathetic nerves – in addition to dysfunction of the renin-angiotensin-aldosterone axis[266,267]. These changes are implicated in the pathophysiology, but are in the main, responsive rather than the primary cause of the syndrome. A further important point is that the upregulation of the SNS is a chronic process, occurring over weeks, months or even years. Animal models which aim to recapitulate the sympathetic excess as the sole means of myocardial insult are therefore failing to incorporate the far more common initial drivers of the pathophysiology, such as ischaemia, valve disease, or the protein malfunction that occurs in dilated cardiomyopathy. A possible exception to this is the use of βAR agonists in a small animal model of Takotsubo cardiomyopathy. In this condition, acute catecholamine surges are believed to play a major part in the pathophysiology, resulting in mid-apical LV akinesis or severe hypocontractility, which is usually reversible. A study by Paur et al in rats found high-dose adrenaline boluses could produce a phenotype in rats similar to that seen in humans, and the effects were attributed to ligand-directed trafficking, or biased agonism – adrenaline's concentration-dependent change from Gs to Gi signalling[268]. However, this model has recently been challenged, with fair questions raised regarding its validity[269].

Finally, it is not known whether the SNS hyperactivity seen in human heart failure preferentially stimulates β1ARs or β2ARs: both β1-selective, and non-selective β-blocker drugs are effective in heart failure. And α-AR effects are also likely to play a part, given that circulating catecholamines will act on the vasculature. Isoprenaline is a non-selective βAR agonist however, with no α-AR activity.

Notwithstanding the above, the importance of the SNS in heart failure is undisputed, and murine knockout models of βARs and G protein α subunits are beginning to shed light on the issues of the differing responses from β1- and β2AR stimulation, and the signalling cascades they and other GPCRs initiate. It is unfortunate that the model has not been more completely described, and more fully validated.

4.2 Correlation of histological and echocardiographic findings

Echocardiography in humans is the most common non-invasive means of assessing the heart's contractile function, and it is considered reliable in this regard. Its main weakness is the dependency of image quality on body habitus: poor endocardial definition limits accuracy of measurements of EF. However, given the relative sizes of

the chest wall and ultrasound probe in humans, different 'windows' of the heart can be tried so as to optimise image quality and measurement accuracy.
The large size of the probe in relation to the murine chest limits the possible views, and chest wall scar tissue can also interfere with image quality. For these reasons, it was deemed important to ascertain that the echo measure, FAC, was related to the extent of scar induced by coronary ligation, and in particular, that moderate and severe impairment could be distinguished from normal function. To my knowledge, this comparison had not been done before.
The strengths of this study were that it compared histological scar to FAC, a parameter that reflects all regions of the LV wall, rather than the 1D parameter FS. This is essential following MI where the scarring is regional. Also, that three histological sections per heart were assessed to ensure representation of the base, mid-LV and apex in the measurement, and reduce the chance of unrepresentative sections influencing the results.
A reasonable number of mice were studied, though larger numbers would have further increased confidence in the results. This study was not taken further as even ten mice involved a considerable amount of work, and this was a sub-study rather than a contribution to investigation of the main hypotheses.

4.3 Conclusion

The human syndrome in which $G\alpha_{i2}$ is elevated, and of possible pathophysiological relevance, is that of heart failure. One of the main goals of this project was therefore to take forward the previous work performed using $G\alpha_{i2}$ knockout mice with structurally normal hearts, by examining the electrophysiological phenotypic effects of LV impairment/heart failure in these mice. At the outset of this work, it was deemed useful to set up two models of heart failure to probe the hyopothesis that $G\alpha_{i2}$ is anti-arrhythmic in the ventricles. The coronary ligation-induced MI model would reflect the regional scarring seen in the most common cause of human heart failure, and importantly, it could be expected that the arrhythmic substrates seen within human ischaemic cardiomyopathy would also be seen in the mouse. It was hoped that the pharmacological model using isoprenaline would not merely provide a technically easier backup, but also that given the sympathetic nervous system's overactivity in the syndrome, it would enable probing of $G\alpha_{i2}$'s role in the β-AR signalling cascades. The

lack of induction of overt LV impairment/heart failure with the latter was surprising, but served as a reminder of the need to use models as close as possible to the human pathophysiology. This is a major strength of the coronary ligation model. In addition, echo was found to be a reliable means of non-invasively assessing the extent of myocardial damage following MI.

5. RESULTS – EFFECTS OF Gαi2 KNOCKOUT IN A MYOCARDIAL INFARCTION MODEL OF HEART FAILURE

5.1 Introduction

The phenotypic effects of cardiac-specific knockout of $G\alpha_{i2}$ were studied *in vivo* in cKOs and littermate controls. LV contractility and electrophysiological parameters were assessed at baseline, and following coronary ligation-induced MI. Prior to reporting these results, the approaches used to assess cardiac-specific $G\alpha_{i2}$ knockout are described.

5.2 Assessment of *GNAI2* gene knockout status

The *GNAI2* gene status and mRNA expression of cKOs was interrogated in three ways, as discussed below. At times, the full *GNAI2*/Cre genetic status ($G\alpha_{i2}^{Flx/Flx}$ Cre+) is used, in addition to or in place of the abbreviated form (cKO) to facilitate readability and help avoid ambiguity. 'Control' mice refer to those without Cre deletion of the gene, i.e. $G\alpha_{i2}^{WT/WT}$ Cre-, $G\alpha_{i2}^{WT/WT}$ Cre+, or $G\alpha_{i2}^{Flx/Flx}$ Cre-.

5.2.1 DNA genotyping

Illustrative examples of expected amplicon bands for *GNAI2* and Cre PCR products on gel electrophoresis are shown in Figure 42. The WT *GNAI2* amplicon is approximately 400bp, and the Flx/Flx amplicon approximately 500bp. The Cre amplicon is 990bp.

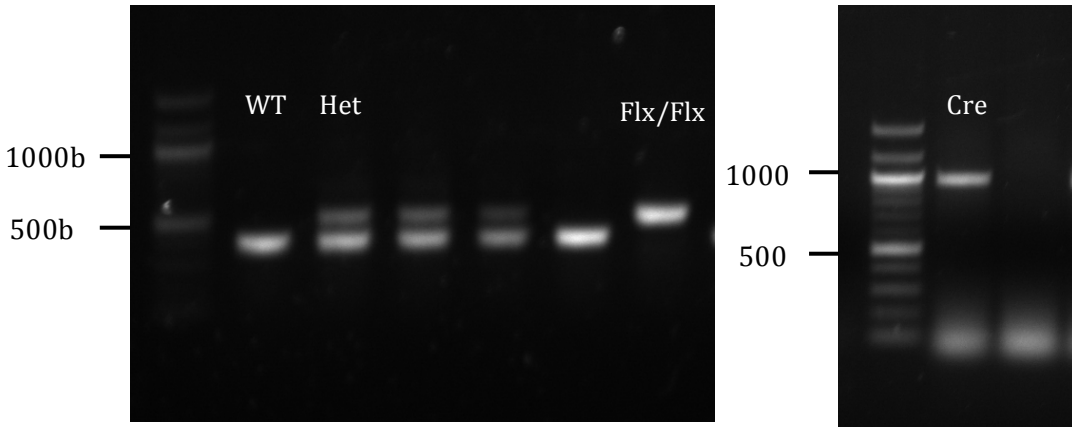

Figure 42 Gel electrophoreses showing illustrative examples of *GNAI2* PCR products (left) and Cre product (right).

Figure 43 shows the PCR products following gel electrophoresis of genomic DNA isolated from ear-notched tissue for the four cKO mice (genotype $G\alpha_{i2}^{Flx/Flx}$ Cre+) used in the RT-qPCR experiments with total RNA, described below. As can be seen, the bands are clear and the results unequivocal. The control mice had genotypes $G\alpha_{i2}^{WT/WT}$ Cre- (3) and $G\alpha_{i2}^{WT/WT}$ Cre+ (1) (gel electrophoresis results not shown).

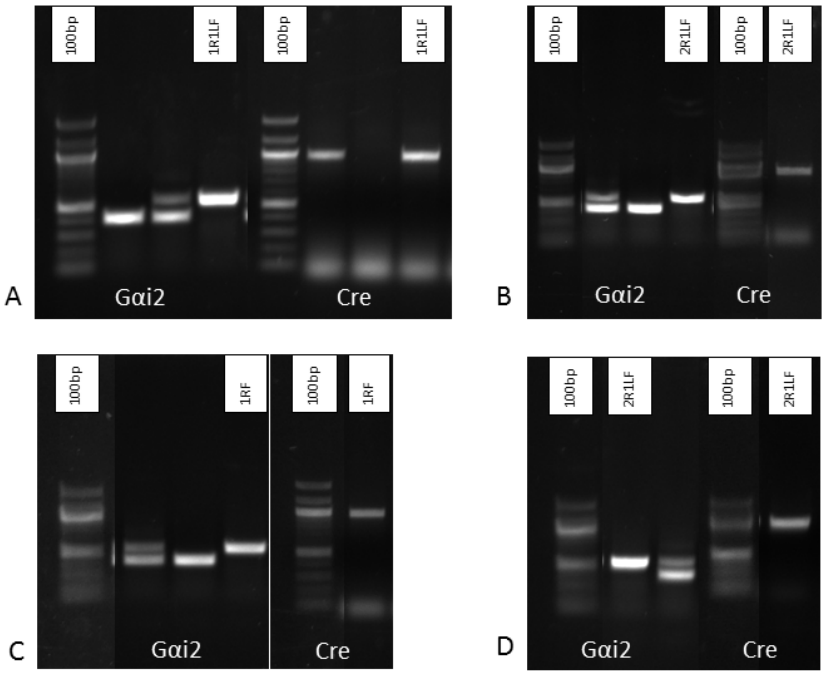

Figure 43 DNA genotyping results for four cKO mice (A,B,C,D) used in subsequent RT-qPCR. First lane in each is a 100bp DNA ladder (New England Biolabs). Lanes marked with white box (e.g. "1RF") are the mouse's result; unmarked lanes are for illustrative purposes only. Results for $G\alpha_{i2}$ and Cre PCRs are shown.

5.2.2 Sanger sequencing of cardiac tissue DNA to assess GNAI2 gene status

I next isolated genomic DNA from the heart and used Sanger sequencing to determine if Cre-mediated deletion of the relevant genomic regions had occurred in mice with genotypes (number) $G\alpha_{i2}^{Flx/Flx}$ Cre+ (2), $G\alpha_{i2}^{WT/WT}$ Cre- (1) and $G\alpha_{i2}^{Flx/Flx}$ Cre- (1). The results are illustrated graphically in Figure 44, following analysis with the UCSC BLAT. For each sequence, the region of the *GNAI2* gene containing exons 2-4 (purple blocks) is magnified for clarity. As can be seen, DNA from mice with genotype $G\alpha_{i2}^{Flx/Flx}$ Cre+ (cKOs) aligns within introns 1 and 4, with a large intervening segment that does not match. This non-matching section includes exons 2-4, compatible with excision. In C ($G\alpha_{i2}^{Flx/Flx}$ Cre-), there is a small section of homology at the primer binding site (black), followed by a section of unmatched DNA reading 5' to 3' (right to left in the figure) which corresponds to the loxP site. Further 3' there is near complete homology as indicated by the black sections. Finally, in D ($G\alpha_{i2}^{WT/WT}$ Cre-, i.e. two WT *GNAI2* alleles), there is near complete homology indicated by the almost continuous black blocks. The short discontinuities are likely reading errors, or possibly intronic mutations.

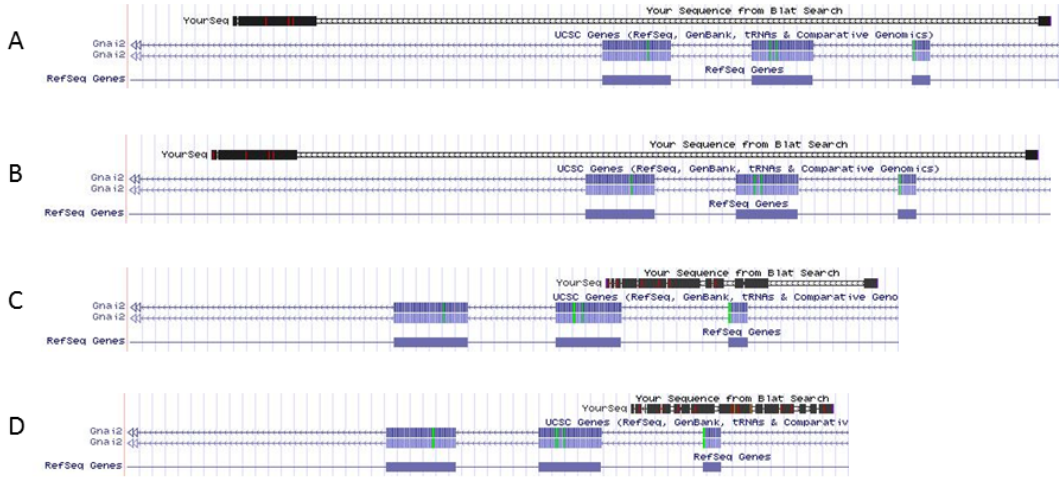

Figure 44 Results from Sanger sequencing showing alignment with the Mus musculus *GNAI2* gene, retrieved with UCSC BLAT searches. Genotypes as follows - A: $G\alpha_{i2}^{Flx/Flx}$ Cre+, B: $G\alpha_{i2}^{Flx/Flx}$ Cre+, C: $G\alpha_{i2}^{Flx/Flx}$ Cre-, D: $G\alpha_{i2}^{WT/WT}$ Cre-. Sanger sequences are shown at top of each strip – black sections represent regions of homology with *GNAI2* reference sequence, while ladder regions indicate unmatched zones. Purple blocks represent exons 2-4.

Figure 45 compares the sequences of A and B from Figure 44. There is near complete homology, indicated by the consensus sequence.

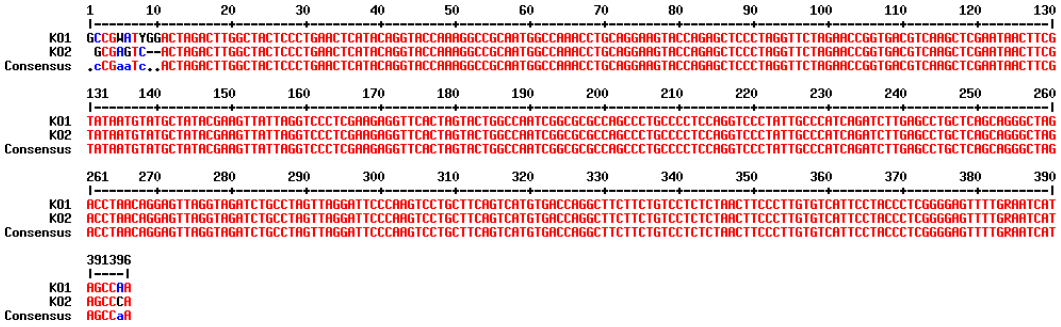

Figure 45 Comparison of Sanger sequences from two cKO mice. Sequences from mice with genotype $G\alpha_{i2}$ $^{Flx/Flx}$ Cre+ (A and B in Figure 44), labelled KO1 and KO2 here, with consensus sequence in the third row.

5.2.3 RT-qPCR results: mRNA expression in mice of different GNAI2 gene status

Yield of extracted total RNA was assessed prior to performing reverse transcription to cDNA, and RT-qPCR: sufficient quantities were present for hearts and livers, but not for tails, which were therefore discarded. Figure 46 shows the threshold cycle (C_t) values obtained for the hearts and livers of four control mice and four cKO mice. As can be seen, the expected marked increase in C_t for the hearts of cKO mice was not observed. Table 5 shows the mean ΔC_t values for each organ by genotype.

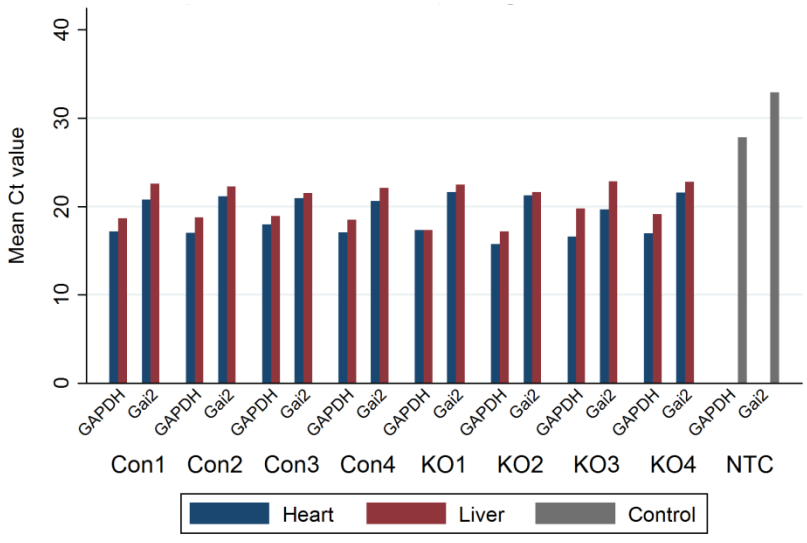

Figure 46 First RT-qPCR results. For hearts and livers of control (Con) and $G\alpha_{i2}$ Flx/Flx Cre+ genotype (cKO) mice. NTC: No Template Controls.

	cKOs		Controls	
	Heart $G\alpha_{i2}$ - GAPDH	Liver $G\alpha_{i2}$ - GAPDH	Heart $G\alpha_{i2}$ - GAPDH	Liver $G\alpha_{i2}$ - GAPDH
Mean ΔCt	4.34	4.07	3.56	3.41

Table 5 Mean ΔCt values in first RT-qPCR. Results for cKOs and controls by organ.

Relative expression using the 'comparative C_t method' for first RT-qPCR:

Heart			Liver		
$\Delta\Delta C_t$	=	0.78	$\Delta\Delta C_t$	=	0.66
$2^{-\Delta\Delta Ct}$	=	0.58	$2^{-\Delta\Delta Ct}$	=	0.63

Therefore, $G\alpha_{i2}$ expression in the hearts of cKOs was 58% of that in controls, while in the liver it was 63%.

To check the results were not due to error given the apparent incomplete cardiac knockout of $G\alpha_{i2}$, the RT-qPCR experiment was repeated with five more cKOs and five more controls. The C_t values are shown in Figure 47, and the mean ΔC_t values for each group of mice and each organ are shown in Table 6.

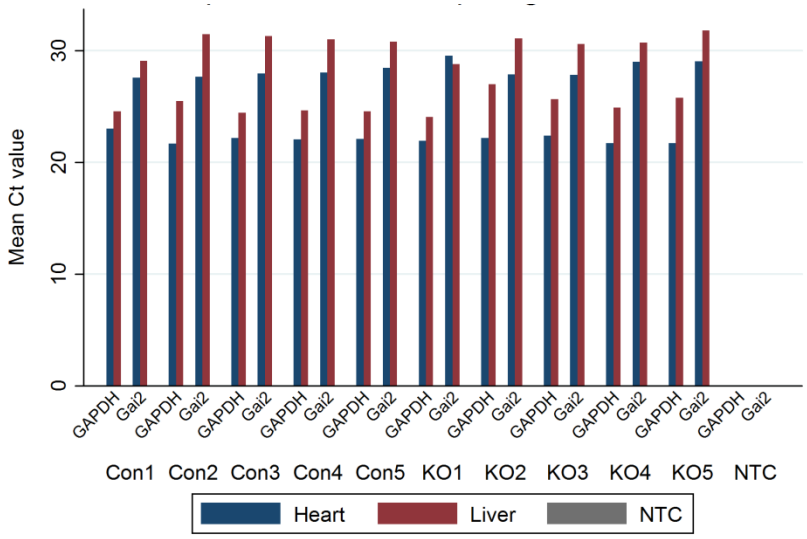

Figure 47 Second RT-qPCR results. For hearts and livers of control (Con) and $G\alpha_{i2}$ Flx/Flx Cre+ genotype (cKO) mice. NTC: No Template Controls.

	cKOs		Controls	
	Heart $G\alpha_{i2}$ - GAPDH	Liver $G\alpha_{i2}$ - GAPDH	Heart $G\alpha_{i2}$ - GAPDH	Liver $G\alpha_{i2}$ - GAPDH
Mean ΔCt	6.67	5.13	5.73	5.99

Table 6 Mean ΔCt values in second RT-qPCR. For cKOs and controls by organ.

Relative expression using the 'comparative C_t method' for second RT-qPCR:

Heart			Liver		
$\Delta\Delta C_t$	=	0.94	$\Delta\Delta C_t$	=	-0.86
$2^{-\Delta\Delta Ct}$	=	0.52	$2^{-\Delta\Delta Ct}$	=	1.82

$G\alpha_{i2}$ expression in the hearts of cKOs in this experiment was 52% of that in controls, while in the liver it was 182%. So again, $G\alpha_{i2}$ expression was not fully knocked out, although the level of knockdown is consistent with that seen in the first RT-qPCR. But inexplicably, $G\alpha_{i2}$ expression in the liver was increased. Combining the two sets of results yields the following overall relative expression values:

Combined RT-qPCR results: relative expression using the 'comparative C_t method':

Heart			Liver		
$\Delta\Delta C_t$	=	0.87	$\Delta\Delta C_t$	=	-0.18
$2^{-\Delta\Delta Ct}$	=	0.55	$2^{-\Delta\Delta Ct}$	=	0.88

So overall $G\alpha_{i2}$ expression in the hearts of cKOs was 55% of that in controls, and in the liver was 88%.

5.3 Myocardial infarction model of heart failure

The number of mice surviving to each stage of the study protocol is illustrated in Figure 48, with the thick arrows indicating survival.

Only one of 34 (3%) mice that underwent coronary ligation died peri-procedurally, i.e. within 24 hours of operation. This death occurred intraoperatively following closure of the chest. Post mortem revealed the right atrium to be tethered to the chest wall, and the endotracheal tube to be blocked with blood. All other deaths occurred within seven days of operation, and prior to follow-up echocardiography. In eight of these mice, post mortem revealed blood in the chest cavity and a pale liver, compatible with cardiac rupture.

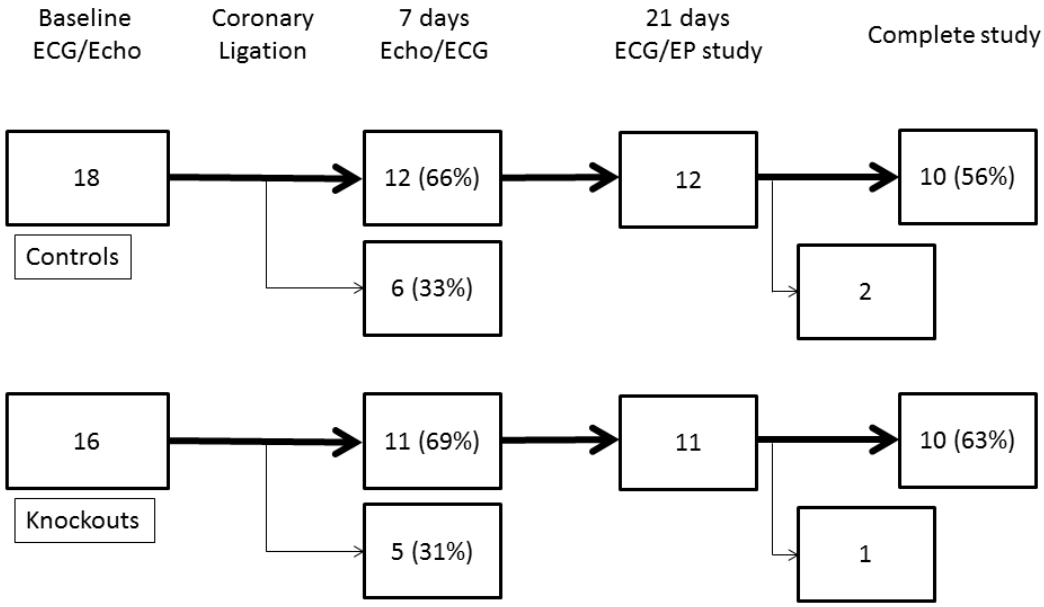

Figure 48 Flow of mice through stages of study protocol. Thick black arrows indicate survival, and lighter grey arrows indicate death. 'Knockouts' here refers to cKOs.

Indeed, in some there appeared to be a hole or tear near the apex. No obvious cause was apparent in the remainder, and the ligature was intact in all.

Survival during the electrophysiological study was 87%. Three deaths occurred during attempted insertion of the catheter, possibly due to vascular tears, pneumothorax, or cardiac damage.

Baseline ECG, echocardiographic and HRV measurements are shown in Table 7. Figures are average values: for parameters assessed as normal, mean is reported; if not, median is reported. The statistical test performed was either unpaired t-test or Wilcoxon Ranksum/Mann-Whitney U. A representative example of an ECG recorded using the ECGenie is shown in Figure 49.

		Controls (n=18) (SD or IQR)	**cKOs** (n=16) (SD or IQR)	p-value
ECG	HR, bpm	675 (71)	671 (88)	0.877
	PR, ms	31.8 (2.0)	31.8 (2.3)	0.977
	QRS, ms	10.4 (0.7)	10.1 (0.8)	0.382
	QTs, ms	17.0 (1.4)	17.5 (1.3)	0.288
	QTc, ms	39.8 (5.9)	40.9 (4.9)	0.581
Echo	LVIDd, mm	4,0 (0.3)	3.9 (0.5)	0.508
	LVIDs, mm	2.8 (0.4)	2.6 (0.5)	0.296
	FS, %	31.2 (28.0-35.0)	33.4 (27.5-39.5)	0.220
	EF, %	58.5 (56.0-65.0)	62.4 (54.0-71.5)	0.201
	EndoD, mm^2	10 (1.6)	9.8 (1.3)	0.663
	EndoS, mm^2	4.5 (1.0)	4.1 (1.1)	0.233
	FAC, %	55 (5.5)	59 (7.5)	0.136
HRV	HR, bpm	677 (75)	670 (86)	0.796
	SDNN, ms	3.70 (2.64-11.10)	9.11 (2.96-18.84)	0.138
	RMSSD	2.97 (1.38-6.97)	9.01 (2.16-21.66)	0.049
	Tpower, ms^2	12.26 (5.28-115.45)	79.97 (6.81-351.19)	0.121
	VLF, ms^2	6.34 (3.65-35.23)	35.75 (3.77-70.56)	0.317
	LF, ms^2	3.45 (0.81-45.61)	16.99 (1.69-144.74)	0.147
	LFnu	54.98 (15.24)	42.07 (11.61)	0.010
	HF, ms^2	1.47 (0.63-11.39)	13.30 (1.44-121.74)	0.053
	HFnu	31.61 (9.52)	39.84 (11.41)	0.029
	LF/HF	2.05 (1.05-2.57)	1.05 (0.76-1.47)	0.020

Table 7 Baseline ECG, echocardiographic and HRV measurements. cKO: cardiospecific knockout. HR: heart rate, PR/QRS/QTs/QTc: intervals as described in text, LVIDd/s: left ventricular internal dimension in diastole/systole, FS: fractional shortening, EF: ejection fraction, EndoD/S: endocardial area in diastole/systole, FAC: fractional area change, NN: time between successive R waves, SDNN: standard deviation of R-R (N-N) intervals, RMSSD: root mean square of successive differences, Tpower: total power, VLF: very low frequency, LF: low frequency, LFnu: LF in normalised units, HF: high frequency, HFnu: high frequency in normalised units, LF/HF: ratio of LF to HF. SD: standard deviation, IQR: interquartile range.

There were significant differences (with $\alpha = 0.05$) between controls and cKOs for several HRV parameters, both in the time and frequency domains. cKOs had higher RMSSD and HF normalised unit values, whilst they had a lower value for LF normalised unit and LF/HF ratio. In addition, cKOs had a markedly higher HF component, though this did not quite reach significance (13.3 ms^2 vs 1.47 ms^2, p=0.053).

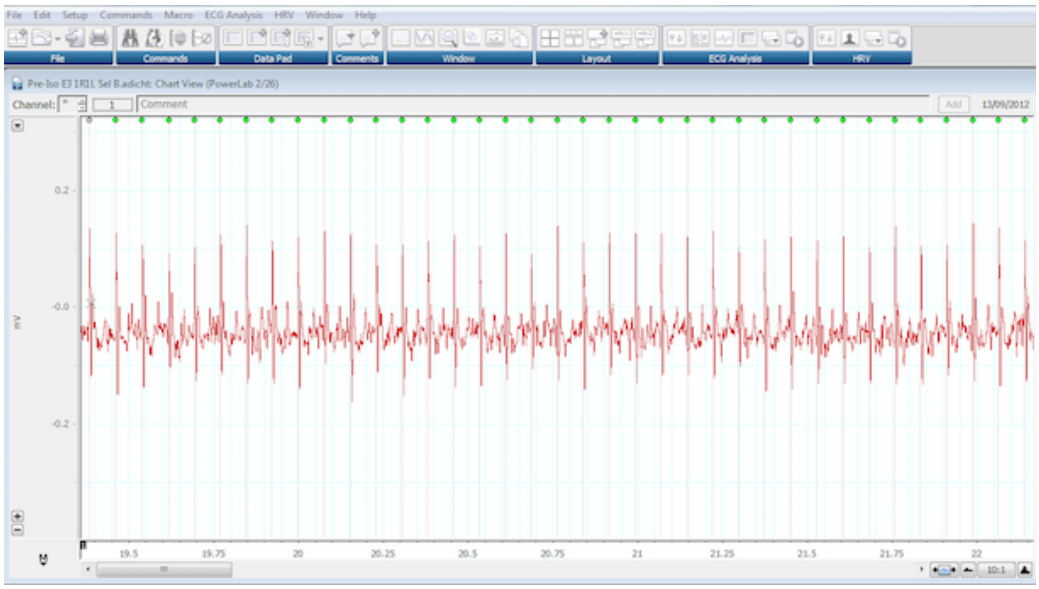

Figure 49 ECG recorded using the ECGenie in LabChart. Green dots mark R waves.

ECGs were recorded during the coronary ligation procedure. Elevation of the ST segment was one of the markers used to indicate successful placement of the ligature, and induction of MI (Figure 50). Some of the cardiac arrhythmias encountered are shown in Figure 51.

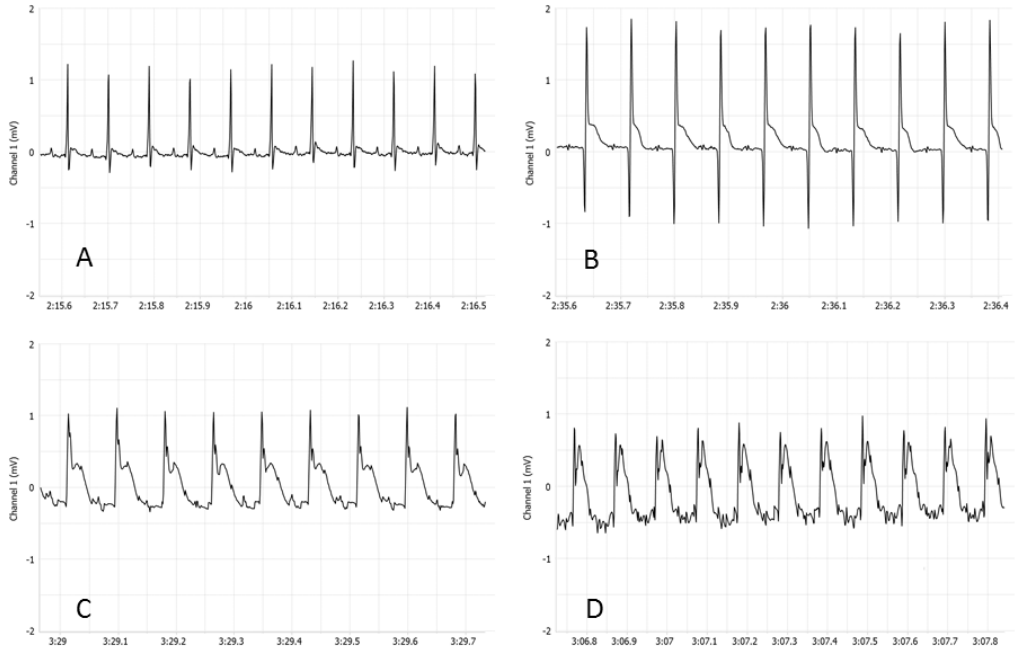

Figure 50 Intra-operative ECGs. Demonstrating normal appearance pre-coronary ligation (A), and worsening degrees of ST elevation immediately following ligation (B to D).

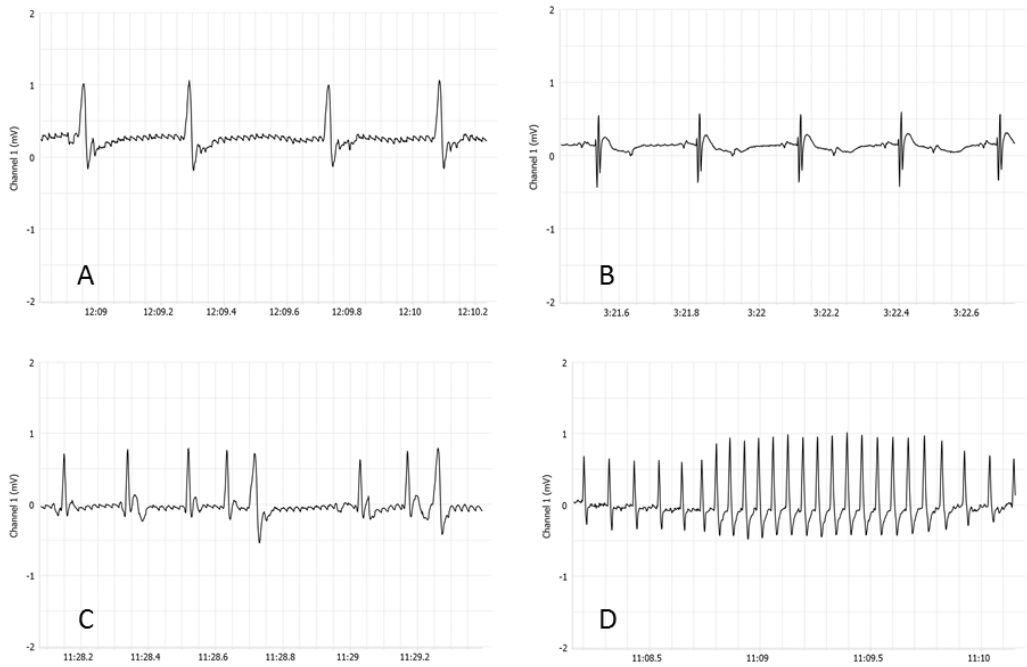

Figure 51 Cardiac rhythm abnormalities encountered during the coronary ligation procedure. Bradycardia of unknown origin (A) and 2:1 heart block (B) portended a poor prognosis. Premature ventricular beats (C) were rarely seen, as was NSVT (D).

In Table 8, average ECG, echo and HRV parameters recorded one week post surgery are reported. QTc was longer for cKOs (p=0.058), although this possible difference must be interpreted with caution, given the difficulty in measurement of the QT interval in mice, particularly following myocardial infarction (see Figure 52).

		Controls (n=12) (SD or IQR)	**cKOs** (n=11) (SD or IQR)	p-value
ECG	HR, bpm	712 (50)	727 (68)	0.560
	PR, ms	31 (2)	30 (2)	0.283
	QRS, ms	12 (11-13)	13 (12-14)	0.092
	QTc, ms	48 (8)	54 (6)	0.058
Echo	EndoD, mm^2	12.4 (4.6)	13.0 (2.8)	0.711
	EndoS, mm^2	7.9 (4.8)	9.3 (3.0)	0.437
	FAC, %	41 (17)	30 (11)	0.093
HRV	HR, bpm	724 (43)	729 (76)	0.824
	SDNN, ms	3.45 (2.20-4.33)	2.81 (1.83-5.82)	0.623
	RMSSD	2.20 (1.87-2.77)	1.97 (1.46-4.70)	0.623
	Tpower, ms^2	10.8 (4.49-19.43)	7.41 (3.60-40.52)	0.667
	VLF, ms^2	5.05 (1.12-12.91)	2.73 (1.92-9.15)	0.806
	LF, ms^2	2.11 (0.91-4.49)	1.88 (0.60-19.89)	0.951
	LFnu	54.97 (24.15)	53.22 (16.34)	0.842
	HF, ms^2	1.16 (0.65-1.92)	0.90 (0.51-9.16)	0.951
	HFnu	25.6 (10.9)	29.1 (11.1)	0.456
	LF/HF	2.73 (1.75)	2.23 (1.34)	0.450

Table 8 ECG, echocardiographic and HRV parameters one week after surgery. cKO: cardiospecific knockout. HR: heart rate, PR/QRS/QTs/QTc: intervals as described in text, LVIDd/s: left ventricular internal dimension in diastole/systole, FS: fractional shortening, EF: ejection fraction, EndoD/S: endocardial area in diastole/systole, FAC: fractional area change, NN: time between successive R waves, SDNN: standard deviation of R-R (N-N) intervals, RMSSD: root mean square of successive differences, Tpower: total power, VLF: very low frequency, LF: low frequency, LFnu: LF in normalised units, HF: high frequency, HFnu: high frequency in normalised units, LF/HF: ratio of LF to HF. SD: standard deviation, IQR: interquartile range.

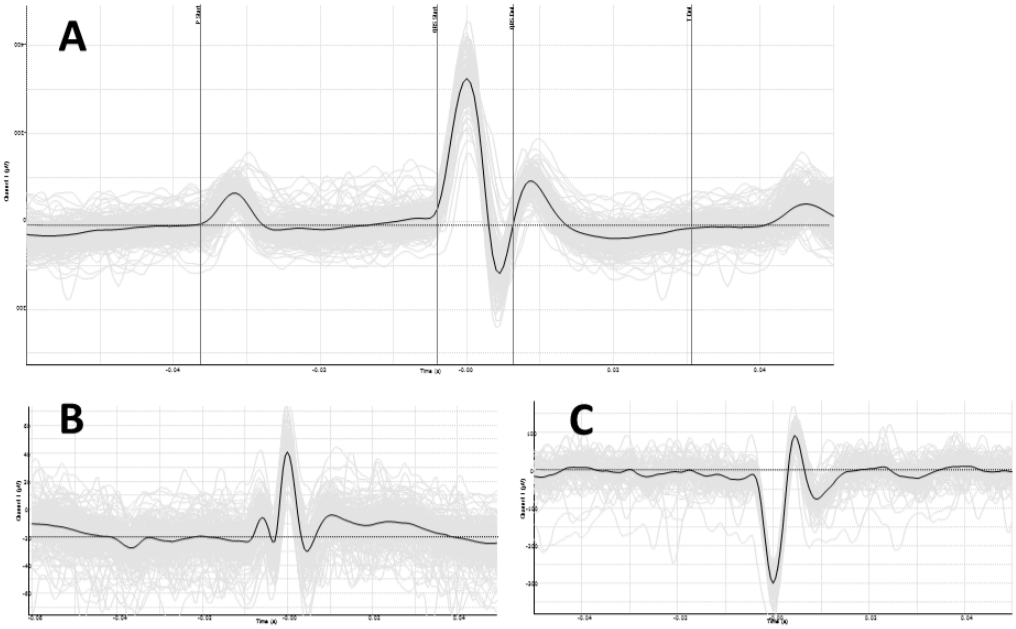

Figure 52 Examples of signal averaged ECG complexes from recordings using the ECGenie. A: a baseline recording, with the following marked by vertical lines – P wave start, QRS start, QRS end, T wave end. B: a post-MI recording to illustrate the difference in T wave morphology due to persistent ST elevation and lack of dip below baseilne seen in A. C: a post-MI recording to show lack of clear T wave.

Examples of FAC measurement and LVIDd/LVIDs measurement in a mouse with severe LV impairment following MI are shown in Figures 53 and 54.

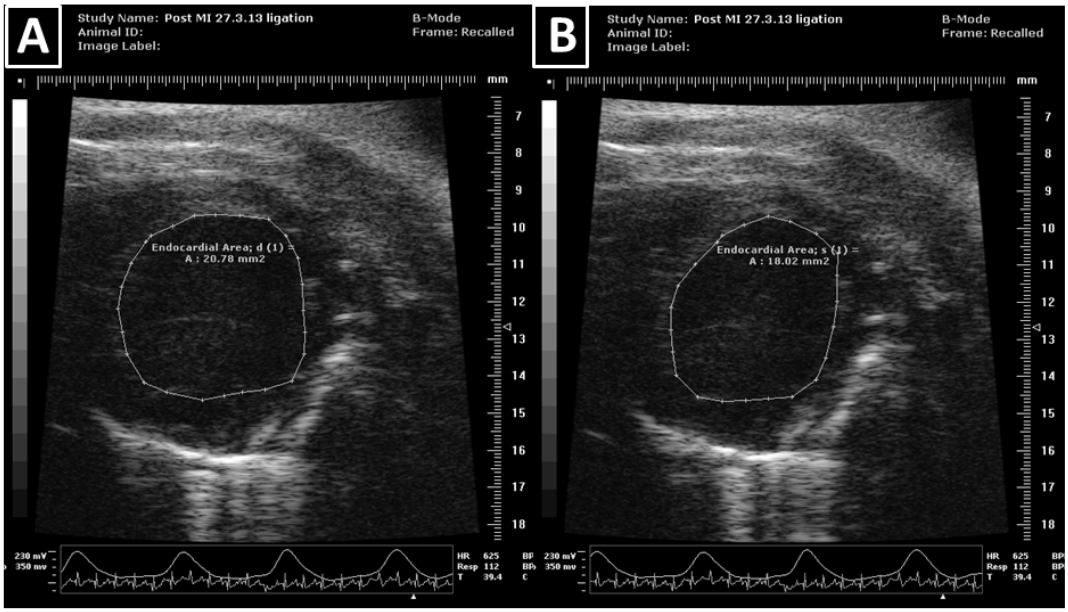

Figure 53 FAC measurements in a mouse with severe LV impairment following coronary ligation-induced MI. The endocardium is traced in diastole (A) and systole (B) to derive the endocardial area from which FAC can be calculated.

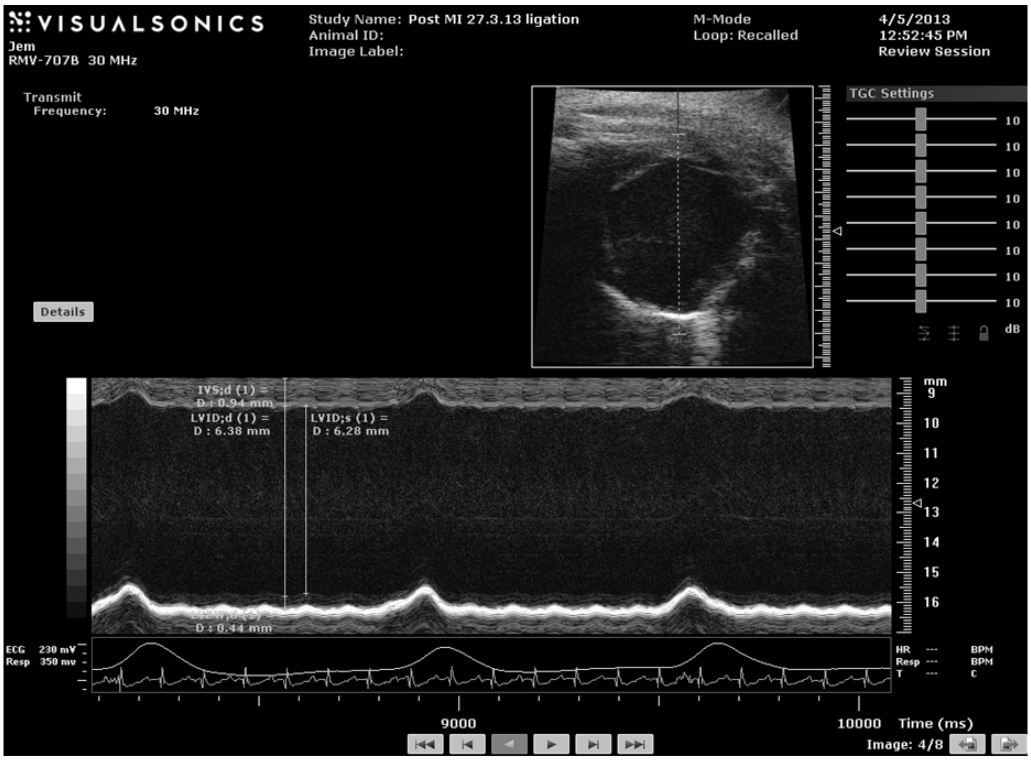

Figure 54 M-mode measurements of LV dimensions from which FS is calculated. Wall thickness measures are also shown.

Figure 55 depicts the mean heart rate before and after surgery. Both groups showed an increase from baseline, although this was only significant for the cKO group ($p=0.002$). Mean QRS and QTc also showed significant increases for both groups compared to baseline (for QRS $p=0.006$ for controls; $p= 0.004$ for cKOs; for QTc $p=0.015$ for controls and $p<0.001$ for cKOs).

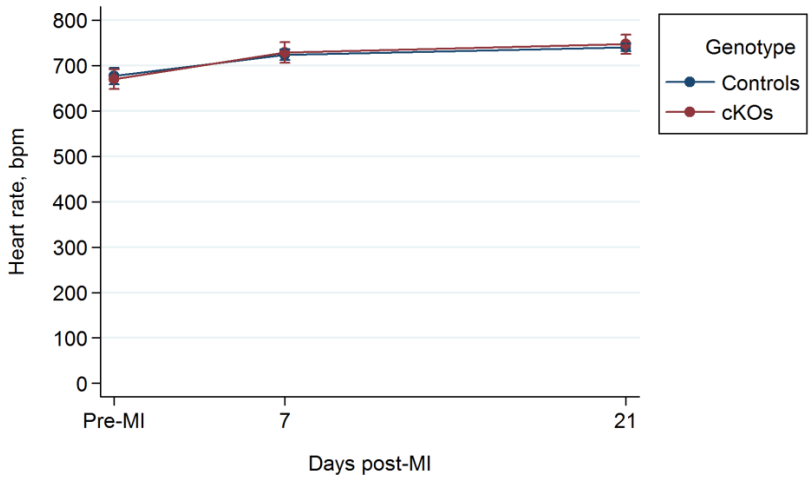

Figure 55 Mean heart rate (+/- SEM) for cKOs and Controls. At baseline, and at one and three weeks following coronary ligation-induced MI in cKOs and controls.

In Figure 56 the decrease in LV contractility following MI is shown. This was of course expected, and is statistically significant for both groups (p=0.028 for controls, and p<0.0001 for cKOs). Of possible interest is the larger reduction in FAC for cKOs than controls (-29% vs -14%), suggesting a greater infarct size in cKOs.

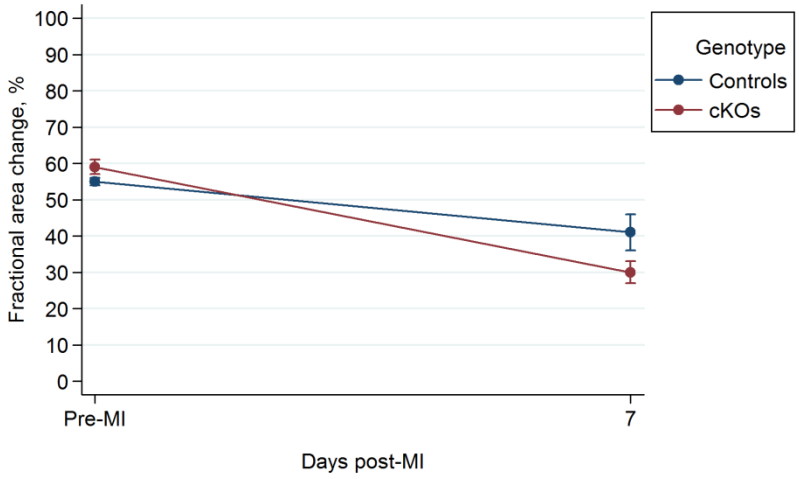

Figure 56 Mean fractional area change (+/- SEM) for cKOs and Controls. At baseline, and at one week following coronary ligation-induced MI in cKOs and controls.

Heart rate variability indices at 21 days post surgery are shown in Table 9. By this stage, there were no significant differences between groups. Compared to baseline, heart rate increased for both groups, but this was only significant for cKOs (p=0.006 vs p=0.209). The following parameters all showed non-significant decreases by day 21 for controls: SDNN, RMSSD, total power, HF, and HF in normalised units. VLF showed a significant reduction (p=0.028). Conversely, reductions in the same parameters compared to baseline were seen for cKOs, and all were significant except VLF: SDNN (p=0.013), RMSSD (p=0.013), total power (p=0.010), HF (p=0.013) and HF normalised units (p=0.014).

	Controls (n=12) (SD or IQR)	**cKOs** (n=11) (SD or IQR)	p-value
HR, bpm	740 (29)	747 (71)	0.742
SDNN, ms	2.47 (2.29-3.44)	2.00 (1.44-4.69)	0.623
RMSSD	1.69 (1.23-2.79)	1.73 (1.24-6.36)	0.758
Tpower, ms^2	5.53 (4.47-9.08)	4.35 (1.75-21.91)	0.667
VLF, ms^2	2.99 (1.53-4.89)	2.32 (0.69-7.95)	0.580
LF, ms^2	1.43 (0.78-1.97)	0.64 (0.43-11.27)	0.758
LFnu	55.35 (23.32)	45.21 (17.80)	0.258
HF, ms^2	0.58 (0.34-1.57)	0.48 (0.23-5.49)	0.758
HFnu	21.48 (19.57-28.72)	26.68 (17.27-37.72)	0.460
LF/HF	2.80 (1.82)	2.05 (1.48)	0.294

Table 9 HRV indices at 21 days following surgery. cKO: cardiospecific knockout. HR: heart rate, SDNN: standard deviation of R-R (N-N) intervals, RMSSD: root mean square of successive differences, Tpower: total power, VLF: very low frequency, LF: low frequency, LFnu: LF in normalised units, HF: high frequency, HFnu: high frequency in normalised units, LF/HF: ratio of LF to HF. SD: standard deviation, IQR: interquartile range.

Mean LF/HF ratio at the three measurement time points is shown for cKOs and controls in Figure 57. As can be seen, there was a non-significant increase for both groups over the study period.

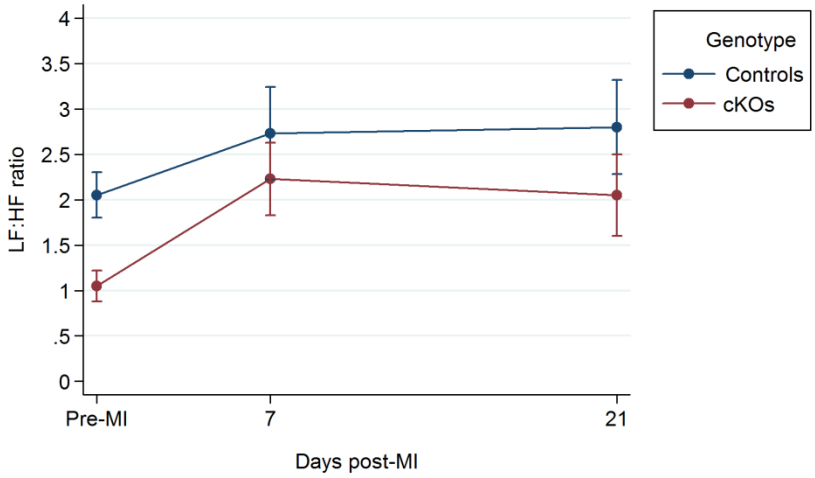

Figure 57 Mean LF:HF power ratio (+/- SEM) for cKOs and Controls. At baseline, and at one and three weeks following coronary ligation-induced MI in cKOs and controls.

The results from electrophysiological testing are shown in Table 10. Wenckebach point was significantly lower for cKOs, whilst VERP was also lower although this was not significant. The slight difference in rates of induction of NSVT during VT stim was non-significant. Illustrative examples of intracardiac EGMs are shown in Figure 58; Wenckebach and VERP can be seen in Figures 59 and 60, respectively.

	Controls (n=10) (IQR)	**cKOs** (n=10) (IQR)	p-value
Wencke, ms	85 (70-90)	60 (60-70)	0.040
VERP, ms	40 (30-40)	30 (20-40)	0.167
NSVT	3/10	5/10	0.650

Table 10 Results from electrophysiological testing. Wencke: Wenckebach point, VERP: ventricular effective refractory period, NSVT: non-sustained VT. SD: standard deviation, IQR: interquartile range.

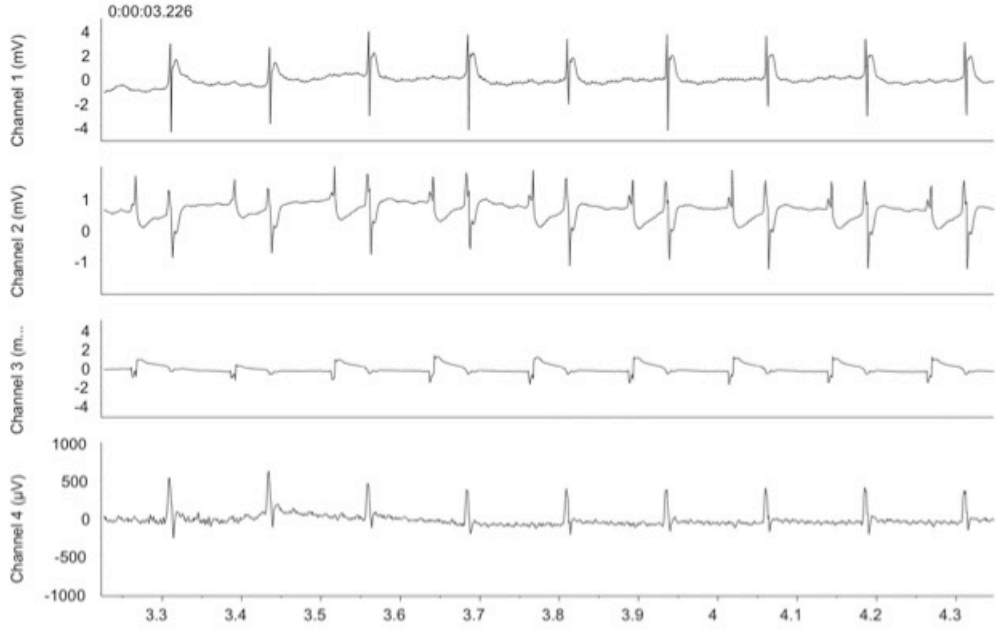

Figure 58 ECG and intracardiac EGMs during electrophysiological study. Channel 1 (top) shows ECG recorded with needle electrodes. Channels 2-4 show EGMs. In channel 2 and 3, atrial and ventricular EGMs can be seen, whereas channel 4 has just ventricular activity.

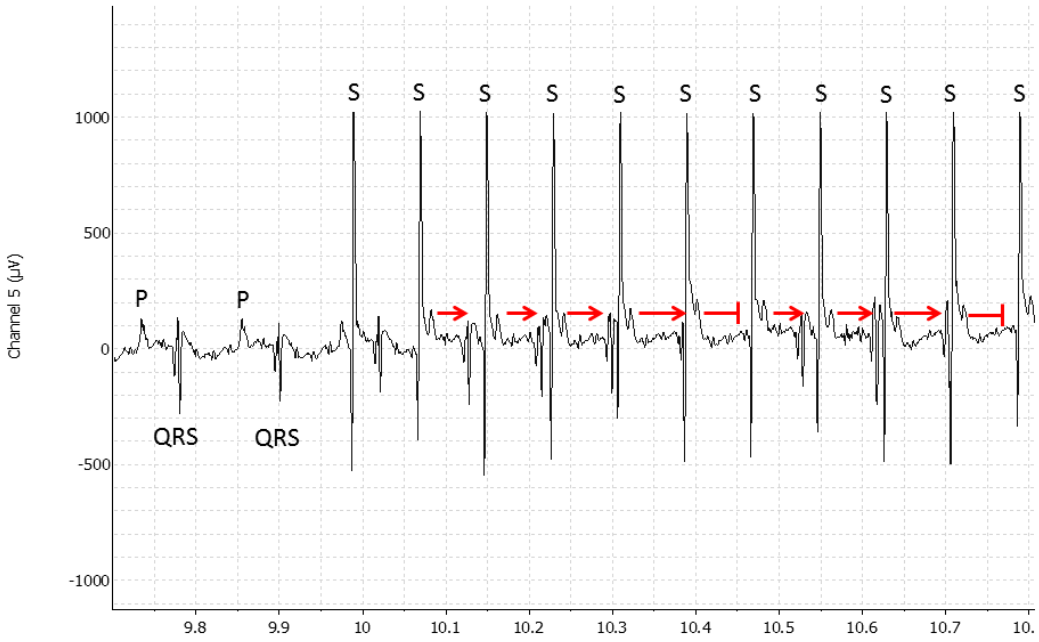

Figure 59 Wenckebach during atrial pacing. At the start of the trace, two spontaneous beats are seen, with atrial P wave and ventricular QRS complexes. Atrial stimulation then begins (S), with atrial capture with the second stimulus. This is conducted to the ventricle, resulting in a QRS (first red arrow). Four such beats are conducted, with the interval between atrial capture and ventricular QRS prolonging progressively, until the fifth beat, where atrial activity is not conducted to the ventricle (red block sign). Conduction then resumes for three beats, before blocking again.

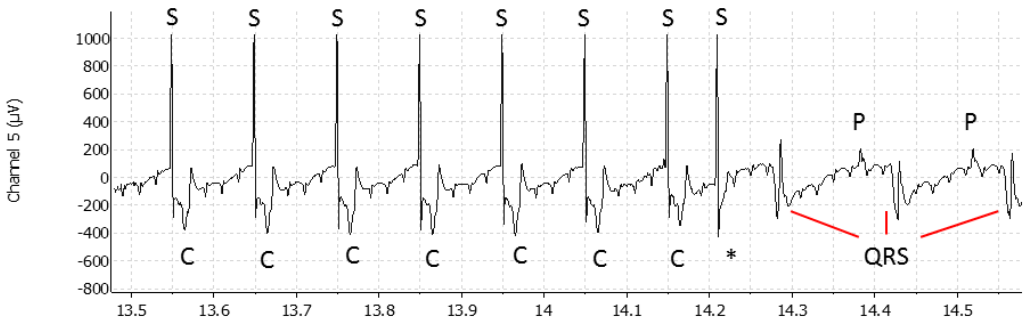

Figure 60 Ventricular effective refractory period (VERP) during programmed electrical stimulation. A series of stimuli (S) result in capture of the ventricle (C), but at the final stimulus which is of a shorter coupling interval than those preceding it, there is no capture (*). Following this there is a spontaneous ventricular escape beat, followed by two sinus beats (P followed by QRS).

6. DISCUSSION - EFFECTS OF Gαi2 KNOCKOUT IN A MYOCARDIAL INFARCTION MODEL OF HEART FAILURE

6.1 Introduction

The bases of the hypothesis that $G\alpha_{i2}$ is anti-arrhythmic in the ventricles were human studies demonstrating elevation of this protein in patients with heart failure. After establishing the coronary ligation-induced MI model of heart failure, this was used to bring the genetically-modified mouse model closer to the human disease state of interest, so as to better reflect the arrhythmic substrates seen in this condition.
The failure to demonstrate complete knockout of $G\alpha_{i2}$ was of course unexpected. The first RT-qPCR analysis of mRNA was performed during the coronary ligation study, and the surprising results were thought attributable to the primer sequences used. As another member of the research group had previously shown near-complete knockout of $G\alpha_{i2}$ in mice with the same genetic modification and Cre under control of the α-MHC promoter (unpublished data), the decision was made to continue with experiments in the expectation that repeating the RT-qPCR with the original primers would demonstrate knockout.
In the end, it seems knockdown rather than knockout was produced in $G\alpha_{i2}^{Flx/Flx}$ Cre+ mice. The issues surrounding this are discussed first, as the results influence to some extent the interpretation of the main study data. The results from cardiovascular phenotyping of cKOs and controls at baseline, and following MI, are then dissected. Contrary to expectations, few differences were noted between groups, despite a reasonable sample size, and rigorous quality control of experimentation and analysis.

6.2 Unexpected knockdown rather than knockout of $G\alpha_{i2}$

Expression of $G\alpha_{i2}$ was assessed in three ways: at the DNA level with PCR and Sanger sequencing, and at the mRNA level with RT-qPCR. Protein expression was not performed as prior experience within the group suggested the antibodies available had poor specificity for $G\alpha_{i2}$ compared to the other $G\alpha_i$ isoforms.

The results from DNA genotyping with PCR and from Sanger sequencing (Figures 43 to 45) were in accordance with knockout of the *GNAI2* gene in cKO mice. With the former, clear PCR amplicon bands were seen at the sizes expected for KO and WT alleles, and for Cre. The Sanger sequencing results demonstrated large gaps over the expected exons when aligned with reference sequences; these gaps were not seen with the Flx/Flx or WT (Cre absent) samples, and correspond to excision of sections of the gene. Further reassurance comes from prior work in our group demonstrating cardiac-specific $G\alpha_{i2}$ knockout with αMHC driven Cre expression (unpublished data). A greater than 10-fold reduction in cardiac $G\alpha_{i2}$ expression was seen in knockout mice, compared to controls.

The failure to demonstrate knockout of $G\alpha_{i2}$ expression in the heart with RT-qPCR of mRNA was clearly unexpected as were the inconsistent results for liver; nevertheless, the pooled data do suggest likely cardiac specificity. The explanation could lie within the tissue, at the tissue removal and mRNA analysis stage, or as a result of calculation error. Genotypic analysis clearly demonstrated the presence of Flx/Flx alleles in the *GNAI2* gene, and the presence of the Cre genetic sequence in ear tissue. So if there were a problem of Cre-mediated excision in the heart it would seem likely to be related to Cre expression or function. Only ventricular tissue was analysed, so contamination by extra-cardiac tissue is unlikely to have occurred. As noted in the *Chapter 1* though, fibroblasts constitute approximately 50% of cells in the heart. While this would have been the case with analyses performed by some of the other groups in which near-complete knockdown was observed, it is noteworthy that in two of these studies this was for cardiac genes of interest such as cardiac myosin binding protein C or SERCA2[200,201]. Assuming these proteins are not expressed in cardiac fibroblasts, deletion in cardiomyocytes would lead to near-total loss of the protein at mRNA level. $G\alpha_{i2}$ on the other hand is more ubiquitously expressed, and without αMHC-driven Cre in fibroblasts, expression may remain, with apparent incomplete knockout when cardiac tissue as a whole is analysed.

However, in one of the original papers describing the use of Cre to achieve cardiospecific gene deletion, Agah et al demonstrated Cre-mediated excision specific for murine ventricular myocytes both *in vitro* and *in vivo*[198]. In both systems, a CAG-CATZ reporter harbouring the chloramphenicol acetyltransferase (CAT) gene flanked by loxP sites was used in conjunction with a LacZ reporter system (the *E. coli* β-galactosidase gene), and Cre under control of the αMHC promoter. Cre-mediated excision of the CAT gene allowed read-through of LacZ, which in the presence of the substrate X-gal produced a colour change in the tissue. PCR analysis confirmed

cardiomyocyte-restricted, Cre-dependent recombination in myocytes both *in vitro* and *in vivo*. In the former, LacZ activity was specific for myocytes (when compared with fibroblasts); in the latter, 90% of ventricular myocytes were LacZ-positive, and CAT activity was reduced by a similar percentage in αMHC-Cre$^+$/CAG-CATZ$^+$ mice relative to expression in mice with CAG-CATZ alone. Thus, myocyte specificity and Cre-efficacy was demonstrated using an exogenous reporter system by the group who provided us with the αMHC-Cre$^+$ mice.

Nevertheless, it is interesting to note that even with gKOs, Köhler et al found that despite almost total loss of $G\alpha_{i2}$ mRNA, protein levels were not nearly so reduced. The authors showed evidence for the specificity of the antibodies used, but did not discuss the incomplete protein knockout seen[89].

Preservation of mRNA was performed in the standard manner used within the group, i.e. by immersion of the tissue in a preservative solution prior to freezing. The ventricles from each heart were placed whole in this solution, and although small, it is possible that cells in the middle of the wall did not come into contact with the preservative, with consequent mRNA degradation.

The use of two sets of primers, and the similar levels of knockdown in the heart seen in both experiments argues against technical error. And finally, the calculation method is in widespread use, and each organ/gene (e.g. heart GAPDH) was repeated in triplicate to ensure consistency.

In summary, incomplete knockout of $G\alpha_{i2}$ in the hearts of cKOs was seen, at the mRNA level. The two most likely reasons are reduced Cre expression or activity, or 'contamination' of cardiomyocyte mRNA by fibroblasts. Further clarification could be achieved using a LacZ reporter mouse to check for diminution of Cre expression or efficacy in recombination, though as noted earlier, our Cre line was provided by the same group who used such a reporter to demonstrate its efficacy. Alternatively, protein analysis could be revisited if it were felt that more suitable antibodies were now available.

6.3 Reasons for choosing (tissue-specific) knockouts rather than 'knockins'

It may at first seem counterintuitive to have chosen to use $G\alpha_{i2}$ knockouts rather than assessing the phenotype where $G\alpha_{i2}$ expression is increased, given that this is what

occurs in heart failure. A gain of function $G\alpha_{i2}$ 'knockin' model has been described in which a mutation leading to substitution of serine for glycine at amino acid 184 prevents RGS binding and resultant insensitivity to GTPase activity[270]. In fact though, both gain and loss of function are useful in elucidating the role of $G\alpha_{i2}$, and knockouts may be more suitable for the heart failure model.

By creating a cohort of mice with LV impairment, those with WT alleles of $G\alpha_{i2}$ may be expected to show elevation of this protein, or at least continue to express it at normal levels. Indeed, this has been demonstrated in wild-type mice which underwent ischaemia-reperfusion injury, compared to sham-operated mice[271]. In contrast, knockouts would have no or minimal expression. The difference between WTs and knockouts therefore would be limited to $G\alpha_{i2}$ expression, and WTs would be expected to show a less arrhythmic phenotype, whereas without the anti-arrhythmic effects of $G\alpha_{i2}$ knockouts would exhibit the converse.

An alternative strategy could have been to use knockin mice where $G\alpha_{i2}$ resistant to inactivation would be compared to basal levels in WT mice, and to study the ease of induction of arrhythmias for example. The expectation here would be that knockins would be more resistant to arrhythmia induction. It would have been incumbent upon me to demonstrate that knockins did indeed have increased activity somehow, which may have thrown up similar issues to those encountered in demonstrating knockout. Ideally, a study comparing WTs, knockouts and knockins with and without heart failure would have been conducted. But the study that was performed was governed by the mouse model available, what has already been studied, and time available.

With regards to the use of tissue-specific knockouts necessitating Cre-loxP technology, the reasons for choosing these remain valid: gKOs are smaller[272], can suffer from immune-related diseases[192–194], and do not breed nearly as easily. The extra-cardiac effects of gene deletion could introduce bias into experiments *in vivo*, and the ease of breeding is important not only from a time perspective as a lone researcher, but also in terms of replacement, reduction and refinement.

6.4 Myocardial infarction model of heart failure

6.4.1 Overview

To examine the electrophysiological effects of $G\alpha_{i2}$ *in vivo*, electrophysiological parameters and LV contractility was assessed for cKOs and littermate controls at

baseline, and following induction of LV impairment with coronary ligation. The flow of mice through the study is shown in Figure 48. The key electrophysiological parameters assessed at each stage were heart rate, corrected QT interval, and HRV indices. A terminal invasive electrophysiological study was performed three weeks following coronary ligation.

6.4.2 Operative survival rate

Peri-procedural mortality was very low at 3%, and mortality up to the point of electrophysiological study was also reasonable at 32%. Both these figures compare favourably with statistics from other investigators[211–214] (see *Section 1.8*). Three of 23 mice (13%) undergoing electrophysiological study died during the procedure; this was unfortunate but considered acceptable given its invasive nature.

6.4.3 Baseline measurements

Heart rate

The lack of an observed difference in heart rate between controls and cKOs appears at first to contradict previous findings with gKOs, which had higher resting heart rates than controls[108]. However, this lack of difference could in fact be expected, given that *GNAI2* gene knockout would not have occurred within the sinoatrial node, which governs heart rate. This is because αMHC-driven Cre expression does not occur in these cells[199]. A further contribution to the difference seen with gKOs may have come from knockout occurring in autonomic nerve fibres innervating the heart, and within the brain. Interestingly, using the RGS-insensitive *GNAI2* knockin model mentioned above, Huang et al found a higher daytime heart rate among knockins compared to controls[270]. These findings are much harder to explain, given that with these animals parasympathetic over-activity would be expected to reduce heart rate, particularly during the day when they are typically asleep.

QTc

The similar QTc seen in controls and cKOs is noteworthy, as it differs from previous findings in gKOs in which QTc was prolonged[94]. The measured values were quite different however: 63.4ms (controls) and 81.1ms (gKOs), compared to 39.8ms (controls) and 40.9ms (cKOs) in the present study. QT interval measurement in humans is not without its problems, and the difficulties of measurement in the mouse are compounded by the more gradual return to baseline of the terminal T wave.. Given the larger number of mice in the present study, and the review of each signal-averaged ECG to ensure accurate interval measurement rather than relying on automated readings, it could be argued that these values are more reliable. Additionally, although in the study by Zuberi et al the prolonged APD seen in knockouts was in accordance with what might be expected if the QT interval were prolonged, APD was measured at room temperature. It is known that there is an inverse relationship between APD and temperature[167,273] and so APD would be expected to be shorter at 37°C, and the magnitude of the difference may be reduced. Alternatively, the incomplete knockout may have prevented QTc differences from emerging, though with moderate $G\alpha_{i2}$ suppression a subtle difference could perhaps be expected.
A possible way to at least partially reconcile the findings of my study (no difference in QTc) with the increased Ca^{2+} currents observed by Zuberi et al, is that the increased Ca^{2+} may in fact make re-excitation possible prior to full repolarisation in a manner analogous to EADs, such that the ERP measured actually reflects a Ca^{2+}-dependent re-activation process.

Heart rate variability

Also difficult to explain are the differences seen in heart rate variability indices. As discussed in the *Chapter 1*, heart rate is under the control of the sinoatrial node (assuming normal cardiac rhythm), which in turn is under the influence of autonomic inputs. Without $G\alpha_{i2}$ knockout in the sinoatrial node (due to absent αMHC and hence Cre expression there), its electrophysiological function could be expected to be the same as in controls. As should the autonomic inputs (a combination of neurones and hormones), given the lack of Cre expression in non-cardiomyocytes. Strangely, not only were there apparent differences between groups, but several differences seen were opposite to those reported for gKOs[108]. For cKOs, RMSSD was 3-fold higher than

in controls, whereas the reverse was found with gKOs. Total and HF power were higher in cKOs than controls, although total power did not reach significance; the converse was seen with gKOs. Normalised LF (LFnu) and LF/HF ratio were lower in cKOs, whilst with gKOs no significant differences were noted.
It is tempting to begin to make inferences regarding possible alterations to the autonomic nervous system in cKOs. However, on the assumption that *GNAI2* knockout was limited to cardiomyocytes, any such inferences seem implausible. Indeed, it would seem more likely that the observed differences resulted from external factors, leading to a type I error. These could be, for example, environmental factors related to the room in which ECG recording was performed, including temperature, smells, and noise, which stressed the animals. Or they could be related to the method of ECG recording for HRV, and the analysis algorithms. One of the strengths of Zuberi et al's work was the use of implantable telemetry devices that enabled significantly longer periods of ECG recording than the short epochs in my study. Also, while those mice had undergone implantation procedures, the recordings were made in their normal environment in a cage. The telemetered ECG data were therefore probably more representative of the mice's normal heart rates.

LV contractility

There was no difference in contractility between cKOs and controls, as assessed by FAC, FS or EF, and LV dimensions were also similar between groups. These findings are in agreement with those of Zuberi et al[94] and Huang et al[270]. Although the latter study investigated gain of function $G\alpha_{i2}$ mice, the lack of difference across three studies supports the idea that $G\alpha_{i2}$ is not directly important in terms of contractility.

6.4.4 Post-myocardial infarction measurements

Heart rate and ECG indices

Heart rate in knockout mice increased significantly from baseline (671 to 727bpm, p=0.002), whereas in control mice heart rate also increased, but this was not significant (675 to 712bpm, p=0.368). It is possible this greater increase in knockouts was related to the more severe LV impairment induced (see below). There were significant

increases from baseline in QRS and QTc duration for both groups. The change in QRS duration is expected and also occurs in humans. It reflects delayed conduction/propagation through the heart as a result of scarred areas, and possibly electrophysiological changes. As already discussed, baseline QT measurement in mice is challenging, and as Figure 52 shows, it can be impossible following MI. Therefore changes in QTc must be interpreted with caution. Even if a clear T wave end can be discerned, prolongation may simply reflect the QRS prolongation seen. Bearing this in mind, comparison between groups post-MI revealed knockouts had significantly longer QTc than controls.

LV contractility

There were no significant differences between groups for echocardiographic indices, although it is noteworthy that cKOs had a lower FAC (30% vs 41%, p=0.093) than controls. This is in keeping with an accumulating body of evidence suggesting that $G\alpha_{i2}$ signalling is protective, at least in the setting of ischaemia. In 2000, Chesley et al showed that β2AR signalling was protective against apoptosis induced by hypoxia or H_20_2, and that this appeared to be mediated by a $G\alpha_i$-PI3K pathway[224]. This was challenged by Oudit et al who found that PI3K signalling was in fact important in the hypertrophy and fibrosis response resulting from βAR stimulation. Subsequently using a $G\alpha_i$-inhibitor peptide, DeGeorge et al showed that mice expressing the peptide had significantly increased infarct sizes compared to WTs. And exploring the effects of increased $G\alpha_{i2}$ activity, Waterson et al reported that infarcts as a proportion of area at risk in Langendorff-perfused mouse hearts were smaller in those hearts with the gain of function (RGS insensitive) mutation[274].
More recently, further support for a protective role of $G\alpha_{i2}$ has been published. Köhler et al reported that $G\alpha_{i2}$ knockouts have increased infarct sizes compared to controls, whereas $G\alpha_{i3}$ knockouts have smaller infarcts[89]. The only possibly contradictory evidence to emerge to date with regard to $G\alpha_{i2}$, is that published by Kaur et al. Using the previously mentioned $G\alpha_{i2}$ gain of function model, isoprenaline induced increased fibrosis and collagen III expression in these mice compared with controls[265].
So on balance it appears that $G\alpha_{i2}$ probably protects against ischaemic cell death, which my results are consistent with. The failure to reach significance may have been due to the low power (46%) – each group would have needed 27 mice to achieve 80% power assuming the same differences in means.

Heart rate variability

There were no significant differences between groups at one week post-MI.
At three weeks, the lack of difference in HRV indices persisted. Compared to baseline, although heart rate was increased for both groups, this was only significant for cKOs. Similarly, whilst SDNN, RMSSD, and total power were lower for both groups compared to baseline, these reductions were only significant for cKOs, whereas conversely, the decline in VLF power seen in both groups was only significant for controls. Both HF and HFnu showed significant reductions for knockouts compared to baseline, whereas the changes were non-significant for controls. These findings are broadly in line with those noted in humans following MI[134].

6.4.5 Electrophysiological studies

In electrophysiological studies, cKOs had a significantly lower Wenckebach point (i.e. occurring at a higher heart rate) compared to controls (60ms vs 85ms, p=0.04). This is difficult to explain, as the Wenckebach point is determined by AV nodal function. The cells comprising the AV node are believed to be more similar to those of the sinoatrial node than working cardiomyocytes, in terms of ion channel expression and electrophysiological behaviour. It is inferred from this that $G\alpha_{i2}$ would not therefore be knocked out in these cells, and as such, the observed difference would seem likely to have arisen by chance.
The lower VERP in knockouts, whilst not significant, is worthy of mention due to its concordance with previous findings[94], and indeed, the values for controls and knockouts in each study are nearly identical. This could be expected, given VERP is dependent upon local activation of cardiomyocytes, rather than activation via the conduction system. As discussed in *Section 1.5*, a reduced VERP can, in some circumstances, be pro-arrhythmic as it facilitates re-entry and afterdepolarisation-mediated triggering of arrhythmia.
The lack of apparent difference in induction of NSVT is somewhat surprising. In contrast to the protocol used by Zuberi et al, no isoprenaline was injected as part of the procedure, and this may have resulted in the lower rate of NSVT in knockouts, although more NSVT was noted in controls. The procedure itself is a fairly blunt tool, and as alluded to in *Section 2.4.4*, is no longer often used in risk prediction in humans due to

problems with specificity and predictive power. Factors that may have influenced the results include anaesthesia and size of infarct.

6.4.6 Summary

The strengths of this study into the effects of $G\alpha_{i2}$ knockout in the setting of heart failure were the reasonable numbers of mice in each group, the low peri-operative mortality and reasonable proportions completing the study. Each mouse was intensively phenotyped using several techniques, all by the same investigator. Although there are drawbacks to this latter approach, it did ensure standardisation of data acquisition and interpretation. The ECG recording made use of a non-invasive technique which avoided the confounder of surgery on measurements obtained, and importantly, permitted repeated recordings on conscious animals.

The main weakness of the study was what appears to have been knockdown rather than knockout of the gene of interest. It is difficult to gauge to what extent this could account for the lack of clear electrophysiological differences between cKOs and controls. Non-significant differences in LV contractility post-MI and VERP however, suggest that some functional effect was achieved.

As was alluded to in Section 1.8, LV contractile impairment is not synonymous with 'heart failure', though there is overlap. Also, the increase in $G\alpha_{i2}$ which has been observed occurs as a result of a part of this syndrome which as yet, is undefined. So while a more complete model of heart failure would potentially have included assessments of organ weights to take account of lung congestion for example, and histologic examination of cardiac wall thickness, it is also worth bearing in mind that these changes may take longer to develop than the 21 days of my experimental protocol. There may have been greater attrition during a longer protocol, and although such changes in organ weight may reflect backwards pressure changes, it is uncertain if this is any more reflective of the change(s) required to elevate $G\alpha_{i2}$ levels. Nevertheless, a recent scientific statement on animal models of heart failure recommends such measurements[203], and this would be important to consider for future work.

In relation to the hypothesis that $G\alpha_{i2}$ is anti-arrhythmic in the ventricles, this study has not produced evidence in support of this.

7. RESULTS - MEA STUDIES

7.1 Introduction

The MEA was used to study the electrophysiological parameters of ERP, local activation time and conduction velocity in slices of murine ventricular tissue. The slices were challenged with drugs, and alteration of temperature, and the response of these parameters measured. In addition, slices from gKOs were compared to littermate controls at baseline, and in the presence of the muscarinic agonist carbachol.

As described in the *Chapter 2*, the vast majority of MEA experiments were performed stimulating at an S1 coupling interval of 250 ms, due to the consistent and stable capture achieved with this cycle length, and the ability to complete the experimental protocol, which was dependent on this. Nevertheless, in some of the early experiments, other cycle lengths were also used, though this was solely for baseline measurements. As such, *Section 7.3* below compares ERPs and conduction velocities at these various stimulation cycle lengths.
Sections 7.4 to *7.8* report experimental results obtained when stimulating solely at a cycle length of 250 ms. The mean values from the original data are displayed graphically, and the values at the same times, drug concentrations or temperature as predicted by the multilevel mixed effects model are given in the text. Presentation of the original data needs no justification; those from the model are presented to show their closeness to the observed values, and in recognition of the fact that they may in fact be more representative of the 'true' values, were these same experiments to be repeated many times. This is because when the explanatory variable (e.g. drug concentration) is classed as continuous, the linear models produce overall lines of best fit. In contrast, when classed as a discrete variable, the responses at each value of the explanatory variable are compared to each other in a manner similar to that of RM-ANOVA. Reassuringly, both methods of statistical analysis produced similar results.

Finally, assessment of $G\alpha_{i2}$ knockout status in the gKOs used for these experiments was limited to PCR of ear DNA samples, as global deletion of the gene had already been demonstrated to abolish protein production[243]. Also, in gKOs gene deletion was not dependent upon the extra step of Cre-mediated excision: if two 'knocked-out' alleles

were incorporated, any protein product would be non-functional due to the design of the modified gene.

Illustrative examples of PCR products are shown in Figure 61. The WT allele gave a 805 bp product and the KO allele a 509 bp product.

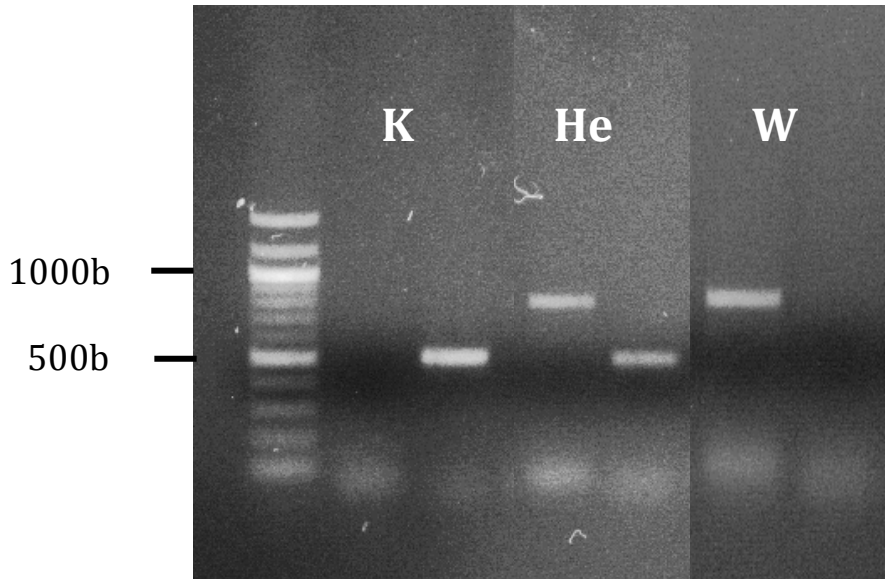

Figure 61 Gel electrophoreses showing illustrative examples of Gαi2 PCR products. KO allele ($G\alpha_{i2}^{-/-}$, 509 bp) and WT allele ($G\alpha_{i2}^{+/+}$, 805 bp). Het: $G\alpha_{i2}^{+/-}$.

7.2 Assessment of Normal Krebs buffer solution

To verify the pH and gaseous composition of the modified Krebs buffer solution used (Normal Krebs) was in the physiological range, the pH was assessed over time for two preprations of the solution (Table 11).

More detailed assessment was made for a further preparation to ensure oxygen, carbon dioxide and $HC0_3^-$ concentrations were physiological. The results are shown in Table 12, and indicate the pH to be slightly lower than the physiological range (7.35 to 7.45), probably as a result of a mild elevation of pCO2.

Time (mins)	pH (solution 1)	pH (solution 2)
0	7.74	7.62
5	7.62	7.45
10	7.55	7.39
25	7.49	7.35

Table 11 pH of the modified Krebs-Henseleit buffer solution during bubbling with carbogen. Two preparations were assessed: solution 1 and 2.

	Baseline	+5 mins	+10 mins	+15 mins
pH	7.82	7.37	7.30	7.27
pO_2	25.3	89.3	93.0	100
pCO_2	2.47	5.83	6.55	7.05
HCO_3^-	37.4	23.9	21.9	21.4

Table 12 Acid-base and gaseous composition during bubbling of modified Krebs-Henseleit buffer solution with carbogen.

7.3 Baseline values of parameters at different cycle lengths

7.3.1 Effective refractory period

In the early stages of experimentation, WT slices were studied at several cycle lengths so as to test how close it was possible to get to physiological heart rates, whilst achieving consistent and reliable results. Baseline ERP measurements are summarised in Figure 62.

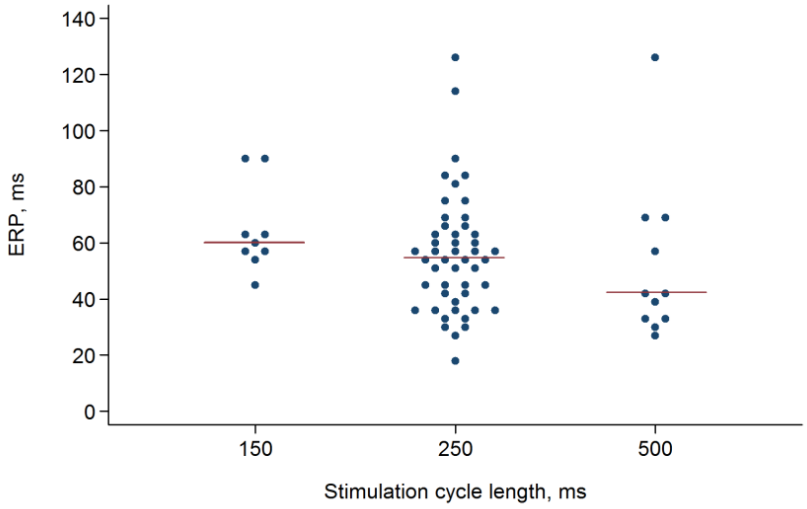

Figure 62 Baseline ERP at different cycle lengths in WT mice. Horizontal lines indicate medians.

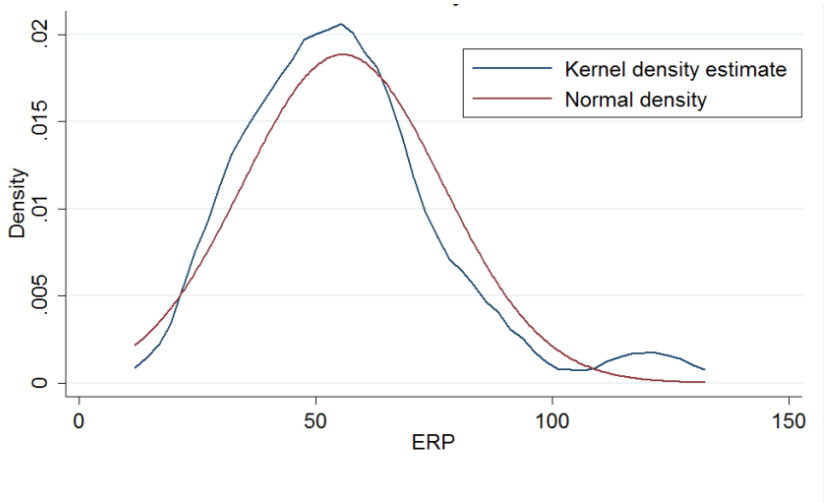

Figure 63 'Kernal density estimate' of ERPs – a means of visualising data values with a superimposed normal plot, to enable assessment of normality.

Figure 63 shows that for a stimulation cycle length (CL) of 250 ms which had by far the largest number of observations, the distribution was reasonably normal, although there was a small second peak. The Shapiro-Wilk test for normality on the other hand suggested the data were not normal.

The robust test of equal variance (Levene's test) did not reject the null hypothesis ($p=0.35$), and in view of this and the fact that analysis of variance (ANOVA) is relatively robust to departures from normality, this was used to test for differences in ERP at different cycle lengths. No between group differences were found ($p=0.428$).

7.3.2 Conduction velocity

Figure 64 summarises the baseline conduction velocity measurements at different stimulation cycle lengths. Figure 65 shows that for a stimulation cycle length (CL) of 250 ms, the distribution was not normal, with a small second peak at higher values. The Shapiro-Wilk test for normality also suggested the data were not normal.

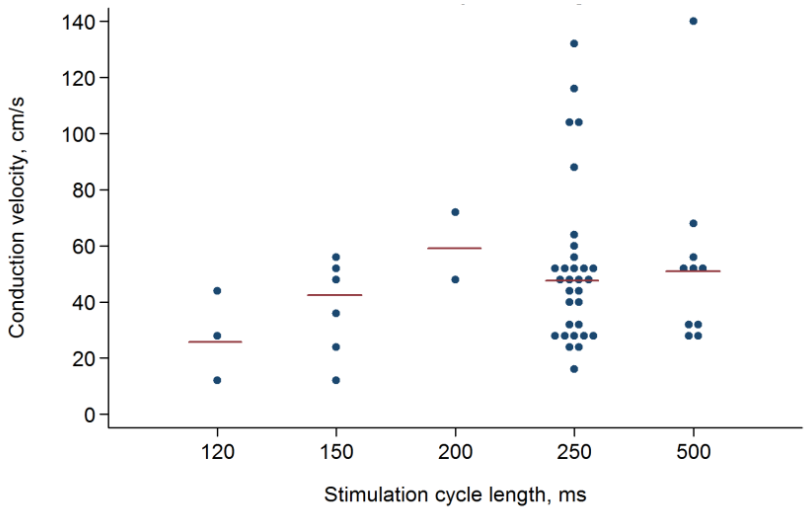

Figure 64 Baseline conduction velocity at different cycle lengths in WTs. Horizontal lines indicate medians.

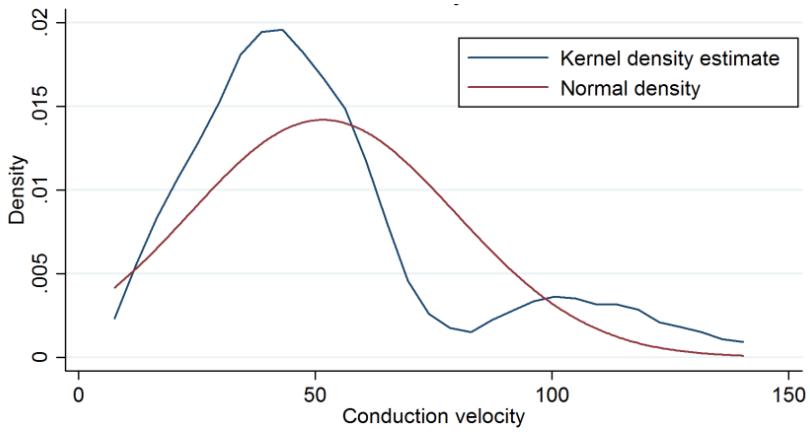

Figure 65 'Kernal density estimate' of conduction velocities – a means of visualising data values with a superimposed normal plot, to enable assessment of normality.

The robust test of equal variance (Levene's test) did not reject the null hypothesis (p=0.84), and in view of this and the fact that ANOVA is relatively robust to departures from normality, this was used to test for differences in conduction velocity at different cycle lengths. No between group differences were found (p=0.475).
A picture of a slice on an MEA as viewed down the microscope is shown in Figure 66.

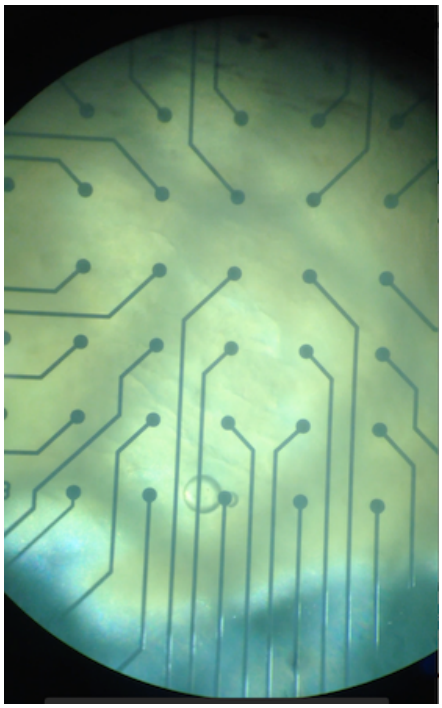

Figure 66 View of ventricular tissue slice on an MEA as viewed through a microscope.

7.4 Control experiments with wild-type slices

7.4.1 Local activation time

Activation times measured from the reference electrode signal (termed 'local activation time') were assessed over 35 minutes at four time points – baseline, 7, 21 and 35 minutes. The results are shown in Figure 67. An illustration of how LabChart was used to calculate the activation time of an electrode's signal using its first temporal derivative is shown in Figure 29.
Model: With time as a continuous explanatory variable, the data were best modelled with random slopes. In this model, there was no significant relationship between local activation time and experimental time (p=0.450). Local activation time at baseline was

2.3 ms, while at 35 minutes it was 2.0 ms. With time as a discrete explanatory variable there was no significant difference between baseline and other time points.

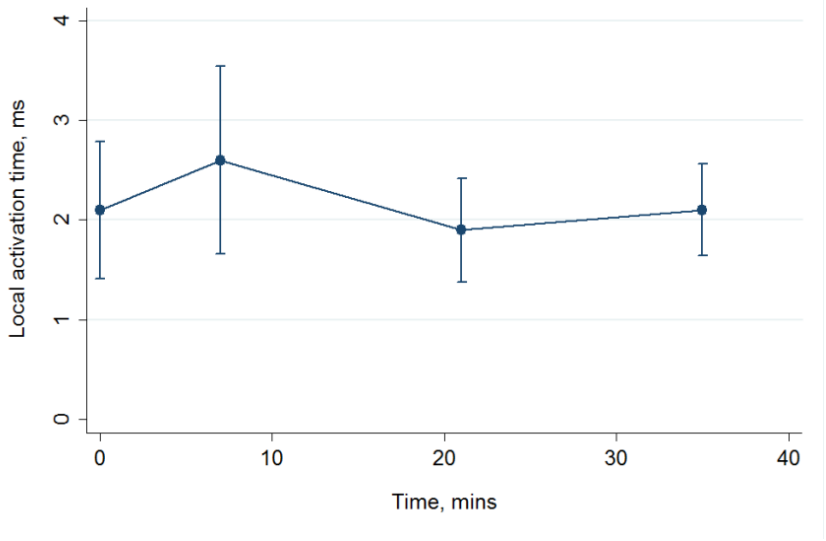

Figure 67 Local activation time in Control experiments with WT mice (n=5).

7.4.2 Effective refractory period

Results are summarised in Figure 68. Model: The relationship between ERP and experimental time as a continuous variable was best modelled with a random intercept model. In this model, there was no significant relationship between ERP and experimental time (p=0.885). Baseline ERP in the model was 43 ms; at 35 minutes it was also 43 ms.

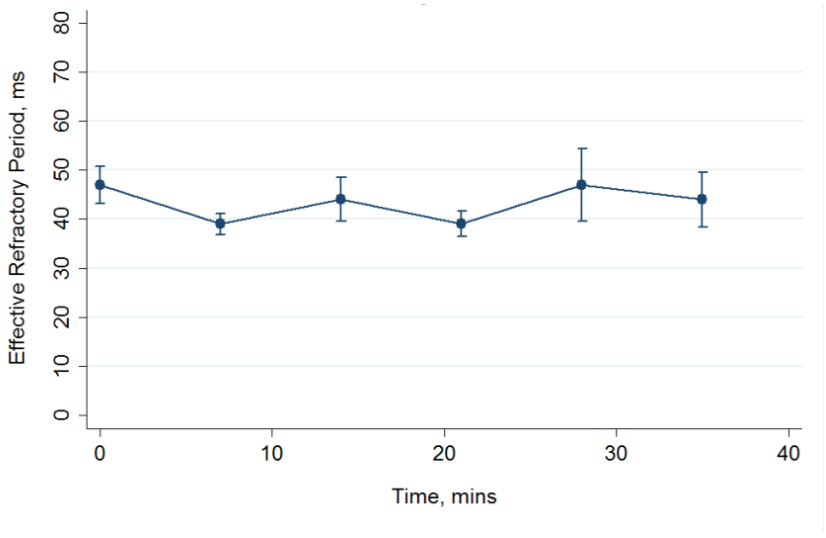

Figure 68 Effective refractory period in Control experiments with WT mice (n=7).

With time as a discrete explanatory variable there were no significant differences between baseline and other time points.

7.4.3 Conduction velocity

Results are summarised in Figure 69.

Model: The relationship between conduction velocity and experimental time as a continuous variable was best modelled with a random intercept model. In this model, there was a small positive linear relationship between conduction velocity and time, which was highly significant (1.2 cm s^{-1} per 7 minutes, p=0.001). Baseline conduction velocity was 37 cm s^{-1}; at 35 minutes it was 43 cm s^{-1}.

With time as a discrete explanatory variable there were small differences between baseline conduction velocity (37 cm s^{-1}) and 7 minutes (+3.6 cm s^{-1}, p=0.049), 21 minutes (+3.6 cm s^{-1} , p=0.049), and 35 minutes (+7 cm s^{-1} , p=0.0001) of experimental time.

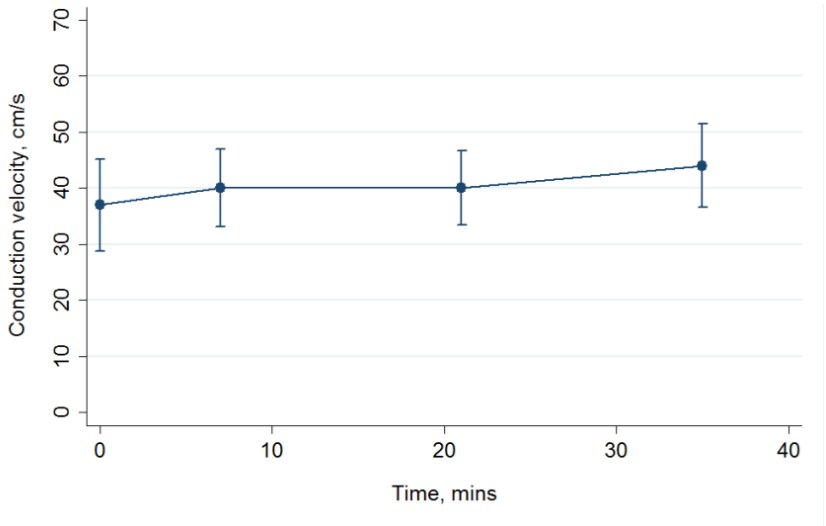

Figure 69 Conduction velocity in Control experiments with WT mice (n=5).

An example of the signals recorded from the MEA during a control experiment is shown in Figure 70.

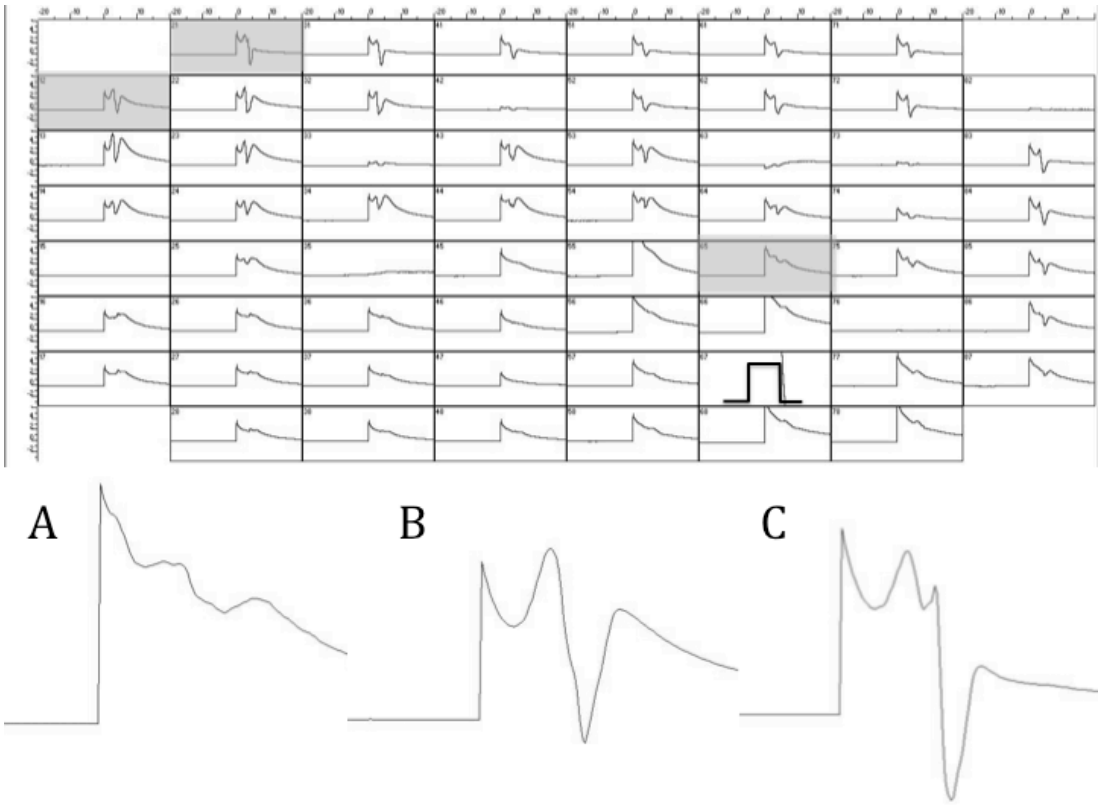

Figure 70 Signals recorded on MEA during control experiment. In the upper part, the signals for each of the 60 electrodes are shown; the stimulus is marked by the square wave; reference and distal electrodes are highlighted in grey. In the lower part, A is the reference electrode signal, and B and C are signals at the distal electrodes used to calculate conduction velocity.

7.5 Carbachol experiments with wild-types and global $G\alpha_{i2}$ knockouts

7.5.1 Local activation time

Results are summarised in Figure 71.

Model: With concentration as a continuous variable the relationship between local activation time and carbachol was best modelled with a random intercept model. For WTs there was no significant relationship between activation time and concentration (p=0.839). Similarly, for gKOs, there was no significant relationship between local activation time and concentration (p=0.117). There was no baseline difference between groups (p=0.139), but at concentration 10^{-6} M the difference between groups approached significance (p=0.0504). In the model, value at baseline for WTs was 2.2 ms, while for gKOs it was 1.6 ms. At maximum carbachol concentration, local

activation time was no different to baseline for either WTs (p=0.839) or gKOs (p=0.117).

With concentration as a discrete explanatory variable there was no significant difference between WTs and gKOs at any concentration, though at 10^{-6} M it approached significance (p=0.08). There were no significant differences compared to baseline for either group.

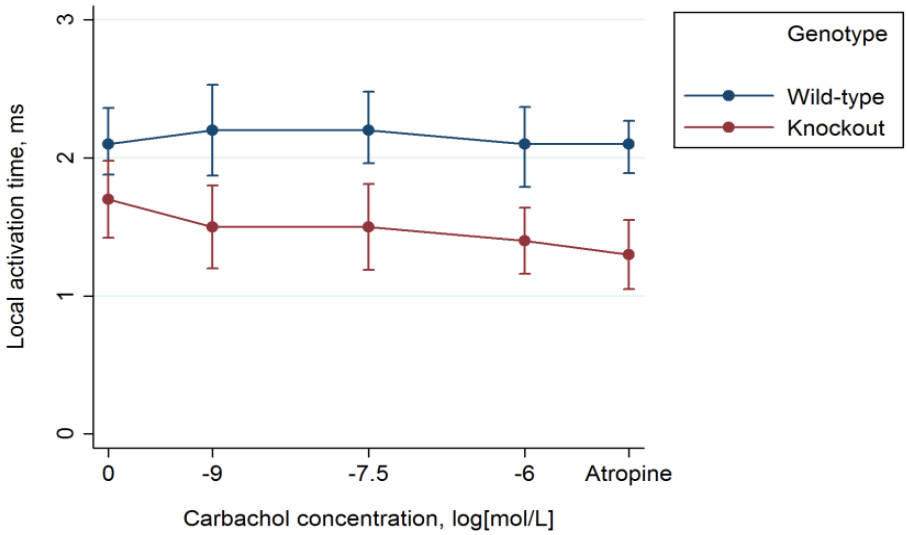

Figure 71 Local activation time with carbachol in WTs (n=6) and gKOs (n=9).

The random intercept model used for local activation times of WT and gKO slices is illustrated in Figure 72. The model predicts the slope of a single line that will best fit the four measurements for each of the 15 mice. In this way, although the slope of the line is the same for all mice, the y-axis intercept can vary. This 'randomness' differentiates the model from multiple linear regression. Compare this to Figure 74 which illustrates a random slopes model.

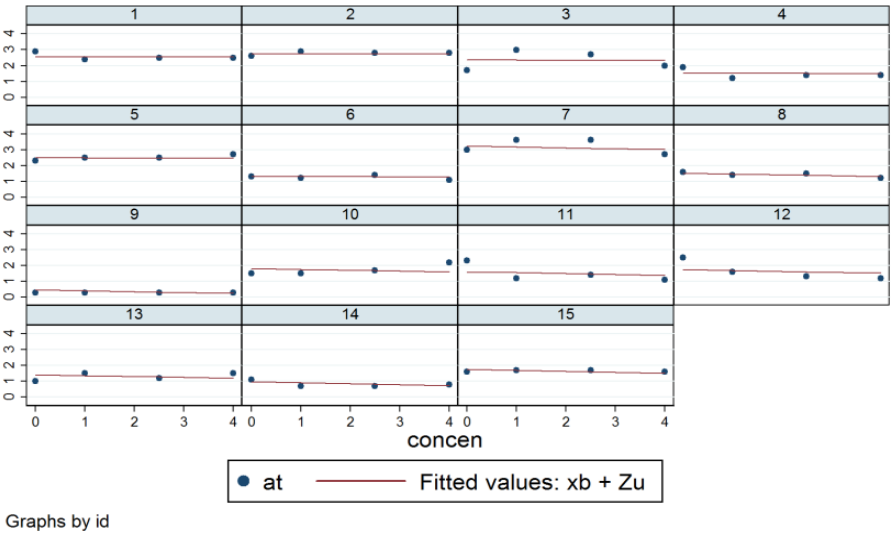

Figure 72 Example of a random intercept model. Original data (dots) and predictions from mixed effects model (lines) are shown for WT and gKO local activation times. The line of best fit is allowed to intersect the ordinate at different values for each slice, though the slope is the same for all in each group (WT or gKO).

7.5.2 Effective refractory period

Results are summarised in Figure 73.

Model: The relationship between ERP and carbachol concentration was best modelled with a random slopes model. For both WTs and gKOs there was no significant relationship between ERP and concentration. There was no baseline difference between groups (p=0.631) and neither was there a significant difference at any concentration. In the model, ERP at baseline for WTs was 61 ms; for gKOs it was 65 ms. There was no difference between ERP at baseline and maximum carbachol concentration for either WTs or gKOs.

With concentration as a discrete explanatory variable, there was no significant difference between WTs and gKOs at any concentration. For WTs, at carbachol concentration $3x10^{-8}$ M, ERP was significantly shorter than at baseline (-7.6 ms, p=0.049). There were no other significant differences.

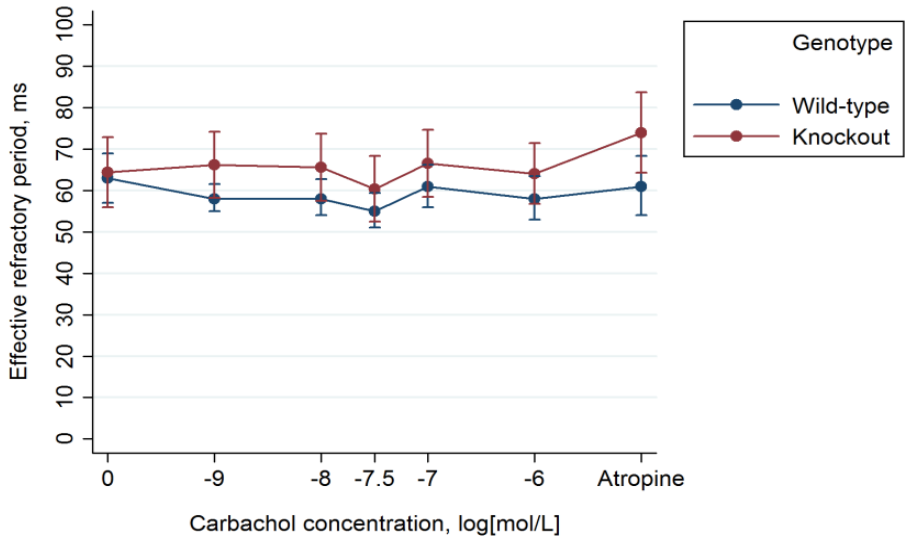

Figure 73 Effective refractory period with carbachol in WTs (n=11) and gKOs (n=11).

The random slopes model used for ERPs of WT and gKO slices is illustrated in Figure 74. In contrast to the random intercept model depicted in Figure 72, a random slopes model allows not only the intercept of each slice's line to vary, but also its slope. So a true (linear) line of best fit is generated for the measurements of each slice. It is not always appropriate to progress from a random intercept to random slopes model however; the appropriateness of doing so is assessed with the likelihood ratio test.

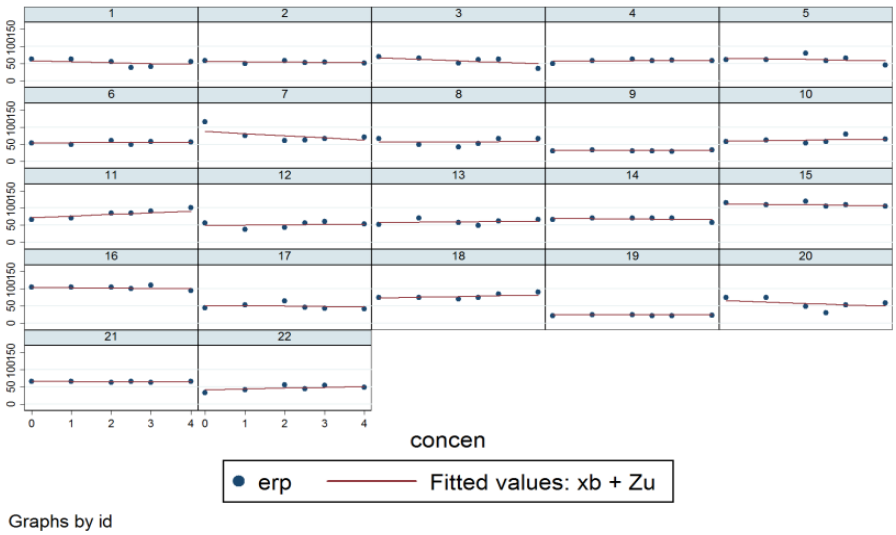

Figure 74 Example of a random slopes model. Original data (dots) and predictions from mixed effects model (lines) are shown for WT and gKO ERPs. The line of best fit is allowed to vary between slices, both with its intersection at the ordinate, and with its slope.

7.5.3 Conduction velocity

Results are summarised in Figure 75.

Model: With concentration as a continuous explanatory variable the relationship between conduction velocity and carbachol concentration was best modelled with a random intercept model. For WTs there was a small positive linear relationship between conduction velocity and concentration which was significant (2.2 cm s^{-1} per unit log[mol/L] increase in carbachol concentration, p=0.044).

For gKOs, there was no significant relationship (p=0.706). There was no baseline difference between groups (p=0.299), and neither was there a significant difference at any concentration. In the model, baseline conduction velocity for WTs was 39 cm s^{-1}; for gKOs it was 51 cm s^{-1}. At maximum carbachol concentration, conduction velocity was +8.8 cm s^{-1} faster than baseline for WTs (p=0.044). For gKOs, it was +1.3 cm s^{-1} (p=0.706).

With concentration as a discrete explanatory variable there was no significant difference between WTs and gKOs at any concentration. For WTs, at $3x10^{-8}$ M carbachol, conduction velocity was significantly faster than baseline (10 cm s^{-1}, p=0.018). There were no other significant differences.

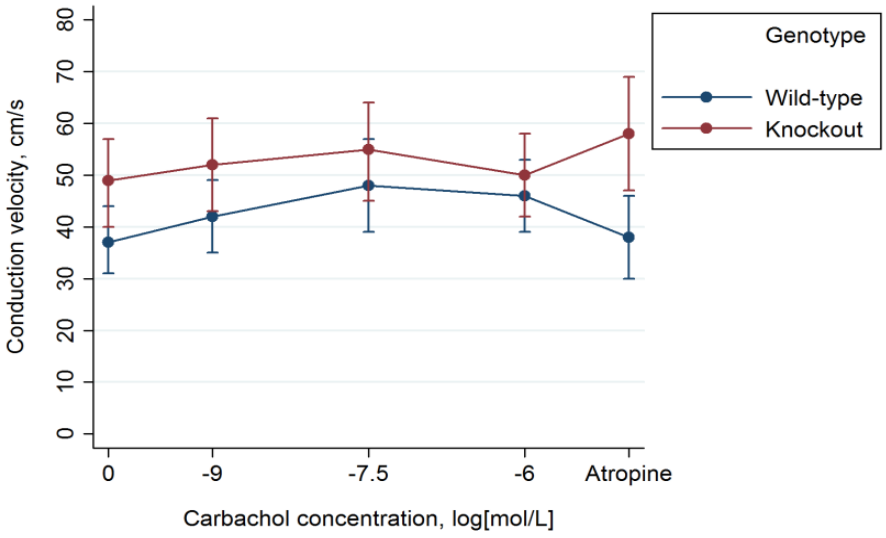

Figure 75 Conduction velocity with carbachol in WTs (n=6) and gKOs (n=9).

7.6 Isoprenaline experiments with wild-type slices

7.6.1 Local activation time

Results are summarised in Figure 76.

Model: The realtionship between local activation time and isoprenaline concentration was best modelled with a random intercept model. There was no significant relationship between local activation time and concentration (p=0.160). In the model, local activation time at baseline was 2.4 ms, and there was no significant difference between this and the value at maximum concentration (p=0.160).

With concentration as a discrete explanatory variable, there were no significant differences compared to baseline.

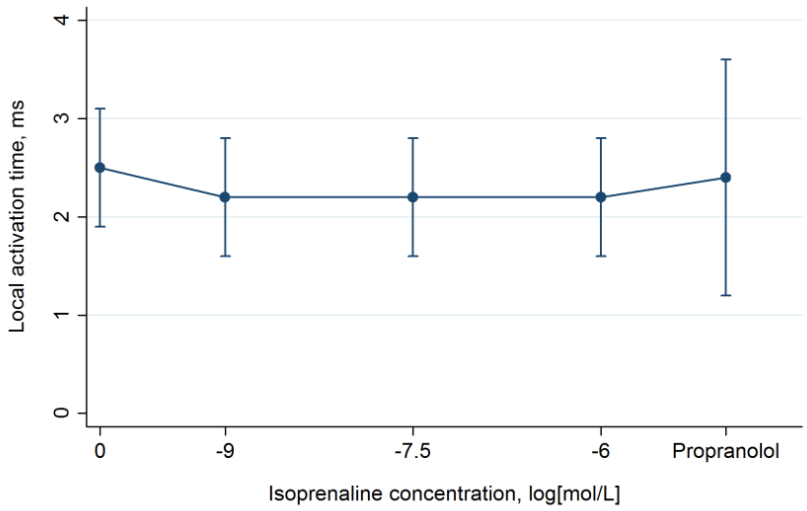

Figure 76 Local activation time with isoprenaline in WTs (n=7).

7.6.2 Effective refractory period

Results are summarised in Figure 77.

Model: the data were best modelled with random intercepts. There was a small positive linear relationship between ERP and concentration which was significant (1.4

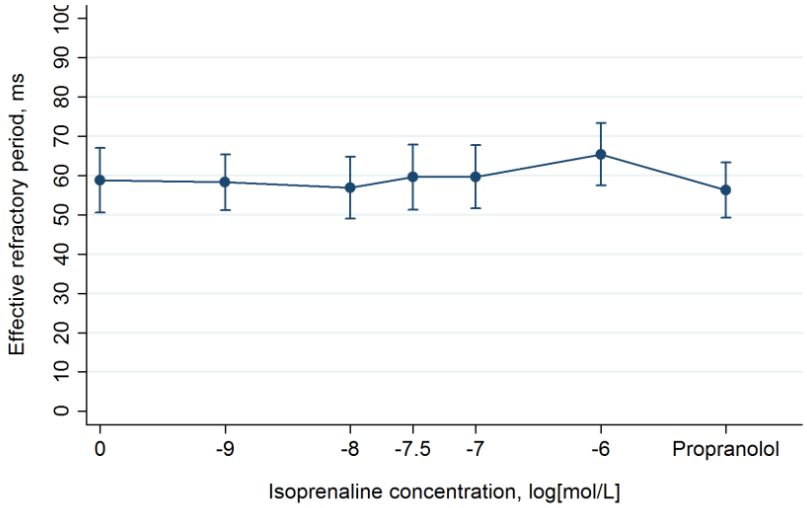

Figure 77 Effective refractory period with isoprenaline in WTs (n=10).

ms per unit log[mol/L] increase in isoprenaline concentration, p=0.033). In the model, mean ERP at baseline was 57 ms; it was significantly longer at maximum concentration than at baseline (+5.7 ms, p=0.033).

With concentration as a discrete explanatory variable, at maximum concentration ERP was significantly longer than baseline (+6.6 ms, p=0.021). There were no other significant differences.

7.6.3 Conduction velocity

Results are summarised in Figure 78.

Model: The relationship between conduction velocity and isoprenaline concentration was best modelled with a random intercept model. There was no significant relationship between conduction velocity and concentration (p=0.377). In the model, conduction velocity at baseline was 68.5 cm s^{-1}. Conduction velocity was 5.8 cm s^{-1} faster at max concentration though this was not significant (p=0.377).

With concentration as a discrete explanatory variable, there were no significant differences compared to baseline.

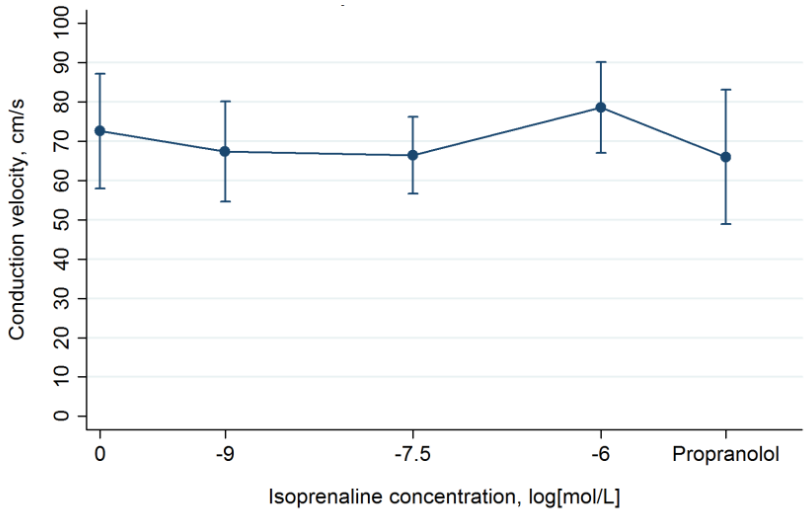

Figure 78 Conduction velocity with isoprenaline in WTs (n=7).

7.7 Mexiletine experiments with wild-type slices

7.7.1 Local activation time

Results are summarised in Figure 79. However, measurements were not possible at maximum concentration for three of the seven slices due to failure to capture, and so the value shown must be interpreted with caution.

Model: With concentration as a discrete explanatory variable there was a highly significant difference between baseline local activation time and that at 10^{-4} M (+1.1 ms, $p<0.00005$). The data were not modelled with concentration as a continuous variable as the lowest concentration (10-5 M) was considered too great a difference from baseline (i.e. 0 M) to consider this increment as equal to the other log unit increments.

For Figure 79 only (not the multilevel model), a value for local activation time of 20 ms was assigned where there had been no capture at 10^{-4} M, for illustrative purposes. This was not done for the statistical model, as the difference was highly significant when these values were treated as missing.

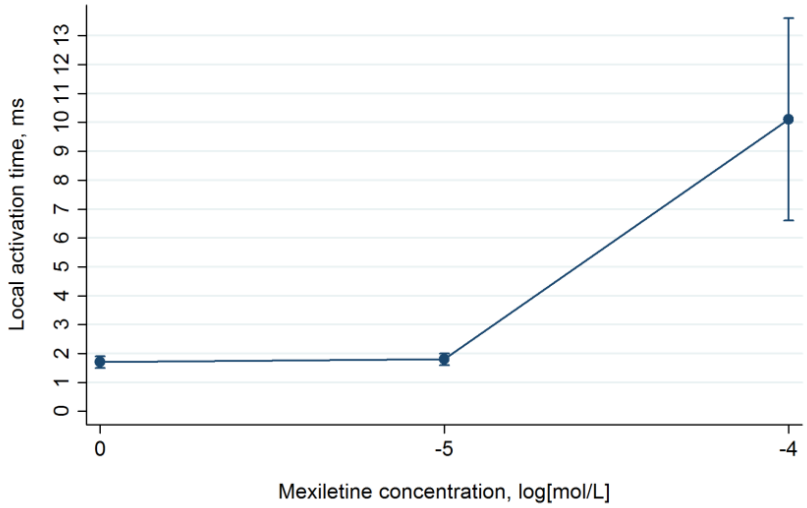

Figure 79 Local activation time with mexiletine in WTs (n=7).

7.7.2 Effective refractory period

Results are summarised in Figure 80. ERP was only measurable for four out of seven of the slices at maximum concentration (mean 71 ms). If these missing values are conservatively estimated at 150 ms, the mean ERP becomes 105 ms.

Model: As for local activation time, concentration was only modelled as a discrete explanatory variable. At 10^{-4} M, where ERP>140, this was conservatively estimated as 150 ms, to avoid missing values. Using a random intercept model, baseline ERP was 55 ms; at 10^{-5} M it was 63 ms (p=0.36), and at 10^{-4} M it was 105 ms (p<0.00005).

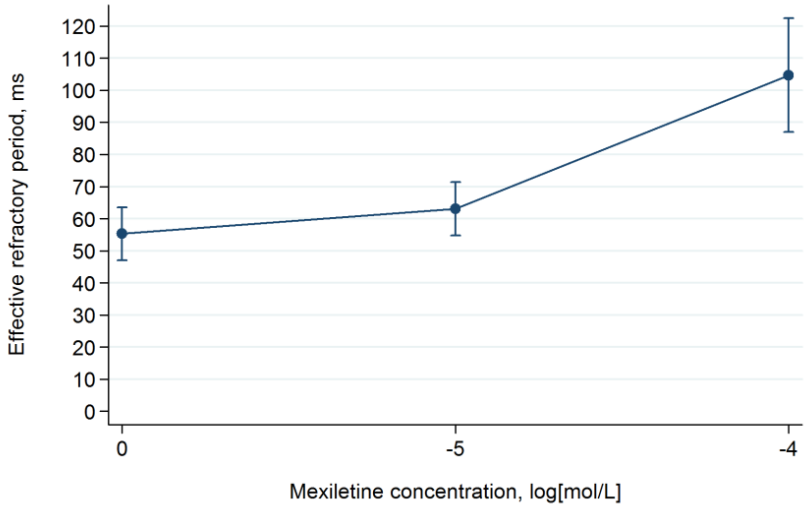

Figure 80 Effective refractory period with mexiletine in WTs (n=7).

7.7.3 Conduction velocity

Results are summarised in Figure 81. Conduction velocity was only measurable for four out of seven of the slices at maximum concentration (mean 44 cm s^{-1}). If these missing values are assigned values of 0 ms, the mean conduction velocity becomes 25 cm s^{-1}.

Model: A random intercept model was used with concentration as a discrete explanatory variable. At 10^{-4} M where conduction velocity could not be measured due to lack of capture/propagation, a value of 0 was assigned. In the model, baseline conduction velocity was 57 cm s^{-1}. At 10^{-5} M it was 60 cm s^{-1} (p=0.638) and at 10^{-4} M it was 25 cm s^{-1} (p<0.0005).

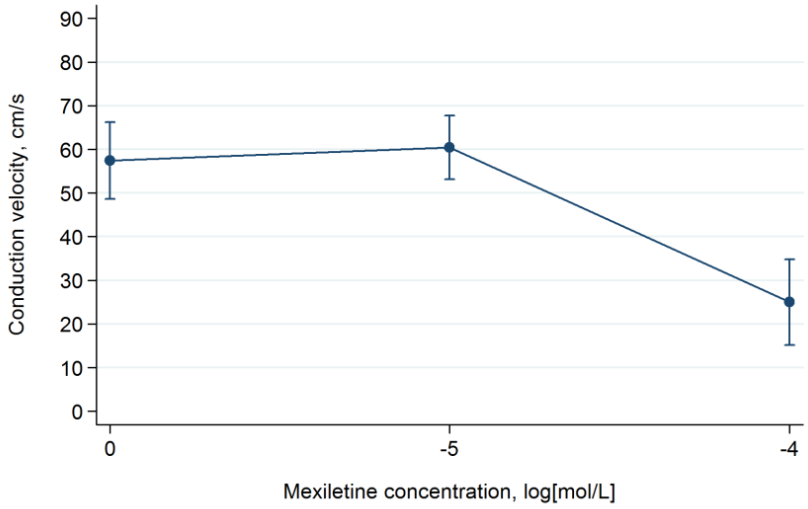

Figure 81 Conduction velocity with mexiletine in WTs (n=7).

An example of the signals acquired at baseline and after 10^{-4} M Mexiletine are shown in Figure 82.

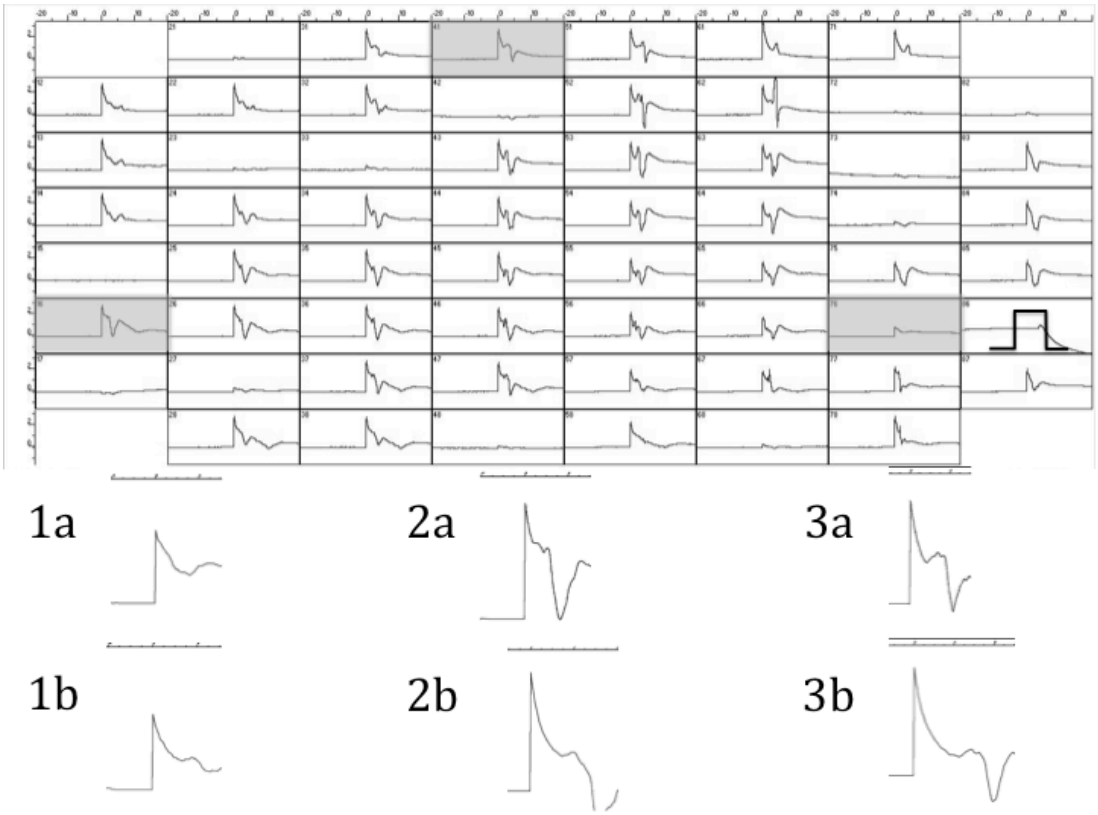

Figure 82 Signals recorded on MEA during mexiletine experiment. In the upper part, the signals for each of the 60 electrodes are shown; the stimulus is marked by the square wave; reference and distal electrodes are highlighted in grey. In the lower part, (1a) is the reference electrode signal at baseline and (2a/3a) are baseline signals at the distal electrodes used to calculate conduction velocity. (1b/2b/3b) are the corresponding signals after receiving 10^{-4} M mexiletine.

7.8 Temperature experiments with wild-type slices

7.8.1 Local activation time

Results are summarised in Figure 83.

Model: With temperature as a continuous explanatory variable, the data were best modelled with random intercepts. There was a highly significant relationship between local activation time and temperature ($p<0.0005$). In the model, local activation time at 34 °C was 1.86 ms; at 37 °C it was 1.64 ms and at 40 °C, 1.43 ms.

With temperature as a discrete explanatory variable there was a significant difference between 37 and 34 degrees ($p<0.00005$). However, there was no significant difference between 37 and 40 degrees ($p=0.296$).

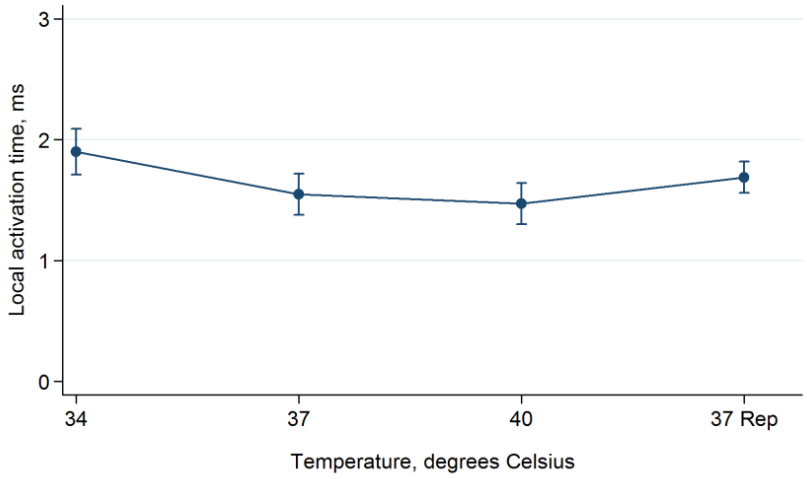

Figure 83 Local activation time according to temperature in WTs (n=11).

7.8.2 Effective refractory period

Results are summarised in Figure 84. Model: The relationship between ERP and temperature was best modelled with a random intercept model. There was a negative linear relationship between ERP and temperature which was highly significant (-4.6 ms per °C increase, p<0.0005). In the model, at 37 °C, ERP was 55 ms; at 34 °C it was 68 ms, and at 40 °C was 41 ms. There were highly significant differences in ERP between 37 °C and both 34 °C and 40 °C. With concentration as a discrete explanatory variable there were highly significant differences between ERP at 37 °C and 34 °C (p<0.00005), and 37 °C and 40 °C (p=0.0018).

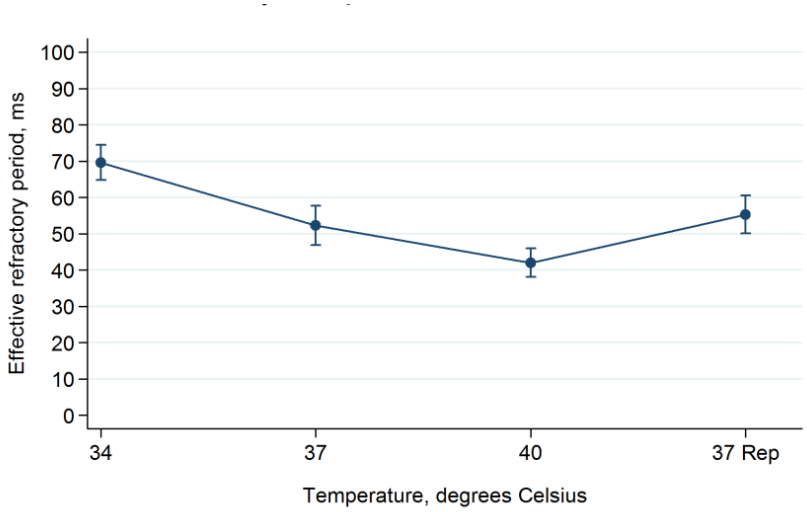

Figure 84 Effective refractory period according to temperature in WTs (n=17).

7.8.3 Conduction velocity

Results are summarised in Figure 85.

Model: The relationship between conduction velocity and temperature was best modelled with a random intercept model. There was no significant relationship between conduction velocity and temperature (p=0.53). In the model, at 37 °C conduction velocity was 59 cm s^{-1}; at 34 °C it was 62 cm s^{-1} and at 40 °C it was 57 cm s^{-1}. There was no significant difference in conduction velocity between 37 °C and 34 °C or 40 °C. When re-modelled with temperature as a discrete variable, there was no significant difference between conduction velocity at 37 °C and 34 °C (p=0.44), nor 37 °C and 40 °C (p=0.89).

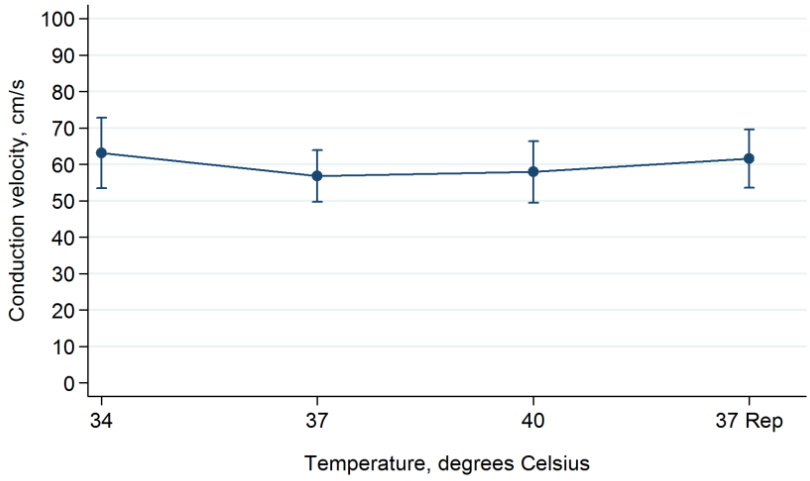

Figure 85 Conduction velocity according to temperature in WTs (n=11).

An example of the signals acquired at 34 °C and at 40 °C are shown in Figure 86.

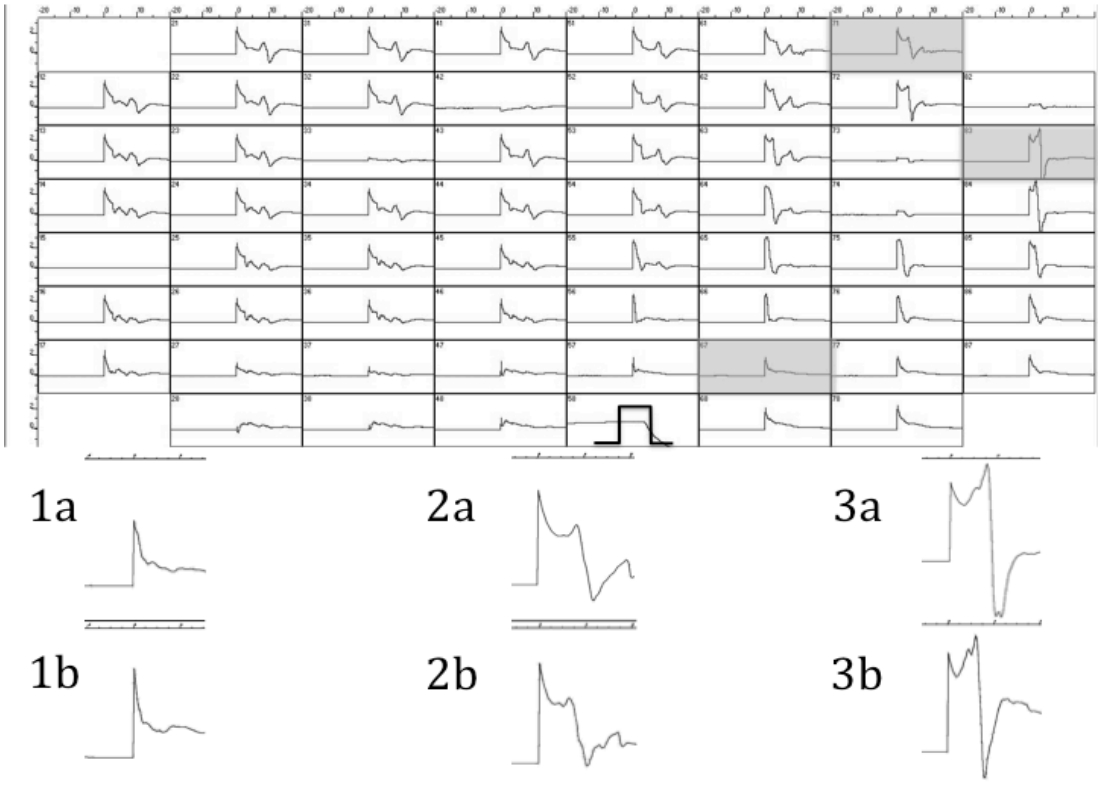

Figure 86 Signals recorded on MEA during temperature experiment. In the upper part, the signals for each of the 60 electrodes are shown; the stimulus is marked by the square wave; reference and distal electrodes are highlighted in grey. In the lower part, (1a) is the reference electrode signal at 34°C and (2a/3a) are signals at the distal electrodes used to calculate conduction velocity also at 34°C. (1b/2b/3b) are the corresponding signals at 40°C.

8. DISCUSSION – MEA STUDIES

8.1 Introduction

Measurement of conduction velocity, and of repolarisation in response to drug challenge *in vivo*, is problematic. Conduction velocity requires knowledge of, or a reasonable estimate of the path of conduction in addition to accurate timings of activation. This is complicated by the 3D propagation of impulses; and achieving this at multiple regions of the contracting heart is a challenge. Yet conduction velocity and repolarisation are two of the key cardiac electrophysiological parameters, and perturbations in these contribute to arrhythmogenesis. New drugs are screened particularly for their effects on repolarisation indices. A current guideline from 2005 recommends a combination of *in vitro* and *in vivo* assessments for this purpose[275]. Although other multicellular and tissue preparations are available, the MEA system in conjuction with tissue slices offers the potential for multiple recordings from the same heart, thus permitting a range of drug doses to be used. Also, the thinness of the slices provides a quasi-2D tissue substrate, simplifying assessment of conduction velocity. Although several groups have published their findings using cardiac slices and the MEA system, it has not been used widely. Initially therefore, the stability and reproducibility of the technique was tested. The methodology was also simplified as far as possible. Baseline studies with WT slices were performed to test the stability of the system. Pharmacological studies in WTs with isoprenaline and mexiletine, thermal studies in WTs, and comparisons of $G\alpha_{i2}$ KOs and WT controls with carbachol were subsequently performed. The results for each of these experiments are discussed first, after which aspects of the methodology and reliability of measurements are critiqued.

8.2 Control experiments with wild-type slices

There were no differences between baseline and 35 minutes for local activation time or ERP. The ERP measurements, as an index of repolarisation, are in keeping with the findings of two other cardiac slice studies. The first, using human and canine slices

showed stable FPD measurements for eight hours[232]. The second demonstrated stable FPD with guinea pig slices for up to 24 hours, and slice viability for 48 hours[236]. Conduction velocity did increase by 1.2 cm s^{-1} per 7 minutes in the model, and although this was highly significant, the magnitude of change was fairly small: an increase of approximately 16% between baseline and end. It is difficult to explain this small, gradual change, but one possibility is a 'warm-up' effect, as BDM is fully washed out of the tissue and near-normal cellular physiology is restored. In particular, the two main protein complexes involved in impulse propagation, the sodium channel and gap junction complexes, may take longer to recover than other ion channels.

8.3 Carbachol experiments with wild-types and global $G\alpha_{i2}$ knockouts

The lack of relationship between local activation time and carbachol concentration for both WTs and gKOs was expected, and in accordance with the findings from the Control experiments. Local activation time is dependent on sodium channel availability, which in turn is partly determined by the resting membrane potential. mACh receptor signalling is not believed to exert influence on the sodium channel, and although it affects GIRK in the atria, the lack of expression of this channel in the ventricles means carbachol, acting via the mACh receptor, is unlikely to have effects on the resting membrane potential either.
For the same reasons, a lack of difference between groups at baseline would be expected. More difficult to explain is the difference that approached significance at 10^{-6} M. Despite the separation of curves, the most likely cause would seem to be chance, an hypothesis supported by the lack of reversal following atropine.

ERP did not vary between baseline and maximum carbachol concentration for either group, in keeping with the results from the Control experiments. Interestingly, with concentration as a discrete variable, ERP was significantly shorter than baseline for WTs at $3x10^{-8}$ M. This was not significant for knockouts, though review of the plotted data shows a mirrored dip. Whether this represents a real effect, or a statistical aberration is difficult to know. It is not concordant with the effects of vagal stimulation in the dog for example, where lengthening of ventricular ERP occurs[276]. Repolarising currents differ markedly between large and small animals which may go some way to explaining the difference.

In contrast to my results *in vivo* at electrophysiological study, gKO tissue slice ERPs were slightly higher than controls, though the differences in both experiments were non-significant. In attempting to reconcile these findings with those of Zuberi et al[94] who found gKOs to have a shorter VERP, several aspects of signalling require consideration. Firstly, GIRK is not expressed in the ventricles, but were it to be, reduced GIRK activity in $G\alpha_{i2}$ knockouts would more likely prolong APD and ERP rather than reduce it. Secondly, there is evidence to support the idea that $G\alpha_{i2}$ negatively regulates the LTCC[94,106,107]. Two of these studies found this to be part of the mACh receptor signalling pathway, though a role for the β2AR cannot be discounted[90]. If the increased Ca^{2+} currents observed in gKOs by Zuberi et al resulted from a lack of mACh receptor - $G\alpha_{i2}$ mediated suppression of the LTCC, then as postulated in the *Chapter 6*, the increased Ca^{2+} could enable re-excitation prior to full repolarisation in a manner similar way to EADs, such that the ERP measured actually reflects a Ca^{2+}-dependent re-activation process. A difficulty with this hypothesis is that with carbachol stimulation of the mACh receptor, LTCC activity should be suppressed in WTs, altering ERP. However, whether this would lead to shortening of ERP, due to reduction in APD, or lengthening, due to less Ca^{2+} availability for EAD-type action potentials, is unclear.
Another important consideration is that a key aspect of *in vivo* experiments is that they study the tissue within its normal environment, under the usual influences of hormones, neural inputs and, pH, oxygen supply, electrolytes and energy substrates. Given the heart is under constant neuromodulation by both branches of the ANS, the lack of these tonic influences may help explain some of the differences between my results for gKOs *ex vivo*, and the *in vivo* results of Zuberi et al. For example, Wainford et al have shown that $G\alpha_{i2}$ signalling in the brain is important in mediating sympathoinhibitory renal nerve-dependent responses in relation to sodium retention and hypertension[277,278]. If similar effects on the cardiac SNS occurred *in vivo* in gKOs, this could potentially affect electrophysiological parameters such as ERP.
A final possibility is that muscarinic signalling effects may only become apparent, in the ventricles at least, in the presence of β2AR signalling. In this way, it could act as a sort of counterbalance. This possibility was considered, but time constraints prevented experiments to investigate it.

Despite slight separation of the curves for conduction velocity, there was no significant difference between WTs and gKOs at any concentration of carbachol. As discussed for local activation time, this is not surprising as there have been no reported effects of

$G\alpha_{i2}$ on either Nav1.5 or gap junctions, although equally, such effects have not to my knowledge been investigated.

The slight increase of conduction velocity with concentration seen for WTs may reflect a similar process to that occurring in the Control experiments, i.e. an effect of time rather than carbachol concentration. In all likelihood, the lack of increase seen for gKOs was due to chance rather than $G\alpha_{i2}$ being implicated in regulation of conduction, and this is supported by the proximity of values for each group at maximum concentration. The one thing favouring a mild effect is the significantly higher value at $3x10^{-8}$ M when modelled with carbachol as a discrete variable – similar but opposite to that which occurred for ERP.

8.4 Isoprenaline experiments with wild-type slices

For both local activation time and conduction velocity, there was no significant relationship with isoprenaline concentration, although it is interesting to note that propranolol had mild opposing effects towards the trend observed for each parameter. Isoprenaline is a non-specific βAR agonist, and its cellular effects are predominantly driven by the $G\alpha_s$ – AC – cAMP – PKA pathway, with PKA phosphorylating and thereby contributing to regulation of a number of proteins involved in ion transport. Published data generally support the idea that βAR signalling increases I_{Na}, via PKA-mediated phosphorylation[279]. However, there is not complete agreement[38]; other proteins such as CamKII may also have a role, and the extent of any $G\alpha_i$-mediated antagonism is unknown.

In terms of functional effects, Lang et al recently reported that both β1AR and β2AR agonism increased conduction velocity in human cardiac wedge preparations[280]. And in a review on the subject, Campbell et al found conduction velocity to be increased with βAR stimulation in intact hearts[279]. Mechanistically, they suggest that due to the non-linear relationship between dV/dt_{max} of phase 0 (an I_{Na}-driven process) and conduction velocity, βAR modulation of gap junction function may also be important, as suggested by previous reports[281]. However, most of the work investigating this has been carried out with neonatal cell preparations, without assessment of the effects on conduction.

Therefore the results in these experiments, particularly with regard to conduction velocity, were it seems unexpected. The cardiac slices may not have been able to

demonstrate changes in this parameter, perhaps as a result of damage incurred during preparation, or due to insufficient tissue volume. Alternatively, it is possible there are species differences in the kinetics of I_{Na} or gap junctions: the majority of studies have used canine models, and the higher heart rates seen in mice may affect activation and conduction, in addition to repolarisation.

Adrenergic effects on APD and ERP are better understood, in large animals at least. In the canine ventricle, ERP shortened in response to sympathetic stimulation, and conversely, sympathetic denervation led to prolongation of ERP[276]. In humans, the effects are well-described, and attributed largely if not wholly to phosphorylation of I_{Ks} by PKA[56]. The resultant increase in K^+ efflux leads to APD shortening, reflected in the normal reduction in QT interval that occurs with exercise. Further evidence comes from patients with LQTS type I, in whom mutations in *KCNQ1* produce ventricular arrhythmias often in response to increased sympathetic activity.
The failure of APD not only to shorten, but to increase marginally with higher concentrations of isoprenaline, was perhaps unexpected. Aliquots of frozen isoprenaline were thawed an hour before commencing the experiments, so oxidisation and loss of pharmacological potency are unlikely to have occurred. Two points deserve mention: firstly, although significant, the increase of ERP was minimal, and may either be a type I error, or represent subtle deterioration in the tissue perhaps. Secondly, as alluded to above, repolarisation in rodents is very different to that in large animals: I_{Ks} is not present in the mouse, and the main murine repolarising currents are less well-studied.

8.5 Mexiletine experiments with wild-type slices

These experiments were performed to check the responsiveness of the cardiac slice technique. For the Control, carbachol and isoprenaline experiments, either no change or a change of small magnitude occurred. It was important to demonstrate that slices could respond to stimuli, and that these responses could be measured: a positive control was required. Similar experiments have been reported previously with cardiac slices using a variety of compounds[231,232,238]. Mexiletine acts effectively as a pure fast sodium channel blocker[282], classed as a IB anti-arrhythmic in Vaughan Williams'

system[283]. It was chosen due to the presence and importance of sodium channels in the murine action potential, and hence the likelihood to elicit a response.
Encouragingly, significant changes of large magnitude were seen in all three measured parameters. The increase in ERP is probably explained by mexiletine preventing re-opening of the channels even after full repolarisation, so that even though APD may not have been prolonged, the longer ERP would reflect an inability of the S2 stimulus to elicit phase 0.

8.6 Temperature experiments with wild-type slices

The effects of variations in temperature were studied because of their clear physiological relevance, implication in arrhythmogenesis, and the suitability of the MEA to study this variable.
The highly significant relationship between local activation time and temperature was not anticipated, although such a dependence has been described. Using isolated perfused rabbit hearts, Spear et al showed that when stimulating the epicardium, local activation time progressively increased as temperature dropped from 36°C to 25°C[284]. Whilst not strictly analogous, the related parameter depolarisation time, was found to be temperature dependent almost 60 years ago[285]. This describes the time taken for phase 0 of the action potential to rise from 10 to 90% of its total amplitude. A negative linear relationship between the log of depolarisation time and temperature was described for frog ventricular fibres *in situ*, with a mean value of 3.3 ms at 37°C. The commonality of depolarisation time and local activation time is their dependence on I_{Na}. Experimental support for the temperature dependence of sodium channel conductance has come from patch-clamp work using rat ventricular myocytes[286].

Temperature's relationship with ERP has been more well-studied, and the results obtained with the MEA finding a significant negative linear relationship of good magnitude are in keeping with what has been published. Accepting the potential differences between atrial and ventricular electrophysiology, Smeets et al showed that in strips of rabbit atrium, cooling led to prolongation of the refractory period[287]. Spear et al showed prolongation of ARIs with lower temperatures[284], and Coronel et al found a negative relationship between temperature and MAP duration in isolated pig hearts[167]. In a similar manner to the sodium channel and local activation time,

repolarising currents have also been shown to exhibit temperature dependence. Kiyosue et al showed that in guinea pig ventricular myocytes, I_K was reduced at lower temperatures, and that APD was prolonged[288].

In the MEA experiments there was no relationship between conduction velocity and temperature. This was surprising given the reported association in the literature. Smeets et al reported an increase in conduction velocity with higher temperatures in rabbit atria[287], and Morley et al found reduction in velocities in mice between 37°C and 25°C[69].

Two obvious explanations for the results exist. The first is that the temperature range studied was too narrow, and centred around 37°C. In contrast, the two studies mentioned above had a maximum temperature of 37°C and a minimum of 25°C to 27°C. The narrow temperature range was chosen deliberately though, as both upper and lower temperatures are quite possible in humans, yet far enough from 'normal' to in theory at least, elicit changes. Oddly though, there was not even a non-significant trend for the MEA results, with conduction velocity at 34°C slightly higher than at 37°C.

The second possibility is that murine conduction does not vary so easily with temperature as it does in the rabbit. Although it is assumed that mammals maintain their temperatures close to 37°C, it is possible that due to their larger body surface area to size ratio, mice may need to be able to tolerate slightly lower temperatures without marked changes in conduction.

Finally, this part of the study had a reasonable sample size (n=11), and the responsiveness of conduction velocity had been demonstrated with mexiletine. Nevertheless, for subtle changes the system or method used may have been too insensitive. A type II error is therefore possible.

The importance of temperature in arrhythmogenicity is best exemplified by Brugada syndrome, where fever can trigger ventricular arrhythmias. A molecular mechanism for the *SCN5A* gene Thr1620Met mutation was demonstrated by Dumaine et al who showed that current decay kinetics and recovery from inactivation of the channel was altered compared to the wild-type channel[289]. Hypothermia has also been implicated as a trigger, but in early repolarisation syndrome[290]. There are conflicting data however on whether hypothermia can trigger ventricular arrhythmias in the presence of J waves related to the low temperature, as opposed to the probable molecular defect of early repolarisation syndrome[291].

Although not investigated in this study, arrhythmic triggers are clearly also important. In this regard, Mugelli et al reported increased afterpotentials when myocardial temperature is raised from 34°C to 37°C [292]; this was investigated in the context of reperfusion arrhythmias following ischaemia.

8.7 Methodology

8.7.1 Choice of experimental model

A number of experimental models and animals have been used to study cellular and tissue electrophysiology. These include, but are not limited to, *in situ* hearts, isolated perfused hearts (murine, leporine, canine, human), and papillary muscle preparations. In terms of recording electrophysiological parameters, this may be achieved with multiple individual electrodes including MAP electrodes, multi-electrode arrays, and potentiometric dyes. The MEA system utilising cardiac tissue slices has several potential advantages (discussed in Section 1.9.2). Amongst these are the potential to obtain several slices from the same heart, which in theory allows for some control of inter-heart variability. This is also a means of maximising experiments from each animal. In terms of the possible measurements and time available, the use of slices permitted pharmacological testing with measurement of ERP, local activation time and conduction velocity.

The alternative *ex vivo* systems available for measuring cardiac electrophysiological parameters include, for example, application of an MEA to the surface of an intact heart which is retrogradely perfused via a Langendorff system. And potentiometric (voltage-sensitive) dyes can also be perfused through the isolated heart or tissue to enable visualisation of depolarisation and repolarisation[293,294].

Advantages of *ex vivo* whole heart experiments include:

- less tissue damage: this maintains not only viability, but also intercellular connections and conduction pathways
- 3D architecture: though not necessarily an advantage with murine hearts, in large animals such as humans transmural electrophysiological differences are present and of pathophysiological importance

Disadvantages include:

- higher metabolic requirements, though this is not usually a problem
- maintaining physiological temperature is more difficult
- only one experiment per heart can be performed
- phototoxicity of potentiometric dyes, resulting in cell death, though this may be more relevant to single-cell or monolayer imaging[295]

These sort of experiments lend themselves particularly to analyses of APD/ARI and activation time assessment. But the problems with conduction velocity are compounded in the whole organ, particularly when as small as the murine heart. And although on the one hand, electrophysiological assessment on the Langendorff perfusion setup obviates the need for slicing, on the other hand it requires the new skills of immobilising the heart to reduce motion artefact, and familiarisation with the different equipment used.
Certainly there are merits to these approaches. But the techniques had not been used before within the group, whereas the MEA system equipment was available in the laboratory, and had been used previously within the group.

The inherently traumatic process of tissue slicing raises the question of slice viability. This was explored comprehensively by Camelliti et al, who found tissue integrity to be maintained when assessed histologically, and a normal distribution of cell types and gap junctions[232]. They also found contractility to be preserved and FPD to be stable for up to 8 hours. Finally, ATP/ADP and phosphocreatine/creatine ratios were similar to intact tissue. Using guinea pig slices, Bussek et al reported viability for over 24 hours [236]. All these findings support the possibility that despite trauma and cell death of myocytes at the periphery of the slice, the bulk of the myocytes and tissue are largely unaffected and function adequately to allow useful experimentation. The results reported for the Control experiments (*Section* 7.4) attest to this: values obtained were both plausible and stable.

8.7.2 Stimulation frequency

Following initial trials with varying stimulation cycle lengths, 250 ms was chosen as the S1 coupling interval for the main study for the reasons described in the *Chapter 2.* Briefly, this was chosen as a workable compromise between the desire to stimulate as

close as possible to physiological heart rates, and the need to preserve tissue vitality and ensure usable signals throughout the protocol. Considering that adaptation of the APD occurs in response to changes in heart rate *in vivo*, can the values for ERP in particular be considered a reasonable reflection of those seen at more physiological heart rates?

The relation of APD and ERP to heart rate at steady state, i.e. adaptation, is well documented, and shows a positive relationship in atrial and ventricular cardiomyocytes[54,55,232]. Although this trend was not seen for the cycle lengths 150-500 ms, this may be accounted for by two things. Firstly, the number of observations at 150 ms was small, and possibly unrepresentative. Secondly, it is possible that in fact over these cycle lengths there was minimal difference in ERP, and that large differences only emerge <150 ms, in a similar way to APD restitution, i.e. the alteration seen following an abrupt change in preceding diastolic interval[296]. Alternatively, the slight paradoxical increase in ERP with shorter cycle lengths was a real phenomenon that occurs with cardiac slices. This may reflect the tissue damage sustained and the *ex vivo* environment.

Importantly, at a cycle length of 250 ms which the majority of experiments were performed with, mean ERP was 56 ms which is not dissimilar to the values obtained *in vivo*. Also, as was seen with the mexiletine and temperature studies, this varied appropriately.

There does not appear to be a strong relationship between conduction velocity and cycle length according to the literature, though it is perhaps less studied than repolarisation. A study using isolated perfused rabbit hearts found remarkably little change in conduction velocity over a range of cycle lengths[297]. And in the murine heart, no change was observed for cycle lengths between 80 and 150 ms[69]. These findings are further supported by the lack of change in QRS duration in humans with exercise, indicating similar total activation times of the ventricles with different heart rates[298]. Therefore, for this parameter it would appear that stimulation frequency is less of a concern. As can be seen from Figure 64, conduction velocity varies little between cycle lengths of 200-500 ms. The number of slices was low for the three shortest cycle lengths so it is difficult to refute the possibility that using slices, conduction velocity is also stable across a range of cycle lengths.

8.7.3 Conduction velocity measurement

The ability to measure conduction velocity is of importance in understanding arrhythmogenesis, and the development of therapies to treat or prevent this. The complex geometry and activation pattern of the human heart makes measurement *in vivo* possible, but difficult, using a limited number of electrodes with an assumption of linear conduction[299]. But without the motion of the contracting heart, more sophisticated means of calculating conduction velocity could be employed, which take into account the non-linear nature of propagation often seen. Herein lies a potential criticism of the method chosen to measure conduction velocity in this study.

The reasons for this choice of measurement technique were explained in the *Section 2.10.* In brief, typically a quarter to a third of the MEA electrodes would show good enough quality signals at baseline. Signals tended to deteriorate through the experiment, such that by the end only a handful were considered usable. Also, without an automated or even semi-automated analysis program for this purpose, the work involved in reviewing and analysing signals, and calculation of conduction velocities was considerable. An advantage of this method was that all signals underwent strict quality control rather than leaving an automated script to determine activation times. Disadvantages were the neglect of other potentially useful signals, and the assumption of linear conduction between the reference electrode proximal to the stimulus, and the distal electrodes.

It is possible for example, that other groups have made use of more electrode data in their conduction velocity calculations using MATLAB-based custom software[232,235]. However, the details are not provided, nor the extent to which calculations were automated. On the other hand, Halbach et al reported relative changes in conduction velocity rather than absolute values, though it was not clear how many electrode signals were used in their analyses[231]. Perhaps surprisingly, despite the range of models and methods of measurement available, most authors report fairly similar values (see *Section 8.8 below*).

Conduction velocity demonstrates anisotropy: it is substantially faster longitudinally than transversely along cardiomyocytes[232]. An incorrect assumption was made at the beginning of the study that myocardial fibres run in a circular direction around the LV cavity, though previously published work demonstrates this not to be the case. In fact, 'tangential' slices along the wall from base to apex are probably the best way of maximising the number of intact longitudinal fibres[235]. Thus, the method of slicing used in this study likely resulted in transected cardiomyocytes, and this may have

contributed to the variability in measurements. Despite this, as will be seen in Section 8.8, the values obtained were in keeping with previously published results.
A final point worth making is that when comparing interventions to controls, the absolute values are not necessarily important, provided they are plausible. If studying the effects of a drug on conduction velocity for example, a relative change is still a useful observation, and perhaps more realistic than placing too much emphasis on absolute values.

8.7.4 Mouse strain

Numerous strains of mice are currently available for use in laboratory research.
The house mouse, *Mus musculus,* first appeared between 1 and 2.5 million years ago[300], and around 1 million years ago three subspecies diverged from their common ancestor: *Mus musculus castaneus*, *Mus musculus musculus*, and *Mus musculus domesticus*[301]. From these were derived the various strains used in research, inbred to ensure genetic homogeneity. The genome of one of these, C57BL/6J serves as a reference sequence.
Genetic differences between inbred strains are beginning to be elucidated with the advent of next-generation sequencing techniques, revealing that overall, as might be expected there is little sequence variation between strains[301,302]. However, even a single base pair change can produce functional consequences, and any resulting phenotypic differences are far from completely characterised. For studies using knockout mice, the strain used is governed by the laboratory which creates the line. The genetic alteration can be transferred to another strain by backcrossing, though this can take several months. The mice used in the MEA studies were all of strain 129Sv.
Several studies have investigated possible differences in cardiac electrophysiology between strains. Brouillette et al showed that *in vitro*, the I_{Kur} current was smaller in ventricular myocytes from C57BL/6 male mice compared to male CD-1 mice[303]. Shah et al found differences in calcium handling in SV129 mice compared to three other strains[304]. *In vivo*, using a precursor to the ECGenie recording system, Chu et al investigated ECG parameters in males and females of three strains of mice (129/Sv, C57BL/6, and FVB). They found within-strain gender differences, but no between strain differences in parameters such as heart rate, PR or QTc intervals, or QRS duration were reported[254]. And using invasive EP studies similar to those I performed in the myocardial infarction model of heart failure (*Section 5.3*), Appleton et al found

differences between FVB, C57 and DBA strains for sinus and AV nodal function, but not for atrial or ventricular depolarisation/repolarisation indices[305]. A large study by Maguire et al however, did report strain-related differences in VERP and VT inducibility, though the VT induction protocol consisted of programmed electrical stimulation and burst pacing, the latter being particularly aggressive.

In summary, small genetic differences exist between inbred strains used in laboratory research, but any resultant phenotypic differences remain to be fully characterised. A small number of studies have investigated possible electrophysiological differences between strains, but the methods vary and there is insufficient evidence as yet to draw meaningful conclusions.

8.8 Plausibility of measurements

8.8.1 Local activation time

This was the activation time at the reference electrode within 400 μM of the stimulating electrode, and assuming constant threshold and current output, changes in this parameter may be assumed to reflect sodium channel availability. As mentioned in the *Section 2.10*, a maximum value of 5 ms was chosen, as based on experience, times in excess of this were deemed to signify unhealthy tissue or a suboptimal location for stimulation that would be less likely to enable completion of the protocol.
In the Control experiments, baseline local activation time was 2.1 ms, and was the same for WTs in the carbachol experiments. In the isoprenaline experiments, baseline value was 2.5 ms; it was 1.7 ms in the mexiletine experiments, and 1.6 ms at 37 °C in the temperature experiments. Thus, there was reasonable consistency with all in the region of 2 ms. Published values vary from under 2 ms to up to 10 ms: using perfused guinea pig hearts and optical mapping, Kanai and Salama found activation times close to the stimulus of 0-3 ms[306]. And using Langendorff-perfused mouse hearts, Tamaddon et al recorded similar activation times in the vicinity of the right atrial pacing stimulus[307]. Times less than 10 ms were recorded by de Bakker et al in their study of propagation paths in infarcted human papillary muscles[308], and typical activation times of 5-10 ms were shown by Bussek et al in their study of cardiac slices[236].

So although the values reported in this study are towards the lower end of what may be considered normal, the best support for their veracity is the clear change seen in activation times across the MEA from the reference to distal electrodes.

8.8.2 Conduction velocity

The method for determining this has been discussed above. But ultimately, its acceptability is dependent upon producing values that are at least plausible. Reassuringly, despite the imperfections of the method, the conduction velocities obtained were generally in the range reported in the literature.

Mean baseline conduction velocity ranged from 27 to 59 cm s^{-1} (median 26 to 59) across all stimulation cycle lengths, with a mean of 52 cm s^{-1} (median 48) at 250 ms. As Figure 65 shows, a cluster of values was also seen around 100 cm s^{-1}. These are all consistent with published experimental data.

In 1970, Durrer et al reported conduction velocities in the isolated perfused human heart of approximately 45 cm s^{-1}, noting that in the specialised conducting system, values of 200 cm s^{-1} were likely. In the same study, values in the canine heart were also assessed: these ranged from 35.5 to 40.3 cm s^{-1} in the in situ heart, with higher velocities of 50.1 to 62.7 cm s^{-1} in the isolated heart[299].

De Bakker et al measured conduction velocities according to cardiomyocyte orientation and propagation path, and found values between 3 cm s^{-1} perpendicular to, and 98 cm s^{-1} parallel to cardiomyocyte fibre direction[308]. Similarly, using isolated rabbit hearts, Gray et al reported values between 13 and 68 cm s^{-1}, with higher values in the longitudinal direction of cells[309]. Using murine hearts perfused with a voltage-sensitive fluorescent dye, Morley et al found conduction velocities in the range of 30-65 cm s^{-1}. And more recently, Dhillon et al reported velocities of 70-80 cm s^{-1} in guinea pig hearts[71].

Taken together, the published data suggest similar values across species, with markedly higher values in the conduction system. Importantly though, the conduction velocities seen in my study are both plausible, and consistent with those previously reported. The variability seen may be accounted for in three ways: firstly, some degree of variation is expected in any study, and is due to the inherent differences in tissue characteristics, due to damage in the preparation process for example. Secondly, longitudinal versus tranverse propagation was not differentiated; as already noted, faster velocities are seen in the former. Finally, were elements of specialised

conducting tissue present in the slices, these may have produced localised regions of faster conduction.

8.8.3 Effective refractory period

Measurement of ERP is less contentious than the other two parameters, due to its relative ease of measurement. Its relation to APD means that it is species dependent. As already noted, those in this study were similar to what was seen at electrophysiological study following myocardial infarction, as well as those recorded by Zuberi et al[94]. Further support comes from the near identical ERPs recorded in a murine study comparing controls with $Cx43^{+/-}$ mice in the setting of ischaemia. Prior to ischaemic challenge, ERP in controls was 55 ms, albeit at a cycle length of 154 ms[310].

8.9 Summary

Murine cardiac slices have been used successfully in conjunction with the MEA system to measure three key electrophysiological parameters: activation, repolarisation, and conduction velocity. The methodology was simplified as far as possible without affecting the ability to derive measurements from the slices. In the absence of drug or thermal challenge, there were no large magnitude changes over time in any of these three parameters, demonstrating stability of the measurements. Of equal importance was that each of the three parameters was responsive to either pharmacological challenge, changes in temperature or both. Strengths of the study include the reasonable numbers of slices studied for each set of experiments, the reasonable consistency in results achieved, and the use of the technique to study four conditions designed to challenge the electrophysiology. Weaknesses could include using limited number of electrode data in conduction velocity calculations, and not studying the effects of isoprenaline in conjunction with carbachol, both in controls and in gKOs.

With regard to the first hypothesis that $G\alpha_{i2}$ is anti-arrhythmic in the ventricles where it mediates parasympathetic signalling effects, it was surprising that there were no differences in ERP between controls and gKOs and that ERP did not prolong for controls with increasing concentration of carbachol. The *ex vivo* nature of the

experiments may go some way to explaining these findings. There were no differences in local activation time or conduction velocity between groups either, though these were perhaps less expected. Overall though, the carbachol experiments have failed to support the hypothesis.

Regarding the second hypothesis, the lack of shortening of ERP with isoprenaline was unexpected and may be reflective of the differences in repolarisation currents in the mouse compared to large animals. The changes in murine ERP and activation time with alterations in temperature were in accordance with our predictions, and likely reflect modulation of channel kinetics or state transitions. That there was no apparent difference in conduction velocity was possibly a result of the relatively narrow range of temperature studied, in comparison to other published reports.

CONCLUSIONS

The syndrome of heart failure can result from a diverse range of diseases. Two features common to heart failure affecting the LV, are sympathovagal imbalance, and an increased risk of arrhythmias. At the molecular level, β1AR density in the LV falls, and $G\alpha_{i2}$ levels increase. The importance of βAR signalling in heart failure is underlined by the fact that antagonists at these receptors reduce both symptoms and mortality, although the mechanisms are incompletely understood. The significance of $G\alpha_{i2}$ elevation however remains uncertain. The absence of this protein in mice without heart failure produced a phenotype consistent with pro-arrhythmic effects. To take this forward, an *in vivo* model of heart failure and an *ex vivo* tissue model were used. The existence of, and some of the effects on cellular electrophysiology of the two limbs of the autonomic nervous system have been known about for over 100 years. Yet our understanding of exactly how these two limbs interact, if it is possible or desirable to modulate either limb independently, and the cellular effects of doing so, remain incomplete. Were the cellular processes affected by βAR agonism better delineated, the goal of achieving efficacious therapies with few side effects may be realised. Similarly, greater insight into the mechanisms of, and in particular triggers of arrhythmia, would enhance our ability to target 'vulnerable parameters' and thereby avoid the pro-arrhythmia often seen with the current range of drugs. Body temperature suggests itself as a possible contributor to arrhythmogenesis, in certain inherited arrhythmia syndromes if not more generally, and the MEA system was taken advantage of to investigate the effects of temperature variation and βAR agonism on key electrophysiological parameters.

Previous studies have shown mAChR agonism to negatively regulate LTCC currents, via $G\alpha_{i2}$. This offers a way of understanding how vagal nerve activity could be protective against ventricular arrhythmias. $G\alpha_{i2}$ has also been shown to couple to the β2AR, and although there is not total consensus, it appears that $G\alpha_{i2}$ is anti-apoptotic, at least in the setting of ischaemia. There is little direct evidence to support a role for $G\alpha_{i2}$ mediating β2AR modulation of the LTCC, and it may in fact be $G\alpha_{i3}$ that is implicated. It is worth noting that although the LTCC has an important role in both calcium-induced calcium release, and maintenance of the phase 2 plateau in the action potentials of

large animals, it is considered to be primarily disorders of the sarcoplasmic reticulum and its associated calcium handling proteins that occur in heart failure[221,311,312]. Confusingly, a recently published study by Lang et al found β2AR stimulation to exert more pro-arrhythmic effects than β1AR stimulation in tissue from failing human hearts[280]. It therefore seems possible that on the one hand, β2AR signalling could be protective against apoptosis, yet on the other, that it is pro-arrhythmic.

The first hypothesis was that $G\alpha_{i2}$ is anti-arrhythmic in the ventricles where it mediates parasympathetic signalling effects. In the MI/heart failure model there was no difference in heart rate between cKOs and controls. This was in contrast to the work of Zuberi et al who found gKOs to have a higher resting heart rate[108]. These apparent discrepant findings are likely attributable to lack of knockout of $G\alpha_{i2}$ in the SA node of cKOs, and possibly to knockout of the protein in autonomic neurons in gKOs. The lack of difference in QTc for cKOs and controls was more surprising, given that QTc has been shown to be longer in gKOs[94]. Measurement of the QT interval is problematic in humans, and particularly so in mice. If a difference exists, it may not have been manifest due to knockdown rather than knockout in cKOs, with resultant amelioration of phenotype. Some differences in HRV were observed, which again, were inconsistent with work in gKOs[108]. The use of the ECGenie to acquire short duration recordings, together with environmental factors suggest at least some of these differences probably arose due to type I errors. And although there was no difference between groups in VERP or rate of NSVT induction with electrophysiological testing, the values of VERP were the same as those reported for gKOs vs controls by Zuberi et al[94]. Thus, with larger numbers this may have become significant. Programmed ventricular stimulation to induce NSVT is a fairly blunt tool, and it may be that scarring post-MI is a more important predictor of this than alterations in $G\alpha_{i2}$ expression.

In the MEA studies, there were no significant differences between ERPs of gKOs and WTs at baseline. In attempting to reconcile this with the findings of Zuberi et al, it is possible that extracardiac knockout in their *in vivo* gKO model of was responsible for the differences. This would implicate the autonomic nervous system in modulation of ventricular refractoriness. ERP was significantly shorter at 3×10^{-8} M in WTs, which if reflecting a real difference, may have been related to $G\alpha_{i2}$ inhibition of the LTCC. Overall though, there were a lack of differences between gKOs and WTs in the presence of carbachol, and it is possible this was because muscarinic signalling effects only become apparent in presence of βAR signalling. There was a slight increase in CV for WTs with increasing carbachol concentration, which may be a time-related or washout effect, though it is worth noting that at 3×10^{-8} M, the increase was opposite to that seen for ERP. So although the effects were small, it is conceivable that the mAChR or $G\alpha_{i2}$ modulates Nav1.5 and gap junctions.

The results from the MI/heart failure model and the MEA studies therefore failed to support the first hypothesis. Several possible explanations exist: the knockdown rather than knockout in the heart failure model, would have meant the $G\alpha_{i2}$ protein level differences between groups were not as large as they might have been. Nevertheless, not even mild differences in heart rate, QTc or VT inducibility were seen. And this would fail to explain the lack of difference seen with the gKOs in the MEA studies. As described above, a possible explanation is that slices were challenged with carbachol in the absence of βAR agonism; it may be that mAChR signalling only exerts its anti-arrhythmic effects in a braking or dampening manner, to counteract pro-arrhythmic sympathetic signalling. Another point worth considering is the increase in $G\alpha_{i3}$ that results when $G\alpha_{i2}$ is knocked out; it is unclear to what extent this may compensate for $G\alpha_{i2}$, or alternatively, act in an opposing manner. Finally, the possibility that $G\alpha_{i2}$ is not anti-arrhythmic must be countenanced. It must of course be remembered that ventricular arrhythmias are common in heart failure; this could be despite, because of, or regardless of the elevations in $G\alpha_{i2}$.

The second hypothesis was that βAR agonism and changes in temperature affect activation, repolarisation and conduction velocity. The lack of effect of isoprenaline on activation and conduction velocity was unexpected, as was the slight increase in ERP as isoprenaline concentration rose. The effects of βAR agonism on these parameters in mice have not been studied as much as they have in large animals including humans, and species differences in I_{Na}, repolarising currents and gap junction modulation may explain the findings. For example, βAR stimulation in the mouse may produce increased Ca^{2+} inflow through the LTCC without the I_{Ks} counterbalance present in humans, with resultant APD and ERP prolongation. Deterioration of the tissue slices is also conceivable, though completion of the protocol for each slice with stable measurements argues against this.

Changes in temperature on the other hand did affect activation and repolarisation properties of slices, in keeping with prior studies, and likely as a result of effects on I_{Na} and repolarising currents. The lack of effect on conduction velocity was surprising; either the reasonably narrow temperature range studied, or perhaps species differences in temperature sensitivity may account for this, possibly related to body surface area to size ratio and the need to tolerate lower temperatures without adverse effects on conduction.

Animal models are an attempt to approximate human physiology or pathophysiology. Their main value is in overcoming ethical issues of experimentation in humans. A model's limitations are accepted if it provides a reasonable reflection of human physiology or pathophysiology, but these limitations must also be recognised. The coronary ligation model of MI is designed to produce LV impairment and the syndrome

of heart failure. The two are not synonymous, although they are sometimes used interchangeably. The distinction is important, but difficult to disambiguate in the mouse. And in the context of addressing $G\alpha_{i2}$'s effects on electrophysiology, it is not clear whether LV impairment or heart failure is important. Another issue is whether sufficient time was allowed for the phenotypic effects of alterations in $G\alpha_{i2}$ levels to develop. Whilst it would have been preferable to leave mice for longer after coronary ligation, there would have been a higher attrition rate. The ECGenie offered the advantage of non-invasive ECG recording in mice. Yet it became apparent that it was difficult to achieve long enough recordings for HRV assessment, and that environmental factors may have influenced the measurements. In fact, trying to measure HRV in the mouse may be demanding too much of the model.

Finally, the *ex vivo* model used with the MEA system produced stable results, with measurements of ERP, local activation time and conduction velocity similar to those previously reported in the literature. However, the quality of the signals was not optimal, likely reflecting the inherent trauma in slicing, or tissue degradation prior to stimulation on the MEA. In addition, the transverse slices used would likely have relatively few myofibres running longitudinally, of relevance due to the anisotropic nature of conduction. It is therefore both surprising, and reassuring, that the measurements obtained were what may be considered normal.

More generally, the purpose of this project was to contribute to the body of knowledge pertaining to the autonomic nervous system's modulation of cardiac electrophysiology. Murine models were used to investigate the effects of autonomic signalling pathways, and in particular, the protein $G\alpha_{i2}$. No observable electrophysiological differences between WT and $G\alpha_{i2}$ KO mice were demonstrated, and βAR agonism had minor effects on repolarisation only. Small changes in temperature on the other hand resulted in significant alterations in activation and refractoriness, suggesting modulation of sodium and potassium currents.
There has been little published previously on the phenotypic effects of alterations of $G\alpha_{i2}$ levels. The use of a pathophysiologically-relevant *in vivo* MI model, combined with an *ex vivo* tissue model, to investigate this and the autonomic control of cardiac electrophysiology, provides a distinct contribution to the field of study.

In simple terms, too much sympathetic and too little parasympathetic activity in the heart is bad, but restoring the balance is no easy task. Several questions remain:

i. Can we modulate the ANS through interventions to achieve better outcomes, and if so, which interventions? Stellate ganglion ablation has been used to reduce sympathetic discharges, and vagal nerve stimulation is under investigation. Pharmacological stimulation of the PNS is currently not possible, though clearly merits investigation.

ii. Can we really manipulate each limb of the autonomic nervous system independently, or is the relationship more complex than that? The anatomical co-localisation, limited in the extra-cardiac ANS but marked in the intrinsic ANS, leads to some functional interdependence.

iii. Can a complex disease state such as heart failure really be treated by targeting a single type of receptor or signalling molecule. Receptors can be promiscuous in terms of the signalling molecules they interact with; and signalling molecules exert diverse effects, and can show redundancy. It is ironic that two of the most successful anti-arrhythmic agents in use today, βAR-blockers and amiodarone, were designed as treatments for angina. Given the poorly-characterised electrical remodelling that occurs in disease states, complexity of intracellular signalling, and the need to balance these factors with acceptable pharmacokinetics and a tolerable side effect profile, it remains to be seen if disease-targeted pharmacotherapy can be realised; and if it can, whether this will be by design, or by chance.

A recently reported trial investigated the use of the centrally-acting sympathoinhibitor, moxonidine in patients undergoing ablation for atrial fibrillation. It reported a significantly lower estimated 12 month recurrence rate with moxonidine (20.0% vs 36.9%, p=0.007)[313]. However, the MOXCON trial from 2003 in which the same drug was investigated in the setting of heart failure, had to be terminated early due to an excess of mortality in the moxonidine group[314]. The effects of vagal nerve stimulation on arrhythmias in ongoing trials are eagerly awaited.

Future directions

Some of the key advantages of mice as a model organism are their small size, easy maintenance, and rapid breeding. These factors contribute to low costs, and help

facilitate genetic modification. However, an important drawback is the difference in their repolarising currents, and hence action potential morphology. Slightly larger animals such as guinea pigs or rabbits show more similarity to humans in this regard, though housing depends on local availability, which is rarely a problem with mice. Another issue is the ease of genetic manipulation: genome sequencing of the guinea pig for example, has not kept pace with that of the mouse. However, it can be expected that such issues will be resolved, and new genetic manipulation techniques are beginning to offer alternatives to the Cre-loxP system commonly used in mice[315].

To take forward the work on $G\alpha_{i2}$ reported in this thesis, larger mammals such as guinea pigs or rabbits could therefore be used to investigate the effects of WT, KO and knockin (gain of function) *GNAI2* alleles. Animals could be phenotyped at baseline and after induction of heart failure, and LTCC currents could be assessed, as could responses to vagal and β2AR stimulation or indeed, blockade. The *ex vivo* work using the MEA system could be corroborated and developed using an epicardial 'sock'/flexible MEA attached to an intact heart perfused on a Langendorff setup. This would remove the traumatic slicing and preservation steps, thereby possibly improving signal quality. Alternatively, or perhaps concurrently, optical mapping with potentiometric dyes could be used to produce visual records of tissue depolarisation and repolarisation.

The relative paucity of data regarding βAR-mediated and thermal effects on I_{Na}, as well as the effect of temperature on potassium currents, could be investigated using the patch-clamp technique. And the ability of alterations in temperature to trigger arrhythmias in ischaemic or scarred tissue could be investigated either *in vivo* or *ex vivo*.

References

1. Priori, S. G. *et al.* Task Force on Sudden Cardiac Death of the European Society of Cardiology. *Eur. Heart J.* **22,** 1374–450 (2001).

2. John, R. M. *et al.* Ventricular arrhythmias and sudden cardiac death. *Lancet* **380,** 1520–9 (2012).

3. Zipes, D. P. *et al.* ACC/AHA/ESC 2006 guidelines for management of patients with ventricular arrhythmias and the prevention of sudden cardiac death: a report of the American College of Cardiology/American Heart Association Task Force and the European Society of Cardiology Com. *Europace* **8,** 746–837 (2006).

4. Kong, M. H. *et al.* Systematic review of the incidence of sudden cardiac death in the United States. *J. Am. Coll. Cardiol.* **57,** 794–801 (2011).

5. National Institute for Health and Clinical Excellence (NICE). Implantable cardioverter defibrillators for arrhythmias. Review of technology appraisal 11.

6. Behr, E. R. *et al.* Sudden arrhythmic death syndrome: a national survey of sudden unexplained cardiac death. *Heart* **93,** 601–5 (2007).

7. Papadakis, M. *et al.* The magnitude of sudden cardiac death in the young: a death certificate-based review in England and Wales. *Europace* **11,** 1353–8 (2009).

8. Pagidipati, N. J. & Gaziano, T. a. Estimating deaths from cardiovascular disease: a review of global methodologies of mortality measurement. *Circulation* **127,** 749–56 (2013).

9. McMurray, J. J. V *et al.* ESC Guidelines for the diagnosis and treatment of acute and chronic heart failure 2012: The Task Force for the Diagnosis and Treatment of Acute and Chronic Heart Failure 2012 of the European Society of Cardiology. Developed in collaboration with the Heart. *Eur. Heart J.* **33,** 1787–847 (2012).

10. Moss, A. *et al.* Improved survival with an implanted defibrillator in patients with coronary disease at high risk for ventricular arrhythmia. *N. Engl. J. Med.* **335,** 1933–1940 (1996).

11. Moss, A. J. *et al.* Prophylactic Implantation of a Defibrillator in Patients with Myocardial Infarction and Reduced Ejection Fraction. *New Engl. J. Med.* **346,** 877–883 (2002).

12. The Antiarrhythmic versus Implantable Defibrillators (AVID) Investigators. A Comparison of Antiarrhythmic-Drug Therapy with Implantable Defibrillators in Patients Resuscitated from Near-Fatal Ventricular Arrhythmias. *N. Engl. J. Med.* **337,** 1576–83 (1997).

13. Bardy, G. H. *et al.* Amiodarone or an implantable cardioverter-defibrillator for congestive heart failure. *N. Engl. J. Med.* **352,** 225–37 (2005).

14. Reddy, V. *et al.* Prophylactic Catheter Ablation For The Prevention Of Defibrillator Therapy. *N. Engl. J. Med.* **357,** 2657–2665 (2007).

15. Kuck, K.-H. *et al.* Catheter ablation of stable ventricular tachycardia before defibrillator implantation in patients with coronary heart disease (VTACH): a multicentre randomised controlled trial. *Lancet* **375,** 31–40 (2010).

16. Mallidi, J., Nadkarni, G. N., Berger, R. D., Calkins, H. & Nazarian, S. Meta-analysis of catheter ablation as an adjunct to medical therapy for treatment of ventricular tachycardia in patients with structural heart disease. *Hear. Rhythm* **8,** 503–510 (2011).

17. Ventricular Tachycardia (VT) Ablation Versus Enhanced Drug Therapy (VANISH). *NCT00905853* at <https://clinicaltrials.gov/ct2/show/NCT00905853?term=NCT00905853&rank=1>

18. Packer, M. *et al.* The effect of carvedilol on mortality and morbidity in patients with chronic heart failure. *N. Engl. J. Med.* **334,** 1349–55 (1996).

19. MERIT-HF Study Group. Effect of metoprolol CR/XL in chronic heart failure : Metoprolol CR/XL Randomised Intervention Trial in Congestive Heart Failure (MERIT-HF). *Lancet* **353,** 2001–2007 (1999).

20. Echt, D. S. *et al.* Mortality and Morbidity in Patients Receiving Encainide, Flecainide, or Placebo. The Cardiac Arrhythmia Suppression Trial. *N. Engl. J. Med.* **324,** 781–8 (1991).

21. Waldo, A. L. *et al.* Effect of d-sotalol on mortality in patients with left ventricular dysfunction after recent and remote myocardial infarction. *Lancet* **348,** 7–12 (1996).

22. Køber, L. *et al.* Increased mortality after dronedarone therapy for severe heart failure. *N. Engl. J. Med.* **358,** 2678–87 (2008).

23. Connolly, S. *et al.* Dronedarone in high-risk permanent atrial fibrillation. *N. Engl. J. Med.* **365,** 2268–76 (2011).

24. Harvey, W. *Exercitatio Anatomica de Motu Cordis et Sanguinis in Animalibus*. (1628).

25. Boyett, M. R. 'And the beat goes on.' The cardiac conduction system: the wiring system of the heart. *Exp. Physiol.* **94,** 1035–49 (2009).

26. Yen Ho, S. & Ernst, S. *Anatomy For Cardiac Electrophysiologists - A Practical Handbook*. (Cardiotext Publishing, 2012).

27. Christoffels, V. M. & Moorman, A. F. M. Development of the cardiac conduction system: why are some regions of the heart more arrhythmogenic than others? *Circ. Arrhythm. Electrophysiol.* **2,** 195–207 (2009).

28. Xin, M., Olson, E. N. & Bassel-Duby, R. Mending broken hearts: cardiac development as a basis for adult heart regeneration and repair. *Nat. Rev. Mol. Cell Biol.* **14,** 529–41 (2013).

29. Camelliti, P., Borg, T. K. & Kohl, P. Structural and functional characterisation of cardiac fibroblasts. *Cardiovasc. Res.* **65,** 40–51 (2005).

30. Rohr, S. Arrhythmogenic implications of fibroblast-myocyte interactions. *Circ. Arrhythm. Electrophysiol.* **5,** 442–52 (2012).

31. Bursac, N. & Kim, J. J. in *Card. Electrophysiol. From Cell to Bedside* (Zipes, D. & Jalife, J.) 297–309 (Elsevier Saunders, 2014).

32. Zipes, D., Libby, P., Bonow, R., Braunwald, E. & (eds). *Braunwald's Heart Disease. A textbook of cardiovascular medicine*. (Elsevier Saunders, 2005).

33. Nygren, A. *et al.* Mathematical model of an adult human atrial cell: the role of K+ currents in repolarization. *Circ. Res.* **82,** 63–81 (1998).

34. Cerrone, M., Agullo-Pascual, E. & Delmar, M. in *Card. Electrophysiol. From Cell to Bedside* (Zipes, D. & Jalife, J.) 215–229 (Elsevier Saunders, 2014).

35. Catterall, W. A. in *Card. Electrophysiol. From Cell to Bedside* (Zipes, D. P. & Jalife, J.) 1–12 (Elsevier Saunders, 2014).

36. Issa, Z. F., Miller, J. M. & Zipes, D. P. *Clinical Arrhythmology and Electrophysiology*. (Elsevier Saunders, 2012).

37. Awad, M. M., Calkins, H. & Judge, D. P. Mechanisms of disease: molecular genetics of arrhythmogenic right ventricular dysplasia/cardiomyopathy. *Nat. Clin. Pract. Cardiovasc. Med.* **5,** 258–267 (2008).

38. Grant, A. O. Cardiac ion channels. *Circ. Arrhythm. Electrophysiol.* **2,** 185–94 (2009).

39. Hodgkin, A. L. & Huxley, F. A Quantitative Description of Membrane Current and its Application To Conduction and Excitation in Nerve. *J. Physiol.* **117,** 500–544 (1952).

40. Roden, D. M., Balser, J. R., George, A. L. & Anderson, M. E. Cardiac ion channels. *Annu. Rev. Physiol.* **64,** 431–75 (2002).

41. Berridge, M. J. Cellular Processes. *Cell Signal. Biol.* 1–137 (2012). doi:10.1042/csb0001007

42. Nerbonne, J. M. & Kass, R. S. Molecular Physiology of Cardiac Repolarization. *Physiol. Rev.* **85,** 1205–1253 (2005).

43. Nerbonne, J. Studying cardiac arrhythmias in the mouse - a reasonable model for probing mechanisms? *Trends Cardiovasc. Med.* **14,** 83–93 (2004).

44. Opthof, T., Coronel, R. & Janse, M. J. Is there a significant transmural gradient in repolarization time in the intact heart?: Repolarization Gradients in the Intact Heart. *Circ. Arrhythm. Electrophysiol.* **2,** 89–96 (2009).

45. Patel, C. *et al.* Is there a significant transmural gradient in repolarization time in the intact heart? Cellular basis of the T wave: a century of controversy. *Circ. Arrhythm. Electrophysiol.* **2,** 80–8 (2009).

46. Rook, M. B., Evers, M. M., Vos, M. a & Bierhuizen, M. F. a. Biology of cardiac sodium channel Nav1.5 expression. *Cardiovasc. Res.* **93,** 12–23 (2012).

47. Davis, R. P., van den Berg, C. W., Casini, S., Braam, S. R. & Mummery, C. L. Pluripotent stem cell models of cardiac disease and their implication for drug discovery and development. *Trends Mol. Med.* **17,** 475–84 (2011).

48. Jalife, J., Delmar, M., Anumonwo, J., Berenfeld, O. & Kalifa, J. *Basic Cardiac Electrophysiology for the Clinician*. (Wiley-Blackwell, 2009).

49. Abriel, H. Cardiac sodium channel Na(v)1.5 and interacting proteins: Physiology and pathophysiology. *J. Mol. Cell. Cardiol.* **48,** 2–11 (2010).

50. Jalife, J. & Milstein, M. L. in *Card. Electrophysiol. From Cell to Bedside* (Zipes, D. P. & Jalife, J.) 205–214 (Elsevier Saunders, 2014).

51. Moore, H. J. & Franz, M. R. Monophasic action potential recordings in humans. *J. Cardiovasc. Electrophysiol.* **18,** 787–90 (2007).

52. Murgatroyd, F. D., Krahn, A. D., Klein, G. J., Yee, R. K. & Skanes, A. C. *Handbook of Cardiac Electrophysiology*. (Remedica, 2002).

53. Sager, P. T. *et al.* Frequency-dependent electrophysiologic effects of amiodarone in humans. *Circulation* **88,** 1063–1071 (1993).

54. Lee, R. J., Liem, L. B., Cohen, T. J. & Franz, M. R. Relation between repolarization and refractoriness in the human ventricle: Cycle length dependence and effect of procainamide. *J. Am. Coll. Cardiol.* **19,** 614–618 (1992).

55. Denes, P., Wu, D., Dhingra, R., Pietras, R. J. & Rosen, K. M. The Effects of Cycle Length on Cardiac Refractory Periods in Man. *Circulation* **49,** 32–41 (1974).

56. Vaseghi, M. & Shivkumar, K. The role of the autonomic nervous system in sudden cardiac death. *Prog. Cardiovasc. Dis.* **50,** 404–19 (2008).

57. Taggart, P. Effect of Adrenergic Stimulation on Action Potential Duration Restitution in Humans. *Circulation* **107,** 285–289 (2002).

58. Franz, M. R. The Electrical Restitution Curve Revisited: Steep or Flat Slope-Which is Better? *J. Cardiovasc. Electrophysiol.* **14,** S140–S147 (2003).

59. Franz, M. R. Bridging the gap between basic and clinical electrophysiology: what can be learned from monophasic action potential recordings? *J. Cardiovasc. Electrophysiol.* **5,** 699–710 (1994).

60. Kléber, A. G. & Rudy, Y. Basic mechanisms of cardiac impulse propagation and associated arrhythmias. *Physiol. Rev.* **84,** 431–88 (2004).

61. Nielsen, M. S. *et al.* Gap junctions. *Compr Physiol* **2,** 1981–2035 (2012).

62. Spector, P. Principles of Cardiac Electric Propagation and Their Implications for Re-entrant Arrhythmias. *Circ. Arrhythmia Electrophysiol.* **6,** 655–661 (2013).

63. Weidmann, S. Heart: Electrophysiology. *Annu. Rev. Physiol.* **36,** 155–169 (1974).

64. Pfenniger, A., Wohlwend, A. & Kwak, B. R. Mutations in connexin genes and disease. *Eur. J. Clin. Invest.* **41,** 103–116 (2011).

65. Severs, N. J., Bruce, A. F., Dupont, E. & Rothery, S. Remodelling of gap junctions and connexin expression in diseased myocardium. *Cardiovasc. Res.* **80,** 9–19 (2008).

66. Kléber, A. G. in *Card. Electrophysiol. From Cell to Bedside* (Zipes, D. & Jalife, J.) 265–275 (Elsevier Saunders, 2014).

67. Valiunas, V. & Brink, P. R. in *Card. Electrophysiol. From Cell to Bedside* (Zipes, D. P. & Jalife, J.) 151–160 (Elsevier Saunders, 2014).

68. Shaw, R. M. & Rudy, Y. Ionic Mechanisms of Propagation in Cardiac Tissue. Roles of the sodium and L-type calcium currents during reduced excitability and decreased gap junction coupling. *Circ. Res.* **81,** 727–741 (1997).

69. Morley, G. E. *et al.* Characterization of conduction in the ventricles of normal and heterozygous Cx43 knockout mice using optical mapping. *J. Cardiovasc. Electrophysiol.* **10,** 1361–1375 (1999).

70. Van Rijen, H. V. M. *et al.* Slow Conduction and Enhanced Anisotropy Increase the Propensity for Ventricular Tachyarrhythmias in Adult Mice with Induced Deletion of Connexin43. *Circulation* **109,** 1048–1055 (2004).

71. Dhillon, P. S. *et al.* Relationship between gap-junctional conductance and conduction velocity in Mammalian myocardium. *Circ. Arrhythm. Electrophysiol.* **6,** 1208–14 (2013).

72. Saffitz, J. E. *et al.* The molecular basis of anisotropy: role of gap junctions. *J. Cardiovasc. Electrophysiol.* **6,** 498–510 (1995).

73. Bukauskas, F. F. in *Card. Electrophysiol. From Cell to Bedside* (Zipes, D. P. & Jalife, J.) 85–94 (Elsevier Saunders, 2014).

74. Jalife, J., Morley, G. E. & Vaidya, D. Connexins and impulse propagation in the mouse heart. *J. Cardiovasc. Electrophysiol.* **10,** 1649–63 (1999).

75. Miquerol, L., Beyer, S. & Kelly, R. G. Establishment of the mouse ventricular conduction system. *Cardiovasc. Res.* **91,** 232–242 (2011).

76. Reaume, A. G. *et al.* Cardiac malformation in neonatal mice lacking connexin43. *Science (80-.).* **267,** 1831–4 (1995).

77. Berridge, M. J. Cell Signalling Pathways. *Cell Signal. Biol.* 1–118 (2012). doi:10.1042/csb0001002

78. Hendriks-balk, M. C., Peters, S. L. M., Michel, M. C. & Alewijnse, A. E. Regulation of G protein-coupled receptor signalling: Focus on the cardiovascular system and regulator of G protein signalling proteins. *Eur. J. Pharmacol.* **585,** 278–291 (2008).

79. Beavo, J. a & Brunton, L. L. Cyclic nucleotide research - still expanding after half a century. *Nat. Rev. Mol. Cell bBology* **3,** 710–8 (2002).

80. Lee, L. C. Y., Maurice, D. H. & Baillie, G. S. Targeting protein-protein interactions within the cyclic AMP signaling system as a therapeutic strategy for cardiovascular disease. *Future Med. Chem.* **5,** 451–64 (2013).

81. Oldham, W. M. & Hamm, H. E. Heterotrimeric G protein activation by G-protein-coupled receptors. *Nat. Rev. Mol. Cell Biol.* **9,** 60–71 (2008).

82. Fredriksson, R., Lagerström, M. C., Lundin, L.-G. & Schiöth, H. B. The G-Protein-Coupled Receptors in the Human Genome Form Five Main Families. Phylogenetic Analysis, Paralogon Groups, and Fingerprints. *Mol. Pharmacol.* **63,** 1256–72 (2003).

83. Huang, C. & Tesmer, J. J. G. Recognition in the Face of Diversity: Interactions of Heterotrimeric G proteins and G Protein-coupled Receptor (GPCR) Kinases with Activated GPCRs. *J. Biol. Chem.* **286,** 7715–7721 (2011).

84. Leaney, J. L., Milligan, G. & Tinker, A. The G protein alpha subunit has a key role in determining the specificity of coupling to, but not the activation of, G protein-gated inwardly rectifying K(+) channels. *J. Biol. Chem.* **275,** 921–9 (2000).

85. Milligan, G. & Kostenis, E. Heterotrimeric G-proteins: a short history. *Br. J. Pharmacol.* **147,** S46–S55 (2006).

86. Logothetis, D. E., Kurachi, Y., Galper, J., Neer, E. J. & Clapham, D. E. The beta-gamma subunits of GTP-binding proteins activate the muscarinic K+ channel in heart. *Nature* **325,** 321–326 (1987).

87. Vivaudou, M. *et al.* Probing the G-protein Regulation of GIRK1 and GIRK4, the Two Subunits of the KACh Channel, Using Functional Homomeric Mutants. *J. Biol. Chem.* **272,** 31553–31560 (1997).

88. Birnbaumer, L. Expansion of signal transduction by G proteins. The second 15 years or so: from 3 to 16 alpha subunits plus betagamma dimers. *Biochim. Biophys. Acta* **1768,** 772–93 (2007).

89. Köhler, D. *et al.* Gαi2- and Gαi3-Deficient Mice Display Opposite Severity of Myocardial Ischemia Reperfusion Injury. *PLoS One* **9,** e98325 (2014).

90. Xiao, R.-P. *et al.* Coupling of Beta 2-Adrenoceptor to Gi Proteins and Its Physiological Relevance in Murine Cardiac Myocytes. *Circ. Res.* **84,** 43–52 (1999).

91. Xiao, R.-P. *et al.* Enhanced G(i) signaling selectively negates beta2-adrenergic receptor (AR)--but not beta1-AR-mediated positive inotropic effect in myocytes from failing rat hearts. *Circulation* **108,** 1633–9 (2003).

92. Dizayee, S. *et al.* Gαi2- and Gαi3-specific regulation of voltage-dependent L-type calcium channels in cardiomyocytes. *PLoS One* **6,** e24979 (2011).

93. Leaney, J. L. & Tinker, a. The role of members of the pertussis toxin-sensitive family of G proteins in coupling receptors to the activation of the G protein-gated inwardly rectifying potassium channel. *Proc. Natl. Acad. Sci. U. S. A.* **97,** 5651–6 (2000).

94. Zuberi, Z. *et al.* Absence of the inhibitory G-protein Galphai2 predisposes to ventricular cardiac arrhythmia. *Circ. Arrhythm. Electrophysiol.* **3,** 391–400 (2010).

95. Fu, Y. *et al.* Endogenous RGS proteins and Galpha subtypes differentially control muscarinic and adenosine-mediated chronotropic effects. *Circ. Res.* **98,** 659–66 (2006).

96. Foerster, K. *et al.* Cardioprotection specific for the G protein Gi2 in chronic adrenergic signaling through beta 2-adrenoceptors. *Proc. Natl. Acad. Sci. U. S. A.* **100,** 14475–80 (2003).

97. Ang, R., Opel, A. & Tinker, A. The Role of Inhibitory G Proteins and Regulators of G Protein Signaling in the in vivo Control of Heart Rate and Predisposition to Cardiac Arrhythmias. *Front. Physiol.* **3,** (2012).

98. Feldman, A. M. *et al.* Increase of the 40,000-mol wt pertussis toxin substrate (G protein) in the failing human heart. *J. Clin. Invest.* **82,** 189–97 (1988).

99. Neumann, J. *et al.* Increase in myocardial Gi-proteins in heart failure. *Lancet* **2,** 936–937 (1988).

100. Böhm, M. *et al.* Increase of Gi alpha in human hearts with dilated but not ischemic cardiomyopathy. *Circulation* **82,** 1249–1265 (1990).

101. Eschenhagen, T. *et al.* Increased messenger RNA level of the inhibitory G protein alpha subunit Gi alpha-2 in human end-stage heart failure. *Circ. Res.* **70,** 688–96 (1992).

102. Kompa, A. R., Gu, X. H., Evans, B. A. & Summers, R. J. Desensitization of cardiac beta-adrenoceptor signaling with heart failure produced by myocardial infarction in the rat. Evidence for the role of Gi but not Gs or phosphorylating proteins. *J. Mol. Cell. Cardiol.* **31,** 1185–201 (1999).

103. Lerman, B. B. *et al.* Right Ventricular Outflow Tract Tachycardia Due To a Somatic Cell Mutation in G Protein Subunit αi2. *J. Clin. Invest.* **101,** 2862–2868 (1998).

104. Zhang, Y. H., Hinde, a K. & Hancox, J. C. Anti-adrenergic effect of adenosine on Na(+)-Ca(2+) exchange current recorded from guinea-pig ventricular myocytes. *Cell Calcium* **29,** 347–58 (2001).

105. Grimm, M. *et al.* Inactivation of Gialpha proteins increases arrhythmogenic effects of beta-adrenergic stimulation in the heart. *J. Mol. Cell. Cardiol.* **30,** 1917–28 (1998).

106. Nagata, K. *et al.* Gαi2 but not Gαi3 Is Required for Muscarinic Inhibition of Contractility and Calcium Currents in Adult Cardiomyocytes. *Circ. Res.* **87,** 903–909 (2000).

107. Chen, F., Spicher, K., Jiang, M., Birnbaumer, L. & Wetzel, G. T. Lack of muscarinic regulation of Ca2+ channels in Gi2α gene knockout mouse hearts. *Am. J. Physiol. Heart Circ. Physiol.* **280,** H1989–1995 (2001).

108. Zuberi, Z., Birnbaumer, L. & Tinker, a. The role of inhibitory heterotrimeric G proteins in the control of in vivo heart rate dynamics. *AJP Regul. Integr. Comp. Physiol.* **295,** R1822–R1830 (2008).

109. Seki, A. *et al.* Sympathetic nerve fibers in human cervical and thoracic vagus nerves. *Hear. Rhythm* **11,** 1411–1417 (2014).

110. Chen, P.-S., Chen, L. S. & Lin, S.-F. in *Card. Electrophysiol. From Cell to Bedside* (Zipes, D. P. & Jalife, J.) 399–408 (Elsevier Saunders, 2014).

111. Sun, J., Scherlag, B. J. & Po, S. S. in *Card. Electrophysiol. From Cell to Bedside* (Zipes, D. & Jalife, J.) 470–474 (Elsevier Saunders, 2014).

112. Shen, M. J. & Zipes, D. P. Role of the autonomic nervous system in modulating cardiac arrhythmias. *Circ. Res.* **114,** 1004–21 (2014).

113. Kimura, K., Ieda, M. & Fukuda, K. Development, maturation, and transdifferentiation of cardiac sympathetic nerves. *Circ. Res.* **110,** 325–336 (2012).

114. Armour, J. a, Murphy, D. a, Yuan, B. X., Macdonald, S. & Hopkins, D. a. Gross and microscopic anatomy of the human intrinsic cardiac nervous system. *Anat. Rec.* **247,** 289–98 (1997).

115. Hou, Y. *et al.* Ganglionated Plexi Modulate Extrinsic Cardiac Autonomic Nerve Input. Effects on Sinus Rate, Atrioventricular Conduction, Refractoriness, and Inducibility of Atrial Fibrillation. *J. Am. Coll. Cardiol.* **50,** 61–68 (2007).

116. Mastitskaya, S. *et al.* Cardioprotection evoked by remote ischaemic preconditioning is critically dependent on the activity of vagal pre-ganglionic neurones. *Cardiovasc. Res.* **95,** 487–94 (2012).

117. Ng, G. A. Vagal modulation of cardiac ventricular arrhythmia. *Exp. Physiol.* **99,** 295–9 (2014).

118. Einbrodt, P. Ueber herzreizung und ihr verhaeltnis zum blutdruck. *Akad. der Wissenschaften Sitzungsberichte* **38,** 345 (1859).

119. Armour, J. A. Functional anatomy of intrathoracic neurons innervating the atria and ventricles. *Hear. Rhythm* **7,** 994–996 (2010).

120. Zipes, D. P. Heart-brain interactions in cardiac arrhythmias: role of the autonomic nervous system. *Cleve. Clin. J. Med.* **75 Suppl 2,** S94–6 (2008).

121. Taggart, P., Critchley, H. & Lambiase, P. D. Heart-brain interactions in cardiac arrhythmia. *Heart* **97,** 698–708 (2011).

122. Brodde, O. E. & Michel, M. C. Adrenergic and muscarinic receptors in the human heart. *Pharmacol. Rev.* **51,** 651–90 (1999).

123. O'Connell, T. D., Jensen, B. C., Baker, A. J. & Simpson, P. C. Cardiac Alpha 1-Adrenergic Receptors: Novel Aspects of Expression, Signaling Mechanisms, Physiologic Function, and Clinical Importance. *Pharmacol. Rev.* **66,** 308–333 (2014).

124. Brodde, O.-E. Beta-adrenoceptor blocker treatment and the cardiac beta-adrenoceptor-G-protein(s)-adenylyl cyclase system in chronic heart failure. *Naunyn. Schmiedebergs. Arch. Pharmacol.* **374,** 361–72 (2007).

125. Xiao, R. P., Ji, X. & Lakatta, E. G. Functional coupling of the beta 2-adrenoceptor to a pertussis toxin-sensitive G protein in cardiac myocytes. *Mol. Pharmacol.* **47,** 322–9 (1995).

126. Kilts, J. D. *et al.* β2-Adrenergic and Several Other G Protein–Coupled Receptors in Human Atrial Membranes Activate Both Gs and Gi. *Circ. Res.* **87,** 705–709 (2000).

127. Zheng, M., Zhu, W., Han, Q. & Xiao, R.-P. Emerging concepts and therapeutic implications of beta-adrenergic receptor subtype signaling. *Pharmacol. Ther.* **108,** 257–68 (2005).

128. Difrancesco, D., Ducouret, P. & Robinson, R. B. Muscarinic modulation of cardiac rate at low acetylcholine concentrations. *Science (80-.).* **243,** 669–671 (1989).

129. Newton, G. E., Parker, A. B., Landzberg, J. S., Colucci, W. S. & Parker, J. D. Muscarinic receptor modulation of basal and beta-adrenergic stimulated function of the failing human left ventricle. *J. Clin. Invest.* **98,** 2756–2763 (1996).

130. Kolman, B. S., Verrier, R. L. & Lown, B. The effect of vagus nerve stimulation upon vulnerability of the canine ventricle: role of sympathetic-parasympathetic interactions. *Circulation* **52,** 578–585 (1975).

131. Vanoli, E. *et al.* Vagal stimulation and prevention of sudden death in conscious dogs with a healed myocardial infarction. *Circ. Res.* **68,** 1471–1481 (1991).

132. Goldberger, J. *et al.* American Heart Association/American College of Cardiology Foundation/Heart Rhythm Society Scientific Statement on Noninvasive Risk Stratification Techniques for Identifying Patients at Risk for Sudden Cardiac Death. *Circulation* **118,** 1497–1518 (2008).

133. Hon, E. H. & Lee, S. T. Electronic evaluations of the fetal heart rate patterns preceding fetal death, further observations. *Am. J. Obstet. Gynecol.* **87,** 814–26 (1965).

134. Task Force of the European Society of Cardiology and The North American Society of Pacing and Electrophysiology. Heart rate variability: Standards of measurement, physiological interpretation, and clinical use. *Eur. Heart J.* **17,** 354–381 (1996).

135. Eckberg, D. L., Drabinsky, M. & Braunwald, E. Defective Cardiac Parasympathetic Control in Patients with Heart Disease. *N. Engl. J. Med.* **285,** 877–883 (1971).

136. Schwartz, P. J. & De Ferrari, G. M. Sympathetic-parasympathetic interaction in health and disease: abnormalities and relevance in heart failure. *Heart Fail. Rev.* **16,** 101–7 (2011).

137. Malik, M. & Schmidt, G. in *Card. Electrophysiol. From Cell to Bedside* (Zipes, D. P. & Jalife, J.) 649–656 (Elsevier Saunders, 2014).

138. La Rovere, M. T., Bigger Jr, J. T., Marcus, F. I., Mortara, A. & Schwartz, P. J. Baroreflex sensitivity and heart-rate variability in prediction of total cardiac mortality after myocardial infarction. *Lancet* **351,** 478–484 (1998).

139. Nolan, J. *et al.* Prospective study of heart rate variability and mortality in chronic heart failure. Results of the United Kingdom Heart Failure Evaluation and Assessment of Risk Trial (UK-Heart). *Circulation* **98,** 1510–1516 (1998).

140. Exner, D. Noninvasive risk stratification after myocardial infarction: rationale, current evidence and the need for definitive trials. *Can. J. Cardiol.* **25 Suppl A,** 21A–27A (2009).

141. Zhou, S. *et al.* Spontaneous stellate ganglion nerve activity and ventricular arrhythmia in a canine model of sudden death. *Hear. Rhythm* **5,** 131–139 (2008).

142. Schwartz, P. J. *et al.* Prevention of Sudden Cardiac Death After a First Myocardial Infarction by Pharmacologic or Surgical Antiadrenergic Interventions. *J. Cardiovasc. Electrophysiol.* **3,** 2–16 (1992).

143. Cardiac Denervation Surgery for Prevention of Ventricular Tacharrhythmias (PREVENT VT). at <https://clinicaltrials.gov/ct2/show/NCT01013714>

144. Takigawa, M. *et al.* Seasonal and circadian distributions of ventricular fibrillation in patients with Brugada syndrome. *Hear. Rhythm* **5,** 1523–7 (2008).

145. Miyazaki, T. *et al.* Autonomic and antiarrhythmic drug modulation of ST segment elevation in patients with Brugada syndrome. *J. Am. Coll. Cardiol.* **27,** 1061–70 (1996).

146. Priori, S. G. *et al.* Executive summary: HRS/EHRA/APHRS expert consensus statement on the diagnosis and management of patients with inherited primary arrhythmia syndromes. *Europace* **15,** 1389–406 (2013).

147. Schwartz, P. J., Crotti, L. & Insolia, R. Long-QT syndrome: from genetics to management. *Circ. Arrhythm. Electrophysiol.* **5,** 868–77 (2012).

148. Zannad, F. *et al.* Chronic vagal stimulation for the treatment of low ejection fraction heart failure: results of the NEural Cardiac TherApy foR Heart Failure (NECTAR-HF) randomized controlled trial. *Eur. Heart J.* **36,** 425–433 (2014).

149. INOVATE-HF. at <https://clinicaltrials.gov/ct2/show/NCT01303718>

150. Shah, M., Akar, F. G. & Tomaselli, G. F. Molecular basis of arrhythmias. *Circulation* **112,** 2517–29 (2005).

151. Pogwizd, S. M. & Bers, D. M. Cellular basis of triggered arrhythmias in heart failure. *Trends Cardiovasc. Med.* **14,** 61–6 (2004).

152. Nattel, S. & Carlsson, L. Innovative approaches to anti-arrhythmic drug therapy. *Nat. Rev. Drug Discov.* **5,** 1034–1049 (2006).

153. Mines, G. R. On dynamic equilibrium in the heart. *J. Physiol.* **46,** 349–383 (1913).

154. Pandit, S. V. & Jalife, J. Rotors and the dynamics of cardiac fibrillation. *Circ. Res.* **112,** 849–862 (2013).

155. Allessie, M. A., Bonke, F. I. & Schopman, F. J. Circus movement in rabbit atrial muscle as a mechanism of tachycardia. III. The 'leading circle' concept: a new model of circus movement in cardiac tissue without the involvement of an anatomical obstacle. *Circ. Res.* **41,** 9–18 (1977).

156. Moe, G. On the multiple wavelet hypothesis of atrial fibrillation. *Arch Int Pharmacodyn Ther* **140,** 183–188 (1962).

157. Krinsky VI. Spread of excitation in an inhomogeneous medium (state similar to cardiac fibrillation). *Biophysics (Oxf).* **11,** 776–784 (1966).

158. Dosdall, D. J. & Ideker, R. E. in *Card. Electrophysiol. From Cell to Bedside* (Zipes, D. P. & Jalife, J.) 475–482 (Elsevier Saunders, 2014).

159. Smith, S. W. *Digital Signal Processing. A practical guide for engineers and scientists*. (Newnes, 2003).

160. Kligfield, P. *et al.* Recommendations for the standardization and interpretation of the electrocardiogram: Part I: the electrocardiogram and its technology. A scientific statement from the American Heart Association Electrocardiography and Arrhythmias Committee, Council on Cli. *J. Am. Coll. Cardiol.* **49,** 1109–27 (2007).

161. Burdon-Sanderson, J. & Page, F. J. M. On the time-relations of the excitatory process in the ventricle of the heart of the frog. *J. Physiol.* **2,** 385–412 (1882).

162. Korsgren, M., Leskinen, E., Sjöstrand, U. & Varnauskas, E. Intracardiac recording of monophasic action potentials in the human heart. *Scand. J. Clin. Lab. Invest.* **18,** 561–564 (1966).

163. Shabetai, R., Surawicz, B. & Hammill, W. Monophasic Action Potentials in Man. *Circulation* **38,** 341–352 (1968).

164. *Monophasic Action Potentials: Bridging Cell and Bedside*. (Futura Publishing Company, Inc., 2000).

165. Kondo, M., Nesterenko, V. & Antzelevitch, C. Cellular basis for the monophasic action potential. Which electrode is the recording electrode? *Cardiovasc. Res.* **63,** 635–644 (2004).

166. Kadish, A. What is a monophasic action potential? *Cardiovasc. Res.* **63,** 580–1 (2004).

167. Coronel, R. *et al.* Monophasic action potentials and activation recovery intervals as measures of ventricular action potential duration: experimental evidence to resolve some controversies. *Hear. Rhythm* **3,** 1043–50 (2006).

168. Ling, G. & Gerard, R. W. The normal membrane potential of frog Sartorius fibers. *J. Cell. Comp. Physiol.* **34,** 383 (1949).

169. Coraboeuf, E. & Weidmann, S. Potentiel de repos et potentiels d'action du muscle cardiaque mesurés à l'aide d'électrodes intracellulaires. *C R Séances Soc Biol* **143,** 1329 (1949).

170. Coraboeuf, E. & Weidmann, S. Potentiels d'action du muscle cardiaque obtenus à l'aide de microélectrodes intracellulaires. *C R Séances Soc Biol* **143,** 1360 (1949).

171. Hoffman, B. F., Cranefield, P. F., Lepeschkin, E., Surawicz, B. & Herrlich, H. C. Comparison of cardiac monophasic action potentials recorded by intracellular and suction electrodes. *Am. J. Physiol.* **196,** 1297–301 (1959).

172. Durrer, D. & van der Tweel, L. H. Excitation of the left ventricular wall of the dog and goat. *Ann. N. Y. Acad. Sci.* **65,** 779–803 (1957).

173. Steinhaus, B. M. Estimating cardiac transmembrane activation and recovery times from unipolar and bipolar extracellular electrograms: a simulation study. *Circ. Res.* **64,** 449–462 (1989).

174. Wyatt, R. F. Comparison of estimates of activation and recovery times from bipolar and unipolar electrograms to in vivo transmembrane APDs. in *Proc IEEE/Eng Med Biol Soc, 2nd Annu. Conf.* 22–25 (1980).

175. Wyatt, R. F. *et al.* Estimation of ventricular transmembrane action potential durations and repolarization times from unipolar electrograms. *Am. J. Cardiol.* **47,** 488 (1981).

176. Chen, P.-S. *et al.* Epicardial activation and repolarization in patients with right ventricular hypertrophy. *Circulation* **83,** 104–118 (1991).

177. Gepstein, L., Hayam, G. & Ben Haim, S. A. Activation-repolarization coupling in the normal swine myocardium. *Circulation* **96,** 4036–4043 (1997).

178. Yue, A. M. *et al.* Determination of human ventricular repolarization by noncontact mapping. Validation with monophasic action potential recordings. *Circulation* **110,** 1343–1350 (2004).

179. Millar, C. K., Kralios, F. a & Lux, R. L. Correlation between refractory periods and activation-recovery intervals from electrograms: effects of rate and adrenergic interventions. *Circulation* **72,** 1372–1379 (1985).

180. Haws, C. W. & Lux, R. L. Correlation between in vivo transmembrane action potential durations and activation-recovery intervals from electrograms. Effects of interventions that alter repolarization time. *Circulation* **81,** 281–288 (1990).

181. Malik, M. & Batchvarov, V. N. Measurement, interpretation and clinical potential of QT dispersion. *J. Am. Coll. Cardiol.* **36,** 1749–1766 (2000).

182. Doyle, A., McGarry, M. P., Lee, N. a & Lee, J. J. The construction of transgenic and gene knockout/knockin mouse models of human disease. *Transgenic Res.* **21,** 327–49 (2012).

183. Sangiorgi, F. Manipulating the mouse genome: approaches and applications. *J. Nucl. Cardiol.* **8,** 591–8 (2001).

184. Sauer, B. & Henderson, N. Site-specific DNA recombination in mammalian cells by the Cre recombinase of bacteriophage P1. *Proc. Natl. Acad. Sci. U. S. A.* **85,** 5166–5170 (1988).

185. Feil, R. *et al.* Ligand-activated site-specific recombination in mice. *Proc. Natl. Acad. Sci. U. S. A.* **93,** 10887–90 (1996).

186. Sohal, D. S. *et al.* Temporally Regulated and Tissue-Specific Gene Manipulations in the Adult and Embryonic Heart Using a Tamoxifen-Inducible Cre Protein. *Circ. Res.* **89,** 20–25 (2001).

187. Minamino, T., Gaussin, V., DeMayo, F. J. & Schneider, M. D. Inducible Gene Targeting in Postnatal Myocardium by Cardiac-Specific Expression of a Hormone-Activated Cre Fusion Protein. *Circ. Res.* **88,** 587–592 (2001).

188. Subramaniam, A. *et al.* Tissue-specific regulation of the alpha-myosin heavy chain gene promoter in transgenic mice. *J. Biol. Chem.* **266,** 24613–20 (1991).

189. Morkin, E. Regulation of myosin heavy chain genes in the heart. *Circulation* **87,** 1451–1460 (1993).

190. Morkin, E. Control of cardiac myosin heavy chain gene expression. *Microsc. Res. Tech.* **50,** 522–31 (2000).

191. Ng, W. A., Grupp, I. L., Subramaniam, A. & Robbins, J. Cardiac myosin heavy chain mRNA expression and myocardial function in the mouse heart. *Circ. Res.* **68,** 1742–1750 (1991).

192. Dalwadi, H. *et al.* B cell developmental requirement for the G alpha i2 gene. *J. Immunol.* **170,** 1707–15 (2003).

193. Wu, J. Y. *et al.* Impaired TGF-beta responses in peripheral T cells of G alpha i2-/- mice. *J. Immunol.* **174,** 6122–8 (2005).

194. Rudolph, U. *et al.* Ulcerative colitis and adenocarcinoma of the colon in Gαi2-deficient mice. *Nat. Genet.* **10,** 143–150 (1995).

195. Mönkkönen, K. S. *et al.* Intracerebroventricular antisense knockdown of G alpha i2 results in ciliary stasis and ventricular dilatation in the rat. *BMC Neurosci.* **8,** 26 (2007).

196. Jantzen, H., Milstone, D. S., Gousset, L., Conley, P. B. & Mortensen, R. M. Impaired activation of murine platelets lacking Gαi2. *J. Clin. Invest.* **108,** 477–483 (2001).

197. Le, Y. & Sauer, B. Conditional gene knockout using Cre recombinase. *Mol. Biotechnol.* **17,** 269–75 (2001).

198. Agah, R. *et al.* Gene Recombination in Postmitotic Cells. *J. Clin. Invest.* **100,** 169–179 (1997).

199. Herrmann, S., Stieber, J., Stöckl, G., Hofmann, F. & Ludwig, A. HCN4 provides a 'depolarization reserve' and is not required for heart rate acceleration in mice. *EMBO J.* **26,** 4423–32 (2007).

200. Chen, P. P., Patel, J. R., Powers, P. a, Fitzsimons, D. P. & Moss, R. L. Dissociation of structural and functional phenotypes in cardiac myosin-binding protein C conditional knockout mice. *Circulation* **126,** 1194–205 (2012).

201. Andersson, K. B. *et al.* Moderate heart dysfunction in mice with inducible cardiomyocyte-specific excision of the Serca2 gene. *J. Mol. Cell. Cardiol.* **47,** 180–7 (2009).

202. Kedzierski, R. M. *et al.* Cardiomyocyte-Specific Endothelin A Receptor Knockout Mice Have Normal Cardiac Function and an Unaltered Hypertrophic Response to Angiotensin II and Isoproterenol Cardiomyocyte-Specific Endothelin A Receptor Knockout Mice Have Normal Cardiac Function and. *Mol. Cell. Biol.* **23,** 8226–8232 (2003).

203. Houser, S. R. *et al.* Animal models of heart failure: a scientific statement from the American Heart Association. *Circ. Res.* **111,** 131–50 (2012).

204. Gao, X.-M., Xu, Q., Kiriazis, H., Dart, A. M. & Du, X.-J. Mouse model of post-infarct ventricular rupture: time course, strain- and gender-dependency, tensile strength, and histopathology. *Cardiovasc. Res.* **65,** 469–77 (2005).

205. Dixon, J. a & Spinale, F. G. Large animal models of heart failure: a critical link in the translation of basic science to clinical practice. *Circ. Heart Fail.* **2,** 262–71 (2009).

206. Monnet, E. & Chachques, J. C. Animal models of heart failure: what is new? *Ann. Thorac. Surg.* **79,** 1445–53 (2005).

207. Cerqueira, M. D. *et al.* Standardized Myocardial Segmentation and Nomenclature for Tomographic Imaging of the Heart. *Circulation* **105,** 539–542 (2002).

208. Fernández, B. *et al.* The coronary arteries of the C57BL/6 mouse strains: implications for comparison with mutant models. *J. Anat.* **212,** 12–18 (2008).

209. Kumar, D. *et al.* Distinct mouse coronary anatomy and myocardial infarction consequent to ligation. *Coron. Artery Dis.* **16,** 41–4 (2005).

210. Icardo, J. M. & Colvee, E. Origin and course of the coronary arteries in normal mice and in iv/iv mice. *J. Anat.* **199,** 473–82 (2001).

211. Borst, O. *et al.* Methods Employed for Induction and Analysis of Experimental Myocardial Infarction in Mice. *Cell. Physiol. Biochem.* **28,** 1–12 (2011).

212. Tarnavski, O. *et al.* Mouse cardiac surgery: comprehensive techniques for the generation of mouse models of human diseases and their application for genomic studies. *Physiol. Genomics* **16,** 349–60 (2004).

213. Gao, E. *et al.* A novel and efficient model of coronary artery ligation and myocardial infarction in the mouse. *Circ. Res.* **107,** 1445–53 (2010).

214. Van den Bos, E. J., Mees, B. M. E., de Waard, M. C., de Crom, R. & Duncker, D. J. A novel model of cryoinjury-induced myocardial infarction in the mouse: a comparison with coronary artery ligation. *Am. J. Physiol. Heart Circ. Physiol.* **289,** H1291–300 (2005).

215. Halapas, A. *et al.* In vivo models for heart failure research. *In Vivo* **22,** 767–80 (2008).

216. Sane, D. C., Mozingo, W. S. & Becker, R. C. Cardiac rupture after myocardial infarction: new insights from murine models. *Cardiol. Rev.* **17,** 293–9 (2009).

217. Fang, L. *et al.* Differences in inflammation, MMP activation and collagen damage account for gender difference in murine cardiac rupture following myocardial infarction. *J. Mol. Cell. Cardiol.* **43,** 535–44 (2007).

218. Cavasin, M. a, Sankey, S. S., Yu, A.-L., Menon, S. & Yang, X.-P. Estrogen and testosterone have opposing effects on chronic cardiac remodeling and function in mice with myocardial infarction. *Am. J. Physiol. Heart Circ. Physiol.* **284,** H1560–9 (2003).

219. Van den Borne, S. W. M. *et al.* Mouse strain determines the outcome of wound healing after myocardial infarction. *Cardiovasc. Res.* **84,** 273–82 (2009).

220. Daaka, Y., Luttrell, L. M. & Lefkowitz, R. J. Switching of the coupling of the beta2-adrenergic receptor to different G proteins by protein kinase A. *Nature* **390,** 88–91 (1997).

221. Shah, A. M. & Mann, D. L. In search of new therapeutic targets and strategies for heart failure: recent advances in basic science. *Lancet* **378,** 704–12 (2011).

222. Nakayama, H. *et al.* Ca2+ - and mitochondrial-dependent cardiomyocyte necrosis as a primary mediator of heart failure. *J. Clin. Invest.* **117,** 2431–2444 (2007).

223. Zhang, X. *et al.* Cardiotoxic and Cardioprotective Features of Chronic β-Adrenergic Signaling. *Circ. Res.* **112,** 498–509 (2013).

224. Chesley, A. *et al.* The β2-Adrenergic Receptor Delivers an Antiapoptotic Signal to Cardiac Myocytes Through Gi-Dependent Coupling to Phosphatidylinositol 3'-Kinase. *Circ. Res.* **87,** 1172–1179 (2000).

225. Oudit, G. Y. *et al.* Phosphoinositide 3-kinase gamma-deficient mice are protected from isoproterenol-induced heart failure. *Circulation* **108,** 2147–52 (2003).

226. Nisch, W., Böck, J., Egert, U., Hämmerle, H. & Mohr, A. A thin film microelectrode array for monitoring extracellular neuronal activity in vitro. *Biosens. Bioelectron.* **9,** 737–741 (1994).

227. Kajikawa, Y. & Schoeder, E. How local is the local field potential? *Neuron* **72,** 847–858 (2012).

228. Buzsáki, G., Anastassiou, C. a. & Koch, C. The origin of extracellular fields and currents — EEG, ECoG, LFP and spikes. *Nat. Rev. Neurosci.* **13,** 407–420 (2012).

229. Burnashev, N. A., Edwards, F. A. & Verkhratskii, A. N. [The use of thin slices of myocardium for recording the currents across single ion channels]. *Fiziol. Zh.* **37,** 119–122 (1991).

230. Pillekamp, F. *et al.* Establishment and characterization of a mouse embryonic heart slice preparation. *Cell. Physiol. Biochem.* **16,** 127–132 (2005).

231. Halbach, M. *et al.* Biochemistry Ventricular Slices of Adult Mouse Hearts - a new Multicellular In Vitro Model for Electro- physiological Studies. *Cell. Physiol. Biochem.* **18,** 1–8 (2006).

232. Camelliti, P. *et al.* Adult human heart slices are a multicellular system suitable for electrophysiological and pharmacological studies. *J. Mol. Cell. Cardiol.* **51,** 390–8 (2011).

233. Langendorff, O. Untersuchungen am uberlebenden Saugethierherzen. *Pflugers Arch.* **61,** 291–332 (1895).

234. Bell, R. M., Mocanu, M. M. & Yellon, D. M. Retrograde heart perfusion: the Langendorff technique of isolated heart perfusion. *J. Mol. Cell. Cardiol.* **50,** 940–50 (2011).

235. Bussek, A. *et al.* Tissue Slices from Adult Mammalian Hearts as a Model for Pharmacological Drug Testing. *Cell. Physiol. Biochem.* **24,** 527–536 (2009).

236. Bussek, A. *et al.* Cardiac tissue slices with prolonged survival for in vitro drug safety screening. *J. Pharmacol. Toxicol. Methods* **66,** 145–51 (2012).

237. Halbach, M. D., Egert, U., Hescheler, J. & Banach, K. Estimation of Action Potential Changes from Field Potential Recordings in Multicellular Mouse Cardiac Myocyte Cultures. *Cell. Physiol. Biochem.* **13,** 271–284 (2003).

238. Himmel, H. M. *et al.* Field and action potential recordings in heart slices: correlation with established in vitro and in vivo models. *Br. J. Pharmacol.* **166,** 276–96 (2012).

239. Ustyugova, I. V, Zhi, L., Abramowitz, J., Birnbaumer, L. & Wu, M. X. IEX-1 deficiency protects against colonic cancer. *Mol. Cancer Res.* **10,** 760–7 (2012).

240. Mouse BLAT search. at <https://genome.ucsc.edu/cgi-bin/hgBlat>

241. Livak, K. J. & Schmittgen, T. D. Analysis of relative gene expression data using real-time quantitative PCR and the 2(-Delta Delta C(T)) Method. *Methods* **25,** 402–408 (2001).

242. Applied Biosystems. User Bulletin #2. ABI PRISM 7700 Sequence Detection System. (2001).

243. Rudolph, U., Spicher, K. & Birnbaumer, L. Adenylyl cyclase inhibition and altered G protein subunit expression and ADP-ribosylation patterns in tissues and cells from Gi2 alpha-/-mice. *Proc. Natl. Acad. Sci. U. S. A.* **93,** 3209–3214 (1996).

244. Collins, K. A., Korcarz, C. E. & Lang, R. M. Use of echocardiography for the phenotypic assessment of genetically altered mice. *Physiol. Genomics* **13,** 227–39 (2003).

245. Rottman, J. N., Ni, G. & Brown, M. Echocardiographic evaluation of ventricular function in mice. *Echocardiography* **24,** 83–9 (2007).

246. Amundsen, B. H. *et al.* A comparison of retrospectively self-gated magnetic resonance imaging and high-frequency echocardiography for characterization of left ventricular function in mice. *Lab. Anim.* **45,** 31–37 (2011).

247. Barbee, R. W., Perry, B. D., Re, R. N. & Murgo, J. P. Microsphere and dilution techniques for the determination of blood flows and volumes in conscious mice. *Am. J. Physiol. Regul. Integr. Comp. Physiol.* **263,** R728–733 (1992).

248. Bowditch, H. P. Über die Eigentümlichkeiten der Reizbarkeit welche Muskelfasern des Herzens zeigen. *Ber Sachs Ges Akkad* **23,** (1871).

249. Maier, L. S., Bers, D. M. & Pieske, B. Differences in Ca(2+)-handling and sarcoplasmic reticulum Ca(2+)-content in isolated rat and rabbit myocardium. *J. Mol. Cell. Cardiol.* **32,** 2249–2258 (2000).

250. Endoh, M. Force-frequency relationship in intact mammalian ventricular myocardium: Physiological and pathophysiological relevance. *Eur. J. Pharmacol.* **500,** 73–86 (2004).

251. Gentry-Smetana, S., Redford, D., Moore, D. & Larson, D. Direct effects of volatile anesthetics on cardiac functiona. *Perfusion* **23,** 43–47 (2008).

252. Janssen, B. J. *et al.* Effects of anesthetics on systemic hemodynamics in mice. *Am. J. Physiol. Heart Circ. Physiol.* **287,** H1618–24 (2004).

253. Mitchell, G. F., Jeron, A. & Koren, G. Measurement of heart rate and Q-T interval in the conscious mouse. *Am. J. Physiol. Heart Circ. Physiol.* **274,** H747–751 (1998).

254. Chu, V. *et al.* Method for non-invasively recording electrocardiograms in conscious mice. *BMC Physiol.* **1,** 4–9 (2001).

255. Gehrmann, J. *et al.* Phenotypic screening for heart rate variability in the mouse. *Am. J. Physiol. Heart Circ. Physiol.* **279,** H733–H740 (2000).

256. Thireau, J., Zhang, B. L., Poisson, D. & Babuty, D. Heart rate variability in mice: a theoretical and practical guide. *Exp. Physiol.* **93,** 83–94 (2008).

257. Wellens, H. J., Schuilenburg, R. M. & Durrer, D. Electrical Stimulation of the Heart in Patients with Ventricular Tachycardia. *Circulation* **46,** 216–226 (1972).

258. Faulx, M. D., Chandler, M. P., Zawaneh, M. S., Stanley, W. C. & Hoit, B. D. Mouse strain-specific differences in cardiac metabolic enzyme activities observed in a model of isoproterenol-induced cardiac hypertrophy. *Clin. Exp. Pharmacol. Physiol.* **34,** 77–80 (2007).

259. Matkovich, S. J. *et al.* Cardiac-specific ablation of G-protein receptor kinase 2 redefines its roles in heart development and beta-adrenergic signaling. *Circ. Res.* **99,** 996–1003 (2006).

260. Horiuchi-Hirose, M. *et al.* Decrease in the density of t-tubular L-type Ca2+ channel currents in failing ventricular myocytes. *Am. J. Physiol. Heart Circ. Physiol.* **300,** H978–88 (2011).

261. Ahn, D. *et al.* Induction of myocardial infarcts of a predictable size and location by branch pattern probability-assisted coronary ligation in C57BL/6 mice. *Am. J. Physiol. Heart Circ. Physiol.* **286,** H1201–7 (2004).

262. Pfeffer, M. a. *et al.* Myocardial infarct size and ventricular function in rats. *Circ. Res.* **44,** 503–512 (1979).

263. Spitznagel, H. *et al.* Cardioprotective effects of the Na(+)/H(+)-exchange inhibitor cariporide in infarct-induced heart failure. *Cardiovasc. Res.* **46,** 102–10 (2000).

264. Wakeno, M. *et al.* Long-term stimulation of adenosine A2b receptors begun after myocardial infarction prevents cardiac remodeling in rats. *Circulation* **114,** 1923–32 (2006).

265. Kaur, K. *et al.* Gαi2 signaling: friend or foe in cardiac injury and heart failure? *Naunyn. Schmiedebergs. Arch. Pharmacol.* **385,** 443–53 (2012).

266. Triposkiadis, F. *et al.* The sympathetic nervous system in heart failure physiology, pathophysiology, and clinical implications. *J. Am. Coll. Cardiol.* **54,** 1747–62 (2009).

267. Mudd, J. O. & Kass, D. a. Tackling heart failure in the twenty-first century. *Nature* **451,** 919–28 (2008).

268. Paur, H. *et al.* High Levels of Circulating Epinephrine Trigger Apical Cardiodepression in a β2-Adrenergic Receptor / Gi–Dependent Manner. A New Model of Takotsubo Cardiomyopathy. *Circulation* **126,** 697–706 (2012).

269. Angelini, P. & Tobis, J. M. Is High-Dose Catecholamine Administration in Small Animals an Appropriate Model for Takotsubo Syndrome? *Circ. J.* **79,** 897 (2015).

270. Huang, X. *et al.* Pleiotropic phenotype of a genomic knock-in of an RGS-insensitive G184S Gnai2 allele. *Mol. Cell. Biol.* **26,** 6870–6879 (2006).

271. DeGeorge, B. R. *et al.* Targeted inhibition of cardiomyocyte Gi signaling enhances susceptibility to apoptotic cell death in response to ischemic stress. *Circulation* **117,** 1378–87 (2008).

272. Moxham, C. M., Hod, Y. & Malbon, C. C. Induction of Gαi2-Specific Antisense RNA in Vivo Inhibits Neonatal Growth. *Science (80-.).* **260,** 991–995 (1993).

273. Hollander, P. B. & Webb, J. L. Cellular membrane potentials and contractility of normal rat atrium and the effects of temperature, tension and stimulus frequency. *Circ. Res.* **3,** 604–612 (1955).

274. Waterson, R. E. *et al.* Gα(i2)-mediated protection from ischaemic injury is modulated by endogenous RGS proteins in the mouse heart. *Cardiovasc. Res.* **91,** 45–52 (2011).

275. International Conference on Harmonsation of Technical Requirements for Registration of Pharmaceuticals for Human Use. *The Non-Clinical Evaluation of the Potential for Delayed Ventricular Repolarization (QT Interval Prolongation) by Human Pharmaceuticals*. (2005). at <http://www.ich.org/products/guidelines/safety/article/safety-guidelines.html>

276. Martins, J. B. & Zipes, D. P. Effects of sympathetic and vagal nerves on recovery properties of the endocardium and epicardium of the canine left ventricle. *Circ. Res.* **46,** 100–110 (1980).

277. Wainford, R. D., Pascale, C. L. & Kuwabara, J. T. Brain Gαi2-subunit protein-gated pathways are required to mediate the centrally evoked sympathoinhibitory mechanisms activated to maintain sodium homeostasis. *J. Hypertens.* **31,** 747–57 (2013).

278. Wainford, R. D., Carmichael, C. Y., Pascale, C. L. & Kuwabara, J. T. Gαi2-Protein-Mediated Signal Transduction: Central Nervous System Molecular Mechanism Countering the Development of Sodium-Dependent Hypertension. *Hypertension* **65,** 178–186 (2015).

279. Campbell, A. S., Johnstone, S. R., Baillie, G. S. & Smith, G. β-Adrenergic modulation of myocardial conduction velocity: Connexins vs. sodium current. *J. Mol. Cell. Cardiol.* **77,** 147–154 (2014).

280. Lang, D. *et al.* Arrhythmogenic Remodeling of β2 versus β1 Adrenergic Signaling in the Human Failing Heart. *Circ. Arrhythmia Electrophysiol.* (2015). doi:10.1161/CIRCEP.114.002065

281. Burt, J. M. & Spray, D. C. Inotropic agents modulate gap junctional conductance between cardiac myocytes. *Am. J. Physiol.* **254,** H1206–1210 (1988).

282. Task Force of the Working Group on Arrhythmias of the European Society of Cardiology. The Sicilian gambit. A new approach to the classification of antiarrhythmic drugs based on their actions on arrhythmogenic mechanisms. *Circulation* **84,** 1831–1851 (1991).

283. Vaughan Williams, E. M. A classification of antiarrhythmic actions reassessed after a decade of new drugs. *J. Clin. Pharmacol.* **24,** 129–147 (1984).

284. Spear, J. F. & Moore, E. N. Modulation of quinidine-induced arrhythmias by temperature in perfused rabbit heart. *Am. J. Physiol. - Hear. Circ. Physiol.* **274,** 817–828 (1998).

285. Hecht, H. H. Normal and Abnormal Transmembrane Potentials of the Spontaneously Beating Heart. *Ann. N. Y. Acad. Sci.* **65,** 700–733 (1957).

286. Milburn, T., Saint, D. A. & Chung, S. H. The temperature dependence of conductance of the sodium channel: implications for mechanisms of ion permeation. *Receptors Channels* **3,** 201–211 (1995).

287. Smeets, J. L. R. M., Allessie, M. A., Lammers, W. J. E. P., Bonke, F. I. M. & Hollen, J. The Wavelength of the Cardiac Impulse and Reentrant Arrhythmias in Isolated Rabbit Atrium. *Circ. Res.* **58,** 96–108 (1986).

288. Kiyosue, T., Arita, M., Muramatsu, H., Spindler, A. J. & Noble, D. Ionic mechanisms of action potential prolongation at low temperature in guinea-pig ventricular myocytes. *J. Physiol.* **468,** 85–106 (1993).

289. Dumaine, R. *et al.* Ionic Mechanisms Responsible for the Electrocardiographic Phenotype of the Brugada Syndrome Are Temperature Dependent. *Circ. Res.* **85,** 803–809 (1999).

290. Bastiaenen, R., Hedley, P. L., Christiansen, M. & Behr, E. R. Therapeutic hypothermia and ventricular fibrillation storm in early repolarization syndrome. *Hear. Rhythm* **7,** 832–834 (2010).

291. Gussak, I., Bjerregaard, P., Egan, T. M. & Chaitman, B. R. ECG phenomenon called the J wave. History, pathophysiology, and clinical significance. *J. Electrocardiol.* **28,** 49–58 (1995).

292. Mugelli, A., Cerbai, E., Amerini, S. & Visentin, S. The role of temperature on the development of oscillatory afterpotentials and triggered activity. *J. Mol. Cell. Cardiol.* **18,** 1313–1316 (1986).

293. Ng, G. A. *et al.* Sympathetic nerve stimulation produces spatial heterogeneities of action potential restitution. *Hear. Rhythm* **6,** 696–706 (2009).

294. Fedorov, V. V. *et al.* Application of blebbistatin as an excitation-contraction uncoupler for electrophysiologic study of rat and rabbit hearts. *Hear. Rhythm* **4,** 619–626 (2007).

295. Herron, T. J., Lee, P. & Jalife, J. Optical imaging of voltage and calcium in cardiac cells & tissues. *Circ. Res.* **110,** 609–23 (2012).

296. Taggart, P. & Lab, M. Cardiac mechano-electric feedback and electrical restitution in humans. *Prog. Biophys. Mol. Biol.* **97,** 452–60 (2008).

297. Reiter, M. J., Landers, M., Zetelaki, Z., Kirchhof, C. J. H. & Allessie, M. A. Electrophysiological Effects of Acute Dilatation in the Isolated Rabbit Heart. *Circulation* **96,** 4050–4056 (1997).

298. Simoons, M. L. & Hugenholtz, P. G. Gradual changes of ECG waveform during and after exercise in normal subjects. *Circulation* **52,** 570–577 (1975).

299. Durrer, D. *et al.* Total excitation of the isolated human heart. *Circulation* **41,** 899–912 (1970).

300. Classic, P. D. Mus musculus (house mouse). at <https://paleobiodb.org/cgi-bin/bridge.pl?a=checkTaxonInfo&taxon_no=104205&is_real_user=1>

301. Frazer, K. *et al.* A sequence-based variation map of 8.27 million SNPs in inbred mouse strains. *Nature* **448,** 1050–1053 (2007).

302. Keane, T. M. *et al.* Mouse genomic variation and its effect on phenotypes and gene regulation. *Nature* **477,** 289–294 (2011).

303. Brouillette, J., Rivard, K., Lizotte, E. & Fiset, C. Sex and strain differences in adult mouse cardiac repolarization: importance of androgens. *Cardiovasc. Res.* **65,** 148–57 (2005).

304. Shah, A. P. *et al.* Genetic background affects function and intracellular calcium regulation of mouse hearts. *Cardiovasc. Res.* **87,** 683–693 (2010).

305. Appleton, G. O. *et al.* Determinants of cardiac electrophysiological properties in mice. *J. Interv. Card. Electrophysiol.* **11,** 5–14 (2004).

306. Kanai, A. & Salama, G. Optical mapping reveals that repolarization spreads anisotropically and is guided by fiber orientation in guinea pig hearts. *Circ. Res.* **77,** 784–802 (1995).

307. Tamaddon, H. S. *et al.* High-Resolution Optical Mapping of the Right Bundle Branch in Connexin40 Knockout Mice Reveals Slow Conduction in the Specialized Conduction System. *Circ. Res.* **87,** 929–936 (2000).

308. De Bakker, J. M. *et al.* Slow conduction in the infarcted human heart. 'Zigzag' course of activation. *Circulation* **88,** 915–926 (1993).

309. Gray, R. A., Iyer, A., Berenfeld, O., Pertsov, A. M. & Hyatt, C. J. Interdependence of virtual electrode polarization and conduction velocity during premature stimulation. *J. Electrocardiol.* **39,** S13–18 (2006).

310. Lerner, D. L., Yamada, K. a., Schuessler, R. B. & Saffitz, J. E. Accelerated Onset and Increased Incidence of Ventricular Arrhythmias Induced by Ischemia in Cx43-Deficient Mice. *Circulation* **101,** 547–552 (2000).

311. Eisner, D., Bode, E., Venetucci, L. & Trafford, A. Calcium flux balance in the heart. *J. Mol. Cell. Cardiol.* **58,** 110–7 (2013).

312. Marks, A. R. Calcium cycling proteins and heart failure: Mechanisms and therapeutics. *J. Clin. Invest.* **123,** 46–52 (2013).

313. Giannopoulos, G. *et al.* Central sympathetic inhibition to reduce postablation atrial fibrillation recurrences in hypertensive patients: a randomized, controlled study. *Circulation* **130,** 1346–1352 (2014).

314. Cohn, J. N. *et al.* Adverse mortality effect of central sympathetic inhibition with sustained-release moxonidine in patients with heart failure (MOXCON). *Eur. J. Heart Fail.* **5,** 659–667 (2003).

315. Cathomen, T. & Ehl, S. Translating the genomic revolution - targeted genome editing in primates. *N. Engl. J. Med.* **370,** 2342–5 (2014).